

UNIVERSITA' DEGLI STUDI DI TRIESTE

Sede Amministrativa di Trieste

XX Ciclo del Dottorato di Ricerca in
Metodologie di Biomonitoraggio dell'Alterazione Ambientale

AN INVESTIGATION IN THE USE OF ADVANCED REMOTE SENSING AND GEOGRAPHIC INFORMATION SYSTEM TECHNIQUES FOR POST-FIRE IMPACT ASSESSMENT ON VEGETATION

(Settore scientifico-disciplinare BIO/07)

DOTTORANDO
Georges H. MITRI

COORDINATORE DEL COLLEGIO DEI DOCENTI
Chiar.mo Prof. Mauro Tretiach
Universita' degli studi di Trieste

RELATORE
Chiar.mo Prof. Enrico Feoli
Universita' degli studi di Trieste

CORRELATORE
Chiar.mo Prof. Ioannis Gitas
Aristotle University of Thessaloniki

ACKNOWLEDGEMENTS

A dissertation does not just appear out of nowhere! Working a PhD dissertation is like walking through a mountained landscape, every hill providing a view over uncharted land and unseen valleys - but at the same time bringing into sight new hilltops, impeding a further view and posing new challenges. Such a journey would not have been possible without the help and support of so many persons to whom I am indebted. I am grateful to them and admit openly that without their help, advice and encouragement this work would not have been plausible.

While most people did not help directly on the work, every one of them contributed in some way towards helping me to get where I am today, even things like just being a friend and going out and having fun. Others were responsible for giving me a push in the right direction in life, and for everyone listed here I am deeply grateful for their help. I appreciated their support, friendship, humour and valuable ideas. The following people deserve a mention for their efforts.

First and foremostly, I would like to thank my supervisors and previous instructors, Professor Ioannis Gitas and Professor Enrico Feoli. Your enthusiasm, guidance, support and boundless ideas were much appreciated. Thank you also for those uplifting comments in times when I doubted that I would ever see the light at the end of the PhD tunnel.

The most instrumental person for this dissertation was my supervisor of research Professor Ioannis Gitas from the Aristotle University of Thessaloniki, Greece. I would like to express my deep gratitude for his support and the valuable time he invested in sharing his knowledge with me. His expertise and his critical comments were always inspiring and substantially contributed to this thesis. Professor Gitas has helped me to gain an international profile in the remote sensing community, by generously giving me the possibility to travel to numerous places all over the Europe and to meet other researchers and even to become an active member of the Forest Fires - European Association of Remote Sensing Laboratories (EARSeL). This international development has strengthened my PhD with experience from a wide range of people and further

motivated my research with fresh ideas. I would also like to thank Professor Gitas for the countless hours I have spent with him discussing research and proof reading papers, talking about life in general, and having a drink as friends after work and when travelling together.

I wish to express my appreciation to the Lebanese National Council for Scientific Research (CNRS) and its director, Dr. Mouïin Hamzé, for providing me with the opportunity and the financial assistance to pursue my PhD studies abroad. Also, I would like to thank Dr. Charle Tabet at the CNRS for his general support and his valuable collaboration in administration matters.

Special thanks go to Dr. Massimo Dragan for his excellent, unconditional and unlimited support and guidance throughout the past three years. Dr. Dragan (the ‘captain’!) provided the right mix of encouragement, challenges, and most important of all friendship.

I am grateful to Professor Serena Fonda Umani, previous coordinator of my PhD studies at the University of Trieste, and to Professor Mauro Tretiach current coordinator of the PhD studies, for their positive contribution to this work. I extend my gratitude to Dr. Andrea Nardini for his collaboration and to the PhD discussion group of professors for all their suggestions and comments through all my work presentations at the university.

My thanks should include all the staff at the Laboratory of Forest Management and Remote Sensing (Aristotle University) and at the Department of Biology (University of Trieste), for the direct and indirect contribution they made to the completion of this work.

In this context, I would like to thank all my friends who provided an ideal environment in which to work and a non-stop support and encouragement, in particular my colleagues Chara, Giorgos, Stavroula, Anastasia, Vasilis, Marco, Daniele, Paola and Kathia for the memorable moments we spent together in our free time. Also, I am indebted to Elena for her sincere friendship and for the indirect contribution she made to the completion of this work. I hope we can always continue our friendship despite that we are no longer fellow suffers in PhDs!

Most importantly of all, I would like to thank my mum Shadia and dad Habib, my sister Joanna and my brother Hadi, for their continued love, support and prayers. They have been a great stability factor and undoubtedly kept me sane through it all. It is through their encouragement and care that I have made it through all the steps to reach this point in life, and I couldn't have done it without them. My family has always taken care of me and I love them all very much.

Last, but most certainly not least, I would like to thank my love Rana who has put up with my crazy PhD life style for the last two years. My research has resulted in being many days away, and some of my travelling has kept me away for weeks at a time. She has always been there supporting me and understood the importance of my work.

I believe that this dissertation has made a real contribution to the field of environmental management and remote sensing science, and I hope that everyone who reads this dissertation finds it useful in his work.

It has been a long, hard and fun journey so far, and I look forward to catching up with everyone and having lots of fun and good times, because that is the most important thing of all. Now it is time to catch up on some sleep and have a holiday! (Well, not really - there is still plenty of other work to go).

TABLE OF CONTENTS

A c k n o w l e d g e m e n t s	i
List of Figures	vii
List of Tables.....	x
Abstract	xii
CHAPTER 1: INTRODUCTION	1
CHAPTER 2: FOREST FIRES IN THE MEDITERRANEAN AND POST-FIRE	
IMPACT ASSESSMENT, AN OVERVIEW	7
2.1 Mediterranean-type ecosystems and the role of forest fires in them.....	7
2.1.1 The Mediterranean ecosystem and its characteristics	7
2.1.2 Mediterranean landscapes.....	8
2.1.3 Forest fires in the Mediterranean and their ecological effects	9
2.1.4 Introduction to post-fire impact assessment	12
2.2 Post-fire impact assessment using Remote Sensing and Geographical Information	
System.....	14
2.2.1 Short-term impact assessment	15
2.2.2 Long-term impact assessment.....	20
2.3 Advanced tools for post-fire impact assessment.....	25
2.3.1 Hyperspectral imaging.....	25
2.3.1.1 Basic concept behind hyperspectral imaging	25
2.3.1.2 Hyperspectral imaging: basic analytical techniques.....	26
2.3.1.3 Hyperspectral imaging of vegetation.....	28
2.3.1.4 Field spectrometry	33
2.3.2 Object-oriented image analysis, concept and methods	33
2.3.2.1 The concept	34
2.3.2.2 Basic aspects in image interpretation	35
2.3.2.3 Classification	36
2.4 Chapter summary	39
CHAPTER 3: ENVIRONMENTAL CONDITIONS IN THASOS AND DATASET	
DESCRIPTION	41
3.1 Study area.....	41
3.1.1 Geography.....	41
3.1.2 Geology and geomorphology.....	42
3.1.3 Climate.....	43
3.1.4 Landcover description	44
3.1.5 History of forest fires.....	47

3.1.6 Post-fire impact assessment	49
3.2 Dataset description	51
3.2.1 Satellite data collection	51
3.2.2 Field and other data collection	53
3.3 Chapter summary	58
CHAPTER 4: SATELLITE DATA PRE-PROCESSING	59
4.1 The concept	59
4.2 Radiometric correction	61
4.2.1 Background	61
4.2.2 Implementation	62
4.2.3 Parameters used and resulting images	64
4.3 Geometric correction	68
4.3.1 Background	69
4.3.2 Implementation and resulting images	71
4.4 Topographic normalization	75
4.4.1 Background	75
4.4.2 Applying the DE_RELIEF algorithm	78
4.4.3 Implementation	79
4.4.4 Resulting images	80
4.5 Chapter summary	82
CHAPTER 5: MAPPING THE TYPE AND SEVERITY OF FIRE USING IKONOS	
IMAGERY	83
5.1 Fire type mapping	85
5.1.1 Segmentation	86
5.1.2 Classification	87
5.1.3 Results and discussion	89
5.2 Fire severity mapping	91
5.2.1 Segmentation	92
5.2.2 Classification	94
5.2.3 Results and discussion	102
5.3 Chapter summary	105
CHAPTER 6: MAPPING VEGETATION RECOVERY USING QUICKBIRD	
IMAGERY	106
6.1 Methodology	108
6.1.1 Segmentation	108
6.1.2 Classification	110
6.2 Results and discussion	119

6.3 Chapter summary	123
CHAPTER 7: MAPPING FOREST REGENERATION AND VEGETATION RECOVERY BY EMPLOYING HYPERSPECTRAL REMOTE SENSING	124
7.1 Analysis of field spectrometry data.....	126
7.1.1 Pine spectral characteristics	127
7.1.1.1 Methodology	128
7.1.1.2 Results and discussion.....	131
7.1.2 Shrub spectral characteristics.....	133
7.1.2.1 Methodology	133
7.1.2.2 Results and discussion.....	135
7.2 Mapping forest regeneration and vegetation recovery using Hyperion	137
7.2.1 Image transformations	140
7.2.2 Methodology.....	142
7.2.2.1 Preliminary steps	143
7.2.2.2 Object-based classification of the Hyperion image.....	147
7.2.3 Results and discussion	149
7.3 Chapter summary	155
CHAPTER 8: MAPPING FOREST REGENERATION AND VEGETATION RECOVERY BY COMBINING VERY HIGH RESOLUTION AND HYPERSPECTRAL IMAGERY	157
8.1 Methodology	160
8.1.1 Segmentation	161
8.1.2 Classification	161
8.2 Results and discussion	169
8.3 Chapter summary	171
CHAPTER 9: GENERAL CONCLUSIONS AND RECOMMENDATIONS.....	172
9.1 General conclusions	172
9.2 Recommendations and future investigations.....	176
REFERENCES	178
APPENDICES	197
APPENDIX 1: Measuring fire severity in the field	198
APPENDIX 2: Collection of hyperspectral data in the field	212
APPENDIX 3: Selected publications	217

LIST OF FIGURES

Figure 1 From left to right: map of Greece, location and satellite image of Thasos	42
Figure 2 Ombrothermic climatic diagram of Thasos for the period 1961 to 1993.....	44
Figure 3 Landcover types in Thasos.....	47
Figure 4 Multitemporal burned areas on the Mediterranean island of Thasos	49
Figure 5 Landsat-TM images showing burned areas from 1985 (left) and 1989 (right)	51
Figure 6 Ikonos image showing the burned area of 2000.....	52
Figure 7 QuickBird image of 2000.....	52
Figure 8 Hyperion image of Thasos	53
Figure 9 CBI ratings (examples of low, medium, and high burn severity in the study area) ..	55
Figure 10 Field spectral measurements	56
Figure 11 Areas of homogeneously regenerated forest and recovered vegetation	57
Figure 12 Numbered field plots overlaid over the Hyperion image	57
Figure 13 Flowchart of the images pre-processing	60
Figure 14 Schematic sketch of radiation components for a flat terrain (solar region)	63
Figure 15 Spectral profile of the Landsat-TM 1985 before and after atmospheric correction	65
Figure 16 Common atmospheric absorption features of the Hyperion scene.....	66
Figure 17 Atmospherically corrected Hyperion	67
Figure 18 Spectral profiles from the atmospherically corrected Ikonos image.....	67
Figure 19 The 1:50 000 map and the ortho-rectified 1985 Landsat image overlaid	73
Figure 20 Accuracy evaluation of the geometric correction of Hyperion	74
Figure 21 Image subset of topographic correction	81
Figure 22 Different levels of image segmentation	87
Figure 23 Fire type class descriptions (middle: Ikonos subsets in false colour)	88
Figure 24 Membership functions.....	89
Figure 25 Ground mapped fire perimeter (white line) and final classification results	89
Figure 26 Flowchart of the methodology for fire severity mapping	92
Figure 27 Hierarchical network of image objects	93
Figure 28 Image subsets show segmentation results at levels 2 and 3	94
Figure 29 A schematic draw of the class hierarchy.....	95
Figure 30 Example of object statistical analysis	96
Figure 31 Schematic overview of the features used in the classification	97
Figure 32 Membership functions of classes (x: feature value, and y: membership value)....	101
Figure 33 Segmentation levels and classification results	102
Figure 34 Left: the points used for accuracy assessment, right: the classification result	103
Figure 35 Fire severity thematic layer over QuickBird.....	108

Figure 36 Subset of image in pixels (left) and segmented subset at level 1 (right).....	109
Figure 37 Image objects at level 2.....	109
Figure 38 Segmented image at level 3	110
Figure 39 Classification results al level 3.....	110
Figure 40 Membership function for class the class ‘land’	111
Figure 41 Classification results at level 1: ‘land’ (dark grey) and ‘water’ (bright grey).....	111
Figure 42 Image of ratio band 1 (bright colour shows shaded areas).....	112
Figure 43 Membership function for the class ‘shadow’	112
Figure 44 Membership function for the class ‘green’	112
Figure 45 Classification of shadow (yellow) green vegetation (green) and other (grey)	113
Figure 46 Membership function for the class ‘green (canopy)’	114
Figure 47 Membership function for the class ‘shadow (bare)’	114
Figure 48 Membership function for the class ‘shadow (canopy)’	115
Figure 49 Membership function for the class ‘shadow (shrubs and small trees)’	115
Figure 50 Membership function for the class ‘other (bare)’	115
Figure 51 Classification results at level 1.....	116
Figure 52 Final classification results at level 2	118
Figure 53 Objects-area ratios.....	120
Figure 54 Relative border of classes	121
Figure 55 Scree plot of the PCA.....	129
Figure 56 Signatures of the selected wavebands for pines	132
Figure 57 Signatures of the selected wavebands for shrub species.....	136
Figure 58 Compared spectral profiles of image endmembers and field spectra.....	139
Figure 59 PC bands 1, 2 and 3 respectively	140
Figure 60 Spatial coherence threshold	141
Figure 61 Flowchart of methodology	142
Figure 62 Feature comparison between ‘vegetation’ (black) and ‘no vegetation’ (blue).....	143
Figure 63 Membership function for the class ‘vegetation’	144
Figure 64 Feature comparison between ‘vegetation’ (black) and ‘no vegetation’ (blue).....	144
Figure 65 Membership function for the class ‘vegetation’	145
Figure 66 Subsets of the preliminary classification results	145
Figure 67 Image subset showing image objects created after segmentation	148
Figure 68 Membership function of NDVI for the class ‘vegetation’	149
Figure 69 Final classification results on image subsets (left: AOI1, and right: AOI2)	150
Figure 70 Flowchart of the methodology	160
Figure 71 Classification scheme.....	162
Figure 72 Ratio of NIR for the class ‘shadows’	163

Figure 73 Membership function for the class ‘vegetation’	163
Figure 74 Membership function for the class ‘not burned’	164
Figure 75 Final classification results at level 2 for AOI1	165
Figure 76 Final classification results at level 2 for AOI2.....	168

LIST OF TABLES

Table 1 Burned area > 0.5 km ² in the year 2000 in some EU countries.....	9
Table 2 Distribution of the burned area by land-cover classes.....	9
Table 3 Landsat-TM characteristics (<i>source: USGS</i>).....	51
Table 4 Ikonos characteristics (<i>source: Space Imaging</i>).....	52
Table 5 QuickBird characteristics (<i>source: DigitalGlobe</i>)	52
Table 6 Hyperion characteristics (<i>source: NASA EO-1 briefing materials</i>).....	53
Table 7 Three composite levels (A-C) including the five strata level (1-4).....	54
Table 8 Regression coefficients and goodness of fit values (Landsat 1985-1989)	66
Table 9 Sun elevation and sun azimuth for the two Landsat TM images of 1985 and 1989... 80	
Table 10 Empirically derived K per band for the 1985 Landsat scene	81
Table 11 Empirically derived K per band for the 1989 Landsat scene	81
Table 12 Fire type mapping contingency matrix.....	90
Table 13 Equations of the mostly used features.....	98
Table 14 The features used in each class.....	99
Table 15 Fire severity confusion matrix.....	104
Table 16 Classification statistics	120
Table 17 Error Matrix.....	122
Table 18 Accuracy statistics.....	122
Table 19 Total Variance explained.....	128
Table 20 Rotated Component Matrix for pines.....	130
Table 21 Wavelengths (nm) correlation for pines	130
Table 22 Reflectance values in the 14 selected wavebands for pines	131
Table 23 Significance (2-tailed) analysis	131
Table 24 Total variance explained	134
Table 25 Rotated Component Matrix	134
Table 26 Wavelengths correlation.....	134
Table 27 Optimal wavebands	135
Table 28 Significance (2-tailed) analysis	136
Table 29 Final output of the Hyperion image (wavelength in nm)	138
Table 30 Band weight assignments	147
Table 31 Best classification results from AOI1.....	151
Table 32 Best classification results from AOI2.....	151
Table 33 Classification stability from AOI1	153
Table 34 Classification stability AOI2	153
Table 35 Error Matrix.....	154

Table 36 Accuracy totals	154
Table 37 Kappa Statistics	154
Table 38 Error Matrix.....	170
Table 39 Accuracy totals	170
Table 40 Kappa Statistics	170

ABSTRACT

Forest fires are a major environmental problem in the Mediterranean region, where large areas are affected each summer. An assessment of the environmental impact of forest fires (in the short-term and in the long-term) requires the collection of accurate and detailed post-fire information related to fire type, fire severity, forest regeneration and vegetation recovery. Advanced tools in remote sensing provide a powerful tool for the study of this phenomenon.

The importance of this work was often emphasized by the European Commission, which focused on the studying of forest fires and their effect on vegetation through the development of appropriate impact assessment and mitigation methods.

The aim of this study was to assess the post-fire impact on vegetation in a Mediterranean environment by employing high quality satellite and field data and by using advanced data processing techniques. The work entailed the development of a whole system integrating very high spatial and spectral resolution remotely sensed data.

For short-term impact assessment, an object-oriented model was developed using very high spatial resolution Ikonos imagery to map the type of fire, namely, canopy fire and surface fire. The results showed that object-oriented classification could be used to accurately distinguish and map areas of surface and crown fire spread (overall accuracy of 87%), especially that occurring in open Mediterranean forests. Also, the performance of object-based classification in mapping three levels of fire severity by employing high spatial resolution Ikonos imagery was evaluated, and accuracy of the obtained results was estimated to be 83%.

As for long-term impact assessment, the mapping of post-fire forest regeneration (pine) and vegetation recovery (shrub) was performed by following three different approaches. First, the developed object-based classification of QuickBird (very high spatial resolution) allowed post-fire vegetation recovery and survival mapping of canopy within two different fire severity levels (86% of classification accuracy). The main effect of fire has been to create a more homogeneous landscape. Second,

statistical analysis of field hyperspectral data allowed a 97% reduction in data volume and recommended 14 best narrowbands to discriminate among pine trees (age and species) and 18 bands that best characterize the different shrub species. Then, hyperspectral Hyperion was employed for mapping post-fire forest regeneration and vegetation recovery. The overall classification accuracy was found to be 75.81% when mapping two different regenerated pine species and other species of vegetation recovery. Third, an object-oriented combined analysis of QuickBird and Hyperion was investigated for the same objective. An improvement in classification accuracy of 8.06% was recorded when combining both Hyperion and QuickBird imageries than by using only the Hyperion image.

Overall, it was observed that advanced tools in remote sensing provided the necessary means for gathering information about the burned areas, the regenerated forests and the recovered vegetations in a successful and a timely/cost effective manner.

CHAPTER 1: INTRODUCTION

Forest fires are an integral part of many terrestrial ecosystems such as boreal forests, temperate forests, Mediterranean ecosystems, savannas and grasslands, among others (Pausas and Vallejo 1999). Fire in the forest can be a “good servant,” ridding forests of unwanted fuel, providing easier access to forest products, and clearing land for other uses. As researchers, managers, policy makers, and concerned citizens, there is a need to maximize the benefits of fire. On the other hand, fire in the forest can be a “bad master,” destroying valuable natural resources, adding carbon to the atmosphere, and killing or injuring humans and animals. Again, as researchers, managers, policy-makers, and concerned citizens, there is a need to reduce these deleterious effects of fire (Landsberg 1994). Additionally, mapping post-fire effects allows forest managers to identify and target areas for intensive or special restoration thus avoiding long-term site degradation.

The average annual number of forest fires throughout the Mediterranean basin was estimated to be close to 50,000 in the last decade, i.e. twice as many as during the 1970s. The annual cumulated burned area in the Mediterranean countries could be estimated to be approximately 600,000 ha (Alexandrian 1995).

Unlike other parts of the world, where a large percentage of fires are of natural origin (especially lightning), the Mediterranean basin is marked by a prevalence of human-induced fires. Natural causes represent only a small percentage of all fires (from 1 to 5 percent, depending on the country), probably because of the absence of climatic phenomena such as dry storms (Canackcioglu and Ozkazanc 1997). Another characteristic common to the entire Mediterranean basin is the high number of fires of unknown cause (Canackcioglu 1986). A point to note, however, is that some countries are characterized by a relatively low proportion of fires resulting from unknown causes (negligence or accidents), which is the case in Croatia (Alexandrian 1995), Greece (Anon 1995) and Portugal (Delattre 1993), where between 25 and 47 percent of fires fall into this category.

Fires in the Mediterranean ecosystems tend to be concentrated in summer when temperatures are high, and air humidity and fuel moisture are low. The fundamental cause of forest fires is linked to:

- changes in traditional land uses, the consequence of which is higher fuel accumulation (García-Ruiz *et al.* 1996); and
- global climatic warming which reduces fuel humidity and increases fire risk and fire spread (Pausas and Vallejo 1999).

Detailed, current information concerning the location and extent of the burned areas, the state and success of forest regeneration, and ecosystem recovery is important for assessing economic losses and ecological effects, monitoring land use and land cover changes, and modelling atmospheric and climatic impacts of biomass burning (Caetano *et al.* 1994, Pereira *et al.* 1997, Gitas 1999). Moreover, accurate assessments aid in evaluating the effectiveness of measures taken to rehabilitate the fire damaged area (Jakubauskas *et al.* 1990).

In order to estimate the ecological impact of fires on the Mediterranean ecosystems, effective analysis techniques need to be implemented. To date, the predominant problems preventing measurement of the impact of forest fires have been the major expense involved in conducting large scale forest investigations and the complex sampling problems associated with collecting relevant descriptive data (Gitas 1999). Given the extremely broad spatial expanse and often limited accessibility of the areas affected by fire, satellite remote sensing is an essential technology for gathering the required information.

Remote sensing images not only provide extensive coverage of wide areas, but also provide comprehensive information about these areas. For almost 30 years, they have been used in many different types of studies covering numerous scientific areas. Due to the absence of precise techniques to map the boundaries of fires occurring in many areas, remote sensing has begun to be widely applied to fill this gap (Díaz-Delgado *et al.* 1998).

Remote sensing from space is especially suitable for forest fire-related research. A significant number of researches were carried out in the last two decades (Chuvieco

and Congalton 1988b, Martín *et al.* 1994, Siljeström and Moreno 1995, Caetano *et al.*, 1995, San Miguel-Ayanz *et al.* 1998) investigating the use of space technology for post-fire assessment, mainly for burned area mapping. Using data from satellites orbiting the earth, it is possible to quickly obtain a general overview of the situation over large areas of terrain, monitor the emergency, identify risks, detect fires and, once the fire has been controlled, assess the damage by mapping the extent of the burned areas, the severity of fire and even post-fire vegetation regeneration.

The wide area coverage and high frequency offered by satellite sensors, as well as their ability to provide information about non visible spectral regions, makes them a very valuable tool for the prevention, detection and mapping of wildland fires. Indeed, remotely sensed data can contribute to a better, cost effective, objective and time-saving method to quantify the location, aerial extent and intensity of fire events (Chuvieco 1999). During the last decade, the range of applications has significantly increased, making satellite remote sensing a solid ally in many forest fire strategic plans (Chuvieco 1997).

Although traditional remote sensing provides an advantageous methodological approach to identifying, mapping and monitoring burned areas compared with the more traditional techniques, it is not free of errors. Despite the advantages of remote sensing in post-fire assessment, several problems have been confronted in burned area and vegetation regeneration mapping using satellite data. Multispectral classification, one of the most common methods for mapping burned areas, is based on the spectral properties of different classes of interest and employs special algorithms designed to perform various types of spectral analysis. However, the use of these classifications has been repeatedly reported to create various types of confusion that can affect the accuracy of mapping, the most important of which can be summarized as follows:

- Spectral overlapping between slightly burned areas and other non-vegetation categories, especially water bodies, urban areas and bare soil (Tanaka *et al.* 1983, Huete *et al.* 1985, Ponzoni *et al.* 1986, Parnot 1988, Lombrana 1995, Siljeström and Moreno 1995, Silva 1996, Caetano *et al.* 1995).
- Spectral overlapping between burned areas and shaded unburned areas (Caetano *et al.* 1994, Pereira *et al.* 1997).

- Spectral overlapping between surface burned areas and unburned forest (Chuvieco and Congalton 1988b, Simpson 1990).
- Spectral overlapping among different vegetation species after regeneration (Thenkabail *et al.* 2004b).

Consequently, spectral based classification methods are difficult to apply when mapping burned areas, forest regeneration and vegetation recovery from satellite images.

However, the development of new remote sensing instruments, both airborne and spaceborne, has provided an opportunity to study vegetation recovery after wildfire (Riano *et al.* 2002). The new generation of very high spatial resolution sensors, such as Ikonos and QuickBird, made it possible to detect small objects not captured by medium-high resolution sensors. Also, hyperspectral data with the typical high number of bands could be used to enable the differentiation of material due to their typical spectra.

With the introduction of advanced remotely sensed data, it is imperative that new methods and techniques be developed to handle these high-dimensional data sets and to accurately extract the required information (Pouliot *et al.* 2002). In the classic image classification approach, the unit is a single pixel (called the pixel-based approach). This pixel-based approach utilises spectral information of the pixels to classify the image. Normally, the different physical properties of earth objects have different spectral information and can be specified by this pixel-based approach. However, the ability of this approach is limited when objects appear to be similar.

Therefore, an alternative analysis approach could be the so-called object-oriented analysis. The concept here is that the information necessary to interpret an image is not represented in a single pixel, but in image objects. Object-based classification, which is based on fuzzy logic, allows the integration of a broad spectrum of different object features such as spectral, shape and texture (when using Very High Resolution) and contextual values, for image analysis. Synergizing all these features is expected to address image analysis tasks that have not been possible until now. Moreover, it is

hypothesized that robust algorithms based on both spectral and contextual information can be further used for operational post-fire impact assessment.

Advanced remote sensing data (recently introduced to the market) and advanced techniques for data processing such as object-oriented analysis are supposed to provide good basis for post-fire impact assessment. The **aim** of this study was to assess the post-fire impact on vegetation in the Mediterranean ecosystem of Thasos using advanced tools in remote sensing. The specific **objectives** were:

1. to investigate the potential use of Very High Resolution (VHR) satellite imagery (Ikonos) in mapping the type and severity of fire;
2. to map vegetation recovery by using VHR satellite imagery (QuickBird) and to examine the relationship between fire severity and vegetation recovery;
3. to map forest regeneration and vegetation recovery by using hyperspectral remote sensing (field spectrometry and Hyperion); and
4. to examine the combination of VHR and hyperspectral satellite imagery in forest regeneration and vegetation recovery mapping.

The following part provides an overview of the main structure of the study with a short description of each chapter.

In chapter 2, an overview on forest fires in the Mediterranean and post-fire impact assessment is given. Section one provides information about the Mediterranean-type ecosystems and the role of forest fires in them. Section 2.2 deals with post-fire impact assessment (in the short term and long term) using Remote Sensing and Geographical Information System. Section two represents advanced tools in post-fire impact assessment (hyperspectral imaging and object-oriented image analysis).

Chapter 3 accounts for the environmental conditions in Thasos (the study area) and dataset description. Section one deals with different aspects of the study area, specifically with geography, geology, climate, landcover description, forest fires and post-fire impact assessment in the study area. Section two describes the collected dataset (e.g. satellite data, field survey data and other ancillary data).

Chapter 4 examines all performed steps related to satellite data pre-processing. Section one describes the radiometric correction applied to the satellite data. Section two describes the geometric correction applied to the images. Finally, section three describes the application of topographic correction to the images. In each of the sections the implementation of the procedure is shown and then the resulting images are discussed.

Chapter 5 represents the research related to short-term impact assessment on vegetation. The first section covers the research related to fire type mapping. Section two covers the research related to fire severity mapping.

Chapter 6 corresponds to the study related to long-term impact assessment on vegetation. In this chapter a Very High spatial Resolution imagery is employed for mapping vegetation recovery after fire. An object-based classification model is developed by using QuickBird imagery.

Chapter 7 deals with hyperspectral remotely sensed data analysis for mapping forest regeneration and vegetation recovery. Field spectrometry information is employed within the first section in order to investigate the spectral properties of naturally regenerated vegetation after fire. Section two aims to map post-fire forest regeneration and vegetation recovery using Hyperion imagery by taking into consideration the previous analysis of the field spectrometry data.

In chapter 8, the combination of Very High Resolution imagery with hyperspectral data is investigated. Both, Hyperion and QuickBird images are combined together using object-oriented analysis for forest regeneration and vegetation recovery mapping.

Finally, chapter 9 presents the major findings of this research and the conclusions drawn. It also includes recommendations and discusses future prospects and needs regarding the topic of research.

CHAPTER 2: FOREST FIRES IN THE MEDITERRANEAN AND POST-FIRE IMPACT ASSESSMENT, AN OVERVIEW

Chapter 1 introduced the subject of this work and stated its aim and its specific objectives. This chapter is divided into three main sections. Section 2.1 provides information about the Mediterranean-type ecosystems and the role of forest fires in them. Section 2.2 deals with post-fire impact assessment (in the short term and in the long term) using Remote Sensing and Geographical Information Systems. Section 2.3 represents advanced tools (hyperspectral imaging and object-oriented image analysis) for post-fire impact assessment.

2.1 MEDITERRANEAN-TYPE ECOSYSTEMS AND THE ROLE OF FOREST FIRES IN THEM

2.1.1 The Mediterranean ecosystem and its characteristics

The Mediterranean-type ecosystem is influenced by a Mediterranean climate (Leisz 1982). Regions of Mediterranean-type climate occur roughly between 30° and 40° latitude around the Mediterranean Sea or on the west coasts of continents where there are cold ocean currents offshore. The Mediterranean Climate is unique in that the wet season coincides with the low sun or winter period, while summers are dry. Total annual precipitation ranges between 380 and 1020 mm per year. Temperatures are those of the subtropics moderated by maritime influence and fogs associated with the cold ocean currents. The result is a very limited, but predictable, growing season when there is both sufficient soil moisture and adequately warm temperatures. Many plants are adapted to withstand drought.

Throughout the world, the Mediterranean biome is characterized by shrubs. In most regions these shrubs are evergreen and have small, leathery (sclerophyllous) leaves with thick cuticles. Sometimes the leaves are so reduced as to appear needle-like. Many typical members of the shrub flora are aromatic (for example, sage, rosemary, thyme, and oregano) and contain highly flammable oils. The dominant trees in the

Mediterranean zone are evergreen oaks and pines. Four species of pine are native to the true Mediterranean region; they are *Pinus pinaster*, *Pinus pinea*, *Pinus halepensis* and the closely related *Pinus brutia* (Gitas 1999). In general, Mediterranean-type areas are among the most diverse areas in the world, second to the tropics.

The Mediterranean region has long been influenced by human activity, in particular the use of fire and the grazing of livestock. We know from classical Greek literature that the Mediterranean region was formerly forested with live oaks, pines, cedars, wild carob and wild olive.

One important factor shaping Mediterranean ecosystems is fire. A large portion of Mediterranean plant species thrive in fire-prone areas such as forest lands, including many types of wooded forests and shrublands. High resilience and outstanding levels of taxonomic (richness in endemic species of restricted area) and ecological (on habitat and landscape scales) diversity characterize Mediterranean forest and shrublands (Moreno *et al.* 1994).

2.1.2 Mediterranean landscapes

A prominent characteristic of vegetation communities and landscape structure in the Mediterranean basin is the high diversity and heterogeneity, in terms of the spatial distribution and arrangement of the abiotic, biotic, floristic and ecological components. In general, the Mediterranean landscape is composed of a “mixture of large, small, distinct and indistinct patches” (Forman and Godron 1986).

This complex spatial nature of the Mediterranean landscapes raises a number of questions associated with the optimum scale of measurements that must be made to represent accurately, in the spatial domain, the phenomenon under study. On the other hand, the irregular terrain relief found across the Mediterranean basin, with high elevations and steep slopes, acts as another source of distortion in the quality of the spectral information provided by satellite sensors. For example, projects carried out in the mountainous areas with irregular relief reported difficulties in discriminating burned from unburned located in shadowed areas (Tanaka *et al.* 1983, Milne 1986, Chuvieco and Congalton 1988a).

The defragmented landscape pattern poses a problem for applied remote sensing, because the huge amount of interchanges in the landscape form and its complexity make the interpretation and processing of the satellite data difficult. Finally, it has been demonstrated that even small differences in geometric resolution have a significant impact on the estimated landscape parameters (Gluck and Rempel 1995).

2.1.3 Forest fires in the Mediterranean and their ecological effects

Fire is an integral part of many ecosystems, including those of the Mediterranean (Trabaud 1994). Mediterranean forest ecosystems are well known to be highly flammable. However, in recent decades the general trend in the number of fires and in the surface burned in European Mediterranean areas has increased spectacularly (Table 1 and Table 2). This increase can be attributed to: (a) land-use changes (rural depopulation results in increasing land abandonment and consequently, fuel accumulation); and (b) climatic warming (which is reducing fuel humidity and increasing fire risk and fire spread).

Table 1 Burned area > 0.5 km² in the year 2000 in some EU countries

Country	Surface burned (ha)
Portugal	107 063
Spain	112 720
France	15 078
Italy	45 101
Greece	106 735
Total	386 697

Table 2 Distribution of the burned area by land-cover classes

Corine land-cover classes	Burned area (ha)	(%) of total burned area
Artificial Surfaces	1160	0.3
Agricultural Areas	76976	19.91
Forests and Semi-natural Areas	289855	74.96
Wetlands	612	0.16
Unclassified Land	18094	4.68
Total	386697	100

With industrial development, Mediterranean countries, mainly European, have experienced: depopulation of rural areas, increases in agricultural mechanisation, decreases in grazing pressure and wood gathering, and increases in the urbanisation of rural areas (LeHou  rou 1993). These changes in traditional land-use and lifestyles

have implied the abandonment of large areas of farm-land, which has led to the recovery of vegetation (García-Ruiz *et al.* 1996) and an increase in accumulated fuel (Rego 1992). In Southern Europe, human activity has dramatically increased fire frequency as a consequence of land abandonment and tourist pressure. As a consequence of these processes, landscapes are becoming homogeneous. In summary, land-use changes produced during the present century in southern Europe are parallel to the changes in the fire regime, from being few in number and affecting small areas, to becoming very numerous and affecting large extensions every year. This trend is not observed in the southern Mediterranean basin where traditional land-uses remain the major socio-economic system.

Although the main reason for fire increase in the last decades is probably changes in land use, climatic factors should be considered as a contributing factor. Fires tend to be concentrated in summer when temperatures are high, and air humidity and fuel moisture are low. Predictions on climate warming (EPA 2001) in the Mediterranean basin indicate an increase in air temperature and a reduction in summer rainfall. These changes would lead to an increase in water stress conditions for plants, changes in fuel conditions and increases in fire risk, with the consequent increase in ignition probability and fire propagation. Analysis of past climate data already show some of these trends (Maheras 1988, Amanatidis *et al.* 1993, Piñol *et al.* 1998). These changes are correlated to an increase in the number of fires. The climate changes that are predicted to occur in the near future as a result of releasing greenhouse gases are likely to induce increased fire risk not only in the Mediterranean area, but also in other fire-prone regions of the world (Torn and Friend 1992).

In view of all of the above, the last two-three decades have been marked in the annual number of fires, total surface burned and geographical distribution of areas affected by fire, in almost all Mediterranean countries. Due to the recent overwhelming number of fires, administrations have been forced to make huge investments in fire, preventing, fighting and resgtoration.

The **ecological effects** of forest fires in the Mediterranean region are very diverse. This is not only because of the complexity of plant communities and the interface of grazing and cutting with burning, but also because of the different responses to the

type, duration and intensity of fire, the season in which it occurs and its frequency (LeHouérou 1987). As explained above, the climatic conditions and the recent changes in landscape structure the European Mediterranean countries have favoured a new fire regime, characterised by frequent, extensive and high intensity fires occurring in the summer and early autumn.

The main effects of fire on soils are: loss of nutrients during burning and the increased risk of erosion after burning. The latter is in fact related to the regeneration traits of the previous vegetation and to environmental conditions (Pausas and Vallejo 1999). Large fires that produce a greater number of intensely burned patches can favour the colonization of invasive, fire tolerant species at the expense of rare/endemic species that are less tolerant to post-fire conditions. Thus biodiversity is also affected by fire. Mediterranean conifers, such as *Pinus halepensis* and *Pinus brutia*, do not resprout, but rely solely on prolific seed germination from cones that burst open from the heat of fire (Dafis 1990).

Recent research shows that these severe fires can be a driving force in landscape homogenization and that burned areas in which flammable shrublands expand can have higher probabilities of reburning than neighbouring unburned areas. The combination of landscape homogenization, the shortening of the fire return interval, the increase in reburning rates and the incidence of large fires constitute a new scenario for Mediterranean ecosystems in which biodiversity is threatened. Climate change predictions and repercussions of forest fires on erosion, water yield and desertification further add to these threats (Moreno *et al.* 1990).

In the face of the adverse impacts of the recent fire regime, the European Commission (DG XII, Directorate General for Science, Research and Development) has recognized the need for a pan-European research effort. In 1990, the four-year environmental programme provided considerable funding for forest fire research. The Fourth Framework Programme paid special attention to the natural role of forest fires. The Fifth Framework Programme (FP) focused on the fight against wildfires through the development of impact assessment and mitigation methods. The European Commission proposal for the Framework Programme (2002-2006) rests the research on forest fires in close liaison with issues of global change. Within the framework of

FP7 a method is needed that allows rapid, standardized, and comparable assessment of the recent state of vegetation (i.e., plant biodiversity) after fire in several countries at the same time. In order to do so, post-fire impact assessment is required, and operational methods for post-fire impact assessment should be developed. Therefore, advanced remote sensing data and techniques should be investigated in order to provide good basis for this assessment.

Finally, the assessment of the ecological effects of fires on biodiversity, soil degradation and on the cycling of carbon and nitrogen requires not only a detailed and accurate mapping of the burned areas but also an accurate mapping of the type and severity of fire and of post-fire forest regeneration and vegetation recovery.

2.1.4 Introduction to post-fire impact assessment

After a forest is damaged by fire, detailed and current information concerning the post-fire vegetation situation is needed to assess economic losses and ecological effects. Moreover, accurate assessments of burned location, fire severity and post-fire vegetation regeneration, aid in evaluating the effectiveness of measures taken to rehabilitate the fire damaged area, and allow forest managers to identify and target areas for intensive or special restoration (Gitas 1999), thus avoiding long-term site degradation (Pereira *et al.* 1977, Jakubauskas 1988, Jakubauskas *et al.* 1990).

Most of the National Forest Services in Mediterranean Europe do not provide cartographic representation of the burned areas (Chuvieco *et al.* 1997). This lack of information results in a poor understanding of the spatial consequences of fires. Traditional methods of burned area mapping, though they can be used with small fires, are not applicable in the cases of large fires due to cost and time limitations (Gitas 1999). According to Chuvieco (1997), satellite remote sensing has supplied an alternative to conventional techniques that is especially suitable for monitoring burned areas.

Given the extremely broad spatial expansion, over which a burned area mapping project may operate, and the often limited accessibility of the areas affected by fire, satellite remote sensing makes it possible for data about the Earth's surface, even

about areas with limited accessibility to be acquired on a regular and permanent basis. According to Caetano *et al.* (1994), satellite remote sensing technology in post-fire assessment has the following potential:

- the acquisition of data that present different spectral reflectance characteristics between burned and unburned vegetation (Tanaka *et al.* 1983), especially in the infrared part of the electromagnetic spectrum;
- the effectiveness of the cost/benefit ratio compared to field measurements, especially in cases of large geographic extent (Lauer and Krumpe 1973);
- the periodical acquisition of the required information (Lee *et al.* 1977) combined with the synoptic view and the minimal time required for data acquisition, and
- the digital form of the data with all the accompanying advantages, such as speed and objectivity of data processing (Richards 1984).

2.2 POST-FIRE IMPACT ASSESSMENT USING REMOTE SENSING AND GEOGRAPHICAL INFORMATION SYSTEM

Post-fire impact assessment requires precise information on extent, type and severity of fire (**short-term impact assessment**) as well as on forest regeneration and vegetation recovery (**long-term impact assessment**). On one hand, information concerning the location and extent of the fire are important to assess economic losses and ecological effects. Distinguishing and mapping areas of surface and crown fire spread has significant applications in the study of fire behaviour, fire suppression and fire effects. Moreover, mapping the severity of fire is necessary in order to locate areas in need of post-fire management for the study of fire impact, forest regeneration and vegetation recovery and for the validation of fire risk and fire behaviour models. On the other hand, monitoring post-fire **forest regeneration** (i.e., pine regeneration) and **vegetation recovery** (i.e., shrub recovery) is important to understand the need for future prescribed burns, to establish post-fire resource management, and to design re-vegetation programs to reduce soil erosion (Keely 2000).

Remote Sensing has proved to be efficient, accurate, objective and operational for burned area mapping (Mitri and Gitas 2004a). However, producing accurate maps of other characteristics of fire regimes, particularly fire type/severity as well as maps of forest regeneration and vegetation recovery, remains more of a challenge.

Fire type/severity maps and forest regeneration and vegetation recovery maps are more dependent on robust field validation (White *et al.* 1996) than maps of fire presence/absence (Hudak and Brocket 2002). Computer-aided analysis of remote sensing data may discriminate distinct spectral classes within a burned area, which may indicate fire severity/type impact, the stage of re-vegetation, original cover type, or a combination of these three (Hitchcock and Hoffer 1974). Trends in reflectance are associated with cover type, fire type/severity (degree of carbonisation), forest regeneration and vegetation recovery (abundance, composition and condition), illumination, change due to slope and the incidence of rainfall, among others. Wavelengths in the visible spectrum are sensitive for changes in the plant physiology, and will appear brighter in fire-altered areas due to the reduced absorption by leaf chlorophylls. Near-infrared (NIR) wavelengths are diagnostic of leaf water stress, and will decrease in fire-damaged areas. Mid-infrared (MIR) wavelengths are sensitive to

alterations in ground exposure and soil colour and increase with fire severity. Wildfires create deep changes in the structure and functioning of natural ecosystems. The development of high spatial and spectral resolution remote sensing instruments, both airborne and spaceborne, has provided an opportunity to evaluate patterns of vegetation recovery after wildfire. Several remote sensing studies have addressed the recovery of the vegetation after fire.

The aim of the following part is to review how remote sensing and Geographical Information Systems (GIS) can be employed in vegetation studies for short-term impact assessment (mapping the burned area, fire type and fire severity) and long-term impact assessment (mapping forest regeneration and vegetation recovery).

2.2.1 Short-term impact assessment

Short-term impact assessment is mostly dealing with mapping direct post-fire effects on vegetation, namely burned area's extent, fire type and fire severity. The work of this study is focused mainly on fire type and severity mapping knowing that burned area mapping was extensively investigated in previous researches (Mitri and Gitas 2004a).

Fire scientists and managers distinguish the following three general types of wildland fire: ground, surface, and crown, depending on the fuel stratum in which the fire burns. While, fire severity is a descriptive term that integrates the ecological changes at a site as a result of fire disturbance. Very few fire type studies and existence fire severity studies have mainly been carried out in the USA (Hitchcock and Hoffer 1974, Lachowski and Anderson 1979, Ryan and Noste 1985, Jakubauskas 1989, Jakubauskas *et al.* 1990, White *et al.* 1996, Medler and Yool 1997, Rignot *et al.* 1999, Turner *et al.* 1999, Key and Benson 1999a, 1999b, 2000, Bertolette and Spotskey 2001, Brumby *et al.* 2001, Redmond *et al.* 2001, Rogan and Yool 2001), and only a few in the Mediterranean ecosystem (Chuvieco and Congalton 1988b, Rodriguez y Silva *et al.* 1997, Rishmawi and Gitas 2001, Rogan and Franklin 2001, Escuin *et al.* 2002, Rogan *et al.* 2002). Other fire type/severity studies have been conducted in Australia (Benson and Briggs 1978, Smith and Woodgate 1985, Milne 1986), Indonesia (Ruecker and Siegert 2000, Siegert and Nakayama 2000) and Alaska (Hall *et al.* 1980, Kasischke *et al.* 1994, Michalek *et al.* 2000).

Landsat-Thematic Mapper (TM) and Multispectral Scanner (MSS) seemed to be the most generally used sensors in short-term impact assessment on vegetation, thanks to the high spatial, spectral and temporal resolution. Some studies (Ruecker and Siegert 2000, Siegert and Nakayama 2000) have used radar imagery for fire impact assessment because of the sensor's advantages under cloudy conditions.

The following section gives an overview of image analysis techniques that have been used in researches dealing with short-term post-fire impact on vegetation (e.g. fire type and fire severity). Results of a specific method may change considerably when applied to other fires or other ecosystems. Moreover, classification accuracies may be affected by several factors such as: - (a) the constraint nature of ground surveys (i.e. the limited line of sight), - (b) the undersampling of fire severity classes, - (c) image registration errors, and - (d) the human agency.

Vegetation indices have been widely applied in this kind of research. The simplest type of vegetation index is obtained by dividing the reflectance from the NIR band by the reflectance of the red visible band (Milne 1986, Jakubauskas *et al.* 1990). The Normalised Difference Vegetation Index (NDVI) is the most commonly used vegetation index. It is an indicator of vegetation abundance and may therefore be used in fire severity/impact mapping (Fox and Stuart 1994, Caetano *et al.* 1995, Rodriguez Y Silva *et al.* 1997, Rogan and Yool 2001, Escuin *et al.* 2002,). Other vegetation indices applied are the Soil Adjusted Vegetation Index (SAVI) (Rodriguez Y Silva *et al.* 1997, Rogan and Yool 2001), the Atmospherically Resistant Vegetation Index (ARVI) (Rodriguez Y Silva *et al.* 1997), Modified SAVI and TM7/4 ratio (Rogan and Yool 2001). A relatively new index is the Normalised Burn Ratio (NBR), a ratio similar to NDVI, but using the reflectance of TM band 7 instead of TM band 4 and sensitive for changes in soil and vegetation moisture. Results of the NBR are very promising for fire severity/impact research (Key and Benson 1999b, 2000, Bertolette and Spotskey 2001, Miller and Yool 2002). Often, the NBR is calculated for both pre-fire and a post-fire satellite scene, then the two pre-/post-fire ratios are differenced and in turn provide a fire severity index that displays low to high fire severity of wildfires.

Multitemporal Principal Component Transformations (PCTs) or multitemporal Kauth-thomas transformation may produce suitable fire severity maps if both pre- and post-burn images are available (Rogan and Yool 2001, Rogan *et al.* 2002). Kauth-Thomas

or Tasseled Cap (KT) Transformation is a linear transformation that establishes three new axes in the spectral data of Landsat-TM. The first feature, brightness, is related to soil reflectance; the second feature, greenness, is strongly related to the amount of green vegetation present in the scene; and the third feature, wetness, is related to canopy and soil moisture. Especially KT wetness is sensitive to differences in moisture levels on the landscape and therefore suitable for fire severity mapping. A disadvantage of the KT transform is that its coefficient table differs per satellite, making comparison between satellites difficult. It is even doubtful whether the KT transform is appropriate for all satellites. Principal Component Analysis (PCA) aims to produce a new dataset, through a linear algebraic expression of the initial variables, in order to minimize the correlation and to associate the variance of the data with the new first components. Areas associated with permanent landscape features are highlighted in the higher order components, while areas of change are emphasized in the lower ones. PCA has proved to be useful for mapping direct post-fire effects, such as the extent of fire and fire severity. However, it considers all data as equally important, while the burned area usually comprises only a part of the scene. Classifications using PCA are therefore often outperformed by classifications that are able to extract the most relevant information such as Kauth-Thomas and Spectral Mixture Analysis (SMA) (Rogan *et al.* 2002). Furthermore, several variations on PCA, such as Bendix-DAS and Canonical Discriminant Analysis (CDA) (Rishmawi and Gitas 2001) have been used in mapping short-term post fire effects.

SMA is a procedure that extracts sub-pixel information by assuming that the spectrum is a (linear) combination of the pure spectra of the materials located in the pixel area, weighted by their fractional abundance. SMA has mainly been used in high spectral resolution sensors, but above mentioned advantages in combination with its ability to solve the topographic problem by desegregating the shade component of the spectral signal make SMA also highly effective in burned area mapping and fire severity assessment (Caetano *et al.* 1995, Rishmawi and Gitas 2001, Rogan and Franklin 2001, Rogan *et al.* 2002). The problem is that results are highly dependent on the input endmembers, and the identification of adequate endmembers might prove difficult in some cases.

Supervised and unsupervised classifications are the two most common classification procedures when mapping short-term post fire effects. Unsupervised classifications of recently burned areas were applied by Hitchcock and Hoffer (1974), Milne (1986), Jakubauskas (1989), Jakubauskas *et al.* (1990), and Bertolette and Spotskey (2001). The main problem encountered was the confusion between shaded areas and severely burned areas. Unsupervised classification can also be used to determine the number of classes that can be distinguished (Benson and Briggs 1978). A disadvantage of unsupervised classification is that it considers the whole scene and does not emphasize on the burned area only. Supervised classification was used for fire severity mapping by Lachowski and Anderson (1979), Chuvieco and Congalton (1988b), Michalek *et al.* (2000), and Escuin *et al.* (2002). Often image transformations such as PCA and KT are performed prior to supervised classification (Rogan and Yool 2001, Rogan *et al.* 2002). Results may also be improved by including a vegetation index (e.g. NDVI) as an extra band to the image to be classified. The definition of training statistics appeared to be the main factor influencing the results.

Another classification technique is density slicing: the converting of the full range of data into a series of intervals or slices, each of which expresses a range in the data. Often, density slicing is applied on a single band (Hall *et al.* 1980, Key and Benson 1999b), or of a vegetation index (difference) image such as NDVI (Fox and Stuart 1994) or of a ratio (Milne 1986).

Imaging radar can provide high-resolution imagery of burned areas, independent of cloud cover, smoke and solar illumination. In addition, radar signals are sensitive to the vegetation volume, structure and moisture content, which provide information complementary to that provided by passive sensors operating at an optical wavelength. For example, optical sensors cannot penetrate healthy canopy cover and may therefore not detect surface burns in areas with a dense overstorey, while radar is capable of penetrating the canopy. Radar has been used for fire impact mapping in Indonesia (Ruecker and Siegert 2000, Siegert and Nakayama 2000), Montana USA (Rignot *et al.* 1999) and Alaska (Kasischke *et al.* 1994). The applicability of satellite Synthetic Aperture Radar (SAR) imagery for burned area mapping in Mediterranean regions has been demonstrated by Gimeno *et al.* (2002). Rainfall greatly influences

the backscatter signal, but it is still unclear in which way. Some authors advice to use imagery taken under dry conditions (Ruecker and Siegert 2000, Siegert and Nakayama 2000), while others suggest to use images taken under wet conditions (Gimeno *et al.* 2002). It seems that the relationship between the burned vegetation and radar backscatter strongly depends upon the ecosystem studied.

High spatial resolution sensors such as Ikonos and Quickbird open a new field of research, with new possibilities such as the detection of smaller objects but also with new problems which need more basic investigations. The currently available very high resolution imagery has a low spectral depth compared to e.g. Landsat-TM, especially in the Mid-Infra-Red (MIR) range of the spectrum, causing confusion between burned areas and non vegetated areas. Typically, pixel-based classifications have difficulties dealing with the rich information content of very high resolution images, which show a very high level of detail and are very strong textured. They produce a characteristic, inconsistent salt-and pepper classification, and they are far from being capable of extracting objects of interest (Mansor *et al.* 2002). It seems that with the introduction of very high resolution sensors classic classification based on pixel-based approaches became limited and that an object-oriented approach is more appropriate. Mitri and Gitas (2004a) used an object-oriented approach on Landsat data to map large burned areas in both Spain and Greece reaching very good results.

Remote sensing is very suitable for the detection of temporal (fire frequency) and/or spatial patterns (heterogeneity) of fire impact. Vazquez and Moreno (2001) mapped fires in the Province of Avila, Spain, over a period of 30 years and calculated fire-regime parameters, such as fire rotation period, and their relation to topographic features or other characteristics of the terrain by means of a spatially explicit analysis. Also, Diaz-Delgado and Pons (2001) have applied a semiautomatic methodology for fire scars mapping from a time series of Landsat MSS images over the forest and shrubby surface of Catalonia (1975-1993). Detected fire scars were incorporated into a Geographic Information System in order to characterize the fire regime of the study area. Fire size distribution and the number of spot fires originated from each fire as well as the maximum distance reached from the main fire are analyzed. Results are a map series of fire history during 21 years as well as a map of the fire recurrence level. The analysis of landscape change using remotely sensed imagery and landscape

pattern metrics is useful to fire sensitivity studies and fire hazard build-up. Several studies (Moreira *et al.* 2001, Lloret *et al.* 2002, Romero-Calcerrada and Perry 2004) suggested that systematic changes have occurred since last decades in landscape composition and structure in Mediterranean areas, and that the landscape changes are likely to result in changes in fire risk and fire regime.

2.2.2 Long-term impact assessment

Wildfires create deep changes in the structure and functioning of natural ecosystems. Monitoring and assessing the impact of post-fire effects (forest regeneration and vegetation recovery) in the long term is important to understand the need for future prescribed burns, to establish postfire resource management, and to design revegetation programs to reduce soil erosion (Keely 2000). Since satellite sensors are able to cover wide areas at a high frequency and are also able to provide information about non-visible spectral regions, they represent a very valuable tool for monitoring of forest regeneration and vegetation recovery after fire. The development of high spatial and spectral resolution remote sensing instruments, both airborne and spaceborne, has provided an opportunity to evaluate patterns of forest regeneration and vegetation recovery after wildfire. Several remote sensing studies have addressed the regeneration and recovery of the vegetation after fire. The remote sensing of post-fire recovery is usually based on the proportion of the green vegetation component in the signal. In general, the NDVI has been widely used, although some studies have investigated the application of SMA. Landsat MSS and TM imagery have been most widely used because they can provide time series since 1975, but the application of SAR imagery showed very promising results in post-fire regeneration and recovery mapping.

The NDVI has been found to be highly correlated with crown closure, leaf area index, and other vegetation parameters. Change in canopy cover or vegetation biomass can be detected by analysing NDVI values from separate dates (Hayes and Sader 2001).

The NDVI of multitemporal Landsat (TM and MSS) imagery is the most widely used tool to assess the process of recovery after fire (Jakubauskas *et al.* 1990, Fiorella and Ripple 1993, White *et al.* 1996, Viedma *et al.* 1997, Kushla and Ripple 1998, Ricotta *et al.* 1998, Salvador *et al.* 1998, Diaz-Delgado *et al.* 1999, Belda and Meliá 2000,

Chen *et al.* 2001, Diaz-Delgado and Pons 2001, García-Haro *et al.* 2001, Metzler and Sader 2002). Furthermore, the NDVI has been used for AVIRIS (Riaño *et al.* 2002), AVHRR (Caetano *et al.* 1995) and SPOT XS and VEGETATION (Henry and Hope 1998, Fraser and Li 2002) imagery. Other indices that have been tested include the normalized difference between Landsat Thematic Mapper bands TM4 and TM5 (Marchetti *et al.* 1995), the Structural Index (TM4/TM5) (Fiorella and Ripple 1993, Kushla and Ripple 1998), the Soil Adjusted Vegetation Index (Henry and Hope 1998), and the Tasseled Cap transformation (Fiorella and Ripple 1993, Kushla and Ripple 1998). Riaño *et al.* (2002) compared two indices, Regeneration index (RI) and Normalized Regeneration Index (NRI), both based on the measure of the vigour of vegetation (green vegetation) for a burned plot (VI_{fire}) and the measure for an unburned control plot (VI_{control}).

Marchetti *et al.* (1995) analyzed vegetation recovery by visual assessment. Other authors have assessed not only changes in vegetation indices after the fire (Fiorella and Ripple 1993), but differences in the indices before and after the fire (White *et al.* 1996, Viedma *et al.* 1997, Kushla and Ripple 1998). Kushla and Ripple (1998) also considered the quotient and the normalized difference in the vegetation index before and after fire. Spatial analysis has been used to understand the recovery after a fire. Hostert *et al.* (2003) used coupling spectral unmixing and trend analysis for monitoring of long-term vegetation dynamics. Ricotta *et al.* (1998) used a fractal algorithm (textural analysis of NDVI) to assess recovery in terms of changes in landscape stability. Viedma *et al.* (1997) used a geostatistical approach and analyzed the semivariogram of TM5 within the burned site to measure changes in homogeneity. Transformed Divergence Analysis of Landsat TM radiance data revealed that forests of varying age and following different regeneration pathways were best discriminated using mid infrared (1.55–1.74 μm) wavelengths (Lucas *et al.* 2002). Short-Wave Infrared (SWIR) reflectance measured by Landsat TM has been found to be sensitive to burned area and biomass. Fraser and Li (2002) found that of all the channels, SWIR was most strongly related to age, and the Short-Wave Vegetation Index (SWVI), where SWIR is substituted for the red, was most closely related to burn regeneration age. Several authors have used the sensitivity of the SWIR/MIR channel for biomass and soil cover, for example, by substituting the SWIR for the red in the NDVI, resulting in a SWVI (Fraser and Li 2002), or a Normalised Difference Moisture Index

(NDMI) (Metzler and Sader 2002). Hall *et al.* (1980) used single-channel density slices of band 7 of Landsat MSS to report the first-year recovery of vegetation.

The study of forest regeneration and vegetation recovery after fire using multitemporal analysis requires atmospheric normalization of the image data, a step that has been included in the image analysis by almost every author. Viedma *et al.* (1997) also applied a topographic normalization. However, these corrections may still be insufficient in accounting for measurement and environmental effects that are external to the changes due to the wildfire. Henry and Hope (1998) even questioned whether remote sensing can be used to study ecosystem recovery after fire. Many authors have described a wide range of noise factors that reduce the detection of regeneration patterns, including radiometric calibration uncertainty, errors in the atmospheric correction, topographic effects and shifts in the phenological state of the vegetation between data acquisitions due to interannual or seasonal climate differences. Diaz-Delgado *et al.* (1998) used control sites located in the same images, but not affected by fire to solve this problem. Their criteria for the control sites include similar environmental conditions and vegetation, ideally located adjacent or close to the burned sites. They used the following Regeneration Index (RI) to correct for external influences: $RINDVI = NDVI_{fire} / NDVI_{control}$

SAR can image volumes of vegetation, and therefore is able to map parameters related to forest biomass, namely, stem volume, total growing stock, or above ground net primary productivity. Rignot *et al.* (1999) found that the recovery process of burned areas was only visible in HV bands. Wagner *et al.* (2002) used a combination of Earth Remote Sensing Satellite (ERS) tandem data and Japanese Earth Resources Satellite (JERS) backscatter to map growing stock volumes. Luckman *et al.* (1997) studied the relationship between radar backscatter and the biomass density of a regenerating tropical forest and they found that backscatter at L-band showed greater variation with vegetation type than at C-band. The relationship between biomass density and C-band backscatter did not appear to be very useful, while L-band (either HH or HV) could be suitable for monitoring biomass density in regenerating tropical forests. In general, it seems that the relationship between SAR backscatter and post-fire recovery greatly depends on the specific ecosystem and wavelength.

The temporal evolution of vegetation recovery interpreted from remote sensing data has been validated with aerial photography and field studies (Kushla and Ripple 1998), in which the values of different indices produced from the images were correlated to increased vegetation cover due to regeneration. Field measurements may be focused on the monitoring of seedling germination, survival and growth (height) in a plot (Tsitsoni 1997, De Luís *et al.* 2001, Bailey and Covington 2002, Kennard *et al.* 2002), or may be along a transect on which samples are taken of plant cover (Caturla *et al.* 2000), tree cover (Ne'eman *et al.* 1999), tree characteristics (Ne'eman *et al.* 1999, Gould *et al.* 2002) or the floristic composition and cover per species (Pausas *et al.* 1999, Wahren *et al.* 2001). Shaw *et al.* (1998) also correlated hyperspectral field measurements to increased vegetation cover. Other authors have searched for a relationship between the remotely sensed indices and the time elapsed since the fire to estimate the period of recovery, principally by using a logarithmic regression model (Fiorella and Ripple 1993, Viedma *et al.* 1997, Diaz-Delgado *et al.* 1998). If the time since the wildfire is known from other sources, the remotely sensed estimation of vegetation recovery can be validated. Availability of Global Positioning System (GPS) to map fire scars has increased knowledge of locations of specific wildfires. The most widely used high spatial resolution sensor to study the regeneration after fire has been Landsat TM. Some studies have used SPOT-XS (Henry and Hope 1998) and SPOT-multispectral (French *et al.* 1996). Hyperspectral sensors have not been extensively used for this purpose; however, for example, Shaw *et al.* (1998) studied regeneration in Scots pines with a high-resolution field spectroradiometer and Ustin and Xiao (2001) studied forest communities in central Alaska using NASA's Advanced Visible/Infrared Imaging Spectrometer (AVIRIS). More recently, Riano *et al.* (2002) assessed the usefulness of hyperspectral AVIRIS to characterize the regeneration process. Hyperspectral sensors have been demonstrated to be useful in change detection and have been shown to detect temporal changes in vegetation (Elvidge and Portugal 1990, Gamon *et al.* 1995, Ustin *et al.* 1998). Most remote sensing fire recovery studies have been conducted in environments with Mediterranean climates (Jakubauskas *et al.* 1990, Marchetti *et al.* 1995, Viedma *et al.* 1997, Diaz-Delgado *et al.* 1998, Henry and Hope 1998, Ricotta *et al.* 1998).

Finally, maps of post-fire forest regeneration and vegetation recovery, in combination with GIS databases, may be used to show the relationship between post-fire recovery

and spatial and temporal patterns in the environment (topography, weather, management), may indicate areas in need of protective measures, and may be used to monitor fire-induced land use changes. For example, by applying a GIS technique together with ancillary data, the relationship between post-fire forest regeneration and vegetation recovery and topographic factors can be investigated. Another application of remote sensing is the production of input for post-fire forest regeneration and vegetation recovery modelling, which may predict recovery in a specific area. For example, Amiro *et al.* (2003) used Leaf Area Index (LAI) and landcover type maps produced by means of AVHRR satellite measurements as inputs for an ecosystem process model in order to estimate net primary productivity. Franklin *et al.* (2001) simulated the effects of different fire regimes on plant functional groups in Southern California using the LANDIS (LANDscape Disturbance and Succession) model.

2.3 ADVANCED TOOLS FOR POST-FIRE IMPACT ASSESSMENT

2.3.1 Hyperspectral imaging

A significant step forward in the world of earth observation was made with the development of hyperspectral imaging. Imaging spectrometers measure reflected solar radiance from the earth in many narrow spectral bands. As a result, imaging spectrometry enables a better identification of objects at the earth surface and a better quantification of the object properties than can be achieved by traditional earth observation sensors such as Landsat TM and SPOT. Imaging spectrometers acquire images in a large number (typically over 40), narrow (typically 0.01 to 0.02 μm in width), contiguous (adjacent and not overlapping) spectral bands to enable the extraction of reflectance spectra at a pixel scale that can be directly compared with similar spectra measured either in the field or in a laboratory (Van der Meer and De Jong 2001).

The objective of hyperspectral imaging is to measure quantitatively the components of the Earth System from calibrated spectra acquired as images for scientific research and applications (Vane and Goetz 1988). The evolution of spaceborne remote sensing has led to the introduction of advanced hyperspectral instruments. Recently, the National Aeronautics and Space Administration (NASA) launched the Earth Observing 1 (EO-1), the world's first satellite that carries a hyperspectral sensor, Hyperion (Pearlman *et al.* 2001, Ungar *et al.* 2003). It is the first spaceborne hyperspectral instrument to acquire both visible near-infrared [(VNIR) 400–1000 nm] and shortwave infrared [(SWIR) 900–2500 nm] spectra.

2.3.1.1 Basic concept behind hyperspectral imaging

When light interacts with a substance, light of certain wavelength is preferentially absorbed while at other wavelengths is transmitted in the substance. Reflectance, defined as the ratio of the intensity of light reflected from a sample to the intensity of the light incident on it, is measured by reflection spectrophotometers which are composed of a light source and a prism to separate light into different wavelengths. This light beam interacts with the sample and the intensity of reflected light at various wavelengths is measured by a detector relative to a reference standard of known

reflectance. Thus a continuous reflectance spectrum of the sample is obtained in the wavelength region measured.

Reflectance spectra have been used for many years to obtain compositional information of the Earth surface. Similarly, it has been shown that spectral reflectance in visible and near-infrared offers a rapid and inexpensive technique for determining the mineralogy of samples and obtaining information on chemical composition. Electronic transition and charge transfer processes (e.g., changes in energy states of electrons bound to atoms or molecules) associated with transition metal ions such as Fe, Ti, Cr, etc., determine largely the position of diagnostic absorption features in the visible and near-infrared wavelength region of the spectra of minerals (Burns 1970, Adams 1974). In addition, vibrational processes in H₂O and OH⁻ (e.g. small displacements of the atoms about their resting positions) produce fundamental overtone absorptions (Hunt 1977). Electronic transitions produce broad absorption features that require higher energy levels than do vibrational processes, and therefore take place at shorter wavelengths (Goetz 1991). The position, shape, depth, and width of these absorption features are controlled by the particular crystal structure in which the absorbing species is contained and by the chemical structure of the mineral. Thus, variables characterizing absorption features can be directly related to the mineralogy of the sample.

2.3.1.2 Hyperspectral imaging: basic analytical techniques

Until recently, the main limitation of remote sensing was that surface information lacked of details due to the broad bandwidth of available sensors. Work on high-spectral resolution radiometry has shown that earth surface mineralogy can be identified using spectral information from sensor data (Goetz 1991). Conventional sensors (e.g. Landsat MSS and TM, and SPOT) acquire information in a few separate spectral bands of various widths (typically in the order of 0.1-0.2 μm), thus smoothing to a large extent the reflectance characteristics of the surface (Goetz and Rowan 1981). Most terrestrial materials are characterized by spectral absorption features typically 0.02-0.04 μm in width (Hunt 1980). High-spectral resolution remotely sensed images are acquired to produce reflectance or radiance spectra for each pixel in the scene.

The spectral pre-processing: imaging spectrometers take indirect measurements of physical parameters in the sense that the digitized signal recorded is directly proportional to the incoming photon energy but not measured in any physically meaningful unit. The relation between the raw digitized signal and a physical meaningful parameter is established after radiometric correction yielding spectral radiance measured as the photon flux power per unit solid angle per wavelength interval. During radiometric calibration the radiometric response function is derived from the relation between the signal, caused on the detectors by the bombardment of photoelectrons, and the incoming radiance. This function translates raw radiance into spectral radiance. The radiometric response function corrected for the spectral response and geometric response as well for the temporal response gives the at – sensor spectral radiance. Most instruments measure physical parameters indirectly by generating and recording a signal, i.e., a Digital Number (DN), which is related to this physical parameter, i.e., radiance. The empirical relationship between the raw signal and the desired physical parameter is done through instrument calibration.

Atmospheric correction: raw calibrated imaging spectrometer data have the general appearance of the solar irradiance curve, with radiance decreasing towards longer wavelengths, and exhibit several absorption bands due to scattering and absorption by gasses in the atmosphere. The major atmospheric water vapour bands (H_2O) are centred approximately at 0.94 μm , 1.14 μm , 1.38 μm and 1.88 μm , the oxygen (O_2) band at 0.76 μm , and carbon dioxide (CO_2) bands near 2.01 μm and 2.08 μm . Additionally, other gasses including ozone (O_3), carbon monoxide (CO), nitrous oxide (N_2O), and methane (CH_4), produce noticeable absorption features in the 0.4-2.5 μm wavelength region. The effect of atmospheric calibration algorithms is to re-scale the raw radiance data provided by imaging spectrometers to reflectance by correcting for atmospheric influence thus shifting all spectra to nearly the same albedo. The result is a data set in which each pixel can be represented by a reflectance spectrum which can be directly compared to reflectance spectra of rocks and minerals acquired either in the field or in the laboratory.

Analytical processing techniques: selection of spectral endmembers for spectral unmixing (McCord 1979) or other types of analysis is crucial to understanding imaging spectrometer data. The set of end-members should describe all spectral

variability for all pixels, produce unique results, and be of significance to the underlying science objectives. Selection of end-members can be achieved in two ways:

1. selecting end-members from a spectral (field or laboratory) library, and
2. deriving end-members from the purest pixels in the image.

The second method has the advantage that selected end-members were collected under similar atmospheric conditions. The end-members resulting through the first option are generally denoted as “known” end-members while the second option results in ‘derived’ endmembers. Identification of the purest pixels in the scene is done through compression of the data using PCA following a method developed by Smith and Woodgate (1985). A very useful tool for interactive endmember selection is the 3D visualiser in the software ENVI.

Deriving image end-members starts by determining the number of end-members needed to optimally characterize the image data using the Minimum Noise Fraction (MNF) transformation (Green *et al.* 1988). The MNF transformation is a two-step principal component transformation where during the first step using the noise covariance matrix the noise is decorrelated to have unit variance and no band-to-band correlation. The second principal component transformation results in a data set where components are ranked in terms of noise equivalent radiance.

Next, the location of the end-member pixels need to be determined from the image data. Here the Pixel Purity Index (Boardman *et al.* 1995) based on the approach developed by Smith and Woodgate (1985) is applied to the MNF transformed data. This approach regards spectra as points in an n-dimensional space (n being the number of bands). Van der Meer and De Jong (2000) point out the importance of proper endmember selection as input to unmixing to avoid singularity and orthogonality problems with matrix inversion of linear systems.

2.3.1.3 Hyperspectral imaging of vegetation

Reflectance studies of vegetation (Gates *et al.* 1965) generally restrict to the green leaf part of the plants giving little attention to the non-green dry vegetation

components. Reflectance properties of vegetation in the visible part of the spectrum are dominated by the absorption properties of photosynthetic pigments of which chlorophyll, having absorptions at 0.66 and 0.68 μm for chlorophyll a and b respectively, is the most important.

Changes in the chlorophyll concentration produce spectral shifts of the absorption edge near 0.7 μm : the red edge. This red edge shifts toward the blue part of the spectrum with loss of chlorophyll. The mid-infrared and short-wave infrared part of the vegetation spectrum is dominated by water and organic compounds of which cellulose, lignin, starch and protein (Elvidge 1990). Absorption features due to bound and unbound water occur near 1.4 and 1.9 μm and at 0.97, 1.20 and 1.77 μm . Cellulose has absorptions at 1.22, 1.48, 1.93, 2.28, 2.34, and 2.48 μm while lignin has absorption features at 1.45, 1.68, 1.93, 2.05-2.14, 2.27, 2.33, 2.38, and 2.50 μm (Elvidge 1990). Starch has absorption features at 0.99, 1.22, 1.45, 1.56, 1.70, 1.77, 1.93, 2.10, 1.32, and 2.48 (Elvidge 1990). The most abundant protein in leaves is a nitrogen bearing compound having absorption features at 1.50, 1.68, 1.74, 1.84, 2.05, 2.17, 2.29, 2.47 μm (Elvidge 1990). Dry plant materials lack the chlorophyll absorptions and intense water absorptions that are characteristic for green leaves and thus lack the intense absorption wing produced by high blue and Ultra Violet (UV) absorptions. Dry plant materials have diagnostic lingo-cellulose absorption features at 2.09 and in the 2.30 μm region (Elvidge 1990).

In vegetation, much variation in spectral properties results from the viewing geometry. Viewing geometry includes the angle of incidence, angle of reflection, and the phase angle: the angle between the incident light and observer (the angle of reflection). These affect the intensity of light received. These effects are marginal for minerals, more pronounced for rocks and soils and of much importance in studying vegetation (Gates *et al.* 1965, Wessman *et al.* 1988, Elvidge 1990).

Remote sensing is increasingly used for measurement required for accurate determinations of the landscape and the state of forest land. With the deployment of early broadband sensors there was a lot of enthusiasm as data, which was previously not feasible to obtain, was now regularly available for large areas of the earth. However, new technologies have shown that while data obtained from broadband

sensors have been useful in many respects, they also have their limitations. Because of their limited number of channels and wide bandwidths, a lot of the data about plant reflectance is lost due to averaging. In remote sensing, the radiation values recorded by the sensor, after atmospheric correction, are a function (f) of the location (x), time (t), wavelength (λ) and viewing geometry (θ) of the ground element, i.e. $R = f(x, t, \lambda, \theta)$. Most natural objects have characteristic features in the spectral signature that distinguishes them from others and many of these characteristic features occur in very narrow wavelength regions. Hence to 'sense' these narrow features the use of narrow band sensors is required. Broadband sensors average the reflectance over a wide range and so the narrow spectral features are lost or masked by other stronger features surrounding them. Thus broadband sensors, such as Landsat TM, cannot resolve narrow diagnostic features as their spectral bandwidths are 100-200nm wide and they are also not contiguous. For this reason hyperspectral remote sensing is a strong alternative for significant advancement in the understanding of the earth and its environment.

Data from imaging spectrometers have been found to yield higher quality information about vegetation health and cover than those obtained from broadband sensors (Collins *et al.* 1983, Curran *et al.* 1992, Penuelas *et al.* 1993, Carter 1994, Kraft *et al.* 1996). However, as with any new technology, it takes times to develop new methods and algorithms to fully utilize the large information content of the hundreds of channels on imaging spectrometers. The following paragraphs look at a number of issues relating to the use of hyperspectral remote sensing in vegetation studies. The discussion will concentrate on the fundamental factors affecting vegetation reflectance, reflectance characteristics of vegetation in different wavelength regions (visible, shortwave-infrared, near-infrared and mid-infrared), and the vegetation reflectance curve.

Leaf optical properties

Incoming solar radiation is the primary source of energy for the numerous biological processes taking place in plants. The interactions between solar radiation and plants can be divided into three broad categories: thermal effects, photosynthetic effects, and photomorphogenic effects of radiation.

Reflectance (400-700 nm): The visible region of the vegetation reflectance spectrum is characterized by low reflectance and transmittance due to strong absorptions by foliar pigments. For instance, chlorophyll pigments absorb violet-blue and red light for photosynthesis. Green light is not absorbed for photosynthesis, hence most plants appear green. The reflectance spectrum of green vegetation shows absorption peaks around 420, 490 and 660 nm. Most of these are caused by strong absorptions of chlorophyll.

The reflectance red-edge (690-720 nm): The red-edge, first described by Collins (1978), is a characteristic feature of the spectral response of vegetation and perhaps is the most studied feature in the spectral curve. It is characterized by the low red chlorophyll reflectance to the high reflectance around 800 nm (often called the red-edge shoulder) associated with leaf internal structure and water content. Since the red-edge itself is a fairly wide feature of approximately 30 nm, it is often desirable to quantify it with a single value so that this value can be compared with that of other species. Eventually, the red-edge inflection point is used. This is the point of maximum slope on the red infrared curve. For an accurate determination of the red-edge inflection point, a large number of spectral measurements in very narrow bands are required so the derivative spectra give a fairly accurate position of the inflection point.

The near-infrared region (700-1300 nm): Plants generally have a high reflectance and transmittance in the near-infrared region. In contrast to light in the visible wavelengths, the energy levels of near-infrared light are not great enough for photochemical reactions and so are not absorbed by chloroplasts and other pigments. Pigments do not contribute to near-infrared reflectance properties of leaves (Billings and Morris 1951). The actual proportion absorbed, scattered or reflected will vary between species and depends on the internal structure of the leaves. Gates *et al.* (1965) and Sinclair *et al.* (1971) have reported that internal leaf structure is the dominant factor controlling the spectral response of plants in the near-infrared. The near-infrared spectra of leaves also change during development, growth. In vegetation canopies, near-infrared reflectance is much higher than that for single leaves. As most of the radiation at near-infrared wavelengths pass through single leaves, the multiple leaf layers of a canopy have an additive effect on reflectance (Belward 1991). Part of

the radiation transmitted by the first leaf layer is reflected back by subsequent layers (Hoffer 1978). It should be noted that after a certain number of leaf layers, addition of extra layers does not increase near-infrared reflectance. This point is referred to as the near-infrared infinite reflectance (Belward 1991).

The mid-infrared region (1300-2500 nm): The mid-infrared domain is characterized by strong water absorptions and minor absorption features of other foliar biochemical contents. The reflectance in this region is much lower than in the NIR. The main water absorption bands are centred at 2660, 2730 and 6270 nm, and overtones are observed at 1200, 1450, 1940 and 2500 nm. As the water absorptions in the mid-infrared are fairly strong, they have a carry-over effect such that the regions between major water absorption bands are also affected. Therefore increased water contents of leaves will not only decrease reflectance in the water absorption bands, but they will also cause a decrease in reflectance in other regions as well. Unlike pigments, where absorptions are caused by electron transitions, water absorptions are caused by transitions in the vibrational and rotational states of the water molecules (Belward 1991). Leaf biochemicals which absorb in the mid-infrared region include lignin, cellulose, starch, proteins and nitrogen. The absorptions of these chemicals are not very strong and so are generally masked by water absorptions in fresh leaves. They are much more clearly distinguishable in dry leaf spectra.

Vegetation reflectance curve: Leaf optical properties are influenced by the concentration of chlorophyll and other biochemicals, water content, and leaf structure (Fourty *et al.* 1996). These leaf characteristics are all very variable and therefore also the reflectance of vegetation is a result of a very complex changing process within the leaves, the canopy and the stand. Physical consideration suggests that the most useful three broad spectral intervals for plant discrimination purposes are those associated with chlorophyll, water, and a third region where both chlorophyll and water are transparent (Gausman *et al.* 1970). Specifically, intervals centred around 680, 850, 1650, and 2200 nm wavelength appear to be most useful to discriminate among different kinds of leaves (Gausman *et al.* 1970). The first interval is in the visible region, and the others correspond to peaks of the atmospheric windows. During the plant growth the NIR reflectance of a given species is almost constant (genetic

determinism); the most important changes appear during maturation (Verdebout *et al.* 1994).

2.3.1.4 Field spectrometry

Field spectrometry is the quantitative measurement of radiance, irradiance, reflectance or transmission in the field (Elvidge 1990). Portable, battery powered spectroradiometers are typically used to make these measurements.

There are many reasons why it is desirable to perform spectral measurement in the field, not all related to remote sensing. Field spectra of ground targets that are homogeneous at the scale of the imaging sensor and collected using ambient solar illumination can be used to convert radiance images to reflectance. Often, field spectra of target materials are collected to allow for more precise image analysis and interpretation (Van der Meer and De Jong 2001). Additionally, various techniques are employed to efficiently use the best hyperspectral signatures to perform supervised classification. This classification is based on the differences in the hyperspectral curves.

Field spectroscopy is also used as a tool to perform feasibility studies to understand if and how a process or material of interest can be detected using remote sensing. Aside from remote sensing, field spectrometers are used to make direct material identifications in the field rather than collecting samples for later laboratory analysis. Applications such as aircraft and satellite sensor calibration, development of remote sensing data exploitation methods, remote sensing feasibility studies, and geologic mapping greatly benefit from the use of field spectrometry (Van der Meer and De Jong 2001).

2.3.2 Object-oriented image analysis, concept and methods

With the introduction of Very High Resolution (VHR) images (i.e. Ikonos and QuickBird satellite imageries) and Hyperspectral imagery (i.e. Hyperion), new approaches such as object-oriented image analysis, have been developed to overcome the limitations of the traditional techniques in satellite imagery processing. The scope of this part is to review the basics of object-oriented image analysis, the general

aspects of image interpretation and to provide an overview of segmentation and classification methods, with a particular focus on fuzzy classification.

2.3.2.1 The concept

Object-oriented image analysis has been developed to overcome the limitations and weaknesses of traditional image processing methods for feature extraction from high resolution images. In spite of years of research into pixel-based image processing techniques such systems are often unable to recognize characteristics that are obvious to human visual inspection. Pixel-based image classification uses the spectral information represented by the digital numbers in one or more spectral bands, and attempts to classify each pixel based mainly on this spectral information. However, important semantic information necessary to interpret an image is not represented in single pixels but in meaningful image objects and their mutual relations (Mitri and Gitas 2004a). The basic difference, especially when compared with pixel-based procedures is that image object analysis does not classify single pixels but rather image objects that have been extracted in a previous image segmentation step (Baatz 1999).

A characteristic of object-oriented image analysis is the multitude of additional information which can be derived based on image objects: tone, shape, texture, area, context, and information from other object layers. Using this information, classification leads to better semantic differentiation and to more accurate and specific results. In a conceptual perspective, the available features can be distinguished as follows:

- intrinsic features: the object's physical properties, which are determined by the imaging situation, basically sensor and illumination. Such features describe colour, texture and form of the objects;
- topological features: features, which describe the geometric relationships between the objects or the whole scene, such as being left, right or at a certain distance to a certain object or being in a certain area within the image; and
- context features: these describe the semantic relationship of objects to one another.

2.3.2.2 Basic aspects in image interpretation

The **scale** is a very important aspect of image understanding in remote sensing. It determines the occurrence or non occurrence of a certain object class and it determines what the objects look like at a certain level of scale.

Another important aspect in understanding the content of an image is information about **context**. There are two types of contextual information: 1) global context, which describes the situation of the image (basically time, sensor and location) and 2) local context, which describes the relationships of objects to one another within a certain area of the image, usually neighbourhood relationships. To make the objects aware of their spatial context, it is necessary to link them. By linking the objects, a network of image objects is created. When taking scale into account, different sized image segmentations represent different scale levels (Mitri and Gitas 2004a). Linking the different sized image objects hierarchically represents their (semantic) scale relationships, as mentioned before. By linking the image objects, they are able to communicate and to “tell each other” their mutual relations. Each object “knows” its neighbours, its sub- and its super-objects. From a classification point of view now, the objects non-intrinsic properties, such as neighbourhood relationships or being a sub or super-object, are describable.

Segmentation is the subdivision of an image into separated regions. For many years, procedures for image segmentation have been a main research focus in the area of image analysis. Many different approaches have been adopted. However, few of them lead to qualitatively convincing results that are robust and are applicable operationally (Hofmann 1998).

In an object-oriented approach, image objects resulting from a segmentation procedure are intended to be rather image object primitives, serving as information carriers and building blocks for further classification or other segmentation processes (Baatz 1999). In this sense, the best segmentation result is the one that provides optimal information for further processing.

Multiresolution segmentation (Baatz and Schape 2000) allows the largely knowledge-free extraction of homogeneous image object primitives in any chosen resolution, taking into consideration local contrasts. It can generally be applied to a very large range of data types; it works on an arbitrary number of channels simultaneously.

2.3.2.3 Classification

Usually classification means the assignment of a number of objects into a certain class according to the class description. Thereby, class description is performed by describing typical properties or conditions pertaining to the desired classes. The objects then become assigned (classified) according to whether they fulfil or not these properties/conditions. In terms of data base language, one can say that the feature space is segmented into distinct regions which lead to a many-to-one relationship between the objects and the classes (Baatz and Schape 1999).

As a result of a classification, each object belongs to one definite class or to no class. Classic classifiers (i.e. maximum-likelihood, minimum-distance or parallelepiped) thereby assign a membership of 1 or 0 to the objects, expressing whether an object belongs to a certain class or not. These classifiers are usually also called hard classifiers since they express the objects' membership to a class only in a binary manner. In contrast, soft classifiers (mainly fuzzy-systems and/or Bayes-classifiers) use a degree of membership/a probability to express an object's assignment to a class.

The membership value usually lies between 1.0 and 0.0, whereas 1.0 expresses a full membership/probability (a complete assignment) to a class and 0.0 expresses an absolutely non-membership (improbability). Thereby, the degree of membership (probability) depends on the degree to which the objects fulfil the class describing properties/conditions. A main advantage of these soft methods lies in their ability to express uncertainties about the classes' descriptions. It makes it also possible to express each object's membership to more than just one class but with different degrees of membership probabilities.

With respect to image understanding, these soft classification results are more able to express human uncertain knowledge about the world, and thus lead to classification

results that are closer to human language, thinking and mind. In other words: soft classifiers are more honest than their hard counterparts. However, many applications using land use or land cover information are unable to handle soft classification results. Thus, soft classification results must be hardened, which can lead to shammed classification truths and accuracies.

Classification methods can basically be separated into *supervised* and *unsupervised* methods. As unsupervised methods are almost user independent, supervised methods have to be trained by the user – usually either by taking samples or by describing the class properties. Therefore, the class describing information must be as accurate, representative and complete as possible. Hence, a class description can just be a general estimation of the desired class' properties. Estimating the properties also means assuming a more or less known uncertainty about the class description. Formulating these uncertainties can only be achieved using soft classifiers.

There are advantages and disadvantages to both unsupervised and supervised classification methods. Unsupervised methods are noticeably faster than supervised, but since they are simply a special kind of sorting algorithms, their results have to be interpreted by the user – which can be tough in some cases and lead to numerous repetitions of the classification with slightly adjusted parameters. Another advantage of unsupervised classifiers is their ability to analyze the objects' statistics completely and systematically. Thus, the results of an unsupervised classification can give useful indications for detectable classes, but formulating uncertainty is only possible in general with regard to the classification parameters, not to the classes and their properties themselves.

In contrast, supervised classification methods can be more labour intensive since the user has to describe the classes' properties either explicitly or by taking samples as typical representatives. Their advantages are firstly their usually higher quality and a priori counting and naming of the classes, and secondly the possibility to formulate explicit class related uncertainty. In cases of misclassifications, the latter point in particular eases the investigation into the potential reasons. Also, the class descriptions themselves are easier to understand since they should be a result of human reasoning and thus be easier to investigate.

Finally, object-oriented image analysis can be based on a fuzzy system of classification. One of the most powerful soft classifiers are classifiers based on fuzzy systems (Civanlar and Trussel 1986, Benz 1999). Fuzzy logic is a mathematical approach to quantifying uncertain statements. The basic idea is to replace the two strictly logical statements 'yes' and 'no' by the continuous range of $[0...1]$, where 0 means 'exactly no' and 1 means 'exactly yes'. All values between 0 and 1 represent a more or less certain state of 'yes' and 'no'. Thus, fuzzy logic is able to emulate human thinking and to take into account even linguistic rules. Fuzzy classification systems are well suited to handling most vagueness in remote sensing information extraction. Parameter and model uncertainties are considered using fuzzy sets defined by membership functions. Instead of the binary "true" and "false", the multi-valued fuzzy logic allows transitions between "true" and "false". Additionally, there are more or less strict realizations of the logic operations "AND" or "OR".

The output of the fuzzy classification system is a fuzzy classification, where the membership degree to each land cover or land use is given for each object. This enables a detailed performance analysis and gives an insight in the class mixture for each image object. This is a major advantage of the soft classification. The maximum membership degree determines the final classification to build the interface to crisp systems.

2.4 CHAPTER SUMMARY

In summary:

- The Mediterranean climate is unique in that the wet season coincides with the low sun or winter period. Summers are dry with high temperatures, while in winters rainfall is high and the temperature is relatively mild. Fire, either natural or man-induced, has been one important factor in shaping Mediterranean ecosystems.
- Post-fire impact assessment requires precise information on extent, type and severity of fire (**short-term impact assessment**) as well as on forest regeneration and vegetation recovery (**long-term impact assessment**).
- On the other hand, monitoring post-fire **forest regeneration** (e.g. pine regeneration) and **vegetation recovery** (e.g. shrub recovery) is important to understand the need for future prescribed burns, to establish post-fire resource management, and to design re-vegetation programs to reduce soil erosion.
- Fire scientists and managers distinguish the following three general types of wildland fire: ground, surface, and crown, depending on the fuel stratum in which the fire burns. While, fire severity is a descriptive term that integrates the ecological changes at a site as a result of fire disturbance.
- Remote sensing is a powerful tool for post-fire impact assessment in the short term and in the long term.
- A wide variety of methodologies, ranging from vegetation indices (mainly NDVI and NBR), image enhancement techniques (PCA and KT) and supervised and unsupervised classification, and SMA, can be applied in post-fire impact assessment. Post-fire recovery monitoring studies are considerably conservative, as they generally use the NDVI index.
- In the short and long term post-fire impact assessment, the use of Landsat-TM and MSS is dominant, due to its many advantages in terms of costs, temporal and spatial resolution and long life span. SAR imagery has been used in several studies with very promising results, especially in monitoring vegetation volumes after fire.
- Advanced remote sensing tools have been recently introduced. The potential use of these tools in post-fire impact assessment is to be investigated.

- Hyperspectral imaging enables a better identification of objects at the earth surface and a better quantification of the object properties than can be achieved by traditional earth observation sensors.
- Very High Resolution imagery provides an advantageous methodological approach to identifying, mapping and monitoring post-fire effects as compared to traditional satellite images.
- With the introduction of Very High Resolution images (e.g. Ikonos and QuickBird satellite imageries) and Hyperspectral imagery, new approaches such as object-oriented image analysis have been developed to overcome the limitations of the traditional techniques in satellite imagery processing.
- The basic difference between image object analysis and pixel-based procedures is that image object analysis does not classify single pixels but rather image objects that have been extracted in a prior image segmentation step.
- Object-oriented image analysis can be based on fuzzy system, which is a mathematical approach to quantifying uncertain statements. The basic idea is to replace the two strictly logical statements 'yes' and 'no' by the continuous range of $[0...1]$, where 0 means 'exactly no' and 1 means 'exactly yes'. All values between 0 and 1 represent a more or less certain state of 'yes' and 'no'.

CHAPTER 3: ENVIRONMENTAL CONDITIONS IN THASOS AND DATASET DESCRIPTION

The most important ecological characteristics of the Mediterranean and the main reasons for post-fire impact assessment and monitoring were presented in chapter 2. Also, it was shown how remote sensing has made enormous progress in recent years in terms of fire related researches. Finally, information on the different techniques used for post-fire impact assessment was provided, and the concept behind object-oriented image analysis was reviewed. The first section of Chapter 3 will describe the environmental conditions of the study area, while section two will provide all information about the datasets that have been collected and employed in this study.

3.1 STUDY AREA

Information on the geography, geology and geomorphology, climate, landcover, and forest fires are given in the following sub sections.

3.1.1 Geography

Thasos is Greece's most northerly island; it is mountainous, roughly circular, and of great natural beauty. Situated close to the mainland, its nearest point is 10 km from the mouth of the Nestos, thus facing the boundary between the Macedonia and Thrace regions. Its surface area is 399 sq. km, while its perimeter is approximately 102 Km; almost circular in shape, it has a length from North to South of 24 km and a width of 19 km, extending from 24°30' to 24°48' East and 40°33' to 40°49' North (Figure 1). The mountain sides are covered with forests, in which pines, planes and walnut trees predominate; timber in Thasos has always been in great demand for ship building.

The northeast part of the island is the most fertile and the greenest part of the island. It is partly ringed by spectacular mountainous limestone palisades, of which the two notable high points are Profitis Ilias, located at 1107 m and Ypsario located at 1203 m, approximately in the centre of the island. The mean elevation is approximately 305 m, while the slopes range from 0 to 80 degrees. On the lower slopes of the mountains is found rich woodland, with pines, oaks, walnuts and sweet-chestnut trees. Thasos

was the most wooded of the Aegean islands and, despite recent extensive forest fires, much woodland remains, particularly above Skala Potamias (Gitas 2000).

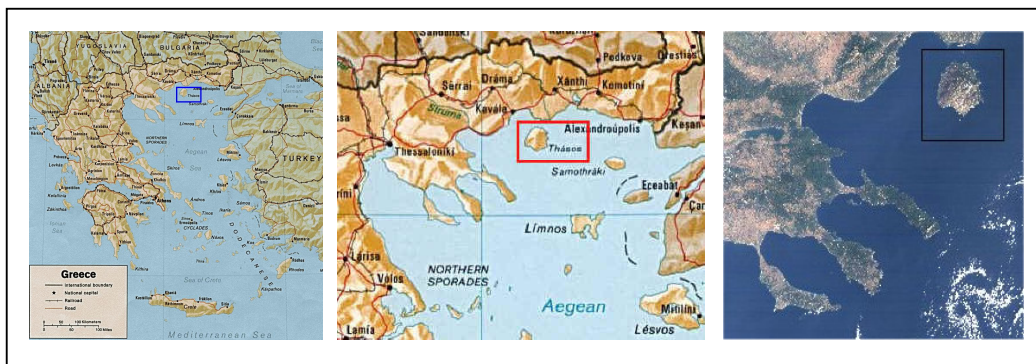


Figure 1 From left to right: map of Greece, location and satellite image of Thasos

3.1.2 Geology and geomorphology

More than 60% of Thasos, especially the highland areas, is composed of metamorphic gneiss. The marble ridge of Mt. Yspari rises out of the surrounding uplands to a height of 1003 m. The island's crystalline base is overlaid by limestones and marbles, and the island is an important source of the latter, with 25 quarries, some of which date back to Roman times, producing 55,000 cubic meters for export each year.

To the east of the island, there is a series of metamorphosed rocks, primarily composed of dolomites, which constitute approximately 25% of the island's total area. 10% of the island, around the coastline, particularly in the areas of soft slopes, is composed of quaternary deposits of clay, sand and gravel.

Soil depth and geology play an important role in determining the characteristics of the hydrology system as well as the characteristics of the vegetation habitats. Almost 50% of the island's surface is covered with shallow soils (5-10cm) due to steep slopes, grazing and repeated forest fires (Gitas 1999). While the remaining surface is covered with deep soils (35%) and bare soil (15%) (Nakos 1995).

The mountainous island can be divided into three geomorphologic areas. The first includes the coast and occupies little space; the second hilly area is extended almost

parallel to the first and is also relatively small. The third area consists of massif rock and occupies most of the island.

3.1.3 Climate

The Climate of Thasos is mild. It is cool in the summer and moderate in winter. The average annual temperature is 17.2 °C and the average summer temperature (July) is 23.4 °C. The mean annual precipitation is 783.48 mm, of which approximately 65% falls in the period between September and April. In general, there are no strong winds affecting the island. Strong North-Northeastern winds blow every summer over the island especially in August.

The dry/hot season starts in May and lasts up to mid September, with August being the driest and July the warmest month of the year. The subclass of the Mediterranean bioclimate of Thasos, using the Emberger (1971) method, was found to be *cool* and *sub-humid* (Gitas 1999).

The meteorological station of Thasos is situated at sea level, in the main city of Limenas, and pertinent data have been recorded by the National Meteorological Service (EMY) of Greece. The ombrothermic climatic diagram for the period 1961 – 1993 (Figure 2) shows a typical Mediterranean climate, with a relatively high mean yearly precipitation (742.3 mm) and a xerothermic period that starts in May and lasts through to September.

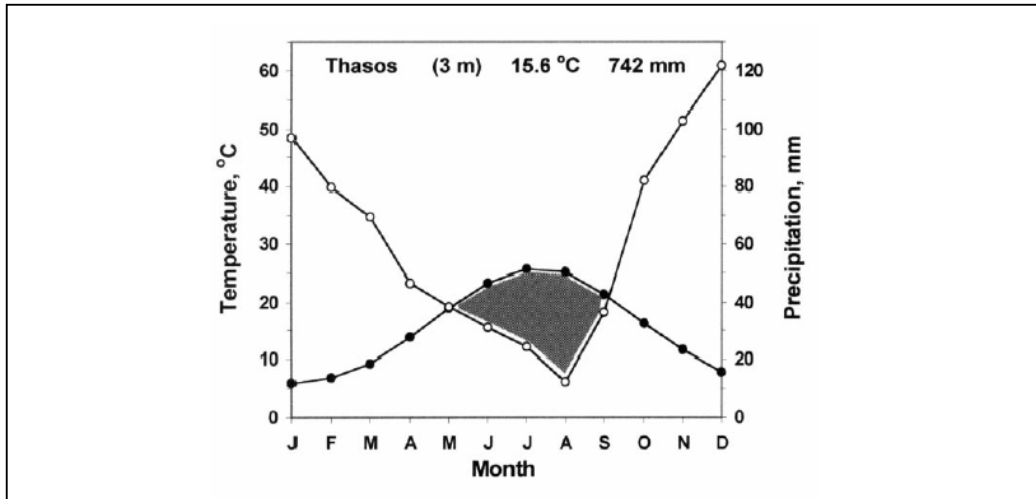


Figure 2 Ombrothermic climatic diagram of Thasos for the period 1961 to 1993

According to the formula of Emberger (Emberger 1971), the Mediterranean-type climate of the island can be further classified to the cold and subhumid variant. It should be noted that the meteorological conditions after the 1985 wildfire have been quite arid. In every one of the eight hydrological years (Oct-Sep) from 1985-86 through to 1992-93, the total yearly precipitation fluctuated between 288.9 mm and 733.6 mm (i.e. for eight consecutive years rainfall has been below the 1961-93 average), while the 1985-93 average is only 440.4 mm (slightly less than 60% of the 30-year-long average value) (Spanos 1996).

3.1.4 Landcover description

Before the two fires of 1985 and 1989, forest and forested lands covered 47.5% of the island (Gitas 1999); making forests the dominant landcover type at the time. Regarding the composition of land uses, 25% of the area of the island was subject to variable agricultural uses, 50% was occupied by forests, 11% by grasslands and only 5% could be characterized as urban land. It is important to note that, in spite of its relevant small size, the island presents 12 endemic plant species. Different kinds of vegetation cover, such as phrygana, maquis and forest, exist in Thasos (Figure 3). The next paragraphs will discuss the different landcover categories according to their characteristics and their location on the island.

Phrygana the most characteristic habitat of the Mediterranean region is garigue, a lowland vegetation community of dry soils, composed largely of spiny or aromatic dwarf shrubs. In Greece, these communities are known as phrygana and there are several variants, depending upon grazing pressure, the incidence of fires, exposure, soils and geology. The only good example on Thasos can be found to the east of the island. By mid summer, drought and trampling reduce the coastal slope of this phrygana to dusty bare ground (Karteris *et al.* 1992).

Adjacent to this low coastal phrygana, freed from trampling and probably less prone to drought, the second type of scrub community can be seen. “*Cistus garigue*” is frequent around much of the island's lowland zone and is especially common in the northern half as an understory in the conifer woods and old olive groves. Pink cistus *Cistus creticus* is the most abundant species but sage-leaved cistus *C. salvifolius* is also widespread. Other species of this community include prickly juniper *Juniperus oxycedrus*, Phoenician juniper *Juniperus phoenicea*, mock privet *Phillyrea latifolia* and Kermes oak *Quercus coccifera*. The southern phrygana has extensive areas with the tree heath *Erica manipuliflora* as a dominant species and Spanish broom *Spartium junceum* is also common.

The third form of phrygana can be regarded as an intermediate stage in the development to maquis. This is a taller scrub community in which Kermes oak *Quercus coccifera* is usually common and species such as Christ thorn *Paliurus mastic tree Pistacia lenticulus*, Judas tree *Cercis* and chaste tree *Vitex agnus-castus* frequently occur. This vegetation type is found on abandoned terraces, neglected olive groves and undisturbed forest clearings but is quite localised and patchy in distribution.

Maquis represents a tall shrub community that presumably represents a phase in succession to secondary deciduous woodland. Pockets of maquis, composed of a variety of species, depending on the degree of shade, soil moisture and geology, occur in many places around the island but some of the most extensive examples can be found in the valley between Prinos and Megalo Kazavitis (where cornelian cherry *Cornus mas* is a conspicuous component) and on the floodplain below Maries (dominated by oriental plane *Platanus orientalis*). *Cistus garigue* and maquis are

common habitats on Thasos; they are widely distributed around the island and the former is currently extending its range as it colonizes lowland slopes cleared of conifers in the recent devastating summer fires (Karteris *et al.* 1992)

Before the forest fire of 1984, one of three large fires that took place between 1984 and 1989, **forest** area covered 47.5% of the island (Gitas 1999). In addition to the phrygana, maquis and forest areas, other existing landcover types included bare land, fields, orchards and human settlements. The human settlements comprised some 38 settlements, with the chief town, Thasos on the north coast. After the fires of 1984 and 1985, forests covered 37.95% of the island (Makedos 1987). Today, as a result of fires, illegal logging, intensive grazing and bad management, the remaining forest has a spatial extent of about 2000 ha in the Northern and Eastern parts of the island.

Pinus brutia was the dominant species of the forests at elevations ranging from sea level up to 800 m, while *Pinus nigra* was the dominant species of the forests found in the mountainous areas of the island (sub-alpine zone). It is worth noting that *Pinus brutia* is well adapted to the Mediterranean climate and can withstand prolonged droughts and the absence of summer rainfall (Gitas 1999). *Pinus brutia* is an obligate reseeders and a typical east Mediterranean tree species. A wildfire usually kills the entire pine tree population and therefore, the regeneration of the species, and also of the forest, is totally dependent upon the recruitment of a postfire cohort of seedlings. A certain fraction of pine seeds can survive the fire, protected by the scales of the closed, serotinous cones; moreover, as a result of heat, these cones open and disperse the enclosed seeds shortly after fire. Pine seed germination and seedling emergence takes place almost exclusively during the first postfire wet season.

The natural, postfire regeneration of *Pinus brutia* forests has been studied in two 40-60-year-old forests on Thasos Island that were burned in the summers of 1985 and 1989 (Spanos 1996). Within the latter burned area (5700 ha), forty experimental sites of various aspects and site index values were established and successively monitored for 5 years, at 6-month intervals. Pine seedling emergence took place late in spring (due to a long drought in that particular year), but exclusively during the first postfire year. By the end of the recruitment period (May 1990), mean pine seedling density was considerably high (2-6 seedlings.m⁻²), while a significant drop in the first

summer was observed. Thereafter, a relatively smooth decline was noted and the density was almost stabilized to about $0.6-2 \text{ seedlings.m}^{-2}$ after 5 years. Annual height growth showed a yearly increment of 17 cm in the year-long postfire period of study. Starting at an age of 4-6 years, an increasing fraction of the sapling population became reproductive so that 9 years later a considerable portion (5-15 %) had already produced cones with fully germinable seeds (Spanos 1996).

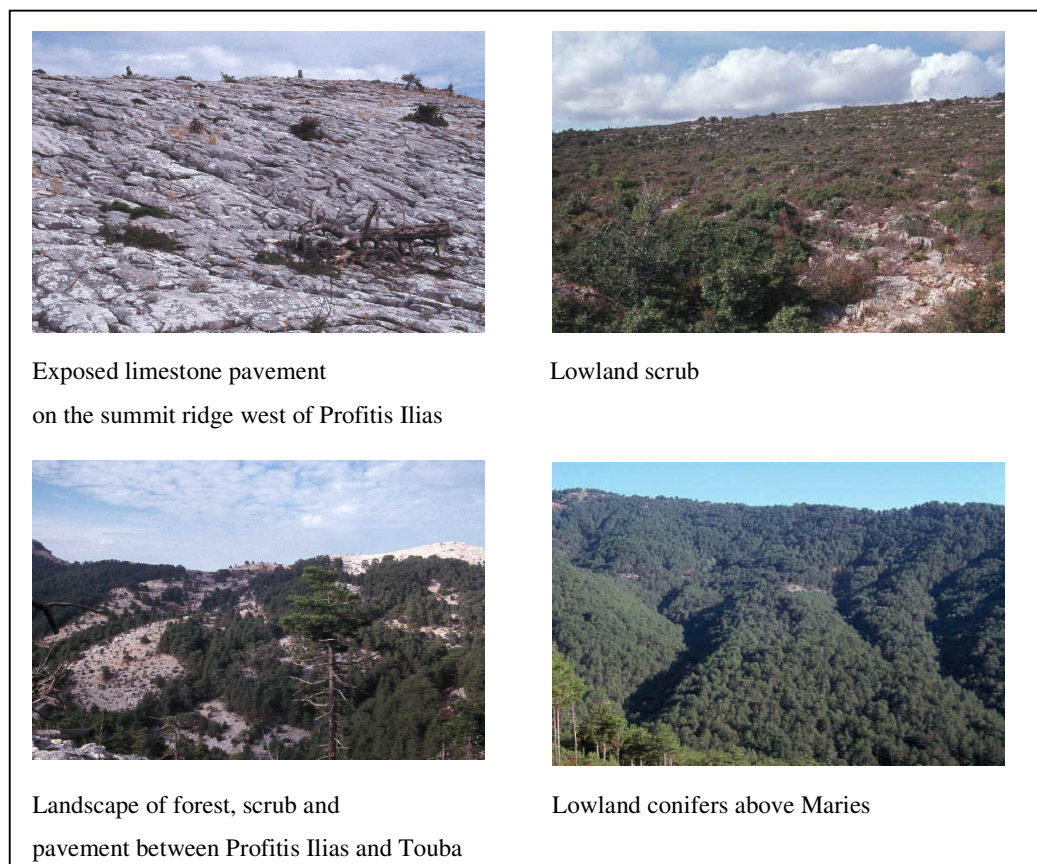


Figure 3 Landcover types in Thasos

3.1.5 History of forest fires

Almost 50% of the total incidents of forest fires on Thasos are caused by lightning, although these fires do not cause any great damage (Makedos 1987). However, fires in Thasos are not caused only by lightning but also by human induced activity.

According to the records of the National Forest Service, Forest Station of Thasos, the biggest forest fires in this century occurred in 1928 (1,500 ha), 1938 (1,700 ha), 1945

(700 ha), 1984 (1,669), 1985 (10, 405 ha), 1989 (8,401 ha) and 2000 (187 ha). However, in the period between 1980 and 1990, there was an overwhelming increase in the number of fires and surface area burned. Indeed, the largest fires in the last century occurred in this period and resulted in the loss of about 20,000 ha of *Pinus brutia* and *Pinus nigra* forests, leaving in behind an affected area that constituted more than half the size of the island (Figure 4). More detailed information about the type of fire and the landcover types destroyed in the fires of 1985, 1989 and 2000 - the examined years in this study – are given in the following paragraph (Gitas 1999).

The fire of 1985 started in the afternoon of August 15th on a day of very low relative humidity (45%), very high temperature (33°C) and strong NE winds (7 BF). The source of ignition was not identified (Forest station of Thasos). It was mainly a crown fire that destroyed 6300 ha of *Pinus brutia* forest and 350 ha of *Pinus nigra*. The fire also destroyed 3300 ha of *maquis*, 420 ha of *phrygana*, and 1500 ha of agricultural land.

The fire of 1989 started on the 16th August at night (22:30 hrs) due to arson (Forest station of Thasos 1989). At the time, relative humidity was 68%, the temperature was 28°C and there were strong NE winds (6 BF). It was mainly a crown fire that destroyed 4600 ha of *Pinus brutia* forest and 1000 ha of *Pinus nigra* forest. The fire also destroyed 2200 ha of *maquis*, 500 ha of *phrygana* and 1200 ha of olive groves. In addition, 23 houses were burned.

On 13th July 2000, a fire started due to unknown reasons. Conditions at the onset of fire were: humidity 65%, temperature 38°C and strong winds (4,1-7 BF). It was a mixed fire (crown and surface) that destroyed an area of 1.95 Km², covered by *Pinus brutia* (Forest Station of Thasos).

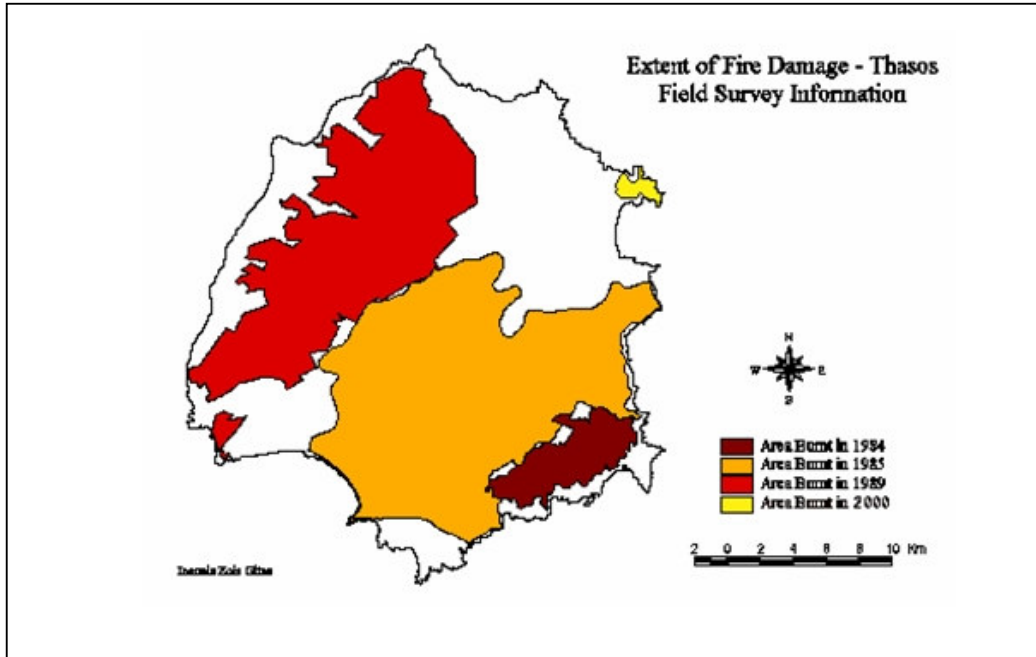


Figure 4 Multitemporal burned areas on the Mediterranean island of Thasos

The climatic and soil conditions of Thasos are quite favourable to the establishment and growth of *P. brutia* stands but during the last decades, the fire interval has gradually decreased (Spanos *et al.* 2000) for most Mediterranean forests of Greece. Moreover, a large part of these forests have reached a critical stage due to both intensive grazing by goats and poor management. The wildfires of 1984, 1985, 1989 and 2000 have destroyed more than 80 % of the total forest area of Thasos of different landcover types (Gitas 1999). Pine seedlings and saplings up to about 20-years old and 2 m in height are scattered throughout the area.

3.1.6 Post-fire impact assessment

In this research, post-fire impact assessment was focused on 1) short term post-fire effect (fire type and fire severity) and 2) long-term post-fire effect (forest regeneration and vegetation recovery). It should be noted that forest regeneration comprises mainly pine forest regeneration, while vegetation recovery comprises shrub (maquis and phrygana) recovery after fire.

Based on all the geographic characteristics of Thasos, it can be concluded that the island represents an ideal site for post-fire impact assessment (Gitas 2003). It can provide the researcher with the opportunity to investigate ways of improving existing methods employed not only in burned area mapping and fire type/severity mapping but also in forest regeneration and vegetation recovery mapping for the following reasons:

- the geomorphology of the island guarantees the existence of the shadowed areas that occur as a result of the irregular terrain found particularly in mountainous areas;
- the large extents of the 1985 and the 1989 fires guarantee the existence of different surface exposures of the burned area and of the regenerated areas; and
- the landcover types in the study are typical of other Mediterranean ecosystems and are representative of most of the landcover types affected by fires in the Mediterranean countries, as well as in Greece. Therefore, successful efforts can make burned area mapping in this study more operational in a number of areas across the Mediterranean region.

3.2 DATASET DESCRIPTION

Satellite images of different spectral and spatial resolution were collected (section 3.2.1). Also, data were collected from several field surveys carried out in the study area in addition to other ancillary data (section 3.2.2).

3.2.1 Satellite data collection

Two Landsat TM images (Miller and Yool 2002) showing burns that occurred in 1985 and 1989 were obtained for this study (Figure 5). The acquisition dates (few weeks after each fire) of the images were the 24th September 1985 and the 19th September 1989. The 1985 image (Table 3) was acquired to map the 1985 burn scar, while the 1989 image was acquired to map the 1989 burn scar.

Table 3 Landsat-TM characteristics (*source: USGS*)

	Spectral range (microns)	Visible bands	Near Infrared Bands	Mid Infrared (microns)	Thermal Infrared (microns)	Spatial resolution at nadir	Swath width (km)	Number of bands
Landsat TM	0.45-1.75	3	1	2 (2.8-2.35)	1 (10.4- 2.5)	30 m	185	7

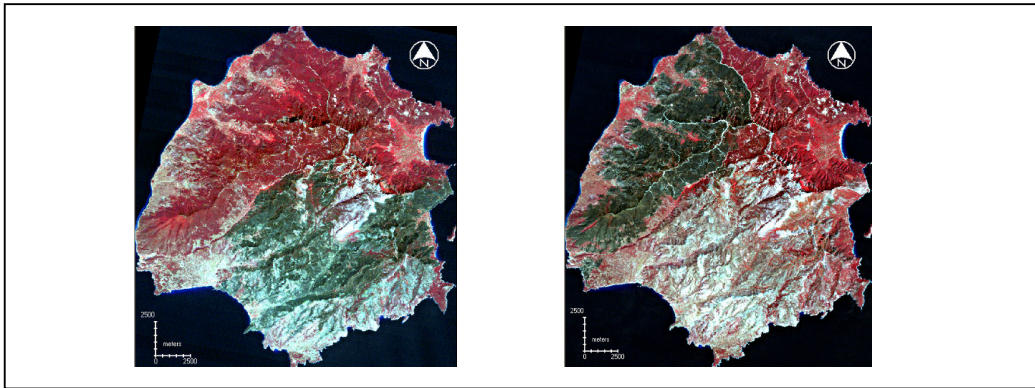
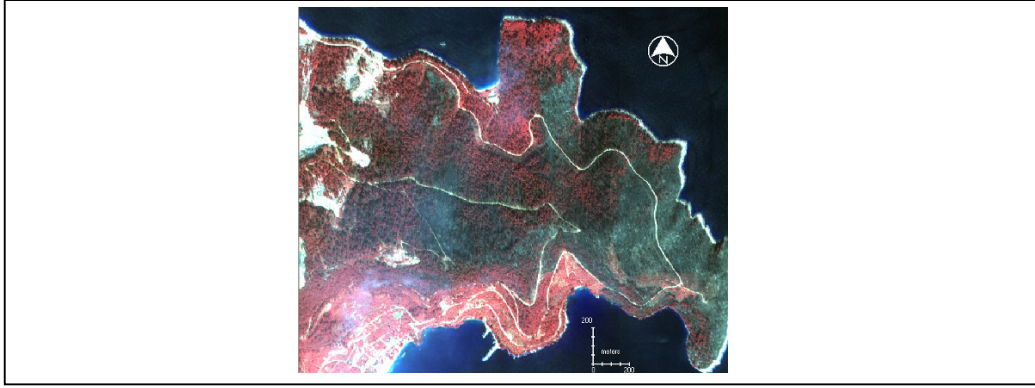


Figure 5 Landsat-TM images showing burned areas from 1985 (left) and 1989 (right)

A post-fire Ikonos (Figure 6) image was acquired on 14th July 2000, one day after the fire. The image of Ikonos (Van der Sande *et al.* 2003) included band 1 (0.445-0.516 micrometers), band 2 (0.506-0.595 micrometers), band 3 (0.632-0.698 micrometers) and band 4 (0.757-0.853 micrometers). Other image characteristics are shown in Table 4.

Table 4 Ikonos characteristics (*source: Space Imaging*)

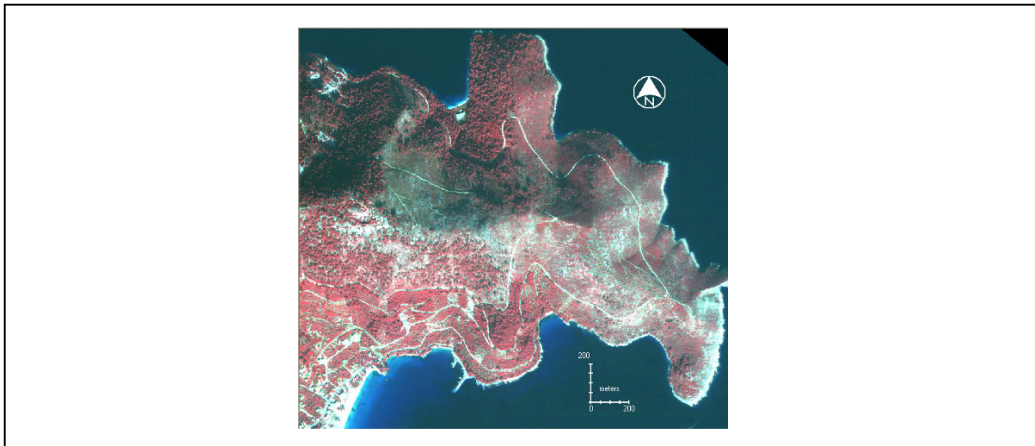
	Spectral range (microns)	Visible bands	Near Infrared Bands	Short Wave Infrared	Spatial resolution	Swath Width (km)	Number of bands
Ikonos multispectral	0.45 - 0.90	3	1	0	4 m	11	4

**Figure 6** Ikonos image showing the burned area of 2000

A single multispectral QuickBird (Figure 7) image was obtained (Table 5). The multispectral Quickbird (Wang *et al.* 2004) image acquired on October 28th of 2004 included a blue band (450 to 520 nm), a green band (520 to 600 nm) a red band (630 to 690 nm) and a Near-IR band (760 to 900 nm).

Table 5 QuickBird characteristics (*source: DigitalGlobe*)

	Spectral range (microns)	Visible bands	Near Infrared Bands	Short Wave Infrared	Spatial resolution at nadir	Swath width (Km)	Number of bands
QuickBird multispectral	0.45-0.9	3	1	0	2.44 m	16.5	4

**Figure 7** QuickBird image of 2000

On the 1st of August 2003 a Hyperion image (level 1 radiometric product) was acquired for the area of Thasos covering a part of the island from south to north (Figure 8). The Hyperion (Thenkabail *et al.* 2004b) image has 220 unique spectral channels (Table 6) collected with a complete spectrum covering from 357 - 2576 nm. Only 198 bands are calibrated. Because of an overlap between the VNIR and SWIR focal planes, there are only 196 unique channels. Calibrated channels are 8-57 for the VNIR, and 77-224 for the SWIR. The bands that are not calibrated are set to zero in those channels.

Table 6 Hyperion characteristics (*source: NASA EO-1 briefing materials*)

	Spectral range	Visible bands	Near Infrared Bands	Short Wave Infrared	Spatial resolution at nadir	Swath width	Spectral coverage	Number of bands
EO-1/ Hyperion	0.4-2.5 microns	35	35	172	30 m	7.5 km	continuous	220

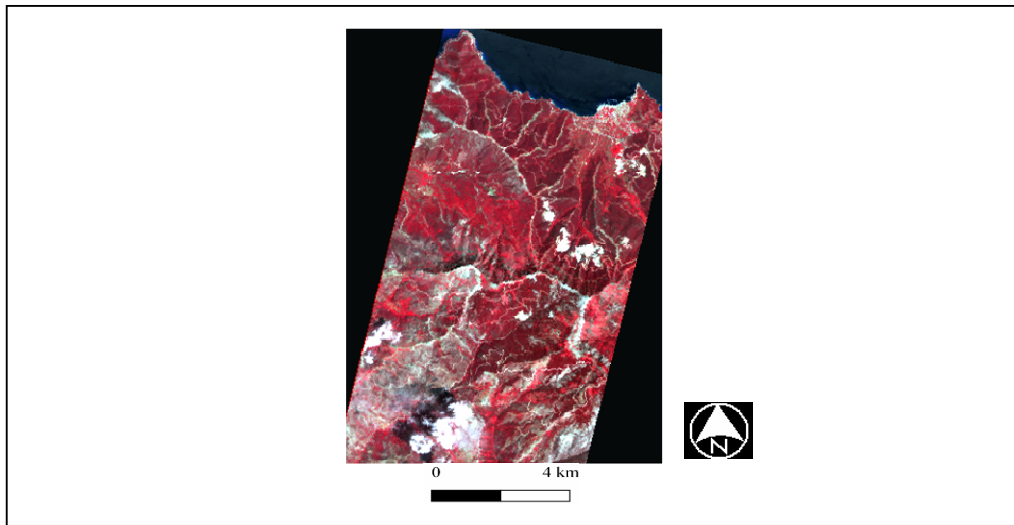


Figure 8 Hyperion image of Thasos

3.2.2 Field and other data collection

Field data were collected during an extensive field survey carried out in the study area. The survey started shortly after the fire event in summer 2000. Moreover, the study area was repeatedly visited every summer season in the following five years for monitoring post-fire effects. The field survey focused on visual assessment of fire type and severity (39 plots), observation of unburned neighbouring plots, the collection of GPS points and documentation of fire type and severity by means of

field digital photography. In addition, adapted version of the FIREMON landscape assessment method was employed (Appendix 1), and consequently the Composite Burn Index (CBI) was calculated for 36 plots in total to be used for classification accuracy assessment. The fire severity measured was defined here as a scaled index gauging the magnitude of ecological change caused by fire (Key and Benson 2002).

The data was made suitable for very high spatial resolution applications and adapted to remote sensing and GIS technologies. Therefore, the methodology of the CBI required a relatively large plot (10x10 m) and allocated independent severity ratings for individual strata and synoptic scores for the entire plot area. Ratings considered criteria such as colour, percentage of fuel consumed, regeneration from pre-fire vegetation and blackening or scorching of trees. Additional measurements, such as vegetation cover, percentage of healthy trees and vegetation type, were taken. Additionally, the effects of fire on individual trees were determined by counting the number of trees alive, dead, resprouting, consumed/down, broken and cut stump. The landscape sampling design was hierarchical and multi-layered. Each strata of a vegetative community was evaluated independently by several criteria and given a rating. There were three composite levels (lettered) and five strata (numbered) (Table 7). CBI scoring is completed for each stratum and averaged to the total composite level.

Table 7 Three composite levels (A-C) including the five strata level (1-4)

A. Total plot	B. Understory	1. Herbs, Low shrubs and Small Trees
		2. Tall Shrubs and Sapling Trees
	C. Overstory	3. Intermediate Trees (pole-sized trees, subcanopy)
		4. Big Trees (mature, dominant/co-dominant, upper canopy)

The total plot CBI comprised all five strata, when all strata were present. When plots did not contain all strata, the missing strata were simply not counted. Ratings could be reported separately by strata, or in their composite forms. Scores were decimal values between 0.0 and 3.0, spanning the possible range of severity from unburned to highest burn effect. Scores could be combined (averaged) to yield aggregate CBI ratings for the understory, the overstory, and the total plot. That was done by adding up scores within each hierarchical level, and dividing by the number of rated factors (Figure 9).

Figure 9 shows figures from the study area for three different examples of CBI ratings (Key *et al.* 2002).




	<p>CBI Ratings:</p> <p>Understory - 1.125 Overstory - 0.7 Total Plot – 0.88</p> <p>Light char and moderate consumption of downed fuels. Regenerated herbs and grass dominate understory. Shrubs show mortality. Canopy not scorched or blackened, and tree charring remains < 1.5 m.</p>
	<p>CBI Ratings:</p> <p>Understory - 1.625 Overstory - 2.5 Total Plot – 1.916</p> <p>Deep char and small fuels mostly consumed. Some pre-fire herbs and shrubs persist. Most tree crowns blackened or largely scorched, a few green crowns remain.</p>
	<p>CBI Ratings:</p> <p>Understory – 1.75 Overstory - 2.66 Total Plot – 2.14</p> <p>Major portions of large downed fuels consumed. Large amounts of exposed mineral soil. Overstory consumed including all branching in crowns.</p>

Figure 9 CBI ratings (examples of low, medium, and high burn severity in the study area)

In the summer periods of 2002, 2003 and 2004, field spectral measurements (Figure 10) of different shrub species as well as of regenerating *P. brutia* and *P. nigra* at different ages were obtained (Appendix 2). Measurements were taken for regenerating trees at different ages. According to Spanos *et al.* (2000) the annual height growth of *P. brutia* showed linear regression kinetics throughout the 5 (and conceivably 9) year-long post-fire period, with a yearly increment of 17 cm. As for *P. nigra*, the tree is moderately fast growing (30-70 cm/year).

Measurements were taken from *P. brutia* and *P. nigra* trees of two groups of ages. The first group represents trees younger than 10 years old and the second group represents trees older of 10 years old and older. A FieldSpec Pro VNIR spectrometer (350-1050 nm range; 3nm spectral resolution; 1.4 nm spectral sampling interval) was employed. A 10° foreoptic was used, and the spectrometer was mounted on a stand of 0.75 m above the target giving a 16.628 cm radius of FOV. At least five measurements were recorded for each age and normalized against a calibrated white reference panel. To reduce the effects of low sun angle, showdown and longer atmospheric pathlengths, scans were recorded within two hours either side of the solar noon and sky conditions were clear for all sampling times.



Figure 10 Field spectral measurements

Also, in the summers of 2003 and 2004 all burned areas were surveyed for locating homogeneous vegetated areas (Figure 11) after fires. Sixty six plots (Figure 12) of minimum 30x30 m large and of homogenously regenerated forest and recovered vegetation were located within the fire affected areas and covered by the Hyperion image.



Figure 11 Areas of homogeneously regenerated forest and recovered vegetation

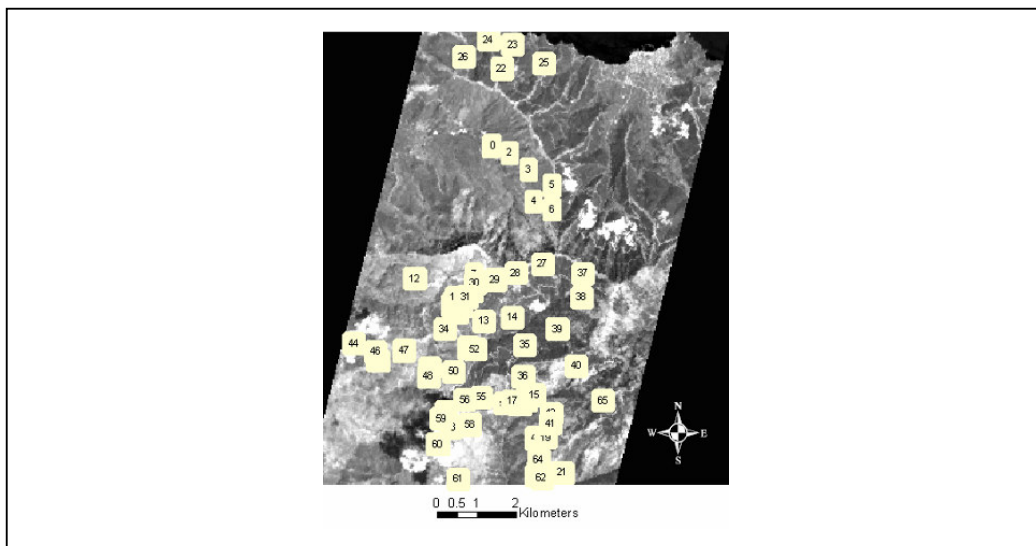


Figure 12 Numbered field plots overlaid over the Hyperion image

The other datasets used in this study were:

- A fire perimeter map of the three fires, published by the Greek Forest Service;
- A 1:50000 Topographic map of Thasos;
- A Digital Elevation Model (DEM) of Thasos, with 10 m pixels size. The elevation grid was generated from a 1:5000 contour map (Gitas 1999).

3.3 CHAPTER SUMMARY

In summary:

- The climate of Thasos is Mediterranean mild. It is cool in the summer and moderate in the winter. The average annual temperature is 17.2 °C and the mean annual precipitation is 783.48 mm.
- In addition to the phrygana, maquis and forest areas, other landcover types that exist include bare land, fields, orchards and human settlements.
- The largest fires on Thasos Island occurred between 1980 and 1990 and resulted in the loss of about 20,000 ha of *Pinus brutia* and *Pinus nigra* forests, leaving behind an affected area that constituted more than half the size of Thasos.
- Based on all the geographic characteristics of Thasos, such as the complex relief types, the diversity of landcover areas and the large extents of the fires, it can be concluded that the island represents an ideal site for operational burned area mapping.
- Image data such as Landsat-TM images, Ikonos, QuickBird and Hyperion were collected and field data such as fire type and severity, areas of homogenously regenerated forest and recovered vegetation, and spectro-radiometer measurements were employed.

CHAPTER 4: SATELLITE DATA PRE-PROCESSING

In Chapter 3 the environmental conditions on the island of Thasos were outlined and the datasets employed were presented. The different satellite data such as Landsat-TM images, Ikonos, QuickBird and Hyperion were collected and field data related fire severity, homogenous regenerated areas and spectro-radiometer measurements were recorded. This chapter deals with the pre-processing of all collected satellite data, a preparatory phase which, in principle, improves data quality to provide the basis for later analyses. After representing the concept behind satellite data pre-processing, each of the chapter sections describes one of the main three image pre-processing steps, namely, radiometric correction, geometric correction and finally topographic correction.

4.1 THE CONCEPT

In this chapter, the main three image pre-processing steps undertaken were:

- radiometric and atmospheric correction, so that the influence of the atmosphere degradation is removed;
- geometric correction, to bring the remotely sensed data into registration with a map in order to make the images and the auxiliary data geographically comparable; and
- topographic correction, to reduce the effect of relief present on the imagery of rugged terrains areas so that image classification accuracy can be improved.

The decision to use atmospheric correction for the Landsat TM and Ikonos images was based on the evidence that burned area discrimination is more accurate when applied to atmospherically corrected satellite images (Mitri and Gitas 2004a). Hyperion image was atmospherically corrected due to the fact that the spectral values were related to ground reflectance. In the case of QuickBird, the work was done on a single-date image data, and the spectral values were not related to ground reflectance. Therefore, the atmospheric correction was not necessary in this case.

The topographic correction of the high spatial resolution imageries of Ikonos and QuickBird was avoided due to the absence of a similar or higher spatial resolution Digital Elevation Model (DEM). Also, the Hyperion image was not topographically corrected in order not to alter the spectral reflectance of the data.

The flowchart of the satellite data pre-processing is described in Figure 13.

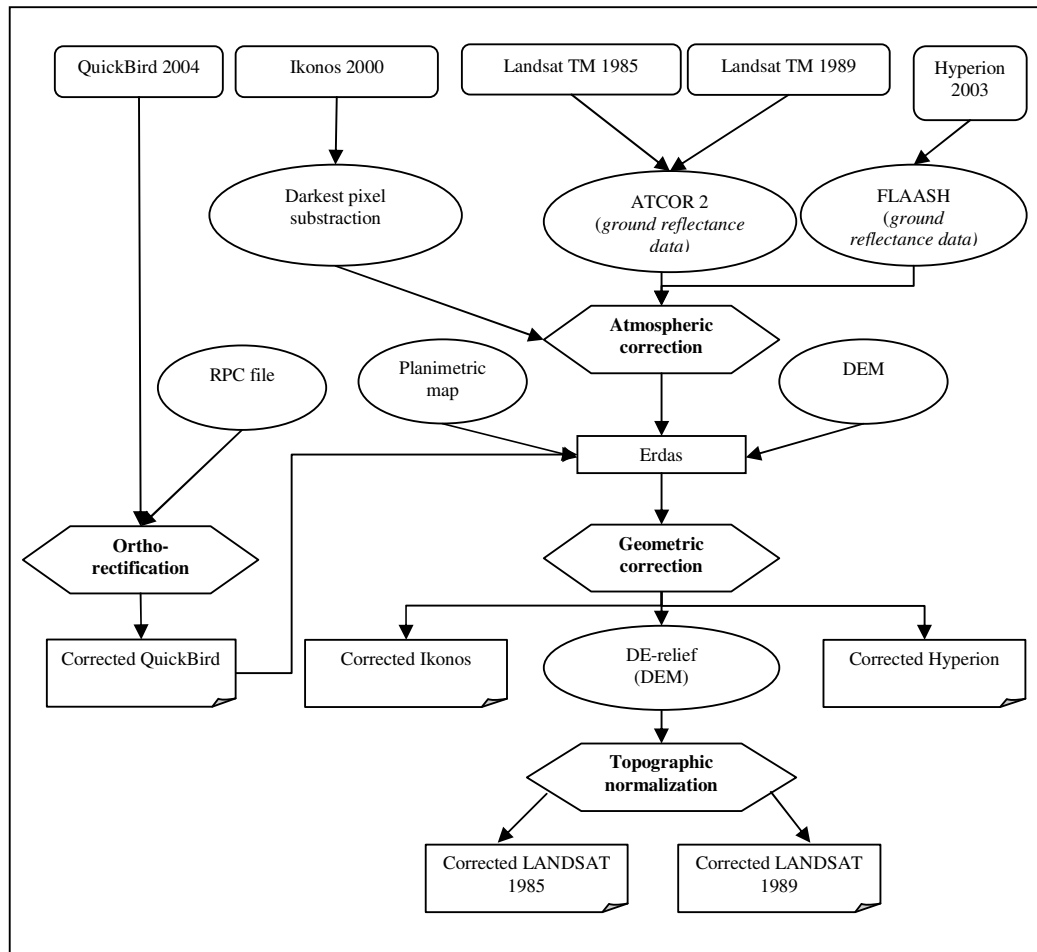


Figure 13 Flowchart of the images pre-processing

4.2 RADIOMETRIC CORRECTION

The main purpose of applying radiometric correction is to reduce the influence of errors or inconsistencies in image brightness values that may limit one's ability to interpret or quantitatively process and analyze digital remotely sensed images.

Radiometric pre-processing influences the brightness values of an image to correct for sensor illuminations or to adjust the values to compensate for atmospheric degradation. Any sensor that observes the earth's surface using visible or near-visible radiation will record a mixture of two kinds of brightness. One brightness is due to the reflectance from the earth's surface - the brightness that is of interest for remote sensing. But the sensor also observes the brightness of the atmosphere itself - the effect of scattering. Therefore, one objective of atmospheric correction is to identify and separate these two components so the main analysis can focus on examination of the correct surface brightness (Campbell 1996).

4.2.1 Background

All electromagnetic radiation must travel through the Earth's atmosphere and along the way several things can alter the radiation in some way, either by redirection or a change in energy level. The further away a sensor is from its target, the larger the atmospheric effects are upon the radiation.

Scattering is the redirection of electromagnetic (EM) energy by particles suspended in the atmosphere. It is dependant upon the number of particles present in the atmosphere, the size of the particles, the wavelength of incoming radiation and the depth of atmosphere that the radiation must travel through.

Particles that are small relative to the wavelength of incoming radiation create Rayleigh scattering. *Rayleigh scattering* is wave length dependent, favouring short wavelengths, and is responsible for the sky appearing blue. *Mie scattering* is produced by particles having a diameter approximately equal to the wavelength of the incoming radiation. Mie scattering is typically created by dust, smoke, haze and water droplets in the lower atmosphere. The scattering produced by very large particles relative to

the incoming radiation is nonselective. As the name implies, nonselective scattering is not wavelength dependent and scatters all wavelengths equally.

Absorption occurs when atmospheric particles do not allow EM radiation to be fully transmitted. The amount of energy absorbed is dependent upon the absorber and the wavelength of incoming radiation. Energy that is absorbed is then re-emitted at longer wavelengths. There are three gasses in the atmosphere that are responsible for most of the absorption in the earth's atmosphere, namely, ozone (O_3), carbon dioxide (CO_2) and water vapour (H_2O). .

Refraction is the deflection of EM radiation as it passes from one medium with one refractive index to a medium with a different refractive index. In the Earth's atmosphere, temperature, composition and humidity all affect the density which in turn affects the refractive index

Digital sensors record the intensity of Electromagnetic Radiation (ER) from each spot viewed on the Earth's surface as a Digital Number (DN) for each spectral band. The exact range of DN that a sensor utilizes depends on its radiometric resolution.

4.2.2 Implementation

The task of earth observing sensors is the mapping of surface properties. However, the surface information is masked, since the signal recorded by spaceborne optical sensors consists of several components and their magnitudes depend on atmospheric conditions. In addition, topographic effects strongly influence the recorded signal. The objective of an atmospheric correction is the elimination of atmospheric and illumination effects to retrieve physical parameters of the earth's surface, e.g. surface reflectance, emissivity and temperature.

This information can be used for monitoring, change detection, surface-vegetation atmosphere transfer (SVAT) modelling, and surface energy balance investigations for climatic modelling and upscaling. Therefore, atmospheric correction is an essential part of pre-processing and a prerequisite for the derivation of certain value adding products.

The Spatially-Adaptive Fast Atmospheric Correction Algorithm (ATCOR2), developed by Richter (1990) and compiled using the MODTRAN-2 and the SENSAT-5 codes, was used in this study for atmospherically correcting the Landsat-TM imaging. The model calculates a ground reflectance image in each spectral band: the first step assumes an isotropic (Lambert) reflectance law neglecting the neighbourhood of each pixel. The second step accounts for the influence of the neighbouring background (adjacency effect).

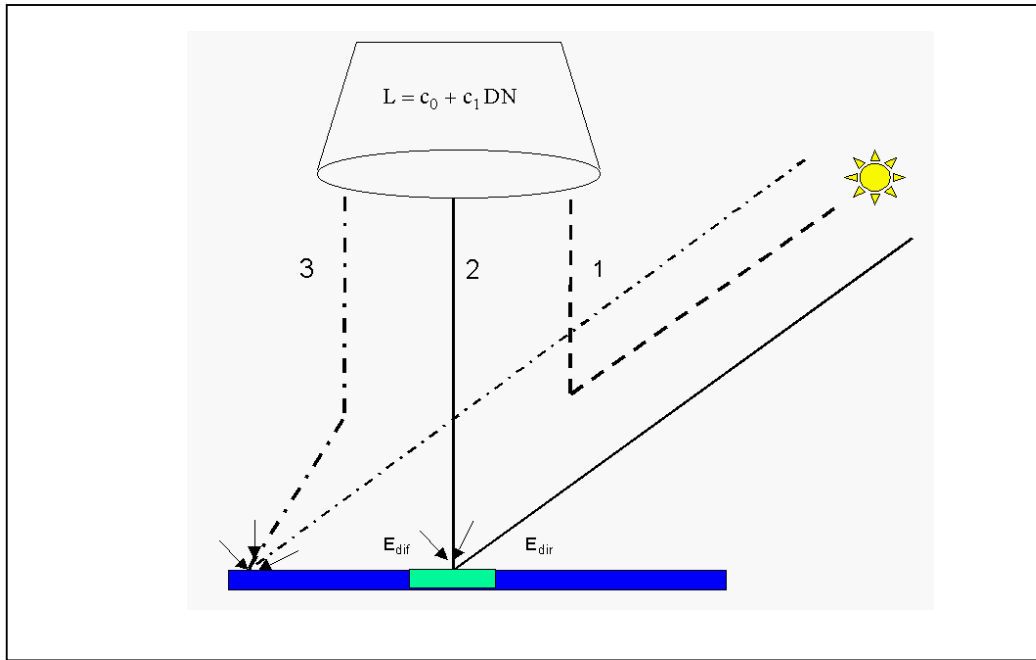


Figure 14 Schematic sketch of radiation components for a flat terrain (solar region)

The at-sensor radiance is split into three components (Figure 14):

Component 1: path radiance: radiation scattered by the atmosphere

Component 2: reflected radiation from the viewed pixel ($E_{dir} + E_{dif}$)

Component 3: radiation reflected by the neighbourhood and scattered into the view direction (adjacency effect).

From the three components mentioned above, only component 2 contains information from the viewed pixel. DN is the digital number recorded in a certain spectral channel, and C_0 , C_1 are the offset and gain of the radiometric calibration relating the

DN to the at-sensor radiance $L = C_0 + C_1 \cdot \text{DN}$. The atmospheric correction process removes the signal components 1 and 3 from the total at-sensor radiance L , so radiance component 2 remains. This information is converted into a surface reflectance value. Here, the input variables are the day of data acquisition and the solar zenith angle. The former is used to calculate the Earth/Sun distance in astronomical units. The radiance into reflectance conversion eliminates the in between scene variability due to the differences in earth/sun distance and sun zenith angle.

From a catalogue of functions stored in lookup tables, the selection of the appropriate atmospheric correction model is required for the removal of atmospheric effects. The user should normally work in a way to specify all the needed input information. An iterative process is used to determine the aerosol types as well as a best approximation of image visibility.

ENVI's (The Environment for Visualizing Images, software version 3.6) atmospheric correction module, called FLAASH (Fast Line-of-sight Atmospheric Analysis of Spectral Hypercubes) for retrieving spectral reflectance from hyperspectral radiance images was employed to atmospherically correct the Hyperion image. The FLAASH module incorporates the MODTRAN41 radiation transfer code (Berk *et al.* 1989, Berk *et al.* 1998, Adler-Golden *et al.* 1999, Matthew *et al.* 2000).

4.2.3 Parameters used and resulting images

The Landsat-TM scenes were processed with the spatially-adaptive correction algorithm of ATCOR2. It was found that the atmospheric correction function for the 1985 image was for a midlatitude summer atmosphere, maritime aerosol, at a visibility of 25 km. For the 1989 image, it was a humid atmosphere, rural aerosol, at a visibility of 25 km.

Figure 15 shows the result of the atmospheric correction for the six different bands of the image. The left figure represents the spectral profile of the Landsat-TM 1985 before the atmospheric correction. The right figure represents the spectral profile from the same image after atmospheric correction.

A broadening of the four histograms is evident. This is due to dependence of atmospheric correction on the type of surface which tends to increase the contrast between low and high reflective surfaces. Also noticeable is a general reduction in reflectance values. This is normal since the contribution of atmospheric Raleigh and aerosol is higher than the ozone absorption, and correction of the atmospheric effects tends to decrease the reflectance values at that wavelength. By contrast, the reflectance values found in channels 4, 5 and 7 (band 6) increase after correction as a result of the weak component of Raleigh and aerosol scattering and the high water vapour absorption.

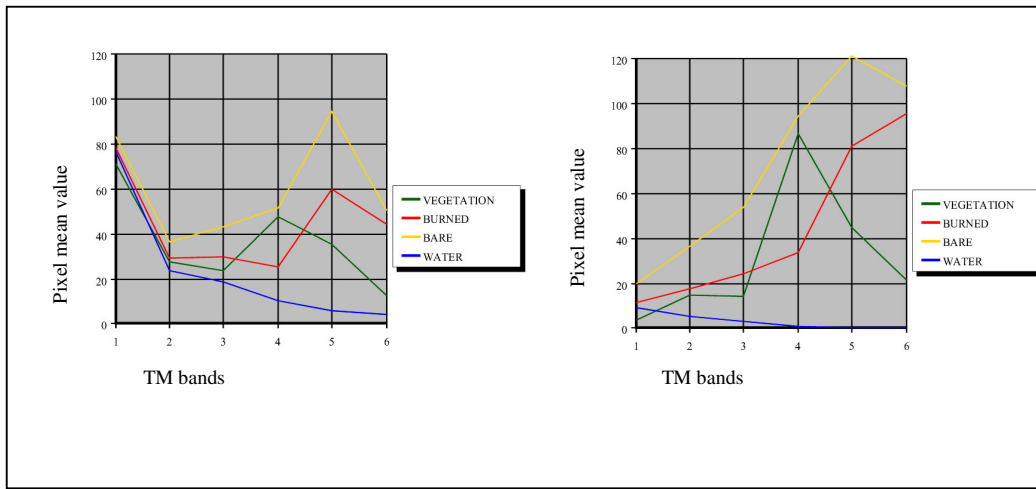


Figure 15 Spectral profile of the Landsat-TM 1985 before and after atmospheric correction

The lack of field radiometry data at the time of image acquisitions did not allow a qualitative determination of the accuracy of the radiometric correction method. However, the effectiveness of the method in reducing the in between-scene illumination was quantitatively studied by regressing the surface-reflectance-corrected spectra of pseudo-invariant targets between the two images of 1985 and 1989 for all bands. Table 8 represents the regression coefficients and goodness of fit values resulting from the regression of the 1985 Landsat image to the 1989 Landsat image. The table shows that the regression coefficients were significantly different from 1 which indicates that the pseudo-invariant targets have the almost the same reflectance values across the two images. Therefore, it can be concluded that the in between-scene illumination variation was greatly reduced. The goodness of fit values for the regression models indicate if the resulting surface-reflectance-corrected spectra have

residual artefacts due to the imperfect radiative transfer models and the imperfect knowledge of the detailed spectral response of the sun (Mather 1999, Clarck *et al.* 1999).

Table 8 Regression coefficients and goodness of fit values (Landsat 1985-1989)

TM Bands	Regression Coefficient	r^2
B1	1.043	0.995
B2	0.913	0.998
B3	0.924	0.995
B4	0.931	0.991
B5	0.922	0.995
B7	0.906	0.996

As for Hyperion, in the raw image water vapour absorption features were located at approximately 721 nm, 823 nm, 940 nm, 1124 nm and 1366 nm. Also a common CO₂ signature that consists of two absorption features was observed near 2000 nm. Figure 16 shows common atmospheric absorption features in the radiance spectrum of a road pixel of the Hyperion scene.

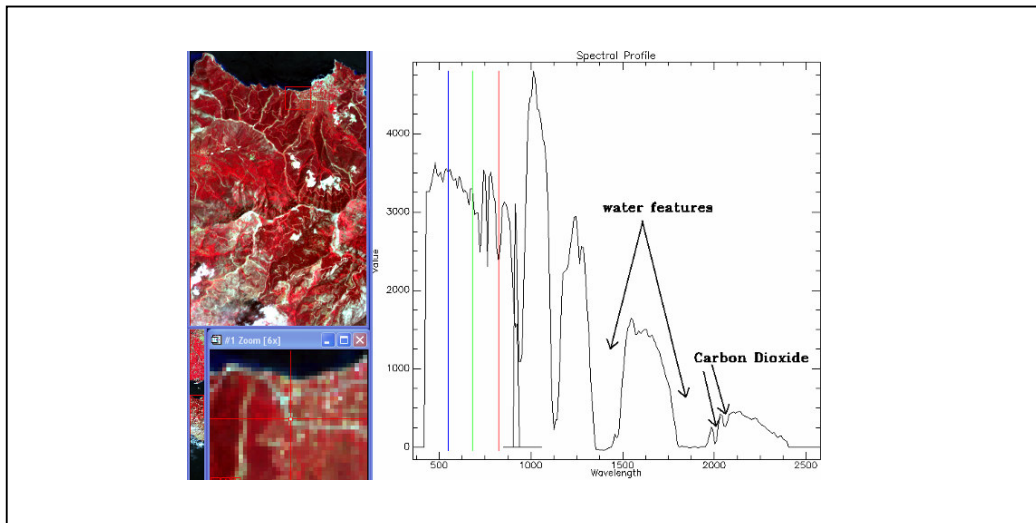


Figure 16 Common atmospheric absorption features of the Hyperion scene

The total number of output bands after atmospheric correction using FLAASH was 198, since out of the original 242, only 8-57 and 77-224 are calibrated and were kept. Output data were scaled to 10000 (10000=100% reflectance). Using the Bad Band Selection tool in Erdas 51 bad (no data) and noisy bands (due to water absorption in the atmosphere), were eliminated. These layers were: 50-55; 71-74; 94-107; 139-160;

194-198. That means the bands that were laminated were: 57; 77-81; 97-100; 120-133; 165-186 and 220-224. The final output image was composed of 147 bands. Final data were scaled from 0 to 1. Figure 17 shows a spectral profile of a road pixel in the atmospherically corrected Hyperion scene.

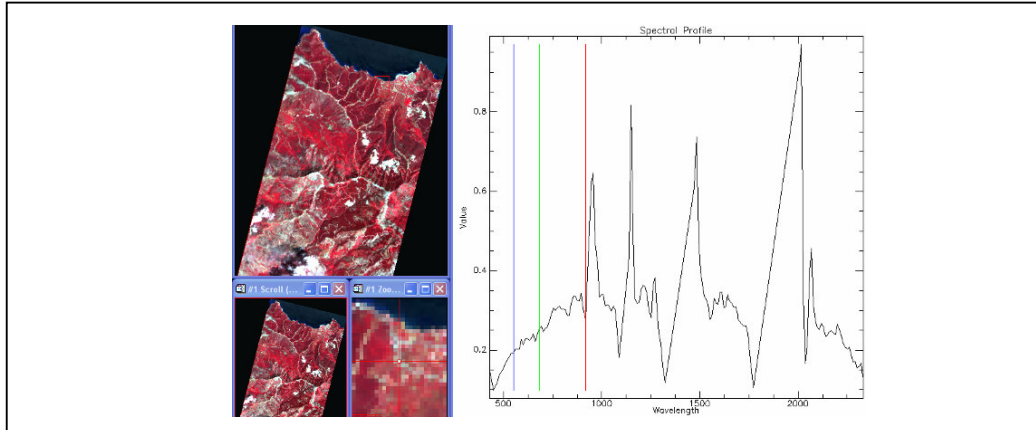


Figure 17 Atmospherically corrected Hyperion

The atmospheric correction of the Ikonos image involved the Darkest Pixel method. From an operational point of view, the Darkest Pixel method, which derives its input parameters from the image itself, and is relatively easy to implement, is to be preferred over more sophisticated techniques that require the acquisition of atmospheric or meteorological data (Hadjimitsis *et al.* 2004). Based on the above, atmospheric correction in this subtracted the minimum value of each spectral channel from each pixel's brightness in that channel (Figure 18).

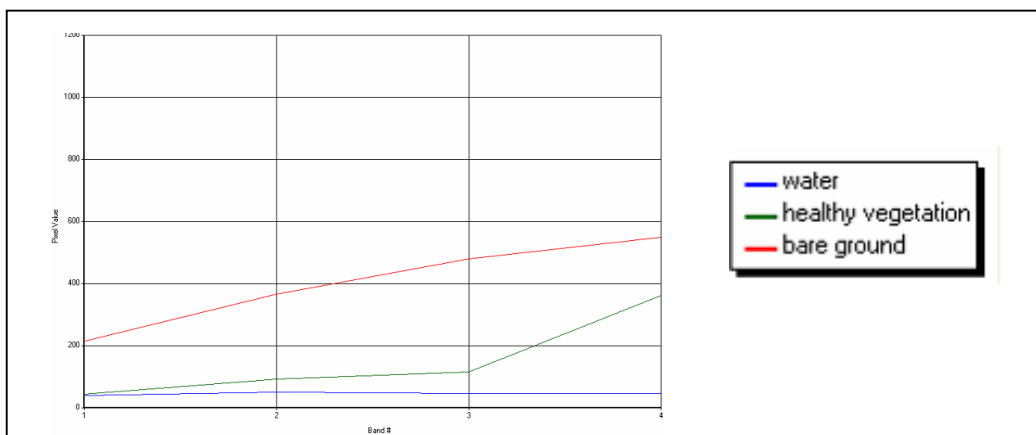


Figure 18 Spectral profiles from the atmospherically corrected Ikonos image

4.3 GEOMETRIC CORRECTION

Raw digital images usually have such significant geometric distortions that they cannot be used as maps, nor be compared with maps or to each other. These distortions are due to the Earth, the satellite, the orbit and the image projection. The contribution of the Earth comes from its rotation, oblateness, and curvature. The satellite causes image distortion by its variation in velocity, attitude, and altitude. The projection of the earth's spherical surface on a flat image and the scan skew of the sensor are also responsible for significant geometric errors (Lillesand and Kiefer 1994, Nguyen and Ho 1988).

The purpose of geometric correction is to compensate for the distortions introduced by these factors so that the image will have the properties of a map. When the image achieves the geometric integrity of a map meaningful image-to-image comparisons can be made, as well as comparisons among images acquired at different times and by different sources. Also in applications which require precise geographical positioning of ground characteristics, such as cartographic mapping or analysis of certain features in specific locations; these images must be geometrically corrected in order to perform image-to-map registration (Nguyen and Ho 1988). The most widely used projection system in remote sensing is Universal Transverse Mercator (UTM). This involves projecting the earth's surface on cylinders touching the earth along its meridians. This projection is well suited for Landsat imagery except in the Polar Regions where there is considerable distortion (Nguyen and Ho 1988).

Using the ERDAS "geometric correction" option "LANDSAT", images can be geometrically corrected and registered. A number of clearly visible small ground features, well-distributed across the original map sheet, must be located on the image. These control points are often road and/or stream intersections. Each control point is located on the displayed image and the equivalent UTM coordinates are keyed in. Three (3) different types of geometric correction (data resampling) techniques are available as follows: Nearest Neighbour, Bilinear Interpolation and Cubic Convolution. The nearest neighbour resampling technique is often used because it offers the advantage of computational simplicity and does not alter the original input pixel values (Lillesand and Kiefer 1994).

4.3.1 Background

Four basic processes must be performed to geometrically rectify or ortho-rectify an image into a map coordinate system (Jensen 1996):

- Identification of Ground Control Points (GCPs) in the original imagery and on the reference map;
- mathematical modelling of the geometric distortion by fitting the GCPs into a polynomial equation using least-square criteria;
- relocation of every pixel in the original input image (x' , y') to its proper position in the rectified output image (x , y);
- extraction of the brightness value for every pixel from its (x' , y') location in the original image and its relocation to the appropriate (x , y) coordinate location in the rectified output image (*image resampling*).

The intent for geometric correction of imagery is to compensate for the distortions introduced by a variety of factors so that corrected imagery will have the geometric integrity of a planimetric map. A transformation equation allows the reference coordinates for any data file location to be precisely estimated and to be transformed from one coordinate space to another. The statistical technique of least squares regression was used to determine the coefficients for the coordinate transformation equations. For each point, a predicted image location is determined and the difference between the predicted image location and known image location is used in the calculation of a Root Mean Square error (RMS_{error}). The RMS_{error} (equation 4.1) is generally reported in units of image pixels; the smaller the RMS_{error}, the more accurate the rectification. According to Luque (2000), the standard range of accepted error is $0 \leq \text{RMS}_{\text{error}} \leq 0.6$.

$$RMS = \sqrt{(x_{\text{prec}} - x_{\text{known}})^2 + (y_{\text{prec}} - y_{\text{known}})^2} \quad (\text{Equation 4.1})$$

The RMS error gives an indication of how “well” the polynomial equation represents the functional relationship between the image and map coordinates.

Three main resampling methods can be used to relocate the brightness values from their original location into the rectified image. The *nearest-neighbour* is a method that uses the input cell value closest to the output cell as the assigned value to the output cell; *bilinear interpolation* calculates the output cell value by calculating the weighted average of the four closest input cells (a 2x2 array) based on distance; and *cubic convolution* Calculates the output cell value by calculating the weighted average of the closest 16 input cells (a 4x4 array) based on distance. The *nearest-neighbour* was the resampling method used in this study. The nearest-neighbour method does not alter the pixel brightness values during resampling (Robinson 1982), whereas the other two methods use averages to compute the output brightness values, often removing valuable spectral information.

The nearest neighbour approach uses the value of the closest input pixel for the output pixel value. To determine the nearest neighbour, the algorithm uses the inverse of the transformation matrix to calculate the image file coordinates of the desired geographic coordinate. The pixel value occupying the closest image file coordinate to the estimated coordinate will be used for the output pixel value in the georeferenced image.

Advantages of the nearest-neighbour approach:

- output values are the original input values. Other methods of resampling tend to average surrounding values. This may be an important consideration when discriminating between vegetation types or locating boundaries;
- since original data are retained, this method is recommended before classification;
- easy to compute and therefore fastest to use.

Disadvantages of the nearest-neighbour approach:

- produces a choppy, "stair-stepped" effect. The image has a rough appearance relative to the original unrectified data;
- data values may be lost, while other values may be duplicated. This loss of data may result in breaks in linear features such as roads, streams, and boundaries.

4.3.2 Implementation and resulting images

The LANDSAT model was used to geometrically correct the two Landsat TM images. The LANDSAT model allows ortho-rectification of Landsat data, such as TM and MSS, which have multiple perspective centres.

Ortho-rectification is a more advanced and more rigorous method of rectifying imagery. Ortho-rectification is a form of rectification that corrects geometric errors inherent with photography caused by relief displacement, lens distortion, and the like.

In the ortho-rectification process, relief displacement was corrected with the use of a DEM by including Z values (elevation from the DEM), Sensor attitude/orientation was corrected by taking into account the exterior orientation (position and orientation), and internal sensor errors were corrected by looking at the internal geometry of the sensor.

A 10-metre grid size Digital Terrain Model (DTM) and a 1:50,000 planimetric map were used in the process. The geometric correction proceeded by identifying GCPs in the Landsat images and on the planimetric map.

Accurate ground control points, locations that were found both on the image and in the map, were essential for an accurate rectification. From the ground control points, the rectified coordinates for all other points in the image are extrapolated. The more dispersed the GCPs are, the more reliable, the rectification will be. The coastline and some road intersections provided excellent locations for the selection of GCPs.

Approximately 30 GCPs were selected spaced as widely as possible across the study areas for each image and using features that are readily identifiable and not likely to move, e.g., road intersections. The GCP coordinates were recorded from the map and from the image and then used in the least squares regression analysis to determine the coordinate transformation equations.

Once a large number of ground control points have been determined, it is a common practice to remove points with high RMS errors and to adjust the points to improve the overall RMS error, taking into consideration that many effects, such as

topography, would introduce complexity in the actual functional relationship that cannot be modelled with a low-order polynomial equation.

The technique that was used in this study for the interpolation was the nearest-neighbour; the value of the image pixel whose centre ends up nearest that of the output grid was placed in the output grid.

The two images were then reprojected using a continuous polynomial approximation into the Greek EGSA projection system, a process by which the geometry of the image areas was made planimetric by referencing to a standard map projection. It was necessary to re-project the images in order to render them geographically comparable with the other datasets used in this study.

The statistical technique of least squares regression was used to determine the coefficients for the coordinate transformation equations. The total $\text{RMS}_{\text{error}}$ associated with the GCPs used for orthorectifying the 1985 and the 1989 Landsat images were equal to 0.31 and 0.37, respectively. These solutions with low RMS were likely to be good fits of the two datasets.

A good fit of the orthorectified Landsat TM image (1985) and the topographic map is shown in Figure 19.



Figure 19 The 1:50 000 map and the ortho-rectified 1985 Landsat image overlaid

The QuickBird image was ortho-rectified using the Rational Polynomial Coefficients (RPC) file provided with the image. The resulted image showed a perfect fit with the topographic map as well as with the ortho-photos of the area.

The Hyperion image was geometrically corrected employing the orthorectified QuickBird image. Ten image to image Ground Control Points (GCPs) were interactively selected on both Hyperion and ortho-rectified QuickBird image covering the same area. The Hyperion image was then reprojected using a continuous polynomial approximation into the EGSA projection system (Greek grid). The statistical technique of least squares regression was used to determine the coefficients for the coordinate transformation equations. The total RMSError associated with the GCPs used for geo-referencing the images was equal to 0.46. The low RMSError obtained using the simple polynomial rectification technique can be attributed to the good distribution of the GCPs over the two images. At an altitude of 600 m, the red

crosshair in the two images (Figure 20) has the same geographic coordinates. The left figure is the geometrically corrected Hyperion and right figure is the ortho-rectified QuickBird. The crosshair was centred over a square of bare ground.

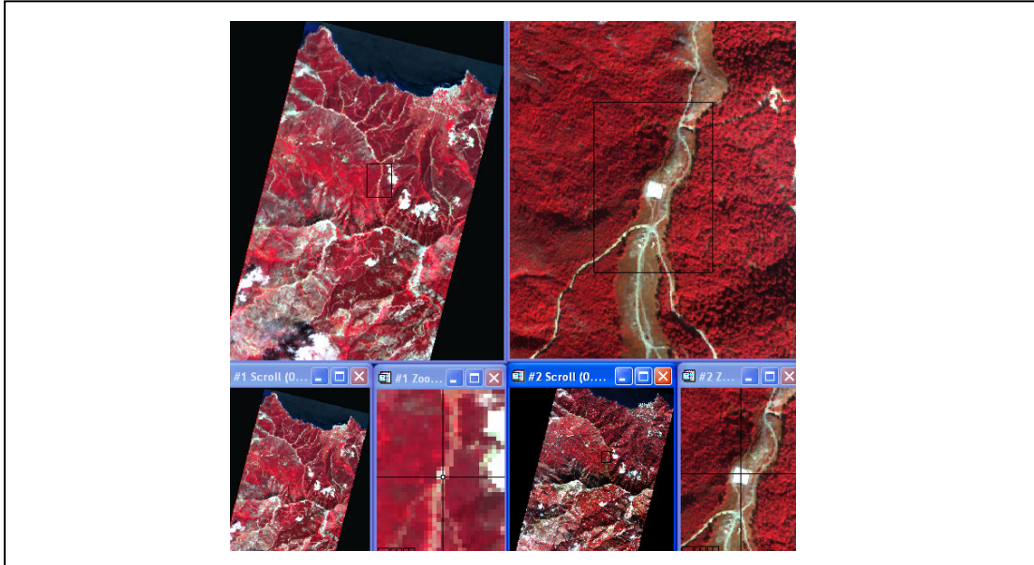


Figure 20 Accuracy evaluation of the geometric correction of Hyperion

The Ikonos image was geometrically corrected and projected to the Greek grid. A set of 20 Ground Control Points (GCPs), which were evenly distributed over the image, was used in the procedure, and the nearest neighbour interpolation method was employed to resample the image. An overall Root Mean Square error (RMSError) of 0.24 was obtained using the simple polynomial rectification technique. The fact that the RMSError was low could be attributed to the absence of high relief in the terrain.

4.4 TOPOGRAPHIC NORMALIZATION

Topography does not only affect the geometric properties of an image but will also have an impact on the illumination and the reflection of the scanned area. This effect is caused by the local variations of view and illumination angles due to mountainous terrain. Therefore, identical land-cover might be represented by totally different intensity values depending on its orientation and on the position of the sun at the time of data acquisition.

Neglecting the atmospheric influence and the adjacency effects, we can state that in the visible and near-infrared bands the direct sun radiation is the only illuminating factor. However, most objects, including forest, have non-lambertian reflectance characteristics and the effects of topography on scene radiance cannot be neglected in rugged terrain. The next section will focus on the correction of slope-aspect effects.

4.4.1 Background

An ideal slope-aspect correction removes all topographically induced illumination variation so that two objects having the same reflectance properties show the same digital number despite their different orientation to the sun's position. Visibly, the result is that the three-dimensional relief impression of a scene gets lost and the image looks flat.

In order to achieve this result, several radiometric correction procedures have been developed. Besides empirical approaches, such as image rationing, which do not take into account the physical behaviour of scene elements, early correction methods were based on the lambertian assumption, i.e. the satellite images are normalized according to the cosine of the effective illumination angle (Smith *et al.* 1980). However, most objects on the earth's surface show non-lambertian reflectance characteristics (Meyer *et al.* 1993). Therefore, the cosine correction had to be extended by introducing parameters, which simulate the non-lambertian behaviour of the surface (Civco 1989, Colby 1991). The estimation of these parameters is generally based on a linear regression between the radiometrically distorted bands and a shaded terrain model. A comparison between four correction methods, including the non-parametric cosine

correction, confirms a significant improvement in classification results when applying the parametric models (Meyer *et al.* 1993).

Cosine Correction: The cosine correction is a statistic-empirical method. Such approaches are based on a significant correlation between a dependent and one or several independent variables. The quality of such correction depends on the degree of explanation of the regression function. The cosine correction is often applied in flat terrain to equalize illumination differences due to different sun positions in multitemporal data sets. It is a strictly trigonometric approach based on physical law assuming a Lambertian reflection characteristic of objects and overlooking the presence of an atmosphere.

$$L_H = L_T \frac{\cos(sz)}{\cos(i)} \quad (\text{Equation 4.2})$$

L_H	=	radiance observed for horizontal surface;
L_T	=	radiance observed over sloped terrain;
sz	=	sun's zenith angle;
i	=	sun's incidence angle in relation to the normal on a pixel.

The cosine correction only models the direct part of irradiance. As weakly illuminated regions receive a considerable amount of diffuse irradiance, these areas show a disproportional brightening effect when corrected (the smaller the $\cos(i)$, the stronger the overcorrection).

C-Correction: bringing the original data into the form:

$$L_T = m \cos(i) + b \quad (\text{Equation 4.3})$$

We can introduce a parameter c which is the quotient of b and m of the regression line. The parameter c is built in the cosine law as an additive term:

$$L_H = L_T \frac{\cos(sz) + c}{\cos(i) + c} \quad (\text{Equation 4.4})$$

$$\text{With } c = \frac{b}{m} \quad (\text{Equation 4.5})$$

c	=	correction parameter;
m	=	inclination of regression line;
b	=	intercept of regression line;
L _H	=	radiance observed for horizontal surface;
L _T	=	radiance observed over sloped terrain;
sz	=	sun's zenith angle;
i	=	sun's incidence angle in relation to the normal on a pixel;

The effect of c is similar to that of the Minnaert constant. It increases the denominator and weakens the overcorrection of faintly illuminated pixels.

Many models have been proposed to remove the effect of relief present on imagery of rugged terrain areas (Gitas 1999). These include classical band rationing (Holben and Justice 1981), Lambertian illumination modelling (Colby 1991), and non-Lambertian illumination modelling (Baker *et al.* 1991). Vegetation and soil cover classes on steeper slopes have been found to be overcorrected using the Lambertian model (Costa-Posada 1997). Overall, of the non-Lambertian models, the Minnaert model is currently the most promising (Costa-Posada and Devreux 1995).

A principle developed by Minnaert (1941) and a method outlined by Smith *et al.* (1980) proposed an equation that allows favouring certain directions of scattering over others, unlike the perfectly diffuse reflector assumed by the Lambertian correction. The equation is as follows:

$$L_s = L_n (\cos(i))^k \cos(e)^{k-1} \quad (\text{Equation 4.6})$$

Where:

- L_s is the scattered radiance.
- i is the angle of incident e.
- e is the angle of exitance: the angle between a perpendicular to the surface and the sensor.
- L_n is the normalized radiance: the theoretical radiance with the sun and the sensor at nadir ($i=0$, $e=0$).
- K is the Minnaert or k constant, it varies between 0 and 1 (when k is 1 the Minnaert model becomes Lambertian).

The normalized radiance can be derived from equation 4.6 as

$$L_n = \frac{L_s}{\cos(i) \cos(e)^{k-1}} \quad (\text{Equation 4.7})$$

The method used to calculate the value K is as follows: logarithmically linearising equation 4.6:

$$\log[L_s \cos(e)] = \log[L_n] + K \log[\cos(i) \cos(e)] \quad (\text{Equation 4.8})$$

4.4.2 Applying the DE_RELIEF algorithm

The De-relief algorithm corrects radiometrically preprocessed remote sensed data for the topographic effect using the Minnaert model (equation 4.6) with a single k coefficient for every different band of the image. Using it for each band separately makes it possible to correct each band with a different k coefficient (Gitas 1999). The method calculates the normalised reflectance for each pixel by first calculating the cosine incidence ($\cos(i)$) and after that the cosine exitance ($\cos(e)$).

$$\cos(i) = \sin(\theta_s) \cos(\theta_z) + \cos(\theta_s) \sin(\theta_z) \cos(A - \theta_a) \quad (\text{Equation 4.9})$$

Where:

Se is the solar elevation

Sa is the solar azimuth

S is the slope

A is the aspect

Pixel slope and aspect can be derived from a digital elevation model (DEM), while solar elevation and solar azimuth can be obtained from the image file metadata. This first step results in an image that resamples the surface illumination conditions at the same acquisition time of the satellite image. Then, the calculation of the normalized reflectance for each pixel is applied on each band individually because k values change with wavelength. From equation 4.7, and since the satellite view angle is close to nadir ($\cos(e) \approx \cos(S)$), the normalised radiance can be expressed as:

$$Ln = Ls \frac{\cos(e)^{1-k}}{\cos(i)^k} \quad (\text{Equation 4.8})$$

Where:

$\cos(i)$ represents the result of the first step of the model

Ls represents the result of the atmospheric correction applied on the image

K represents the result of a regression of equation C with all of the data of the image

4.4.3 Implementation

The De-Relief programme was used in order to topographically normalize the two Landsat images of 1985 and 1989. The procedure followed for the correction of the 1985 image is described in this section. The other Landsat image of 1989 was corrected in an identical way. Table 9 shows the sun elevation and sun azimuth of the two Landsat TM images of 1985 and 1989.

Table 9 Sun elevation and sun azimuth for the two Landsat TM images of 1985 and 1989

	1985	1989
Solar elevation	42.4	44
Solar Azimuth	142.4	140

The first step was to calculate the cosine intercept. Slope and aspect images were derived from the DEM of Thasos, while sun elevation and sun azimuth were obtained from the metadata file.

After the cosine incidence had been calculated, it was used in the second step of the model, together with the slope raster map, the atmospherically corrected single TM bands, and the k constant. The k value was used for each band individually, and the best value which produced the best result was chosen empirically.

Once the K values were determined using linear regression analysis, the Minnaert correction method was applied to the two Landsat TM images. The results of the analysis are shown in Tables 10 and 11.

4.4.4 Resulting images

The final result of the topographic normalization was the topographically corrected Landsat TM 1985 and Landsat TM 1989 images. It was not possible to evaluate the effectiveness of the topographic correction quantitatively; however, topographic normalization greatly reduced the illumination variation across the scene. This was visually evaluated.

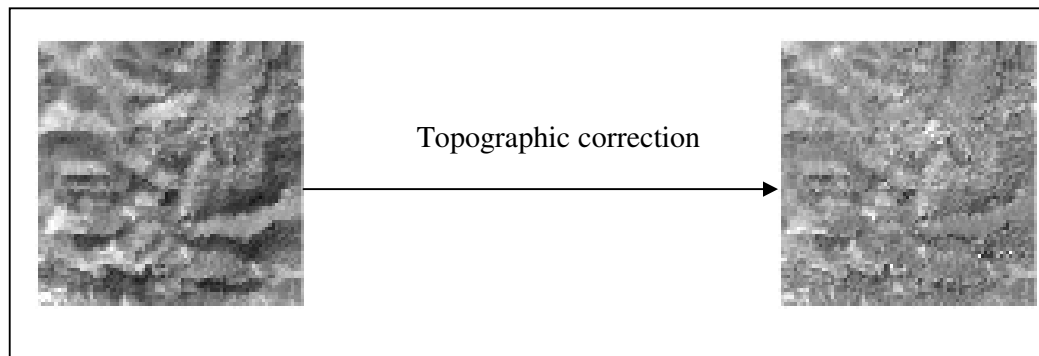
The Near Infra Red (NIR) band (band 4 in Landsat-TM) is severely affected by the topographic effect (Kawata *et al.* 1988). A comparison between the band 4 of the original image and the topographically normalized band 4 showed a reduction of the topographic effect. In Figure 21 the left image represents a subset of the original 1985 Landsat TM (band 4) showing the effects of topography on scene radiance resulted from rugged terrain. The right image represents a subset of the topographically corrected Landsat TM (band 4) showing how the topographic effect was suppressed in shaded areas after applying the topographic correction.

Table 10 Empirically derived K per band for the 1985 Landsat scene

TM bands	k
Band 1	0.7
Band 2	0.65
Band 3	0.6
Band 4	0.55
Band 5	0.5
Band 7	0.45

Table 11 Empirically derived K per band for the 1989 Landsat scene

TM bands	k
Band 1	0.65
Band 2	0.7
Band 3	0.6
Band 4	0.5
Band 5	0.55
Band 7	0.6

**Figure 21** Image subset of topographic correction

4.5 CHAPTER SUMMARY

In summary:

- The satellite images are largely contaminated by the effects of atmospheric particles through absorption and scattering of the radiation from the earth surface. The objective of the atmospheric correction was to retrieve the surface reflectance (that characterizes the surface properties) from remotely sensed imagery by removing the atmospheric effects.
- In the case of the Landsat TM images, the Spatially-Adaptive Fast Atmospheric Correction Algorithm (ATCOR2) was employed. The model calculated a ground reflectance image in each spectral band.
- FLAASH (Fast Line-of-sight Atmospheric Analysis of Spectral Hypercubes) for retrieving spectral reflectance from hyperspectral radiance images was employed to atmospherically correct the Hyperion image.
- The accuracy of the radiometric correction method applied to the images was not quantitatively determined. This is due to the lack of field radiometry work at the time of image acquisition.
- The effectiveness of the method applied to the Landsat TM images in reducing the in between-scene illumination was quantitatively studied. The atmospheric correction for the Landsat images was very effective in reducing the in between-scene illumination variation.
- The satellite images were geometrically corrected and reprojected (Greek EGSA projection system).
- A correction of the images for topographic corrections (using DE-relief algorithm) was applied to the Landsat TM images. The topographic correction of the high spatial resolution imageries of Ikonos and QuickBird was avoided due to the absence of a similar or higher spatial resolution Digital Elevation Model (DEM). Also, the Hyperion image was not topographically corrected in order not to alter the spectral reflectance of the data.
- The topographic correction appeared to be an improved means of eliminating or, at least, greatly reducing illumination variation induced by topography, as similar surfaces on opposite sides of the ridges appeared to have similar brightness values.

CHAPTER 5: MAPPING THE TYPE AND SEVERITY OF FIRE USING IKONOS IMAGERY

Chapter four presented the different pre-processing steps of the satellite data used in this work and described the undertaken atmospherically, geometrically and topographically corrections of the images. In this chapter, a classification approach for fire type and severity mapping using object-oriented image analysis and employing the pre-processed Ikonos image will be developed. The area under investigation was burned in 2000 as describe in chapter 3. Section one will deal with the first main objective of the study, which is fire type mapping. Section two will deal with the second main objective, which is fire severity mapping.

Traditional methods of recording fire type and fire severity included field work or observations from an airborne platform and then mapping (manually) resource damage into predetermined classes. As fire sizes increase, and time becomes a constraining factor, traditional methods become costly and labour-intensive to the point where accurate mapping of severity classifications is precluded (Bertolette and Spotskey 2001).

Although remotely sensed data have been shown to provide accurate post-fire information shortly after the fire event (Smith and Woodgate 1985, Milne 1986, Chuvieco and Congalton 1988b, Jakubauskas *et al.* 1990, White *et al.* 1996, Patterson and Yool 1998, Beaty and Taylor 2001, Escuin *et al.* 2002, Pollet and Omi 2002), the accurate mapping of the type and severity of fire seems to be in its early stages.

Previous studies for detecting fire severity from remotely sensed data concentrated on analyzing post-fire AVHRR, MODIS, SPOT, AVIRIS, ASTER, among others (Chuvieco and Martin 1994, Barbosa *et al.* 1999, Van Wagtendonk *et al.* 2004, Roy *et al.* 2005), Landsat Multispectral Scanner (MSS) and Thematic Mapper (Hunt and Rock 1989, White *et al.* 1996, Patterson and Yool 1998, Key and Benson 2000, 2002, Key *et al.* 2002, Diaz-Delgado *et al.* 2003), Enhanced Thematic Mapper Plus (Rogan and Franklin 2001, Brumby *et al.* 2002) and ERS-2 SAR images (Siegert and Ruecker 2000). However, burned areas were not always discernable from unburned

background and acceptable results were not obtainable in the case of insufficient radiometric and spatial resolutions. Fire severity mapping presented a series of problems, caused by spectral confusion between vegetation affected by surface fire and unburned vegetation, between moderately burned vegetation and sparse vegetation, and between burned shaded and unburned shaded vegetation (Rogan and Franklin 2001).

Therefore, new types of satellite data such as Ikonos imagery, whose high spatial resolution is comparable with that of an aerial photo, are opening up a new frontier in remote sensing (Tanaka and Sugimura 2001). The new generation of very high spatial resolution sensors, such as Ikonos, made it possible to detect small objects not captured by medium-high resolution sensors. Therefore, these high spatial resolution sensors could overcome some of the problems encountered mainly when using Landsat-TM imagery in fire severity mapping. One major application in which very high resolution images are expected to bring new insight is in the provision of post-fire related information (Gitas and Rishmawi 2003, Van Wagtendonk *et al.* 2004).

Very high spatial resolution imagery of high quality provided by new satellite sensors is characterized by high user interpretability, rich information content, sharpness, accuracy, high image clarity and integrity. Pixel-based classification is aggravated by the rich information of this imagery (De Wit and Clevers 2004). Therefore, object-based classification, which deals with objects (group of pixels), represents an advanced tool for classifying high spatial resolution imagery.

The two main objectives of this chapter are:

1. To map the type of fire using object-based classification of Ikonos imagery.
2. To map the severity of fire using object-based classification of the same Ikonos imagery.

5.1 FIRE TYPE MAPPING

The type of fire, the main focus of the first section in this chapter, is related to environmental conditions such as topography, wind, fuel type, and condition of the fuel. Fire scientists and managers distinguish the following three general types of wildland fire: ground, surface, and crown, depending on the fuel stratum in which the fire burns (Scott and Reinhardt 2001). More specifically:

- A ground fire is one that burns in ground fuels such as duff, organic soils, roots, and rotten buried logs.
- A surface fire is one that burns in the surface fuel layer, which lies immediately above the ground fuels but below the canopy or aerial fuels.
- A crown fire is one that burns in elevated canopy fuels.

Distinguishing and mapping areas of surface and crown fire spread has significant applications in the study of fire behaviour, fire suppression and fire effects (Albini and Stocks 1986, Stephens 1998, Rogan and Yool 2001, Scott and Reinhardt 2001, Graham 2003).

The aim of this study was to develop an object-based classification model to map the type of fire using very high spatial resolution imagery. The specific objectives were:

- to distinguish between surface burn and canopy burn using a post-fire Ikonos image; and
- to assess the accuracy of the classification results by employing field survey data.

The development of the object-oriented model involved two steps: segmentation and classification using the software ecognition (Benz *et al.* 2004, Gitas *et al.* 2004, Mitri and Gitas 2004a, 2004b). Image objects were extracted from the image in the segmentation procedure prior to classification. The methodology is detailed below.

5.1.1 Segmentation

The segmentation used was a bottom-up region-merging technique starting with one-pixel objects. In numerous subsequent steps, smaller image objects were merged into bigger ones. The procedure simulates an even and simultaneous growth of segments over a scene in each step. The algorithm guarantees a regular spatial distribution of treated image objects. The underlying patented algorithm is essentially a heuristic optimization procedure that minimizes the average heterogeneity of image objects for a given resolution over the whole scene. Heterogeneity itself is based not only on the standard deviation of image objects, but also on their shape. Weighting between spectral and shape heterogeneity enables adjustment of the segmentation results to the considered application.

Segmentation parameters were determined empirically in order to produce highly homogeneous objects in specific resolutions and for specific purposes. A series of segmentations was generated by adjusting the parameters of scale, band weights, colour, and shape. As burned areas appeared to be more visible in Ikonos bands 3 and 4 than in bands 1 and 2, a weight number of '2' was assigned to bands 3 and 4, and a weight number of '1' was assigned to bands 1 and 2. The sum of all chosen weights for image layers was normalised to 1. Additionally, segmentations based on higher colour weights (80%) and lower shape weights (20%) appeared to better match the ground features of the image.

Next, a three-level graded scale (15, 60, and 150) of segmentation (Figure 22), namely small objects (level 1), middlesized objects (level 2), and large objects (level 3), was created.

The scale parameter used in the segmentation is an abstract term which determines the maximum allowed heterogeneity for the resulting image objects. In heterogeneous data, the resulting objects for a given scale parameter are smaller than in more homogeneous data. By increasing the scale value, the size of image objects is increased. Super-objects at levels 3 and 2 would provide information about the classification of the sub-objects at level 1.

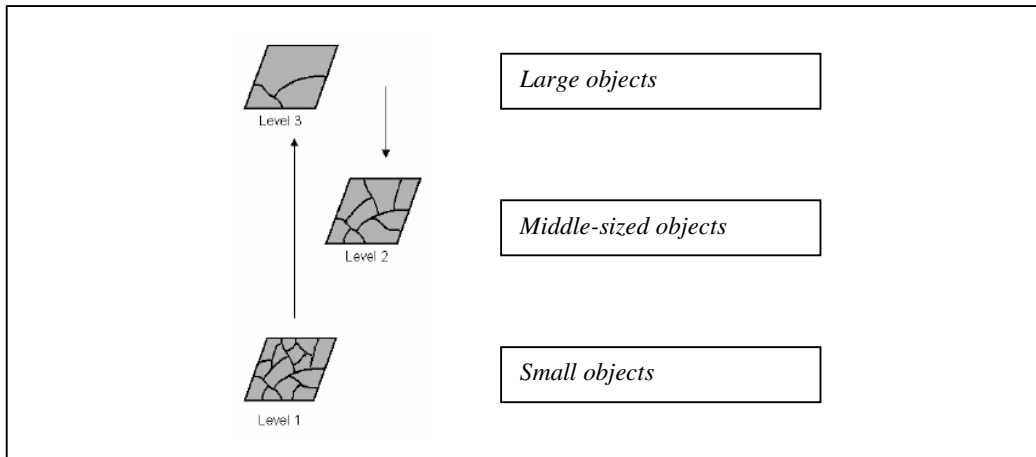


Figure 22 Different levels of image segmentation

5.1.2 Classification

Classification was based on fuzzy logic and consisted of a combination of several conditions (Figure 23) that had to be fulfilled for an object to be assigned to a class. The fuzzy sets were defined by membership functions that identify those values of a feature that are regarded as typical, less typical, or not typical of a class, i.e. they have a high, low, or zero membership, respectively, of the fuzzy set.

Classifications were carried out at the three segmentation levels. The classes were:

- Level 1: 'surface burn', 'canopy burn', 'healthy vegetation', and 'other';
- Level 2: 'water', 'bare soil', and 'other'; and
- Level 3: 'healthy vegetation', 'heavily burned', and 'slightly burned'.

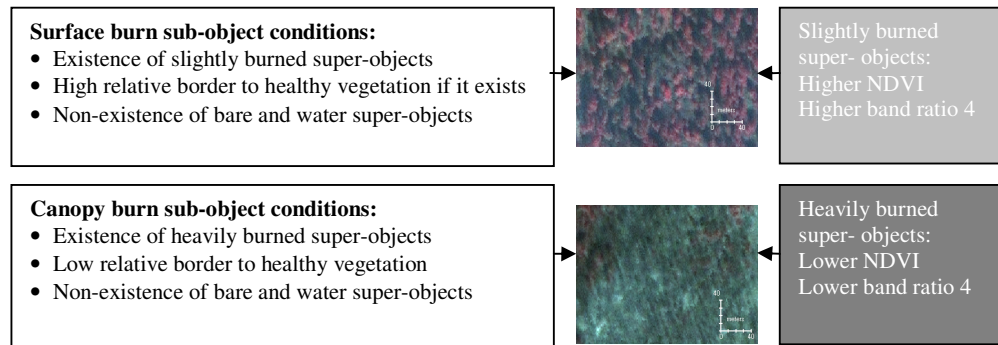


Figure 23 Fire type class descriptions (middle: Ikonos subsets in false colour)

Features based on object spectral information as well as object contextual information, such as neighbourhood and relation to super-objects and to sub-objects, were used in the classification. The features based on object spectral information were: the Normalized Difference Vegetation Index (NDVI)-like index (digital numbers have been used instead of reflectances or radiances) and the band ratio of near infra-red (NIR). The object NDVI was calculated from the NDVI values of all n pixels forming an image object, whereas the object band ratio of NIR corresponded to the NIR mean value of an image object divided by the sum of all spectral layer mean values.

Membership functions were adapted for each chosen classification feature. They offered a transparent relationship between feature values and the degree of membership to a class. Figure 24 shows membership functions of heavily burned super-objects for the features 'NDVI' (upper left), 'band ratio 4' (upper right), and of canopy burn sub-objects for the features 'existence of' (lower left) and 'high relative border to' (lower right).

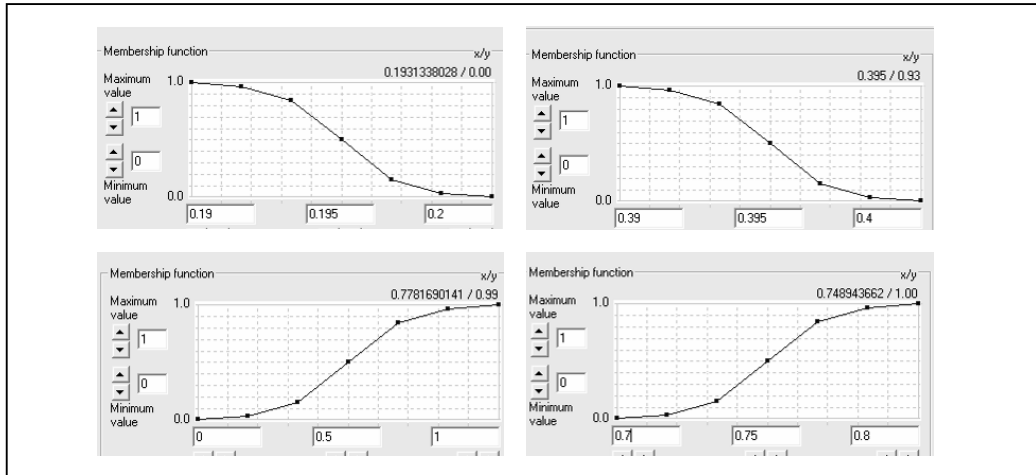


Figure 24 Membership functions

5.1.3 Results and discussion

The classification at level 1 resulted in the production of a fire type map of the study area. Figure 25 shows a ground mapped fire perimeter (white line) and the final classification results of the Ikonos image (burned canopy in dark grey and burned surface in light grey). An area of 80 ha, representing 43% of the total burned area, was classified as canopy burn, whereas an area of 106 ha, representing 57% of the total burned area, was classified as surface burn.

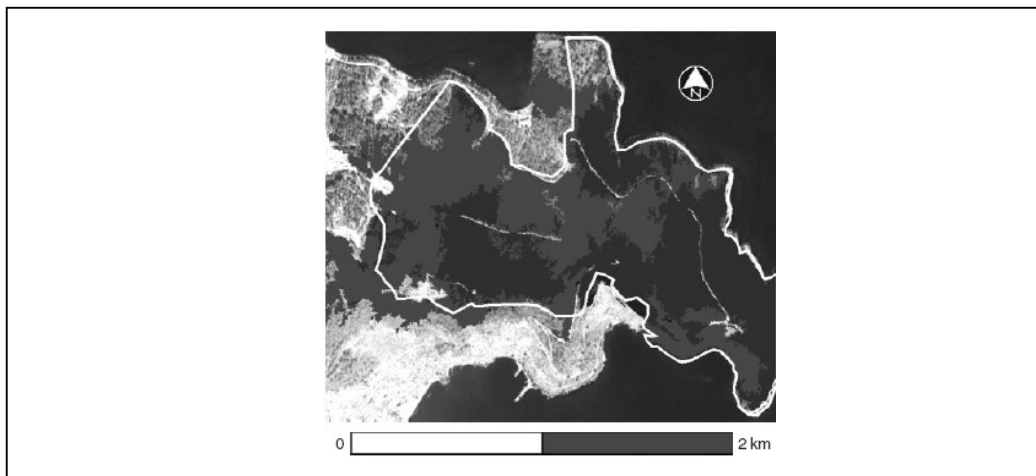


Figure 25 Ground mapped fire perimeter (white line) and final classification results

The results of the classification were compared to the data collected during the field survey. The comparison resulted in the production of a classification error matrix (Table 12). The overall accuracy of the classification was 0.87, whereas the total Kappa Index of Agreement was 0.74. The examination of the error matrix revealed a slight confusion between the surface burn and the healthy vegetation classes.

This confusion is related to the presence of dense healthy vegetation on the image, which completely covers areas of surface burn. This confusion could be attributed to the inability of the optical sensor to penetrate dense canopy to detect fire-affected areas.

Table 12 Fire type mapping contingency matrix

	<i>reference data</i>			
<i>Classified data</i>	<i>canopy burn</i>	<i>surface burn</i>	<i>total</i>	<i>commission error</i>
canopy burn	13	0	13	0
surface burn	3	21	24	0.125
unclassified (non-burned)	0	2	2	-
Total	16	23	39	-
Producers accuracy	0.8125	0.913043		
Users accuracy	1	0.875		
KIA per Class	0.71875	0.773913		

Close examination of the map produced revealed the spatial distribution of the two classes of burn to be highly homogeneous. Also, the border line between surface burn and canopy burn appeared to be very irregular as a result of fire transition from surface burn to canopy burn, and vice versa. In addition, the road network seemed to control the extent of the surface fire, but not the canopy fire.

The resulting map of the total burned area (surface burn plus canopy burn) was compared with the fire perimeter map generated by the Forest Service using traditional survey methods. The vectorised fire perimeter from the classified image was overlaid onto the official fire perimeter. The area measured by the Greek Forest Service was 187 ha, whereas that of the classification result was 186 ha, i.e. a difference of only 1 ha. The common area between the fire perimeter from the classification and that of the Forest Service was 87%. The boundary derived from the classification was rather more detailed than that derived by the Forest Service.

5.2 FIRE SEVERITY MAPPING

This section investigates the subject of fire severity mapping. In recent decades, the number of fires and total surface burns in the European Mediterranean region has increased spectacularly (Pausas and Vallejo 1999), incurring significant impacts on vegetation (De Luís *et al.* 2001). The magnitude of these impacts, measured as fire severity, is related directly to the level of damage done to vegetation, leaf litter and soil (Rogan and Franklin 2001). Fire severity maps are therefore required to locate areas in need of post-fire management where fire impact, timber recovery and the validation of fire risk and fire behaviour models can be examined (Caetano *et al.* 1995).

Although fire severity is a very general concept, it is often defined in less general terms, namely fire impact, which is described as the immediate evident effect of fire on the ecosystem in terms of biophysical alteration (e.g. crown scorch, soil exposure, depth of burn, fuel consumption) (Kafka *et al.* 2001). According to White *et al.* (1996), fire severity is a descriptive term that integrates the physical, chemical and biological changes to a site as a result of fire.

The aim of this study was to develop an object-oriented (Wicks *et al.* 2002, Gitas *et al.* 2004, Mitri and Gitas 2004a, 2004b) model for mapping fire severity in the Mediterranean using very high spatial resolution data of Ikonos. The specific objectives were:

- to differentiate among three levels of fire severity, namely, slightly, moderately and heavily burned; and
- to assess the accuracy of the classification results by employing field data.

The approach applied for fire type mapping is represented in the following sub-sections. The pre-processed image was firstly segmented and then classified using the same software eCognition. Each step followed in the analysis is presented in the flowchart (Figure 26). The numbers in the starbursts represent the steps followed. Image objects were generated at different scales. The whole image object classification was based on fuzzy logic. The following sections describe the different followed steps.

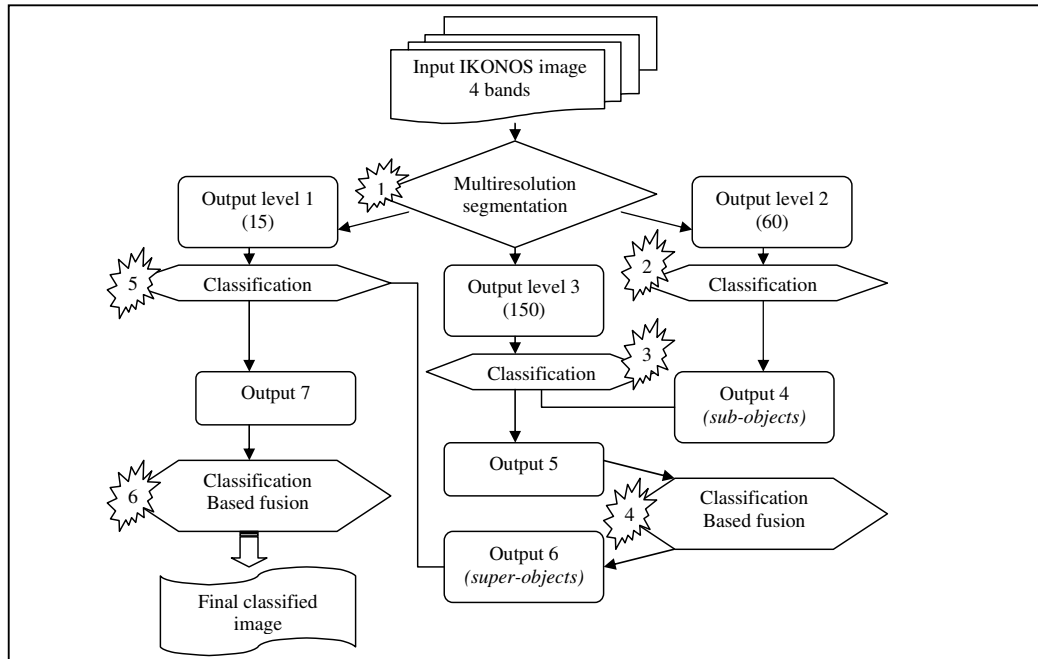


Figure 26 Flowchart of the methodology for fire severity mapping

5.2.1 Segmentation

Multiresolution segmentation was firstly applied to the image. The strategy behind image segmentation was to create three different levels of image objects at different scales. Since it is possible to produce image objects in different resolutions, an object-oriented image analysis can contain a hierarchical network with different object levels of different resolutions. This structure represents image information on different scales simultaneously. Thus, different object levels can be analyzed in relation to each other.

Image objects can be classified by extracting information from classified sub-objects or super-objects (Figure 27). For instance, in a burned area, the possibility of partially burned canopies being classified as slightly or moderately burned is much greater than if they were located in unburned vegetation.

The segmentation used in this study was also a bottom up region-merging technique starting with one-pixel objects. The three levels of segmentation, (level 1, level 2 and

level 3), were generated using increasing scales of 15, 60 and 150, respectively (Figure 27). Individual canopies were found to be best delineated using scale 15. In order to improve the delineation of some specific features such as individual canopies, the shape heterogeneity for image segmentation was considered only at level 1. At level 2, a scale of 60 was useful for extracting large homogeneous image objects of water. Finally, scale 150 was found to be useful for representing broad forested areas.

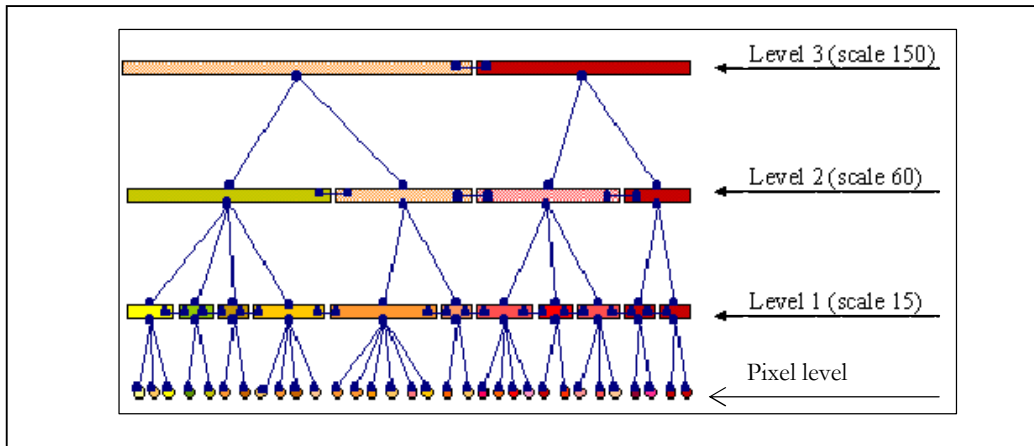


Figure 27 Hierarchical network of image objects

Image layers can be assessed differently depending on their importance or suitability for the segmentation result. The higher the weight assigned to a layer, the greater the amount of information will be used during the segmentation process. Segmentation was achieved by assigning more weights to the NIR band. Several studies have indicated that NIR is the best spectral region for burned area detection and mapping (Lopez and Caselles 1991, Pereira and Setzer 1993, Caetano *et al.* 1994, Chuvieco and Congalton 1988b, Koutsias and Karteris 1998, Sifakis *et al.* 2004). This indeed is the case, since only few other landcover types tend to be darker than burned areas in the NIR part of the spectrum.

Figure 28 shows how multiresolution segmentation at levels 2 and 3, for instance, worked on the Ikonos image. At level 2, image regions of different texture were separated, even when they were of a similar spectral mean value (e.g., shadows and burns). The results of image segmentation at level 3 showed larger homogeneous image objects (e.g. burns) and smaller heterogeneous image objects (e.g. group of

canopies). Statistics based on both spectral values and contextual values were extracted from the objects at different levels.

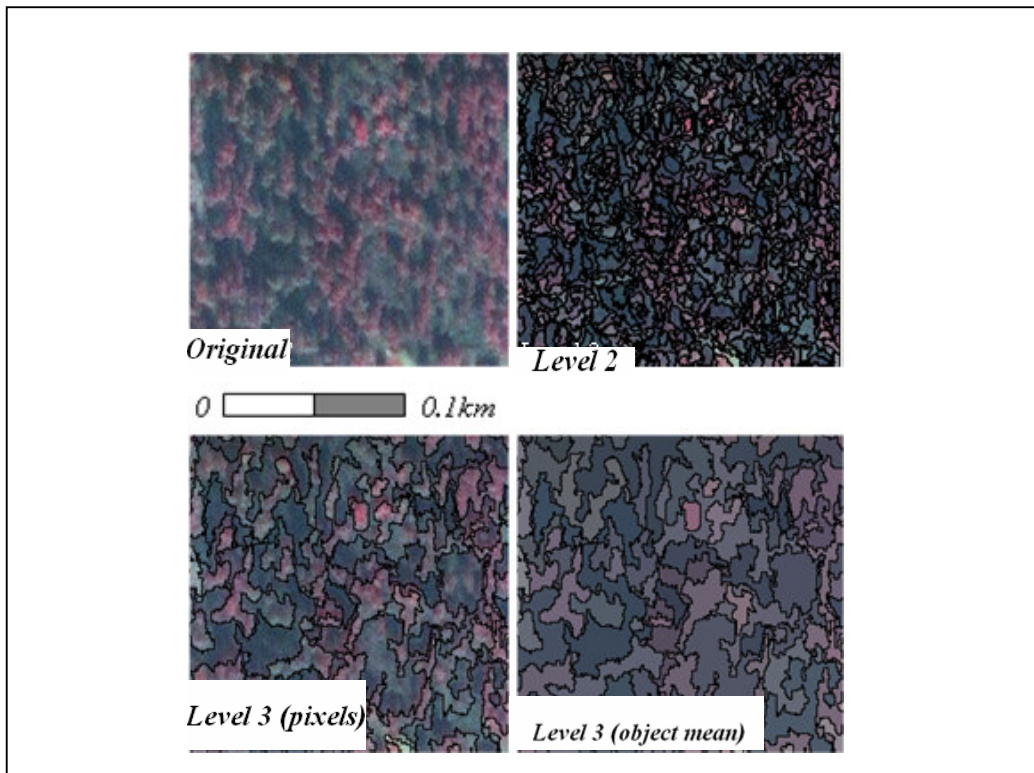


Figure 28 Image subsets show segmentation results at levels 2 and 3

5.2.2 Classification

An individual representative plot of each severity and landcover case was selected independently in order to develop the classification rules. Sample image objects were defined in relation to these representative plots. The Ikonos image was classified into fire severity classes by training and building up a knowledge base for the classification of image objects. The frame of knowledge base for the analysis and classification of image objects was the so-called class hierarchy, which contained all classes of a classification scheme.

The largest number of classes was created at level 1 due to the presence of highly homogeneous segments resulting from an optimal separation and representation of image regions. The medium average size of objects at level 2 showed better

representation of *water* objects, which was mainly due to the size of objects. At level 3, the bigger sized objects would allow a better discrimination between *moderately burned* and *heavily burned*. Classifications were carried out at the three segmentation levels (Figure 29). The classes were:

- level 1: *healthy vegetation*, *water*, *bare*, *shadow in burned*, *slightly burned* and *burned* (with its two subclasses *heavily burned* and *moderately burned*), and *others*;
- level 2: *water*, *bare*, *healthy vegetation* and *others*; and
- level 3: *healthy vegetation* and *burned area* (with the subclasses *slightly burned*, *moderately burned* and *heavily burned*).

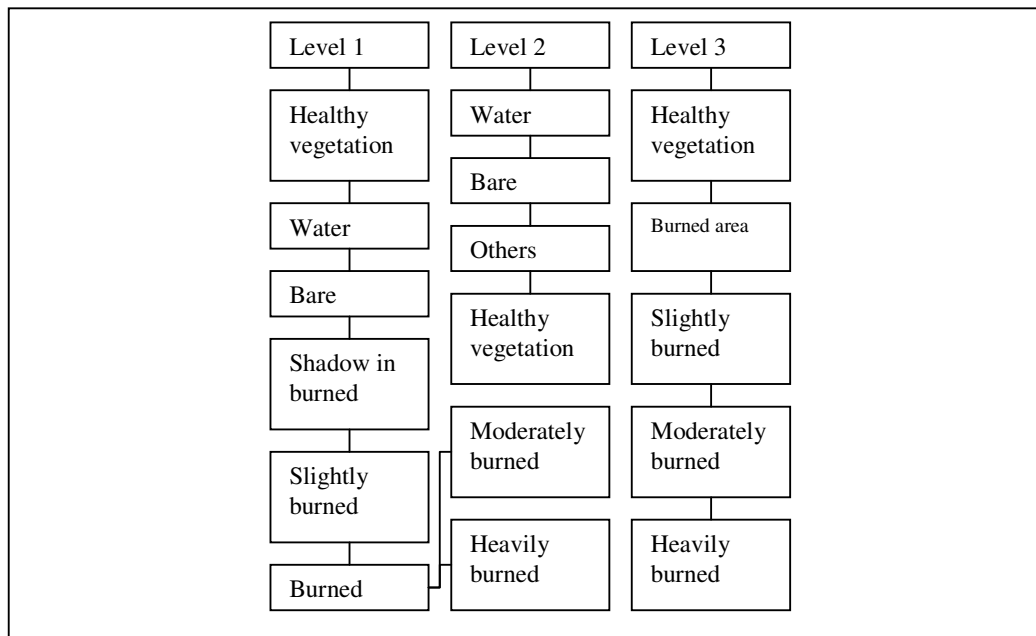


Figure 29 A schematic draw of the class hierarchy

The features selected for the classification are briefly discussed below. Class descriptions are performed using a fuzzy approach defined by membership functions that identify those values of a feature that are regarded as typical, less typical, or not typical of a class. For the construction of a meaningful knowledge base, it was of utmost importance to know which features are suited to the separation of target classes and how to specify these features.

A careful examination of the object features values helped in defining the object features that would be used in the classification. A representation of object statistics is shown in Figure 30 (the reflectance was scaled by 1000 – left figure: bands 3 and 4 object mean values, and right figure: NDVI object mean values - LV: Lowly vegetated and HV: highly vegetated).

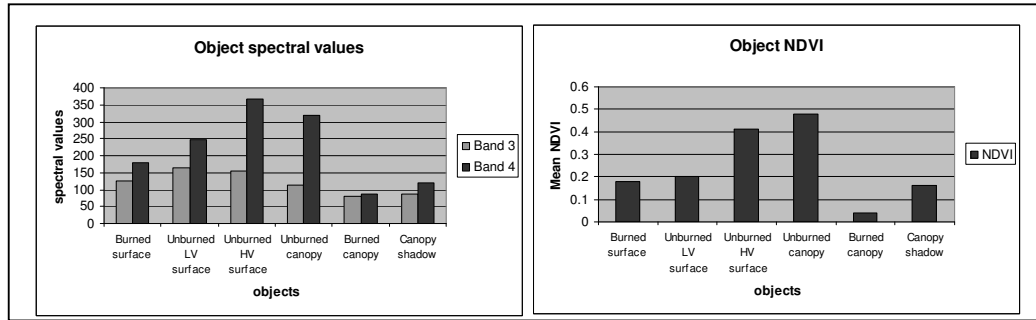


Figure 30 Example of object statistical analysis

The statistical analysis performed on the pre-defined sample objects, provided all the information necessary to achieve high quality classifications by comparing and analyzing single or all image objects in terms of features for classification. Thus, it was possible to evaluate whether image objects would be classified correctly or not before performing the actual classification. Figure 31 shows the object features that were used in the class descriptions.

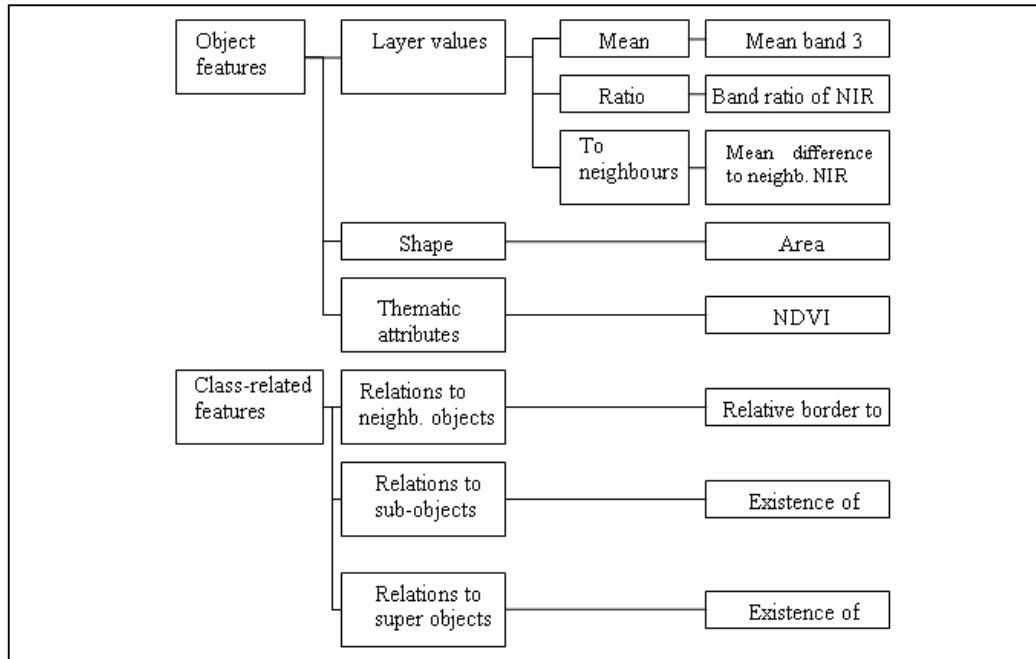


Figure 31 Schematic overview of the features used in the classification

Features based on object spectral information as well as object contextual information, such as neighbourhood and relation to super-objects and to sub-objects, were used in the classification. The features based on object spectral information were: the ‘mean band 3’, the ‘NDVI’, the ‘mean difference to neighbours’ and the ‘band ratio of NIR’.

The mean digital number of band 3 was calculated from the layer values of all n pixels forming an image object. The object NDVI was calculated from the NDVI values of all n pixels forming an image object. As for the feature ‘mean difference to neighbours’, the layer mean difference for each neighbouring object was computed and weighted with regard to the length of the border between the objects or the area covered by the neighbour objects. The object ‘band ratio of NIR’ corresponded to the Near Infra-Red (NIR) mean value of an image object divided by the sum of all spectral layer mean values. The mathematical equations for the previously discussed features are presented in Table 13.

Table 13 Equations of the mostly used features

Feature	Equation	Description
Band mean value	$\bar{C}_L = \frac{1}{n} \sum_{i=1}^n C_{Li}$	Layer mean value \bar{C}_L calculated from the layer values C_{Li} of all n pixels forming an image object.
Mean difference to neighbours	$\Delta_{CL} = \frac{1}{l} \sum_{i=1}^n l_{Si} (\bar{C}_L - \bar{C}_{Li})$	l border length of the image object of concern l_{Si} border length shared with direct neighbour i \bar{C}_L layer mean value of the image object of concern \bar{C}_{Li} layer mean value of neighbour i n quantity of neighbours
Ratio	$r_L = \frac{\bar{C}_L}{\sum_{i=1}^{n_i} \bar{C}_i}$	The ratio of layer L is the layer L mean value of an image object divided by the sum of all spectral layer mean values

Following, the classification process is described and strategies for classification are given. In the classification process, level 2 was the first to be classified. Water was classified using the ratio of NIR and the mean of band 3 because of their low values in comparison to other landcover classes. The second classification was applied to level 3. The NDVI was used to discriminate between *burned* and *healthy vegetation* and to distinguish between *moderately burned* and *heavily burned*. In a procedure called classification-based fusion, objects classified as *moderately burned* and *heavily burned* at level 3 were merged into image objects representing an entire *burned* area by creating a new level of classification. At this new level, potential slightly burned objects were identified, taking into account the presence of *healthy vegetation* objects and their neighbouring burned objects.

At level 1, it was crucial to identify the canopy shadows and to allocate them to the right class for better classification accuracy. Mainly contextual features were used at this level to extract information from the super-objects and the neighbouring objects. At this level water objects were classified based on existence of water super-objects at

level 2. Single trees in open stands cast a shadow on forest understory, resulting in a mosaic of shaded and illuminated pixels. The spectral signature of the shaded pixels is very close to that of surface burned areas. The feature ‘mean difference to neighbours in NIR’ proved to be effective in identifying shaded objects. The shaded objects were assigned to the appropriate classes of fire severity using classification-based fusion at level 1, taking into consideration the extracted information from the super-objects, as well as from the objects at the same level. Table 14 presents most of the spectral and contextual features that were used for each class at the three levels.

Table 14 The features used in each class

Class	Spectral features	Contextual features
Healthy vegetation (1)	-	Existence of healthy vegetation (3) super-objects
Water (1)	-	Existence of water (2) super-objects
Bare (1)	-	Existence of bare (2) super-objects
Shadow in burned (1)	Mean difference to neighbours	Existence of burned area (3) super-objects
Burned (1)	-	Existence of burned area (3) super-objects
Slightly burned (1)	-	Relative border to shadow in burned (1); existence of slightly burned (3) super-objects
Moderately burned (1)	-	Existence of moderately burned (3), ‘Not’ slightly burned (1); Relative border to healthy vegetation (1).
Heavily burned (1)	-	Existence of heavily burned (3) super-objects
Water (2)	Band ratio of NIR	-
Healthy vegetation (2)	NDVI	-
Bare (2)	Mean band 3	-
Others (2)	-	‘Not’ water
Healthy vegetation (3)	NDVI	Existence of healthy vegetation (2) sub-objects
Burned area (3)	NDVI	Relative border to healthy vegetation (3)
Slightly burned (3)	NDVI	Existence of healthy vegetation (2) sub-objects; Relative border to healthy vegetation (3)
Moderately burned (3)	NDVI	-
Heavily burned (3)	NDVI	-

Membership functions were adapted for each chosen feature. They offered a transparent relationship between feature values and the degree of membership to a class (Figure 32). The membership function is basically defined by its left and right border values in combination with the function slope. The way a feature value is translated into a membership value is defined by the function slope. The represented function slope starts at 0, which mean ‘exactly no’ (no assignment) and rises to 1,

which means ‘exactly yes’ (full assignment). All values between 0 and 1 represent a more or less certain status of ‘yes’ and ‘no’. Thereby, the degree of membership/probability depends on the degree to which the objects fulfil the class-describing properties/conditions. A major advantage of this fuzzy method lies in its ability to express uncertainties about the classes’ descriptions.

For successful classification a deliberate choice of membership function was crucial. The selection of these membership functions and the setup of thresholds were based on an expert knowledge. The better the knowledge about the real system is modelled by the membership functions, the better the final classification result. Also, it was possible to create advanced fuzzy rules by combining membership functions and by using basic operators such as “and” and “or”. The most crucial membership functions of the classification and their thresholds were presented in Figure 32.

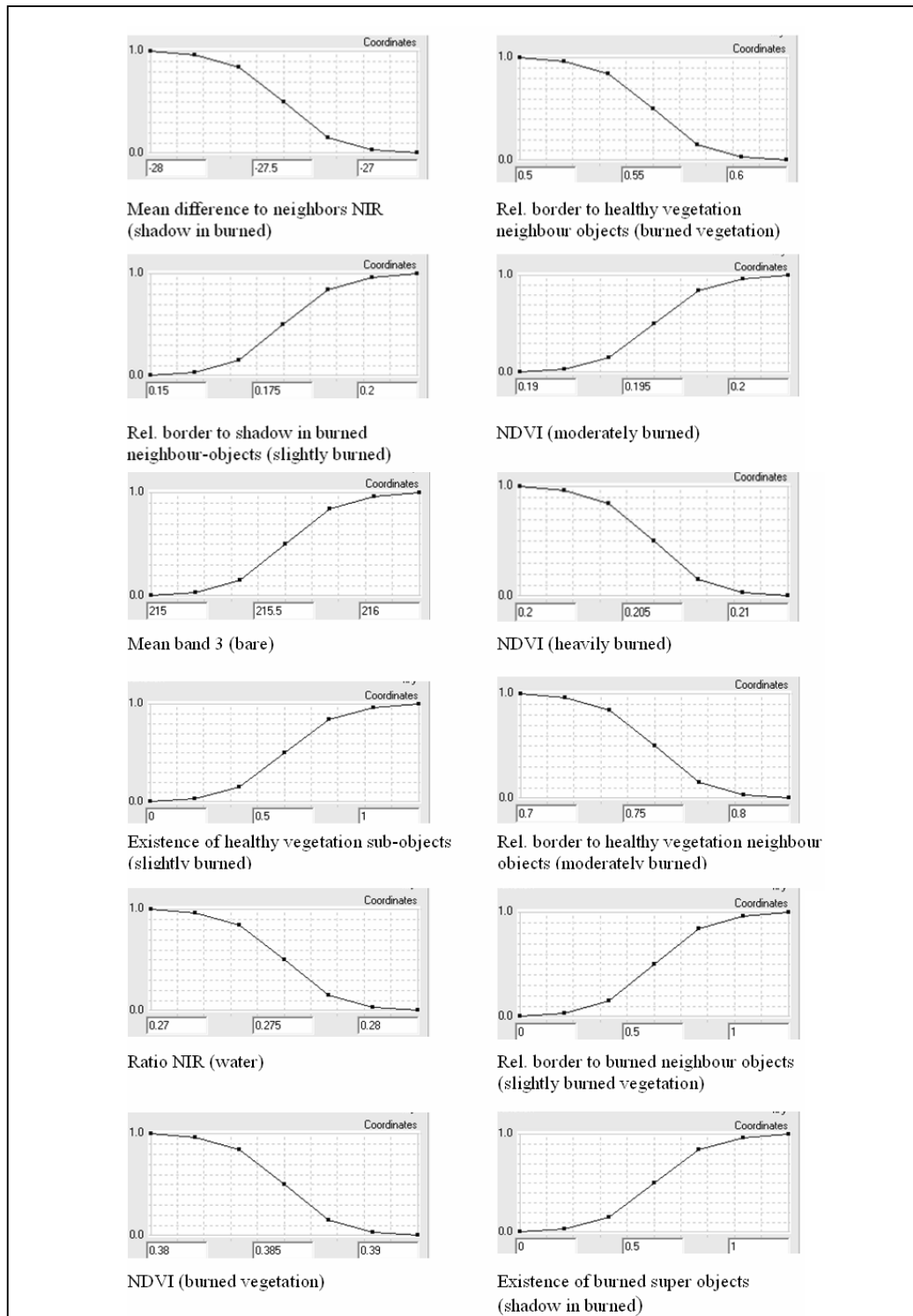


Figure 32 Membership functions of classes (x: feature value, and y: membership value)

The final results of the classification showed the three different classes of fire severity: *slightly burned*, *moderately burned* and *heavily burned* (Figure 33). In

Figure 33 (*image subset, **classification-based fusion), the results are shown for an image subset at different the different levels of segmentation.

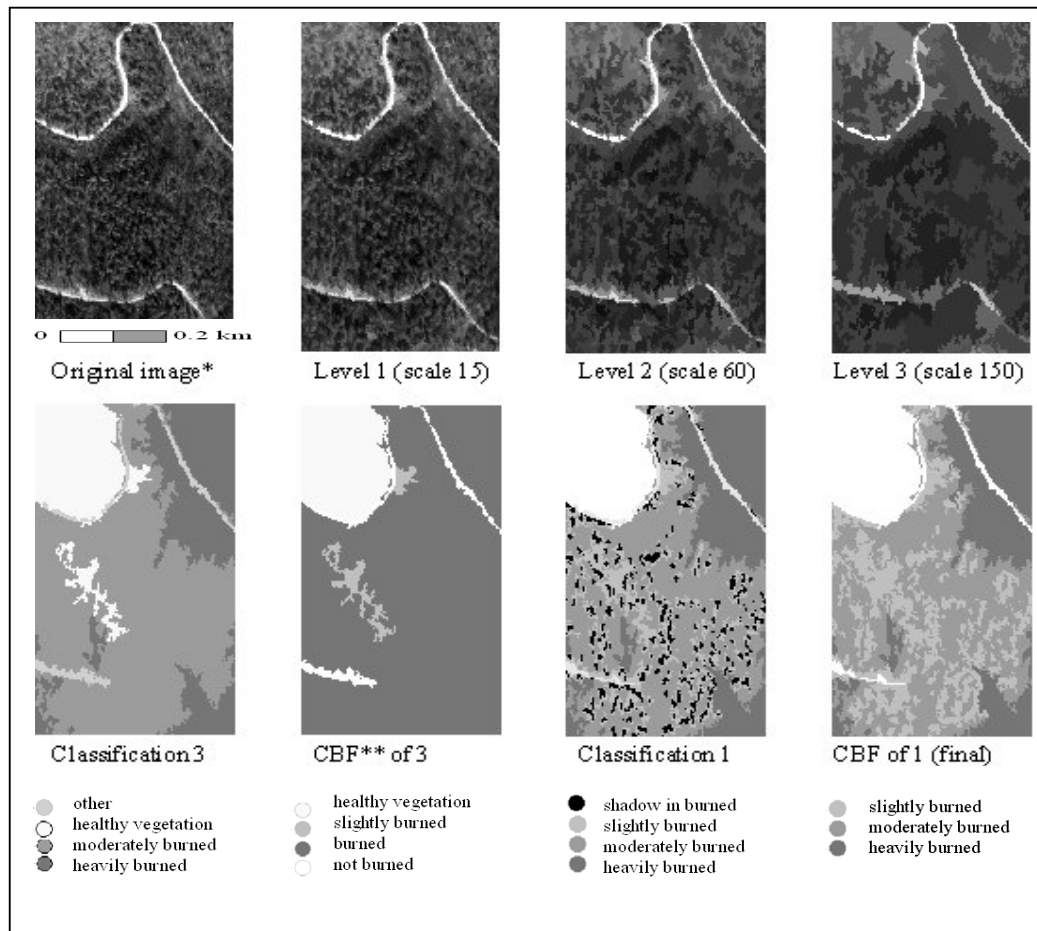


Figure 33 Segmentation levels and classification results

5.2.3 Results and discussion

An area of 0.89 km^2 , representing 42% of the total burned area, was classified as heavily burned, while an area of 0.72 km^2 , representing 35% of the total burned area, was classified as moderately burned. Fire affected areas with low fire severity accounted for only 0.47 km^2 , representing a remaining area of 23%.

According to the map produced from the classification (Figure 34), severely affected areas appeared to form large continuous regions while slightly and moderately affected areas created a mosaic. All three types of severity appeared in various aspects and slopes.

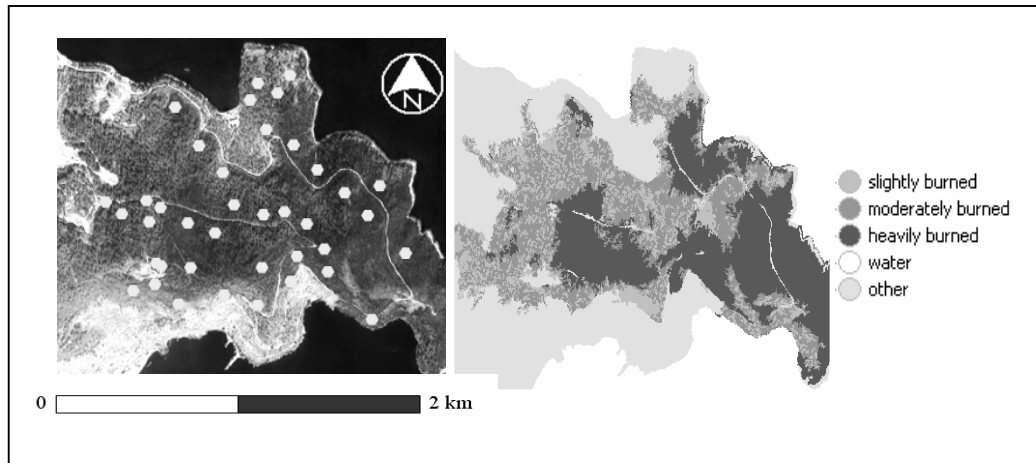


Figure 34 Left: the points used for accuracy assessment, right: the classification result

In order to assess the accuracy of the classification, field-collected data (as described before) from 36 widely dispersed plots were employed; Key and Benson (2002) suggest that burned areas smaller than 4 km² may be covered by as few as 20 to 40 plots. The threshold level of fire severity for each plot was adjusted, taking into consideration the factors that might directly influence surface reflectance (Key *et al.* 2002). Subsequently, three classes of fire severity were distinguished:

- Heavily burned (CBI >1.7: the crowns of most, if not all, trees were burned).
- Moderately burned ($1 < \text{CBI} \leq 1.7$: extensive burning of the understory, but no burning of at least the larger trees).
- Slightly burned ($\text{CBI} \leq 1$: the predominant vegetation comprised burned shrubs).

Another step was the selection of some image objects as sample objects. These sample objects were geographically matched (location and spatial extent) with the field collected plots. The polygon sampling units were initially conceptualized as previously segmented homogeneous objects and identified on Earth from the high spatial resolution imagery of Ikonos and the GPS points. Polygons sampling units were irregular in shape and differed in size (approximately 100 m²). In all cases, each of these polygons sampling units covered only one image object and was compared to the corresponded classified object (Table 15).

The overall classification accuracy was found to be 0.83, while the Kappa Index of Agreement (KIA) was 0.74. A closer examination of the accuracies of the individual classes revealed that the class ‘heavily burned’ was the most accurately identified, followed by the class ‘moderately burned’ and ‘slightly burned’ consecutively.

Table 15 Fire severity confusion matrix

User Class \ Sample	Slightly burned	Moderately burned	Heavily burned	Sum
Slightly burned	5	3	0	8
Moderately burned	2	11	1	14
Heavily burned	0	0	14	14
Sum	7	14	15	-
Producer’s accuracy	0.625	0.785	1	-
User’s accuracy	0.714	0.785	0.933	-
KIA per class	0.632	0.649	0.89	-
Overall accuracy	0.833	-	-	-
KIA	0.741	-	-	-

A closer look at the accuracy assessment results indicated that the misclassified objects were partially located within areas of dense canopy. This could be attributed to the inability of the optical sensors to penetrate dense canopy to detect fire affected areas, while the confusion between the ‘slightly burned’ and ‘moderately burned’ classes can be attributed to:

- the shadowing from tree crowns; and
- the relatively poor spectral information of Ikonos and the way this information is related to the fire severity classes resulted from the CBI scoring system.

The main limitation faced in this study was the impossibility of discriminating forest understory by the use passive optical remote sensing system. The discrimination of forest understory might probably be done with airborne LIDAR (Baltasvias 1999), which is able to penetrate the forest canopy and record accurate information of the ground fuel condition after fire.

Finally, the ability of the object-based classification to combine spectral with contextual information seemed to be the main advantage of the method not only for mapping fire severity, but also for deriving other information of particular interest to forest scientists and managers (such as object area, neighbouring and texture among others).

5.3 CHAPTER SUMMARY

In summary:

- An object-oriented model was developed using very high spatial resolution Ikonos imagery to map fire type on the Mediterranean island of Thasos.
- The main conclusion drawn is that object-oriented classification can be used to accurately distinguish and map areas of surface and crown fire spread (overall accuracy of 87% and Kappa Index of Agreement 0.74), especially that occurring in open Mediterranean forests.
- Classification accuracy was mainly affected by the density of the canopy. This could be attributed to the inability of the optical sensors to penetrate dense canopy to detect fire affected areas.
- The ability of the object-based classification to combine spectral with contextual information seemed to be the main advantage of the method not only when mapping fire type, but also when mapping the total burned area. Another advantage is its ability to derive other information of particular interest to forest scientists and managers.
- The performance of object-based classification in the mapping of fire severity by employing high spatial resolution Ikonos imagery was also evaluated.
- The general conclusion drawn was that object-based classification resulted in mapping 3 classes of fire severity. When assessed with field collected data the overall classification accuracy was estimated to be 83% while the KIA was 0.74.
- Classification accuracy percentages were consistently higher in the case of heavily burned areas.
- The shadowing from tree crowns, the poor spectral resolution of Ikonos together with the inability of the sensor to penetrate dense canopy were identified as being the main sources of classification confusion.
- A combination of the Ikonos imagery with other types of data such as RADAR and LIDAR, which are able to penetrate the forest canopy, might be worth investigating in the future.

CHAPTER 6: MAPPING VEGETATION RECOVERY USING QUICKBIRD IMAGERY

Chapter five presented an approach for fire type and severity mapping using object-oriented image analysis and employing the pre-processed Ikonos image. While this approach proved to be efficient, accurate, and objective for mapping direct and short term post-fire effects, producing accurate maps of long-term post-fire effects (i.e. forest regeneration and vegetation recovery), remains more of a challenge. This chapter will mainly investigate the possibility of mapping post-fire vegetation recover. Also, it is intended to understand better the interactions between vegetation recovery and fire severity. The methodology is presented in section one. Section two will discuss the results and the last section will summarize the chapter.

The occurrence of fire may be result of vegetation community structure and composition (White 1979). Until the 1960s, fire was seen as a disaster to be prevented if possible (Kornas 1958, Molinier 1968). Leopold *et al.* (1963) reported the negative aspects of fire suppression in ecosystems: excessive fuel build-up, homogeneous age structure and loss of diversity. Nowadays fire is considered a natural force in most plant communities and should be allowed to play a greater role where possible (Perry 1994). In Mediterranean ecosystems, fire is considered an important influence on the vegetation structure (Avrelo *et al.* 2001). Fire effects on plant and soil mainly vary according to fire severity (White *et al.* 1996, Perez and Moreno 1998).

Fire produces immediate effects on aerial vegetation, which become evident by total plant death or by partial destruction. High canopy trees may escape ground fires because the vertical discontinuity of fuel prevents fire reaching the canopies. Fire also has important and immediate effects on soil. Moreover, topography, aspect or slopes in the burned area have a considerable effect (Diaz-Delgado *et al.* 1998) either on plant recovery or plant damage.

After fire, autosuccession leads to recovery of preburn communities (Naveh 1975, Trabaud 1994). Unfortunately, interactions between fire severity and plant

regeneration, as well as those between topoclimatic and vegetation factors, are poorly known, especially at the scale of a whole, large fire.

Remote sensing imagery represents a potential tool for mapping direct post-fire effects (Caetano *et al.* 1994, White *et al.* 1996, Mitri and Gitas 2004a) and monitoring post-fire vegetation recovery (Diaz-Delgado and Pons 2001). This study try to investigate the possibility to map vegetation recovery after fire and to understand better the long term effects of fire severity on plant recovery after four years from the date of fire.

High severity of fire may cause irreversible plant damage, thus limiting plant regrowth. High plant damage would imply less ability for vegetation to recover. The use of remote sensing imagery can bring some insights into the overall relationship between fire severity and vegetation recovery at a larger scale (i.e. for large fires). Moreover, advances in this subject can aid the definition of new post-fire management criteria in burned areas under different fire severity levels.

The aim of this work is to map vegetation recovery after fire using object-based classification of QuickBird imagery. The specific objectives are:

- to distinguish between unburned forest and unburned shrub vegetation;
- to investigate the overall relationship between fire severity from one side and vegetation recovery from the other side; and
- to assess the accuracy of the produced results using field collected data.

Forest regeneration (mainly pine regeneration) was not observed in the field after the fire of 2000, except in very restricted areas. This could be attributed to the topographic and climatic conditions of the site. Therefore, any effort to map forest regeneration after in the area affected by the fire of 2000 was excluded. It should be noted that post-fire vegetation recovery are not only correlated with the severity of fire but also with other important factors such as topography, geology and climate.

6.1 METHODOLOGY

In the area that was burned in 2000, a fire severity map was previously (Chapter 5) built using a recent Ikonos image. In this study, only two classes of fire severity, namely, highly severe and moderately-slightly severe fire were generalized from the previous severity results. It should be noted that the map was manually improved taking into consideration the confusion errors and the burned area map produced by the Greek forest service. It is supposed to understand better the relationship severity-regeneration/recovery with less number of severity classes. Figure 35 represents the fire severity thematic layer (dark polygons represent severe fires and bright polygons represent slightly-moderately severe fires).

First, the Quickbird image was segmented and second, an object based classification was applied.

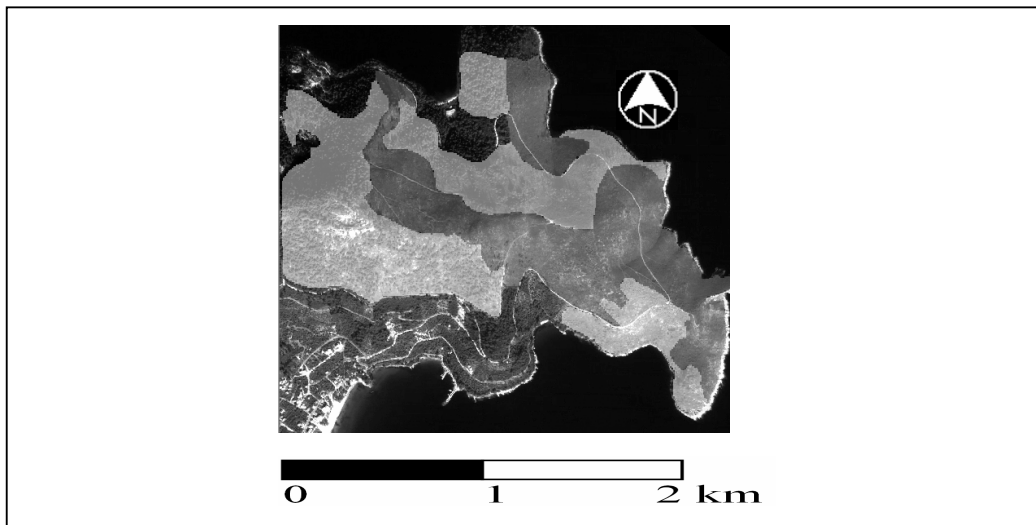


Figure 35 Fire severity thematic layer over QuickBird

6.1.1 Segmentation

Three different levels of image segmentation were created: level 1, level 2 and level 3. The segmentation parameters at level 1 employed an abstract scale of 10, shape factor of 0.1, and compactness-smoothness 0.5 (Figure 36).

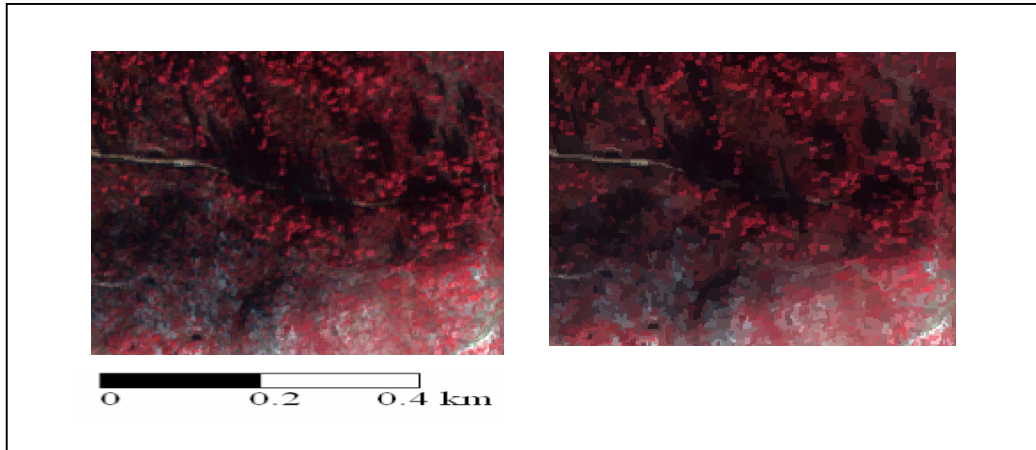


Figure 36 Subset of image in pixels (left) and segmented subset at level 1 (right)

Level 2 was created after classifying level 1 by a procedure called classification based fusion. This procedure produced new objects by merging objects from classes of same structure group into new objects (Figure 37).

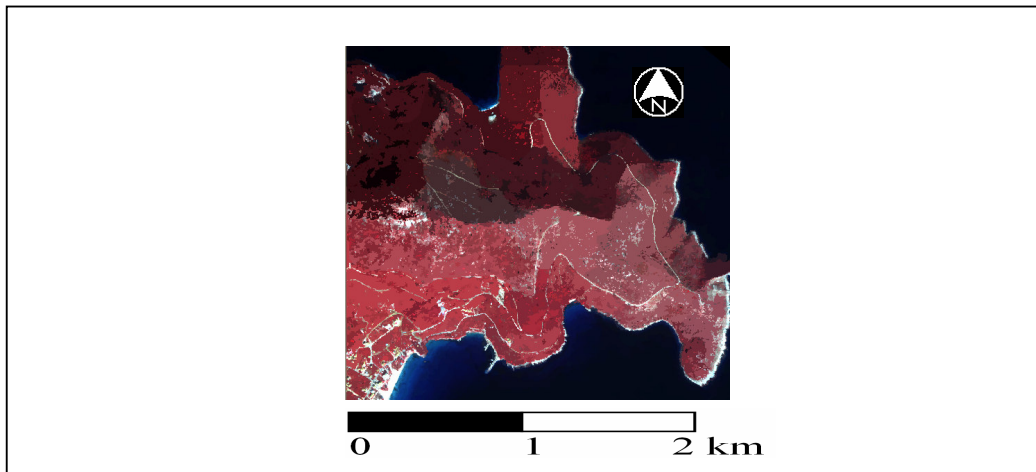


Figure 37 Image objects at level 2

At level 3 the image was segmented by employing only the thematic layer, which is the edited severity map. The reason to do that was to produce objects that fit with the polygons of fire severity at a large scale (Figure 38). The scale used for the segmentation of this level was 200.

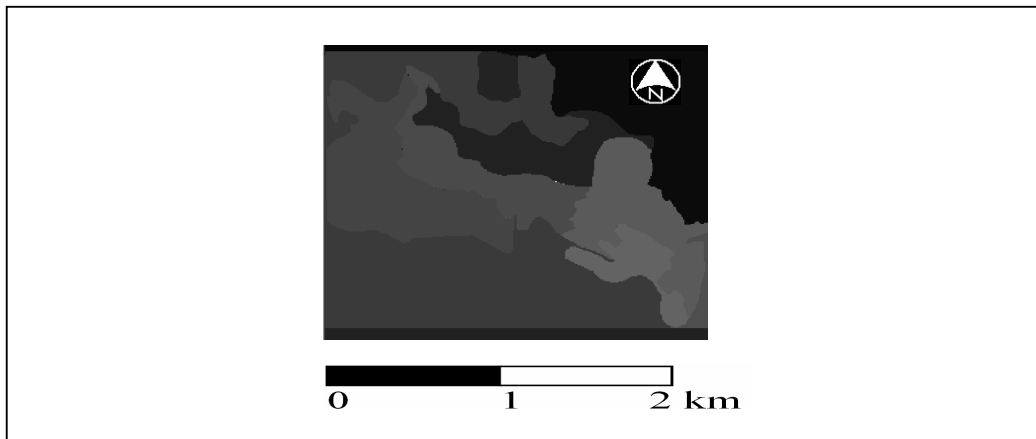


Figure 38 Segmented image at level 3

6.1.2 Classification

First, the segmented image at level 3 was classified. At this level classification was based completely on attribute data from the thematic layer. Three classes were created: slight-moderate fire, severe fire and other. Figure 39 shows the classification results at level 3 (severe fire in dark grey, and slight-moderate fire in light grey).

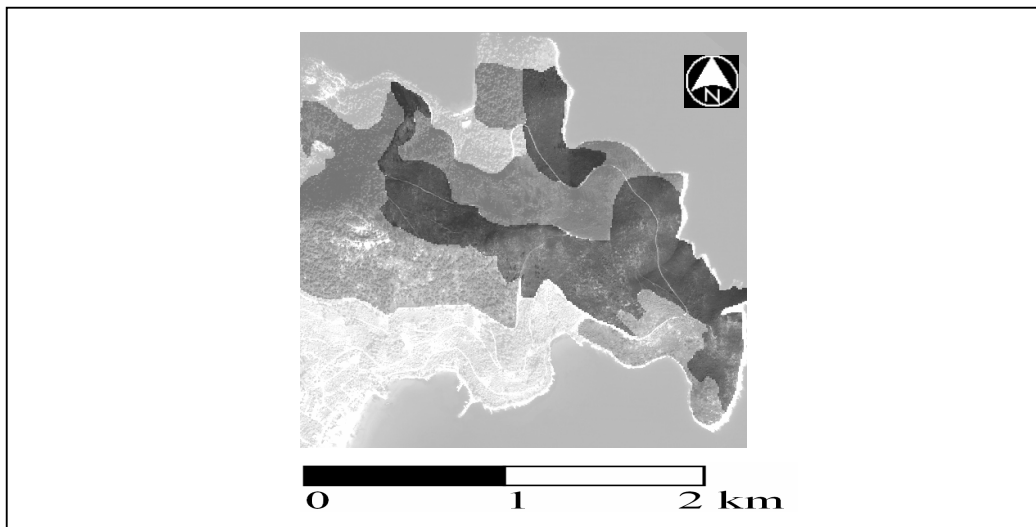


Figure 39 Classification results at level 3

Then, the segmented image at level 1 was classified. At this level, the first step was to distinguish between land and water. This was done by using a membership function of the feature NDVI for the class 'land' (Figure 40). The results map had two classes namely, land and water (Figure 41).

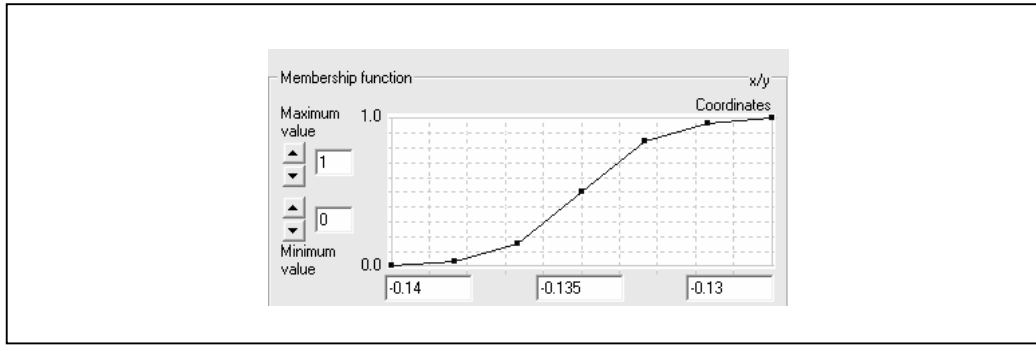


Figure 40 Membership function for class the class 'land'

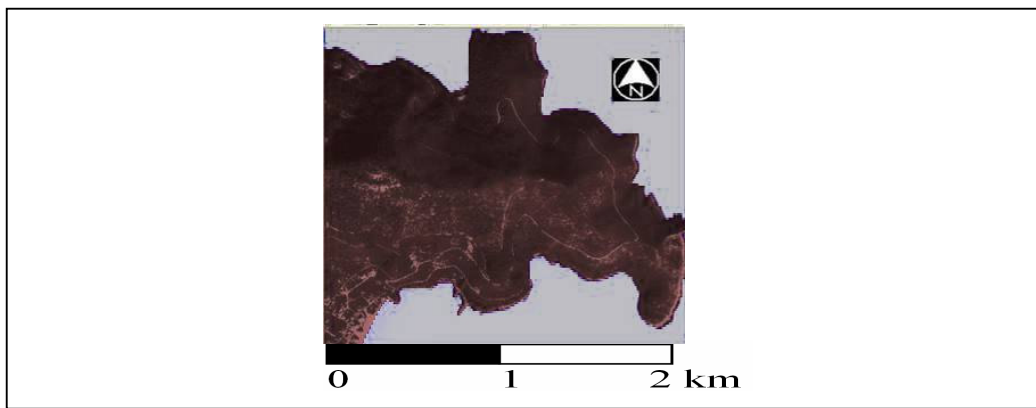


Figure 41 Classification results at level 1: 'land' (dark grey) and 'water' (bright grey)

The second step was to locate shaded areas and green vegetation. The ratio of band 1 showing high contrasts for these two categories was used for this classification (Figure 42). The ratio of band 1 is the band mean value of an image object divided by the sum of all spectral band mean values. The membership function of this feature for the class 'shadow' is shown in figure 43.

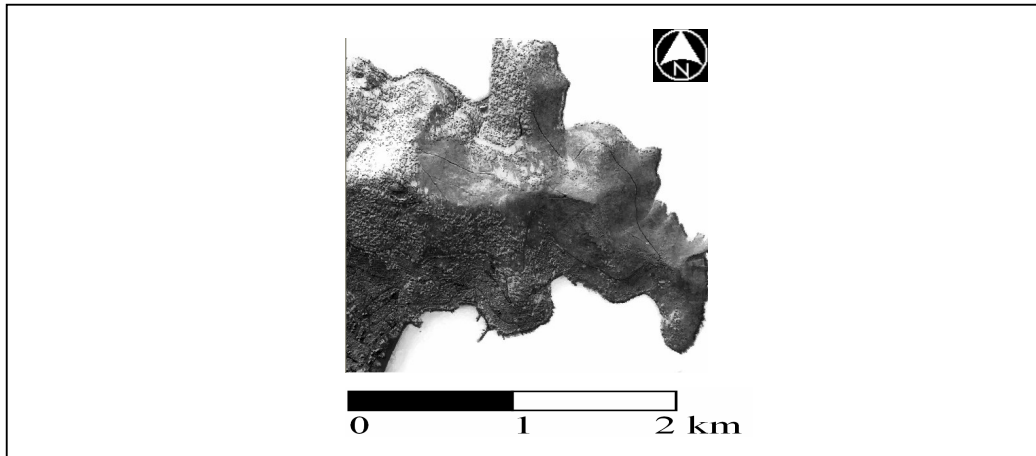


Figure 42 Image of ratio band 1 (bright colour shows shaded areas)

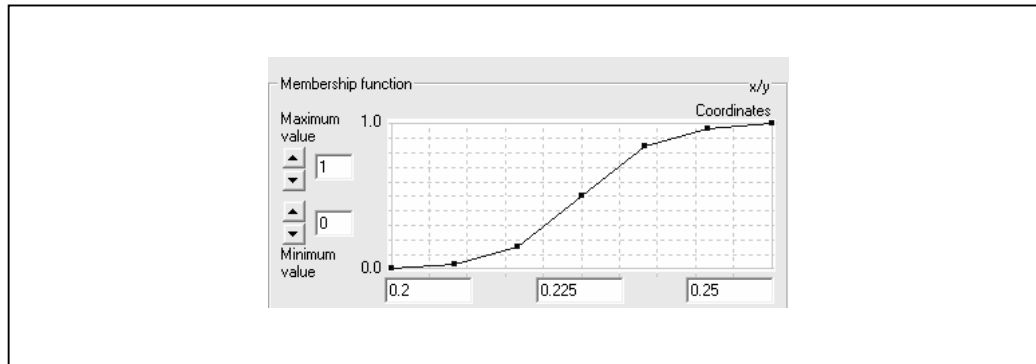


Figure 43 Membership function for the class 'shadow'

Green vegetation represented by a class called 'green' was described by a membership function of NDVI (Figure 44). The results showed a map of three land classes, namely, 'shadow', 'green vegetation' and 'other' (Figure 45).

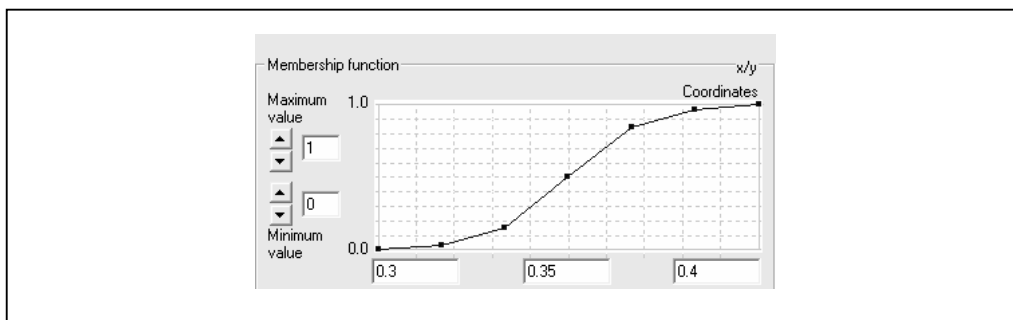


Figure 44 Membership function for the class 'green'

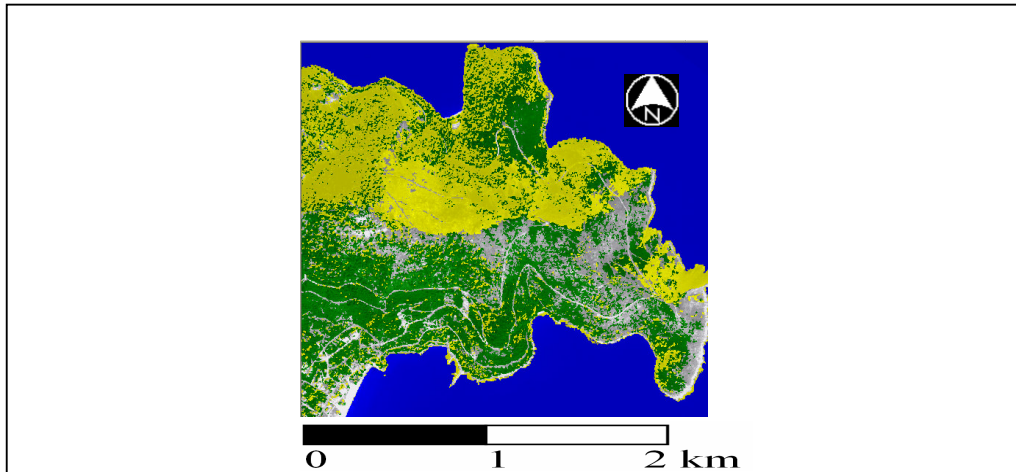


Figure 45 Classification of shadow (yellow) green vegetation (green) and other (grey)

The next step was intended to define different sub-classes for the parent classes of ‘green’, ‘shadow’, and ‘other’.

The parent class green was subdivided into two sub-classes: ‘green (canopy)’ and ‘green (shrubs and small tree)’. In the set of conditions for an object to be classified as ‘green (canopy)’ was:

If (existence of not burned super-objects) or (existence of ‘slight-moderate fire severity’ super-objects) and (relative border to ‘shadow’ neighbour objects is low) then objects are classified as ‘green (canopy)’.

The feature relative border is the ratio of the border of an object shared with neighbouring objects assigned to a defined class to the total border length. The feature relative border to ‘shadow’ neighbour objects was used for the class ‘green (canopy)’ (Figure 46). The class ‘shadow’ is resulted from projected shades of individual canopies or group of canopies.

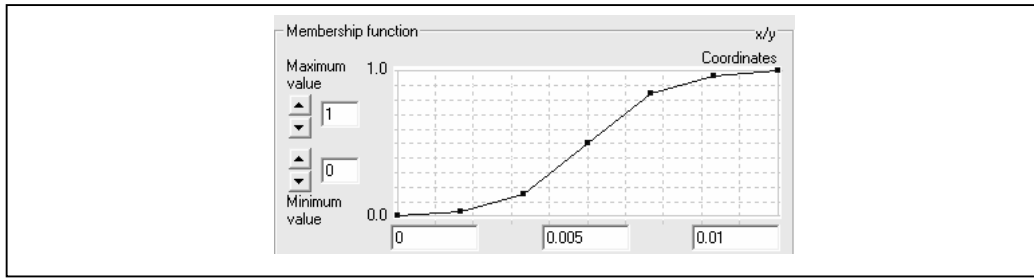


Figure 46 Membership function for the class ‘green (canopy)’

The rest of the objects that are also sub-classes of the parent class ‘green’ and were not satisfied by the previous conditions were classified as ‘green (shrubs and small trees)’. The class ‘shadow’ was subdivided into the following 4 sub-classes:

1. Shadow (bare)
2. Shadow (canopy)
3. Shadow (shrubs and small trees)
4. Shadow (other)

‘Shadow (bare)’ represents all the bare ground area that is located on a dark slope. ‘Shadow (canopy)’ spots areas where canopy shades are projected on the ground. ‘Shadow (shrubs and small trees)’ represents the small shaded areas caused by this kind of vegetation type. The class ‘shadow (bare)’ was described by the feature ratio of band 3 (Figure 47).

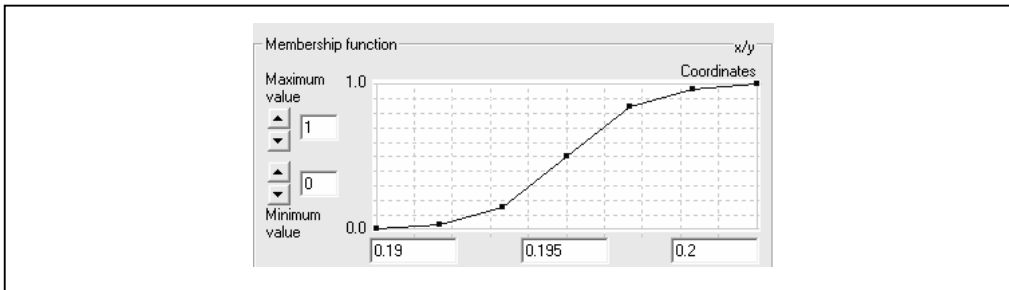


Figure 47 Membership function for the class ‘shadow (bare)’

‘Shadow (canopy)’ was described by a contextual feature called relative border to ‘green (canopy)’ neighbour objects (Figure 48). The class shadow (shrubs and small trees) was defined by the membership function of relative border to green (shrubs and small trees) neighbour objects (Figure 49).

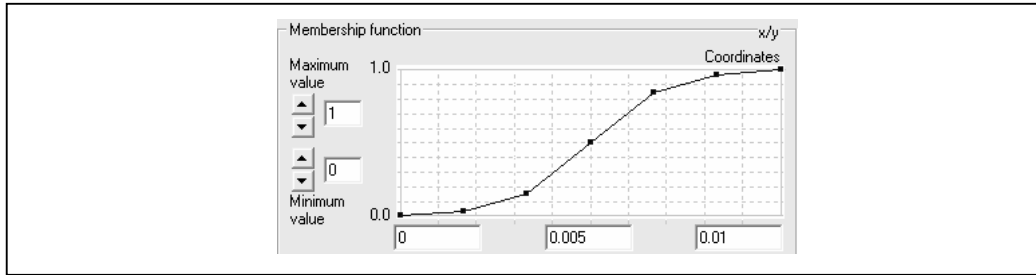


Figure 48 Membership function for the class 'shadow (canopy)'

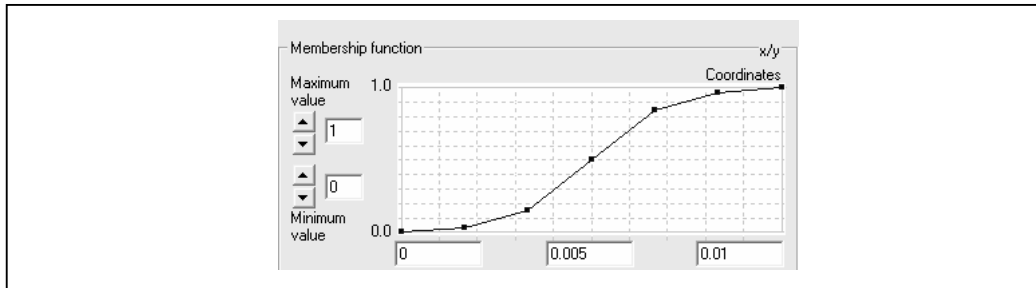


Figure 49 Membership function for the class 'shadow (shrubs and small trees)'

The class 'shadow (other)' describes the rest of the objects, which did not satisfy any of the previous conditions.

Finally, the parent class 'other' was subdivided into two sub-classes: 'other (bare)' and 'other (sparse vegetation)'. The class 'other (bare)' was described by a membership function of Mean band 3 (Figure 50), and the class 'bare (sparse vegetation)' described the rest of the objects that did not satisfy the conditions of the class 'other (bare)'. Figure 51 shows the classification results at level 1.

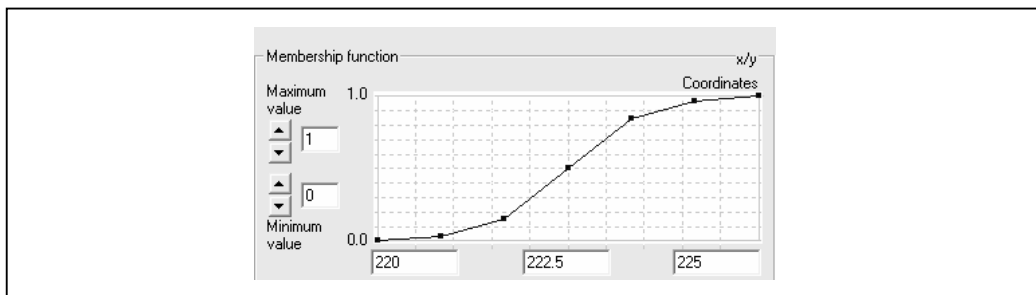


Figure 50 Membership function for the class 'other (bare)'

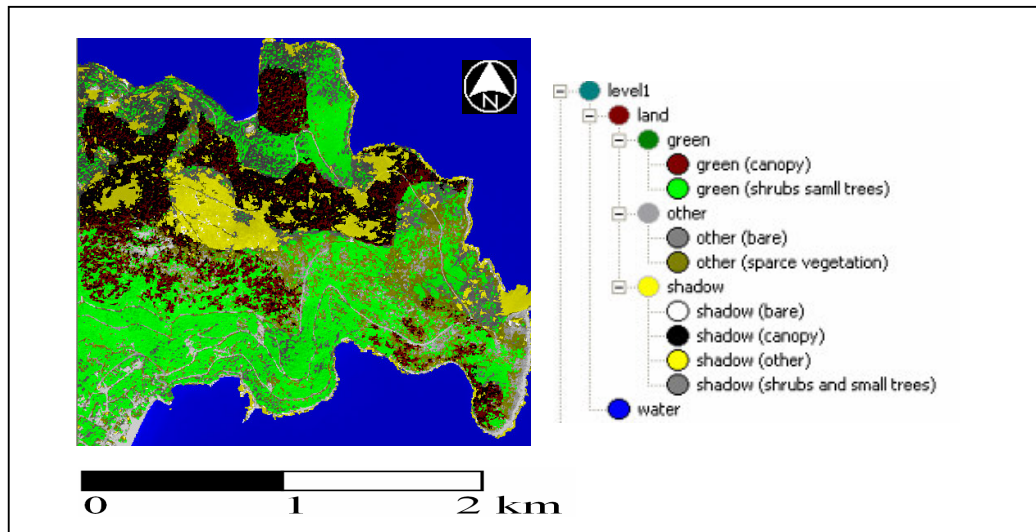


Figure 51 Classification results at level 1

A procedure called classification based segmentation was then applied to level 1 by merging classified objects according to defined structure groups and by creating a new level of these merged objects called level 2. The three defined structure groups were:

- structure group 1: ‘green (canopy)’ and ‘shadow (canopy)’;
- structure group 2: ‘green (shrub and small trees)’ and ‘other (sparse vegetation)’;
- structure group 3: ‘shadow (other)’.

It should be noted that objects belonging to the same structure group and neighbouring each others were merged into one object. Seven classes were created at level 2, these classes are the following:

1. Green canopy
2. Green canopy (slight-moderate fire)
3. Shrub
4. Shrub regeneration (slight moderate fire)
5. Shrub regeneration (severe fire)
6. Bare
7. water

‘Green canopy’ represents mainly *Pinus brutia* trees untouched by fire. ‘Green canopy (slight-moderate fire)’ represents mainly *Pinus brutia* trees that were affected by slight moderate fire. ‘Shrub’ represents unburned shrub cover. ‘Shrub regeneration (slight-moderate fire)’ represents shrub regenerated in areas affected by slight-moderate fire. Finally, ‘shrub regeneration (severe fire)’ represents shrub regenerated in areas affected by severe fire.

The class of ‘green canopy’ had the following set of conditions:

If (not existence of ‘slight-moderate fire’ super-objects) and [(existence of ‘green (canopy)’ sub-objects) or (existence of ‘shadow (canopy)’ sub-objects) or (existence of ‘shadow (other)’ sub-objects and relative border to ‘green (canopy)’ neighbour objects is higher than 0.6) or (existence of ‘green (shrubs and small trees)’ sub-objects and relative border to ‘green (canopy)’ neighbour objects is higher than 0.6)] then objects are classified as ‘green canopy’.

The class of ‘green canopy (slight-moderate fire)’ had the following set of conditions:

If (existence of ‘slight moderate fire’ super-objects) and [(existence of ‘green (canopy)’ sub-objects or (existence of ‘shadow (canopy)’ sub-objects) or (existence of ‘green (shrubs and small trees)’ sub-objects and relative border to ‘green canopy (slight-moderate fire)’ neighbour objects is higher than 0.6) or (existence of ‘shadow (other)’ sub-objects and relative border to ‘green canopy (slight moderate fire)’ neighbour objects is higher than 0.6)] then objects are classified as ‘green canopy (slight-moderate fire)’.

The class of ‘shrub regeneration (severe fire)’ had the following set of conditions:

If (existence of ‘severe fire’ super-objects) and [(existence of ‘green (shrubs and small trees)’ sub-objects or existence of ‘other (sparse vegetation)’ sub-objects or existence of ‘shadow (other)’ sub-objects or existence of ‘shadow (shrubs and small trees)’ sub-objects)] then objects are classified as ‘shrub regeneration (severe fire)’.

The class of ‘shrub regeneration (slight-moderate fire)’ had the following set of conditions:

If (existence of ‘slight-moderate fire’ super objects) and [(existence of ‘shadow (other)’ sub-objects and relative border to ‘green canopy (slight-moderate fire)’ neighbour objects is less than 0.6) or (existence of ‘green (shrubs and small trees)’ sub-objects) or (existence of ‘other (sparse vegetation)’ sub-objects) or (existence of ‘shadow (shrubs and small trees)’ sub-objects)] then objects are classified as ‘shrub regeneration (slight-moderate fire)’.

The class ‘bare’ had the following set of conditions:

If (existence of ‘other (bare)’ sub-objects) or (existence of ‘shadow (bare)’ sub-objects) then objects are classified as ‘bare’.

Finally if none of these conditions is satisfied then objects are classified as ‘shrub’. The membership function existence of ‘water’ sub-objects was used to describe the class ‘water’ at level 2. The final classification results are shown in Figure 52.

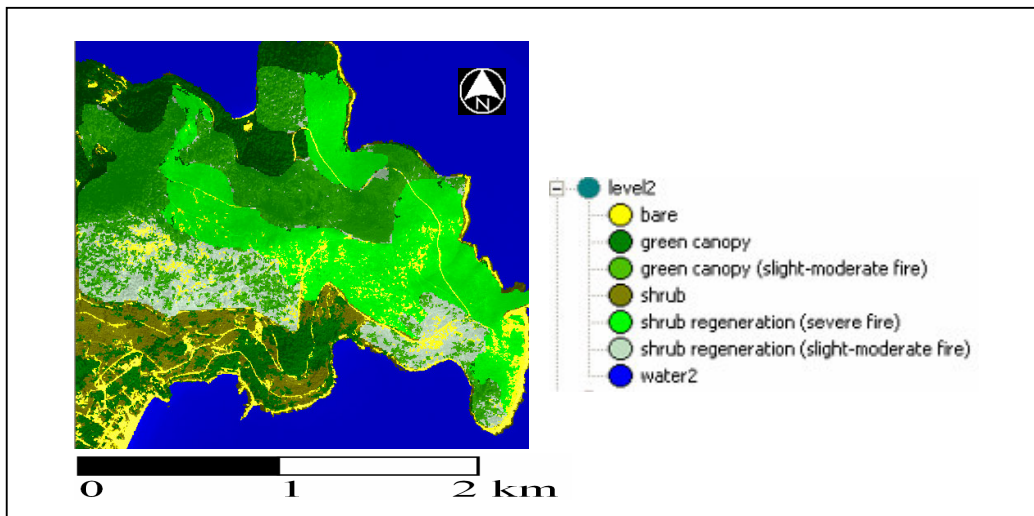


Figure 52 Final classification results at level 2

6.2 RESULTS AND DISCUSSION

Statistics were extracted from the produced map of vegetation recovery (Table 16). By referring to Table 16, it was observed that the class A (shrub regeneration after severe fire) has the largest number of image objects comprising 42% of the total recovered vegetation within the burned area. Class B (shrub regeneration after slight-moderate fire) represents 17% and class C (green canopy within slight-moderate fire) represents 41 % of the total regenerated area (Figure 53). After a more careful investigation of the results (Figure 54), it was observed a close neighbouring of ‘green canopy (slight-moderate fire)’ to ‘shrub regeneration (slight-moderate fire)’, and a distant neighbouring to ‘shrub regeneration (severe fire)’. This can be attributed to the absence of severe fire in areas where green canopy is still alive.

It should be noted that after approximately five years, 87% of the severe fire area was regenerated by shrub vegetation and almost complete absence of *brutia* regeneration that could be detected by the remotely sensed data. Also, a total vegetation cover of 88% was mapped within the area that was slightly-moderately burned.

By visually comparing the produced results to the data collected from the field, it was found that fires of slight-moderate severity produced a highly selective mortality, depending on the species and size of each individual. While fire of high severity, has killed all individuals, independently of species or size. In this fire, mortality of *P. brutia* was very high, especially in areas affected by severe fire. The percentage of dead pine individuals was over 90%. Forest regeneration of pine trees was rarely observable in the field and thus could not be mapped by satellite imagery.

The shrub understory in the study area is floristically rich, comprising various evergreen sclerophylls (maquis) species (e.g. *Quercus coccifera*, *Pistacia terebinthus*, *P. lentiscus*, *Arbutus unedo*) as well as phryganic subshrubs (e.g. *E. manipuliflora*, *Cistus creticus*). Most shrub vegetation was also burned in all types of fire severity considered. Nevertheless, due to their sprouting ability many of them resprouted and were able to recover after fire.

Variability observed in post-fire recovery response can be partially explained by fire severity and by the dominant species or land cover. Main differences among the most abundant land covers (*P. brutia* and shrub vegetation) indicated a capacity of an immediate recovery response for the shrub vegetation due to resprouting ability, and very low regeneration capacity of areas dominated by *P. brutia*.

The fire was a driving force in landscape homogenization. The fire producing severely burned patches favoured the colonization of invasive, fire tolerant shrub species sometimes at the expense of rare/endemic species less tolerant to post-fire conditions. The landscape homogenization constituted a new scenario for the study area ecosystem in which biodiversity is threatened.

Table 16 Classification statistics

Class	Number of objects	Sum area (km ²)	Mean relative border to A	Mean relative border to B	Mean relative border to C
A = shrub regeneration (severe fire)	1218	0.77	0.85	0.01	0.02
B = shrub regeneration (slight-moderate fire)	742	0.30	0.04	0.07	0.72
C = green canopy (slight-moderate fire)	335	0.75	0.02	0.3	0.62

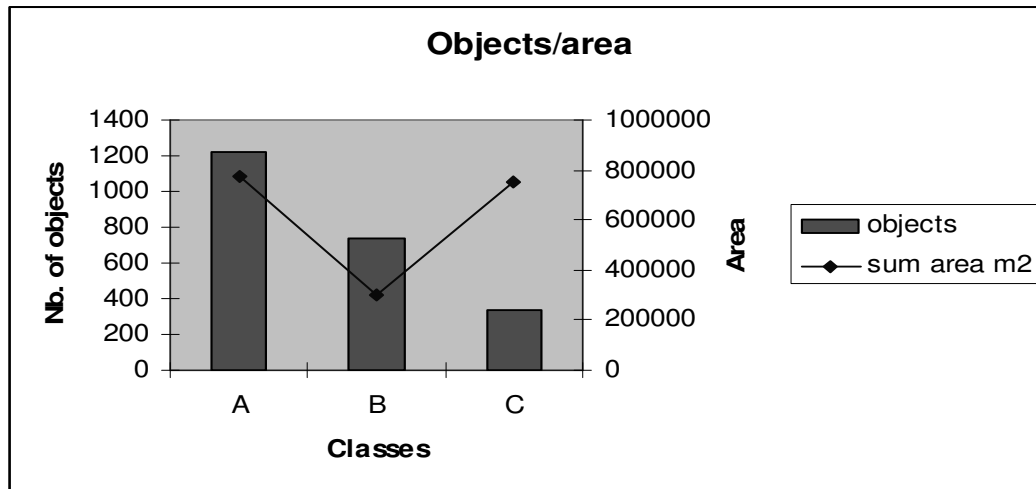


Figure 53 Objects-area ratios

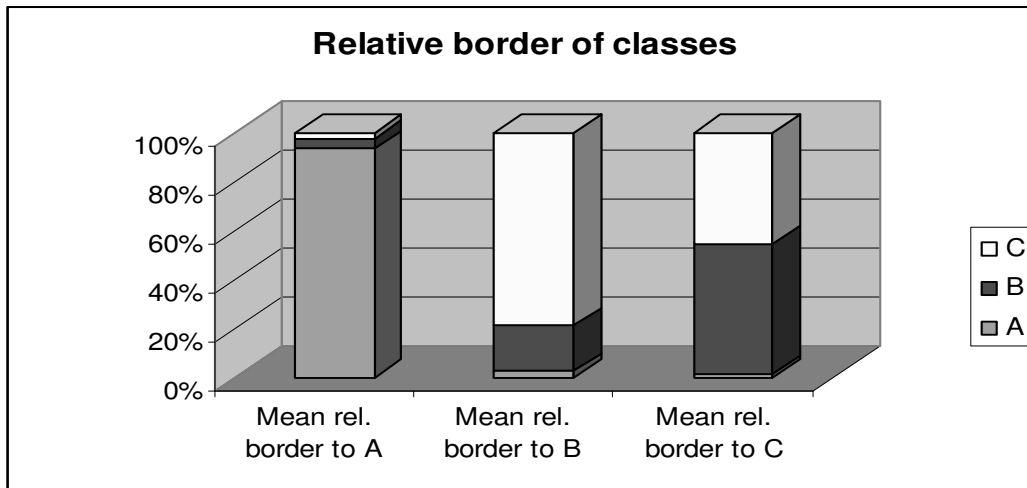


Figure 54 Relative border of classes

The final map was compared to 52 plots surveyed in the field in order to assess the accuracy of the results. An error matrix was produced (Table 17) and accuracy totals were extracted (Table 18).

The overall object-based classification accuracy of the total of classification was estimated to be 86% and the overall Kappa statistics was 0.83. Producer's and user's accuracy showed that vegetation recovery was mapped with higher accuracies in areas of severe fire and with lower accuracies in areas of slight-moderate fire. Some confusion was reported between 'green canopy (slight-moderate fire)' and 'shrub regeneration (slight-moderate fire)' due to the low spectral information of the QuickBird image. Because of the absence of green canopy in areas of severe fire, the class 'shrub regeneration' was mapped with high accuracy. It should be noted that the use of thematic layer of fire severity helped in locating potential areas of vegetation regeneration therefore high accuracies of vegetation regeneration mapping were recorded.

An important issue to be discussed is that the high spatial resolution imagery helped in identifying even small spots of vegetation recovery. However the low spectral confusion of the image did not make it always possible to distinguish in high accuracy between green canopy and shrub regeneration. Therefore high spectral resolution

imagery is needed to improve the results when mapping forest regeneration and vegetation recovery.

Table 17 Error Matrix

User class \ Sample	Bare	green canopy	green canopy (slight-moderate fire)	shrub	shrub regeneration (severe fire)	shrub regeneration (slight-moderate fire)	water	total
Bare	4	0	0	0	0	0	0	4
green canopy	0	4	0	0	0	0	0	4
green canopy (slight-moderate fire)	0	0	14	0	2	1	0	17
Shrub	0	1	0	3	0	0	0	4
shrub regeneration (severe fire)	0	0	1	0	12	0	0	13
shrub regeneration (slight-moderate fire)	0	0	2	0	0	4	0	6
Water	0	0	0	0	0	0	4	4
Total	4	5	17	3	14	5	4	52

Table 18 Accuracy statistics

User class \ Sample	bare	green canopy	green canopy (slight-moderate fire)	shrub	shrub regeneration (severe fire)	shrub regeneration (slight-moderate fire)	Water
Producer	1	0.8	0.8235	1	0.8571	0.8	1
User	1	1	0.8235	0.75	0.923	0.6667	1
Hellden	1	0.8889	0.8235	0.857	0.8889	0.7273	1
Short	1	0.8	0.7	0.75	0.8	0.5714	1
KIA per class	1	0.7833	0.7378	1	0.8095	0.7739	1
Overall Accuracy	0.8654						
KIA	0.8298						

6.3 CHAPTER SUMMARY

In summary:

- Unburned forest was successfully distinguished from unburned shrub as a first step before vegetation recovery mapping.
- Pine forest regeneration was almost absent, while forest survival was successively distinguished from vegetation recovery.
- Variability observed in post-fire vegetation recovery response can be explained by fire severity and by the dominant species or land cover. Within vegetation recovery, shrub vegetation showed immediate recovery capacity after fire due to resprouting ability, while forest regeneration had very low recovery capacity.
- In this fire, mortality of *P. brutia* was very high. The percentage of dead individuals was over 90%, and most shrub vegetation was also burned in all types of the considered fire severity classes.
- The fire was a driving force in landscape homogenization. The fire producing severely burned patches favoured the colonization of invasive, fire tolerant species sometimes at the expense of rare/endemic species less tolerant to post-fire conditions.
- When comparing the final forest regeneration map to field data, it was found that the overall classification accuracy was estimated to be 86% and the overall Kappa statistics was 0.83. Few classification confusions were observed between survived forest and recovered vegetation.
- High spectral resolution imagery is needed to improve the results when mapping vegetation recovery especially for distinguishing among different species.

CHAPTER 7: MAPPING FOREST REGENERATION AND VEGETATION RECOVERY BY EMPLOYING HYPERSPECTRAL REMOTE SENSING

The potential use of very high spatial resolution imagery for mapping the type and the severity of fire and vegetation recovery was previously investigated. However, these high spatial resolution image data containing limited spectral information lead often to classification errors between similar vegetation classes. It was found that high spectral resolution imagery is needed to improve the results when mapping forest regeneration and vegetation recovery especially when distinguishing among different species. As a result, hyperspectral imagery with the typical high number of bands could be used due to their narrowband spectra. Besides, there is an increasing use of handheld spectroradiometer data for “ground truthing” of hyperspectral imagery, as well as conducting pilot studies where hyperspectral data may eventually be used. In section one, field spectrometry measurements were employed to investigate the spectral properties of naturally regenerated vegetation after fire. Section two will aim to map post-fire forest regeneration and vegetation recovery using Hyperion hyperspectral imagery.

Forest regeneration and vegetation recovery are the key measures to ensure forest sustainability. Monitoring post-fire forest regeneration and vegetation recovery is important to understand the need for future prescribed burns, to establish post-fire forest management, to design re-vegetation programs to reduce soil erosion and land degradation, and finally to monitor biodiversity (Di Castri and Mooney 1973, Le Houerou 1987, Naveh 1991, Keely 2000, Twele 2004).

The development of new hyperspectral remote sensing instruments, both airborne and spaceborne, has provided an opportunity to study vegetation recovery after wildfire (Riano *et al.* 2002). Moreover, handheld spectroradiometers have been frequently used to collect “ground truth” information (Shaw *et al.* 1998, Schmidt *et al.* 2004).

Monitoring post-fire forest regeneration and vegetation recovery can greatly benefit from the use of remote sensing therefore the use of spectral data for species

discrimination. The direct remote sensing of individual organisms or species assemblages requires not only detailed spatial information but also spectral information of regenerating species after fire. Spectral analysis done by Twele and Barbosa (2003) revealed that vegetation regeneration is related to gradual spectral changes over time with different vegetation communities following different spectral pathways. Until present, little research has been done on spectral response related to early stand development (Nilson and Peterson 1994, Pouliot *et al.* 2002).

A number of recent studies have indicated the advantages of using discrete narrowband data from specific portions of the spectrum, rather than broadband data, to obtain the most sensitive quantitative or qualitative information on vegetation characteristics (Elvidge and Chen 1995, Carter 1998, Blackburn and Steele 1999, Thenkabail *et al.* 2000, Thenkabail *et al.* 2004a, 2004b). Hyperspectral data for vegetation studies proved to be a progress in detecting plant stress (Carter 1994, 1998), measuring chlorophyll content of plants (Blackburn and Steele 1999), identifying small differences in percent green vegetation cover (McGwire *et al.* 1999), and extracting biochemical variables such as nitrogen and lignin (Curran 1994). Also, hyperspectral data represent an important input for discriminating land cover types (Janetos and Justice 2000), analyzing crop moisture variations (Penuelas *et al.* 1993, 1995), and leaf pigment concentrations (Blackburn and Steele 1999), modelling quantitative biophysical and yield characteristics of agricultural crops (Thenkabail 2003), improving detection changes in sparse vegetation (Elvidge *et al.* 1993, Lyon *et al.* 1998), and assessing absolute water content in plant leaves (Bauer *et al.* 1981).

In the next section, field hyperspectral measurements were employed to investigate the spectral properties of naturally regenerated vegetation after fire. The section after will aim to map post-fire forest regeneration and vegetation recovery using Hyperion hyperspectral imagery taking into account the findings of the first section. The area under investigation has a part that was burned in the fire of 1984, 1985 and another part that was burned in the fire of 1989. The major forest species present are *P. brutia* and *P. nigra*. In addition to the forests, other types of Mediterranean shrub vegetation are also present (Gitas 1999, Spanos *et al.* 2000).

7.1 ANALYSIS OF FIELD SPECTROMETRY DATA

Field spectrometry measurements were employed to investigate the spectral properties of naturally regenerating pine (*brutia* and *nigra*) and recovering shrub (different species) on the Mediterranean island of Thasos. Because of the great spectral variability for vegetation, if only very few well-placed wavebands could account for most of the spectral variability in forested landscapes then recording in less wavebands becomes more desirable.

In the summer periods of 2002, 2003 and 2004, spectral measurements of regenerating *P. brutia* and *P. nigra* were obtained. Measurements were taken for regenerating trees at different ages. According to Spanos *et al.* (2000) the annual height growth of *P. brutia* showed linear regression kinetics throughout the 5 (and conceivably 9) year-long post-fire period, with a yearly increment of 17 cm. As for *P. nigra*, the tree is moderately fast growing (30-70 cm/year). Data were collected from *P. brutia* of 10 years and above (this group was called mature *brutia*) and from younger trees of the same specie. Also, measurements were taken from *P. nigra* trees of 10 years and above (the so called group of mature *nigra*) and from younger trees of the same specie.

A FieldSpec Pro VNIR spectrometer (350-1050 nm range; 3 nm spectral resolution; 1.4 nm spectral sampling interval) was employed. A 10° foreoptic was used, and the spectrometer was mounted on a stand of 0.75 m above the target giving a 16.628 cm radius of FOV. At least five measurements were recorded systematically for each target and normalized against a calibrated white reference panel. Over a fifty hyperspectral data samples were gathered for the two pine species (mature and young) and for the shrub species *Quercus coccifera*, *Erica manipuliflora*, *Laurus nobilis*, *Arbutus unedo* and *Cistus incanus* and fern.

To reduce the effects of low sun angle, shadow and longer atmospheric pathlengths, scans were recorded within two hours either side of the solar noon and sky conditions were clear for all sampling times.

The reflectance spectra in the database were averaged within the same category (age and specie), and then they were resampled by selecting every three values from 0.35 to 1.1 μm and averaging them to one value to reduce the volume of data for analysis and to reduce noises. All values below 0.4 μm and above 0.9 μm were removed due to the large noises. Previous studies (Thenkabail *et al.* 2000, Broge and Leblanc 2000, Thenkabail *et al.* 2002) have shown that wavebands in immediate neighbourhood of one another provide similar information, hence becoming redundant. Also, the first spaceborne hyperspectral sensor, Hyperion, onboard Earth Observing-1 (EO-1) carries a 10-nm wide wavebands in 400- 2500 nm. Given these facts, the data were then aggregated into 60 narrowbands, each of 10.0 nm wide wavebands. The wavebands centres begin at 428 nm and progressively centred at every additional 10-nm such as at 438 nm, 448 nm, and so on until 988 nm. The filtered spectra were used to build a spectral library with Envi (version 4.1).

7.1.1 Pine spectral characteristics

In this study, field spectral measurements were performed on two kinds of pine trees namely, *Pinus brutia* and *Pinus nigra*. The east Mediterranean pine (*P. brutia*) is a tree of great ecological and economic importance for the eastern Mediterranean region (Nahal 1983, Nahal 1984) and a significant forest tree species of the northeastern coast and several Aegean Sea islands of Greece. It grows prolifically in well lit conditions and is adapted to infertile soils and dry climates (Panetsos 1981). The geographical range of *P. brutia* extends from the Greek Aegean islands through Turkey to Lebanon and northern Iraq (Critchfield 1966). *P. nigra* (generally called Black Pine in Europe), is a variable species of pine, occurring across southern Europe from Spain to the Crimea, and also in Asia Minor, Cyprus, and locally in the Atlas Mountains of northwest Africa. It is found at elevations ranging from sea level to 2 000 m, most commonly from 250-1 600 m (Panetsos 1981).

The aim of this work was to investigate the hyperspectral characteristics of post-fire pine regeneration. The specific objectives are:

1. to locate the wavebands that best characterize the pine of the two different species; and

2. to locate the wavebands that best characterize young and mature pine of the two specific species.

7.1.1.1 Methodology

There is no single best approach in hyperspectral analysis to determine the optimal number of bands that provide the best estimates of forest or vegetation characteristics. Past research has incorporated reflectance from individual narrowbands (Mariotti *et al.* 1996), various ratio indices (Aoki *et al.*, 1981, Carter 1994, Lichtenthaler *et al.* 1996, Lyon *et al.* 1998), derivatives of reflectance spectra (Curran *et al.* 1991, Elvidge and Chen 1995), or combinations of these (Thenkabail *et al.* 2000, 2002), and linear mixture modelling approach (McGwire *et al.* 1999, Mass 2000).

In this study, the optimal wavebands that best characterize *P. brutia* and *P. nigra* were determined based on a comprehensive analysis of all samples taken from young and mature trees of both species using Principal Component Analysis (PCA), correlation analysis and Stepwise Discriminant Analysis (SDA). All statistical analyses were performed using the software SPSS.

Principal Component Analysis (PCA) deals with all the variability in a set of variables. PCA helps in determining 1) wavebands that have greatest influence in PC1, PC2 and so on, and 2) *percent* variability explained in each PCA. The analysis was applied on the full set of dataset. The results (Table 19) showed that the first three principal components (PCs) explained 96% of the variability in the various pine trees. Thereby, in order to explain the 96% of the variability, the 60 wavebands were reduced to three PC wavebands (PC1–PC3), thus reducing data volume by approximately 96%.

Table 19 Total Variance explained

Component	Initial Eigenvalues		
	Total	% of Variance	Cumulative %
1	42.870	71.450	71.450
2	11.539	19.231	90.681
3	3.728	6.214	96.895

The scree plot (Figure 55) was useful to determine the optimal number of components. The eigenvalue of each component in the initial solution was plotted. The components on the steep slope were to be extracted, while the components on the shallow slope contribute little to the solution. The last big drop occurred between the second and the third components, so using the first three components was a good choice.

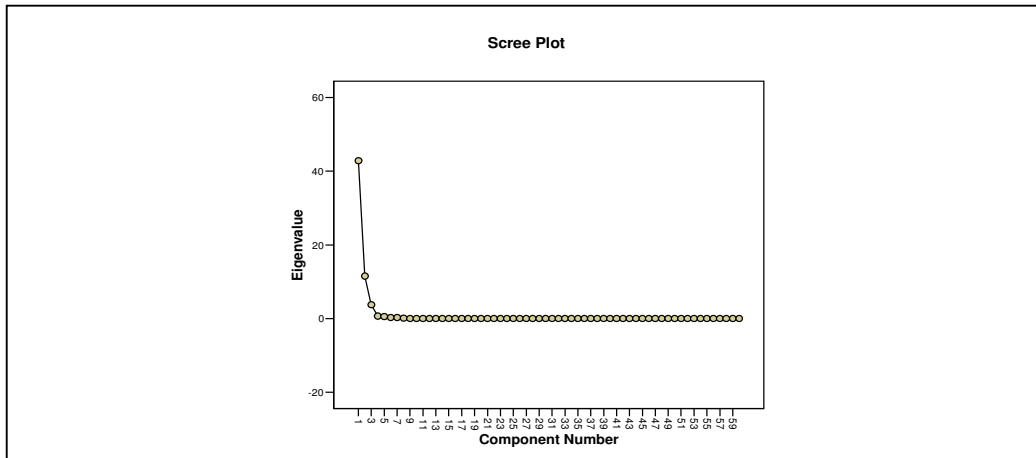


Figure 55 Scree plot of the PCA

The new PC wavebands were computed using factor loadings (or eigenvectors) of each of the 60 wavebands and multiplying the factor loadings with their respective waveband reflectivity. The wavebands that provided the highest factor loadings were listed for the Principal Component PC 1, PC 2 and PC 3 (Table 20). The importance of the waveband was judged by its factor loadings. The PC1 had centred wavebands between 784 nm and 967 nm. This implied that these wavebands had the highest factor loadings from all of the 60 wavebands in the entire spectral range of 428-988 nm with 72% of variability.

It was observed that the Near Infra-Red (NIR) bands dominated the PC1, with the blue bands dominating the PC2 (19% of variability). The bands between green and red dominated PC3, explaining an additional 6% of the variability. All these results indicated the overall importance of visible and NIR wavebands.

Table 20 Rotated Component Matrix for pines

	PC1	PC2	PC3
479.311	-	0.981	-
591.037	-	-	0.9
794.641	0.943	-	-
865.941	0.955	-	-
907.288	0.966	-	-
957.730	0.948	-	-

Extraction Method: Principal Component Analysis. Rotation Method: Varimax with Kaiser Normalization.

Correlation analysis measures how variables or rank orders are related. Pearson's correlation coefficients, with their significance levels, were computed (Table 21). A very high correlation (R^2) between any two wavebands indicates similar or redundant information. The areas of lowest correlation between wavebands indicate that the two bands contained unique information about the target plant.

Table 21 Wavelengths (nm) correlation for pines

428.441	Wavebands with the least redundancy. $R^2 < 0.08$
479.311	
591.037	
672.346	
702.917	
957.738	
967.828	

Stepwise Discriminant Analysis (SDA) was used to discriminate or separate pine trees of different ages and species using Wilk's lambda. At each step, if a band in the model failed to meet the criterion (f test), the worst variable was removed. Otherwise, the band that contributed most to the discriminatory power of the model was entered. When all variables in the model met the criteria and the remaining variables were excluded, the stepwise selection process was stopped. The values of Wilk's lambda were indicative of separability or discriminatory power of spectral bands (i.e., the less the value of Wilk's lambda, the greater spectral differentiation between the species types). The most frequently occurring wavebands that achieved the optimal Wilk's lambda values for trees were centred at: 458.961, 621.506, 733.489, 957.738, and 988.048 nm.

7.1.1.2 Results and discussion

Careful data analysis of PCA, variable correlations, and SDA showed 14 optimal bands (in 400–900 nm spectral range) that best characterize and classify pine trees of different age and specie (Table 22).

Table 22 Reflectance values in the 14 selected wavebands for pines

	brutia young	brutia mature	nigra young	nigra mature
428.441	0.016174	0.042095	0.02912	0.016538
458.961	0.022023	0.034823	0.027416	0.025831
479.311	0.023438	0.039809	0.029977	0.025766
591.037	0.086857	0.073467	0.0575	0.059613
621.506	0.059996	0.069342	0.051279	0.050325
672.346	0.033676	0.062163	0.035335	0.035084
702.917	0.140824	0.13207	0.106823	0.118864
733.489	0.3111	0.2676	0.273509	0.316694
794.641	0.362848	0.325583	0.336054	0.390634
865.941	0.372931	0.345643	0.348922	0.40488
907.288	0.373412	0.343685	0.355518	0.40371
957.738	0.356778	0.30468	0.326634	0.346761
967.828	0.349454	0.352995	0.302467	0.352498
988.048	0.348882	0.335748	0.312276	0.340473

A significance (sig.) analysis of the optimal bands from the pine results was performed using paired-samples *t* test (Table 23). A study of this type consisted of two measurements taken on different pine species or different age. If the change of specie or age had no effect, the average difference between the measurements is equal to 0 and the null hypothesis holds. On the other hand, if the change of specie or age did have an effect (intended or unintended), the average difference is not 0 and the null hypothesis is rejected. The Paired-samples *t* test procedure is used to test the hypothesis of no difference between two variables. Since the significance value for change was less than 0.05, it was concluded that the difference in reflectance is not due to chance variation, and can be attributed to the difference in age and species.

Table 23 Significance (2-tailed) analysis

	<i>T</i>	Sig. (2-tailed)
young - mature (<i>brutia</i>)	-4.987	0.001
young (<i>brutia</i>) – young (<i>nigra</i>)	3.700	0.003
mature (<i>brutia</i>) - mature (<i>nigra</i>)	-4.134	0.001
young - mature (<i>nigra</i>)	-3.153	0.008

The 14 wavebands previously listed for pine trees have a high level of relevance in providing various pine regeneration and specie characteristics (Figure 56).

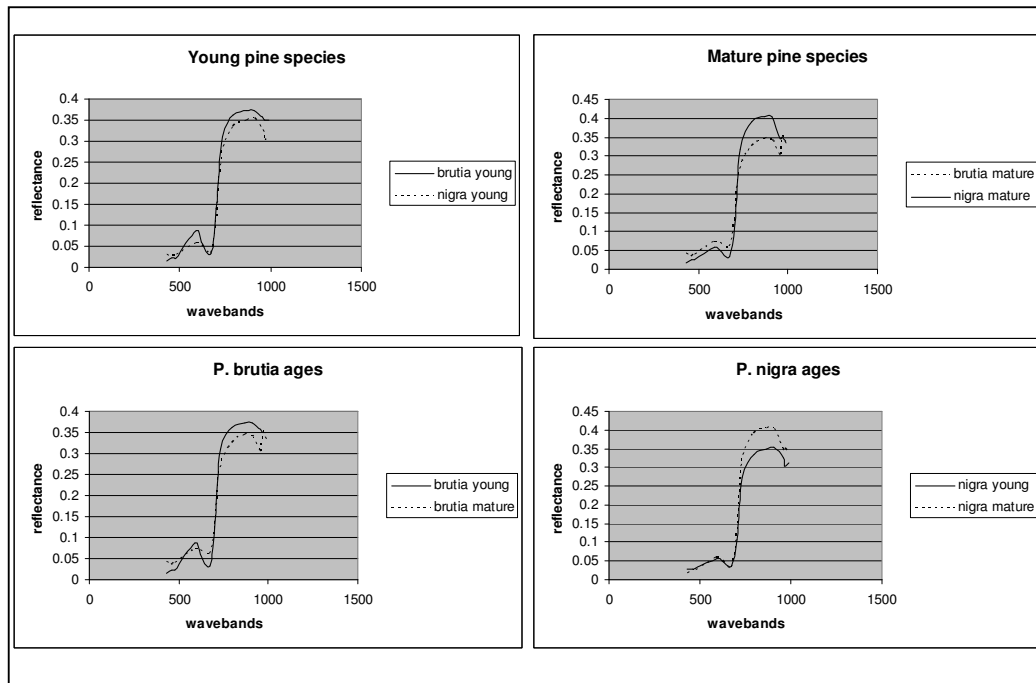


Figure 56 Signatures of the selected wavebands for pines

When young *P. brutia* was compared to young *P. nigra*, a significant difference was observed at 591 nm and slightly higher values for *P. brutia* species were observed in the NIR region. At mature ages of both species, *P. brutia* was distinguished easily from *P. nigra* in the NIR region with much higher values recorded near 865 and 907 nm for *P. nigra* mainly due to the leaf water content.

After a further careful investigation of the results from the same specie at different ages, it was observed that the red region of the *P. brutia* reflectance spectrum was characterized for the young trees by lower reflectance and transmittance due to strong absorptions by foliar pigments for photosynthesis. The mature *brutia* trees showed higher reflectance due to the low absorption of violet-blue and red light by the chlorophyll pigments. The reflectance spectrum of *P. brutia* showed absorption peaks around 458 and 672 nm. Most of these are caused by strong absorptions of chlorophyll. In the NIR region, higher reflectances were recorded for young *P. brutia*

trees. On the other side, *P. nigra*, young trees could be distinguished easily from mature trees in the NIR region with lower NIR values for the younger trees.

Based on what has been observed above, the wavebands centred at 591, 794 and 865 nm are recommended for discrimination between the two young pine species, while wavebands centred at 672 and 907 nm are recommended for discrimination between the two mature pines species. Moreover, wavebands centred at 672 and 957 nm are best selected to discriminate between young and mature brutia and wavebands centred at 865 and 907 nm are best selected to discriminate between young and mature nigra.

7.1.2 Shrub spectral characteristics

Field observations showed that several Mediterranean shrub species were present on the burned site after fires. Hyperspectral measurements of *Quercus coccifera*, *Erica manipuliflora*, *Laurus nobilis*, *Arbutus unedo* and *Cistus incanus* and fern were taken.

Hyperspectral data offer a wide range of possibilities as they provide a set of spectral information that can be very useful for discriminating shrub species within a given area. This is indeed possible as certain plant species show a typical spectral signature (as previously demonstrated with the pine species). Therefore, it is necessary to know which bands best suit the discrimination of the species under study, something that depends upon species specific biochemical characteristics related to foliar chemistry (Martin *et al.* 1998).

The main aim of this work is to determine hyperspectral wavebands (0.4-1.1 μm) that best characterize the main shrub species present after fire in the study area.

7.1.2.1 Methodology

Like before, the optimal wavebands that best describe the spectral characteristics of some shrub species were determined based on a comprehensive analysis using PCA, correlation analysis and SDA.

The **PCA** was applied to the pre-processed spectral measurements of the different measured shrub species. The results (Table 24) showed that the two Principal

Components (PCs) explained 97% of the variability among the different species. The new PC wavebands were computed using factor loadings (or eigen vectors) of each of the 60 wavebands and multiplying the factor loadings with their respective waveband reflectivity (Table 25). It was observed that Near Infra-Red (NIR) dominated PC1 while blue and green wavebands dominated PC2.

Table 24 Total variance explained

Component	Initial Eigenvalues		
	Total	% of Variance	Cumulative %
1	39.320	65.533	65.533
2	18.925	31.541	97.074

Table 25 Rotated Component Matrix

	PC1	PC2
479.311	-	0.997
509.82	-	0.988
651.995	-	0.996
784.43	0.996	-
835.421	0.994	-
926.999	0.992	-
957.738	0.990	-

Extraction Method: Principal Component Analysis. Rotation Method: Varimax with Kaiser Normalization.

In the **correlation analysis**, Pearson's correlation coefficients, with their significance levels, were computed (Table 26). A very high correlation (R^2) between any two wavebands indicates similar or redundant information. The areas of lowest correlation between wavebands indicate that the two bands contained unique information about the species.

Table 26 Wavelengths correlation

458.961	Wavebands with the least redundancy. $R^2 < 0.08$
489.488	
672.346	
723.305	
753.863	
774.236	
865.941	
957.738	

In a **Stepwise Discriminant Analysis**, the discriminatory power of hyperspectral data was assessed for the different shrub species under examination employing SDA. The

most frequently occurring wavebands that achieved the optimal Wilk's lambda values were centred at: 428.441, 601.194, 937.568, and 977.918 nm.

7.1.2.2 Results and discussion

Careful data analysis of PCA and variable correlations and SDA established 18 optimal bands that best characterized the different species (Table 27). These 18 bands are supposed to have a high level of relevance in providing various specie characteristics.

Table 27 Optimal wavebands

	<i>C. incanus</i>	<i>Q. coccifera</i>	<i>E. manipuliflora</i>	<i>fern</i>	<i>L. nobilis</i>	<i>A. unedo</i>
428.441	0.016995	0.027629	0.025258	0.032373	0.014981	0.008406
458.961	0.042907	0.033484	0.025787	0.032012	0.018089	0.011619
479.311	0.054571	0.035324	0.024762	0.034948	0.018219	0.015429
489.488	0.054405	0.036551	0.025235	0.033387	0.018813	0.013523
509.82	0.064392	0.042437	0.030529	0.047068	0.024709	0.023039
601.194	0.111431	0.090045	0.043902	0.087626	0.052195	0.042528
651.995	0.099298	0.065289	0.037	0.056983	0.025829	0.029474
672.346	0.093	0.061175	0.033667	0.045167	0.019802	0.024336
723.305	0.329879	0.219925	0.170266	0.462583	0.298144	0.251198
753.863	0.40181	0.323718	0.229333	0.600262	0.477079	0.375524
774.236	0.413643	0.349881	0.240333	0.619807	0.496242	0.393657
784.43	0.419753	0.357596	0.244646	0.623387	0.498751	0.397828
835.421	0.437267	0.388444	0.263514	0.645348	0.506995	0.41981
865.941	0.453157	0.40251	0.27298	0.655027	0.513906	0.437912
926.999	0.448092	0.411603	0.283287	0.660352	0.511442	0.444959
937.568	0.51516	0.403241	0.321977	0.636977	0.513042	0.426008
957.738	0.426693	0.402598	0.323436	0.609944	0.493537	0.411374
977.918	0.459588	0.405885	0.278934	0.626415	0.483412	0.364666

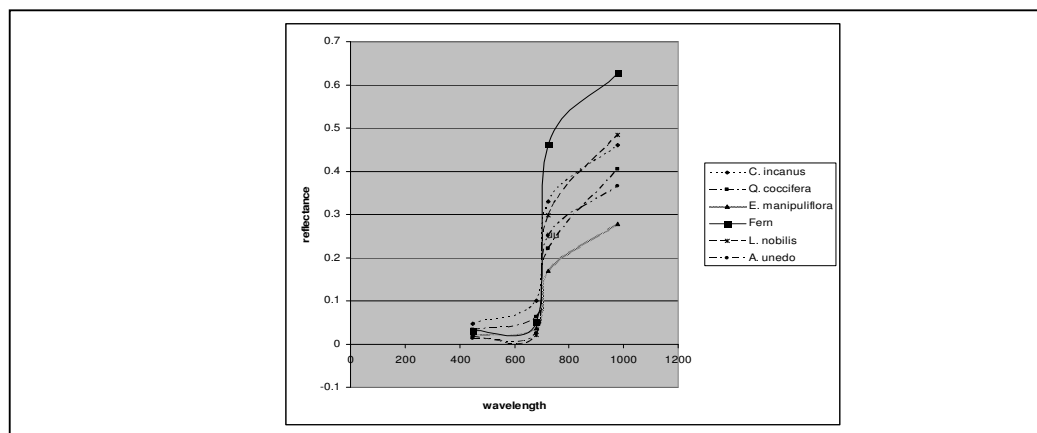
Significance analysis of the selected wavebands was investigated using paired-samples *t* test. The Paired-samples *t* test procedure was used to test the hypothesis of no difference between two variables.

The sig. (2-tailed) column (Table 28) displays the probability of obtaining a *t* statistic whose absolute value is equal to or greater than the obtained *t* statistic. Since the significance value for change for some pairs is less than 0.05, it was concluded that the difference in reflectance was not due to chance variation, and could be attributed to the difference species. However for some pairs (2 out of 15) the significance value was greater than 0.1 showed that the change of specie did not significantly change reflectance.

Table 28 Significance (2-tailed) analysis

	<i>T</i>	Sig. (2-tailed)
<i>C. incanus</i> – <i>Q. coccifera</i>	5.656	0.000
<i>C. incanus</i> – <i>E. manipuliflora</i>	6.497	0.000
<i>C. incanus</i> – <i>Fern</i>	-3.643	0.002
<i>C. incanus</i> – <i>L. nobilis</i>	-0.592	0.562
<i>C. incanus</i> – <i>A. unedo</i>	6.060	0.000
<i>Q. coccifera</i> – <i>E. manipuliflora</i>	5.716	0.000
<i>Q. coccifera</i> – <i>Fern</i>	-4.480	0.000
<i>Q. coccifera</i> – <i>L. nobilis</i>	-2.974	0.009
<i>Q. coccifera</i> – <i>A. unedo</i>	-0.234	0.818
<i>E. manipuliflora</i> – <i>Fern</i>	-4.920	0.000
<i>E. manipuliflora</i> – <i>L. nobilis</i>	-4.207	0.001
<i>E. manipuliflora</i> – <i>A. unedo</i>	-3.790	0.001
<i>Fern</i> – <i>L. nobilis</i>	6.107	0.000
<i>Fern</i> – <i>A. unedo</i>	5.623	0.000
<i>L. nobilis</i> – <i>A. unedo</i>	4.623	0.000

The actual proportion absorbed, scattered or reflected varied significantly among most of the species depending mainly on the internal structure of the leaves. The NIR region was crucial for characterizing most of the species. The two pairs, *C. incanus* - *L. nobilis* and *Q. coccifera* – *A. unedo* showed very close spectral signatures in their selected bands. However in the visible range *C. incanus* showed much higher reflectance than that of *L. nobilis* and *Q. coccifera* showed also higher reflectance in comparison to *A. unedo*. The NIR spectra were highly influenced by the different leaf structures of the species. In this sense, the NIR reflectance of species such as fern was much higher than that of *E. manipuliflora*. While in the visible range the two species showed very similar reflectance values. Finally, it was observed that the best recommended wavebands for species discrimination with the least confusion were centred at 448, 682, 723 and 977 nm (Figure 57).

**Figure 57** Signatures of the selected wavebands for shrub species

7.2 MAPPING FOREST REGENERATION AND VEGETATION RECOVERY USING HYPERION

The aim of this study was to map post-fire forest regeneration and vegetation recovery using hyperspectral Hyperion. The specific objectives were:

- to distinguish between unburned and regenerated or recovered vegetation;
- to distinguish between forest regeneration and vegetation recovery;
- to distinguish between the two dominant forest species, namely *Pinus brutia* and *Pinus nigra* ;
- to distinguish between mature and young pine of same specie; and
- to assess the accuracy of the results using field data.

On the 1st of August 2003 a Hyperion image (level 1 radiometric product) of the study area was acquired (chapter 3). The volume of data collected from Hyperion is about 75 times greater than that for an equivalent area from six non-thermal Landsat ETM+ bands. It is imperative that new methods and techniques such as object-oriented analysis be developed to handle these high-dimensional data sets. At the same time, it will be important to identify and drop redundant bands. This will require determining the most sensitive wavebands for a given application. Optimizing the Hyperion image will help reduce the volume and dimensionality of the data sets, and keep few selected bands that capture most of the pertinent information (Prasad *et al.* 2004).

Sixty two plots of minimum 30x30 m large and of homogenously regenerated forest and recovered vegetation were surveyed in the field (Chapter 3). These plots will be used for accuracy assessment of the classification results.

The Hyperion image was atmospherically and geometrically corrected (Chapter 4). The final output of the image contained 147 bands as shown in Table 29. After image corrections different tasks of Hyperion image transformations were performed. These specific tasks were addressed:

1. to produce uncorrelated output bands using PCA; and
2. to reduce data dimensionality using MNF.

Table 29 Final output of the Hyperion image (wavelength in nm)

Band Nb.	Wavelength	Band Nb.	Wavelength	Band Nb.	Wavelength	Band Nb.	Wavelength
8	428.441	45	804.841	111	1241.08	162	1753.46
9	438.611	46	815.047	112	1251.2	163	1763.62
10	448.791	47	825.235	113	1261.3199	164	1773.79
11	458.961	48	835.421	114	1271.4399	187	2007.38
12	469.141	49	845.591	115	1281.5601	188	2017.5
13	479.311	50	855.771	116	1291.6	189	2027.61
14	489.488	51	865.941	117	1301.75	190	2037.64
15	499.651	52	876.120	118	1311.75	191	2047.77
16	509.82	53	886.290	119	1321.84	192	2057.9099
17	519.974	54	896.470	134	1472.29	193	2068.05
18	530.135	55	906.640	135	1482.3	194	2078.2
19	540.283	56	916.819	136	1492.3	195	2088.3501
20	550.439	82	947.658	137	1502.3	196	2098.51
21	560.584	83	957.738	138	1512.29	197	2108.6699
22	570.738	84	967.828	139	1522.2	198	2118.8401
23	580.892	85	977.918	140	1532.2	199	2129
24	591.037	86	988.048	141	1542.21	200	2139.0701
25	601.194	87	998.048	142	1552.225	201	2149.23
26	611.343	88	1008.15	143	1562.23	202	2159.3999
27	621.506	89	1018.25	144	1572.25	203	2169.5701
28	631.662	90	1028.36	145	1582.25	204	2179.74
29	641.831	91	1038.48	146	1592.28	205	2189.8999
30	651.995	92	1048.60	147	1602.3101	206	2200.0601
31	662.172	93	1058.73	148	1612.35	207	2210.22
32	672.346	94	1068.86	149	1622.29	208	2220.3601
33	682.535	95	1079	150	1632.33	209	2230.51
34	692.720	96	1089.14	151	1642.39	210	2240.5601
35	702.917	101	1139.76	152	1652.45	211	2250.6899
36	713.107	102	1149.91	153	1662.52	212	2260.8201
37	723.305	103	1160.05	154	1672.6	213	2270.95
38	733.489	104	1170.2	155	1682.6899	214	2281.0601
39	743.679	105	1180.35	156	1692.79	215	2291.1699
40	753.863	106	1190.5	157	1692.89	216	2301.27
41	764.039	107	1200.64	158	1713.01	217	2311.3701
42	774.236	108	1210.6801	159	1723.03	218	2321.47
43	784.43	109	1220.8199	160	1733.16	219	2331.5701
44	794.641	110	1230.9399	161	1743.3	-	-

Values of image endmember were compared to field spectra data in order to evaluate whether there is a significant difference between the two variables. The previous statistical analysis resulted in recommending at least 23 best narrowbands in total (from 60 hyperspectral bands), in the range of 0.4 to 0.99 μm to discriminate among pine trees (age and species) and other shrub species. The most frequently occurring waveband centres were: 428.441, 458.961, 479.311, 489.488, 509.820, 591.037, 601.194, 621.506, 651.995, 672.346, 702.917, 723.305, 733.489, 753.863, 774.236, 784.430, 794.641, 835.421, 865.941, 957.738, 967.828, 977.918 and 988.048 nm. Reflectance values at these wavebands were employed. The Paired-samples t test procedure was used to test the hypothesis of no difference between two variables for *P. brutia* and *P. nigra* regeneration. The paired sample correlation for *P. brutia* regeneration was 0.859 with a Sig. (2-tailed) value of 0.437 and a t value of 0.815. As for *P. nigra* regeneration the correlation was 0.892 with a Sig. value of 0.08 and a t value of 1.946. Those observations showed the possibility that difference in reflectance between field spectra and image endmembers was due to chance variation, and can't be attributed to the source of data collection (Figure 58).

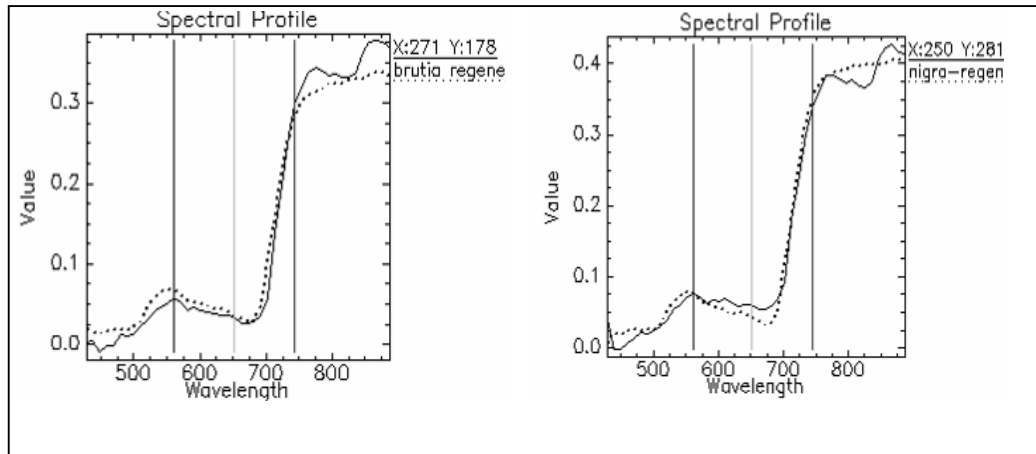


Figure 58 Compared spectral profiles of image endmembers and field spectra

7.2.1 Image transformations

A couple of image transformation techniques were used in order to reduce the large number of bands into more meaningful and noiseless bands.

PCA was used to produce uncorrelated output bands, to segregate noise components, and to reduce the dimensionality of data sets. Because hyperspectral data bands are often highly correlated, the Principal Component (PC) Transformation is used to produce uncorrelated output bands. This is done by finding a new set of orthogonal axes that have their origin at the data mean and that are rotated so the data variance is maximized. PC bands are linear combinations of the original spectral bands and are uncorrelated (Richards 1999). Only 10 PC bands were output of the analysis. The first PC band contained the largest percentage of data variance and the second PC band contains the second largest data variance, and so on. The last PC bands appeared noisy because they contained very little variance, much of which was due to noise in the original spectral data. Principal Component bands produced more colourful composite images than spectral colour composite images because the data is uncorrelated (Figure 59).

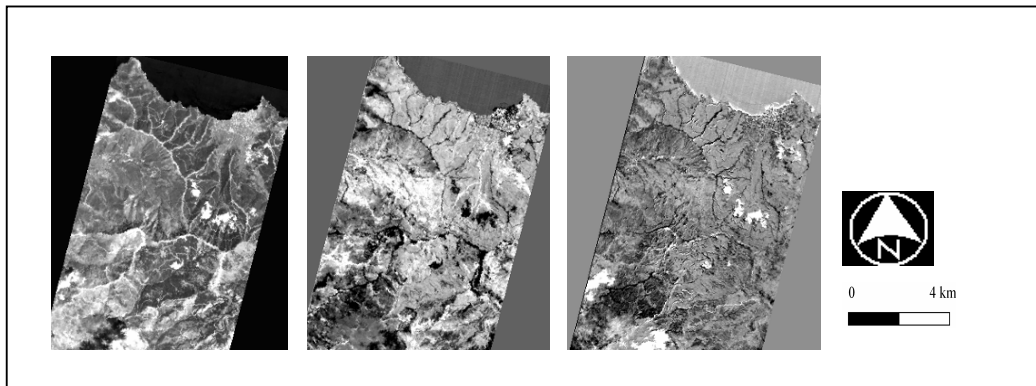


Figure 59 PC bands 1, 2 and 3 respectively

The Minimum Noise Fraction (MNF) transformation was used to determine the inherent dimensionality of image data, to segregate noise in the data, and to reduce the computational requirements for subsequent processing (Boardman and Kruse 1994). The MNF transformation (Green *et al.* 1988) is essentially two cascaded Principal Component transformations. The first transformation, based on an estimated noise

covariance matrix, decorrelated and rescaled the noise in the data. This first step resulted in transformed data in which the noise has unit variance and no band-to-band correlations. The second step was a standard Principal Components transformation of the noise-whitened data. For the purposes of further spectral processing, the inherent dimensionality of the data was determined by examination of the final eigenvalues and the associated images. The inherent dimensionality of the data was determined by the eigenvalues and MNF image. The MNF data space was divided into two parts: one part associated with large eigenvalues and coherent eigenimages, and a complementary part with near-unity eigenvalues and noise-dominated images (Figure 60). Using only the coherent portions by thresholding the MNF bands separates the noise from the data, thus reducing the amount of data to be analysed and improving spectral processing results (Green *et al.* 1988, Harsanyi and Chang 1994, Boardman *et al.* 1995). Finally only 17 eigenbands were selected.

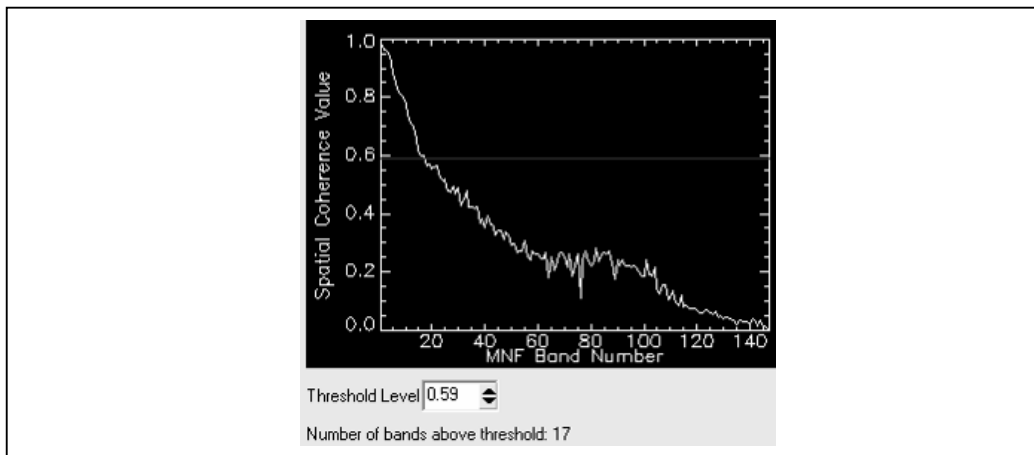


Figure 60 Spatial coherence threshold

In order to facilitate the analysis of such big amount of data, the work was performed on image subsets of the area under investigation. The same procedure of object-oriented image analysis will be applied on each of the image subset separately avoiding processing errors due to the big amount of data.

7.2.2 Methodology

The different layers bands were selected to be imported to an object-oriented analysis.

These layers were the following:

- Hyperion reflectance bands (147 layers)
- PCA layers (only the first three PC bands)
- MNF layers (only the ten first MNF bands)

The methodology comprised three consecutive steps. Step 1 and 2 were performed as a preliminary procedure in order to select a number of training sites by taking field survey information into account. The whole analysis was based on object-based classification. The flowchart of the followed methodology is presented below (Figure 61).

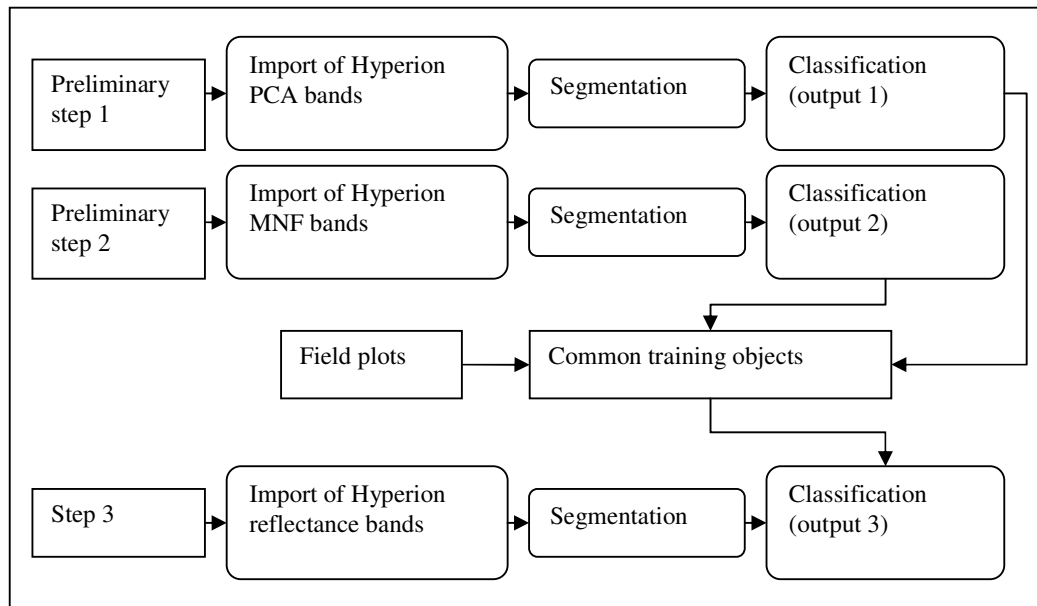


Figure 61 Flowchart of methodology

At each of the previously presented steps, the same classification scheme was applied. Two main classes were distinguished: ‘vegetation’ and ‘no vegetation’ and five sub-classes for vegetation were identified:

1. brutia mature
2. brutia regeneration
3. nigra mature
4. nigra regeneration
5. other (shrubs and trees)

Classification of the two main classes was based on membership functions while the classification of the sub-classes was based on applying standard nearest neighbour to the classes.

7.2.2.1 Preliminary steps

Preliminary step 1: the first three PCA layers were imported considered for segmentation and then for classification. The PCA image was segmented using an abstract scale of 0.3. The resulted objects were close in size to the image pixels. After segmentation the previously discussed classification scheme was applied. Statistics of object for a specific feature were compared between each other (Figure 62). A careful observation of the object statistics allowed selecting the features and thresholds for classification.

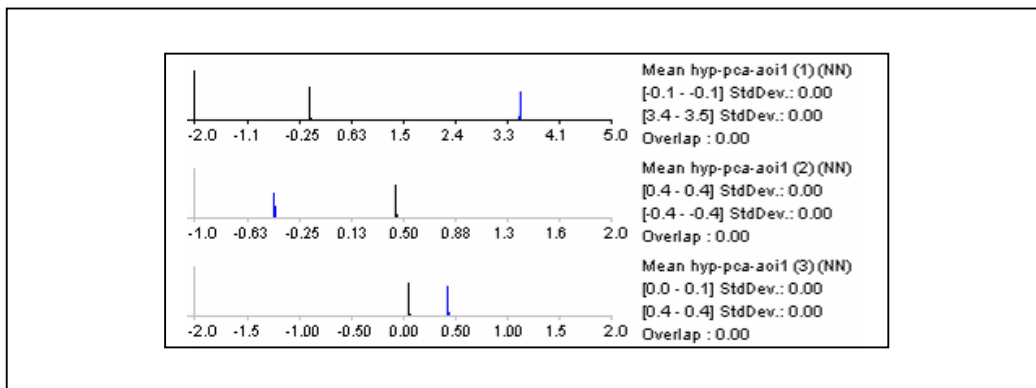


Figure 62 Feature comparison between ‘vegetation’ (black) and ‘no vegetation’ (blue)

The class ‘vegetation’ was classified using a membership function of mean PCA 2 (Figure 63).

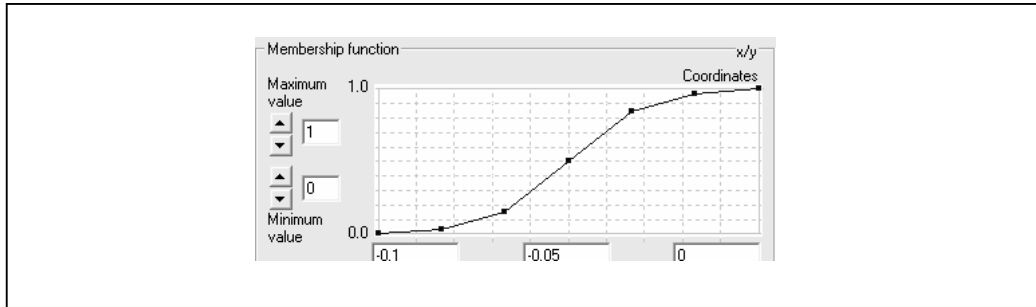


Figure 63 Membership function for the class ‘vegetation’

The subclasses of ‘vegetation’ were classified by applying a standard nearest neighbour classification and employing training sites.

Preliminary step 2: all MNF layers were imported for segmentation. An abstract scale of 1 was used for image segmentation. Also object statistics were observed before selecting the features for classification and setting up the thresholds. Figure 64 shows a feature comparison between ‘vegetation’ (in black) and ‘no vegetation’ (in blue) for the first five MNF bands.

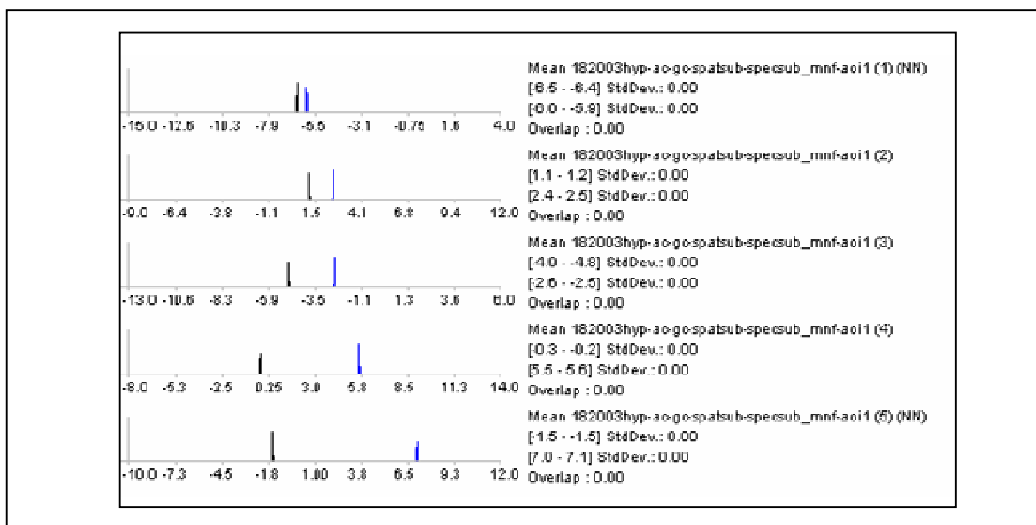


Figure 64 Feature comparison between ‘vegetation’ (black) and ‘no vegetation’ (blue)

The class ‘vegetation’ was classified using membership function of mean band 5 (Figure 65).

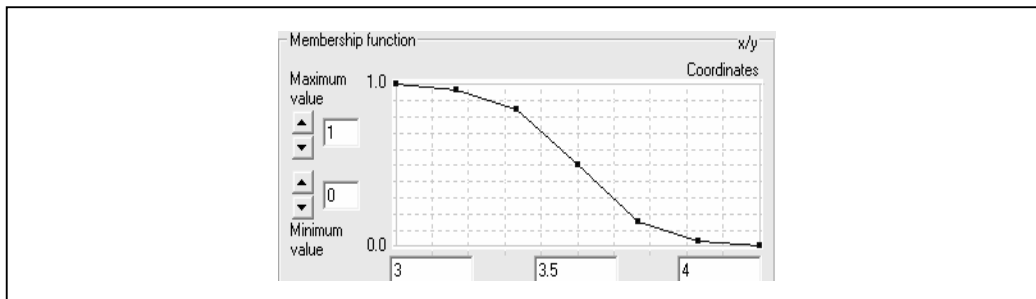


Figure 65 Membership function for the class ‘vegetation’

As in the previous step, the subclasses of ‘vegetation’ were classified by applying a standard nearest neighbour classification and employing samples.

Results of the preliminary steps and discussion: the classification of the PCA and MNF bands was not an aim in itself. The main purpose behind these two preliminary classifications was to locate common training image objects that can be used later in the classification of the Hyperion reflectance image. Some of the objects that were similarly classified in the two output images were compared to some of the collected field data. Matching samples (around three per each classification category) were selected as training image objects for the next classification in step 3. Figure 66 show subsets of the classified PCA and MNF bands. The corresponding subsets show *P. brutia* regeneration in darkest grey (lower) mapped from PCA and MNF bands (upper -left to right).

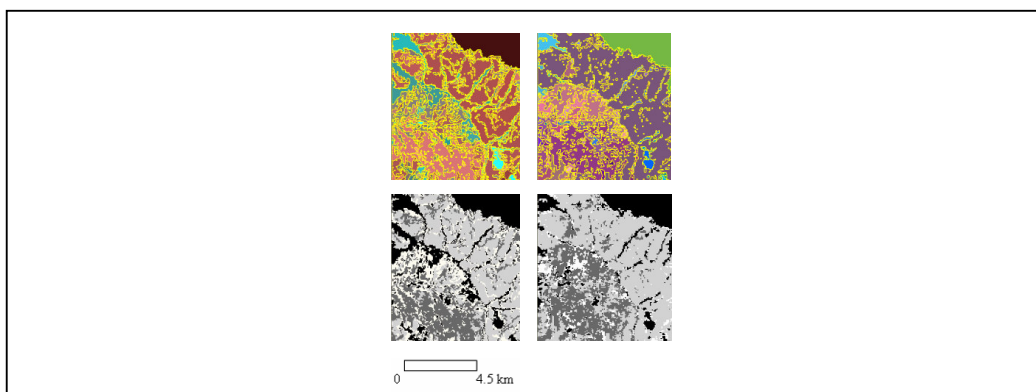


Figure 66 Subsets of the preliminary classification results

From the visual inspection of the preliminary results it was found that the quality of a final classification result could be affected negatively due to the following two reasons:

1. The low spatial resolution of the image makes it not possible to identify accurately the pixels of mixed vegetation types.
2. The topographic effects, canopy shadows, and illumination conditions (spectral overlap).

Also, it was observed from an operational point of view, that the speed performance of data processing was quite acceptable when using PCA and MNF bands, while the use of a full Hyperion image (147 bands) is expected to slow remarkably the processing performance of the data, giving a possibility of internal algorithm errors to be generated.

Based on what has been mentioned above, it was important to find a solution that could satisfy the need of a high quality classification and that could be at the same time operational. The basic strategy was focused on reducing complexity. Image analysis typically implies dealing with complex dependencies. To make this complexity accessible and transparent, it was important to reduce complexity wherever it is possible, specifically in the context of the image to be analysed and in the creation of the classifications schemes and the class descriptions.

Therefore it was found useful to work on two different subsets of the image, namely Area of Interest 1 (AOI1) and AOI2. It should be noted that the aim of the study is to map vegetation regeneration after fire. Consequently, the two subsets were carefully selected in order to have the most representative vegetation regeneration covers.

The study is developed on an operational basis. However, in another type of application, unburned mature brutia and nigra forests can be identified and masked out easily by using fire perimeters (produced by the forest services or from accurate burned area maps) in addition to a Digital Elevation Model, knowing that *P. nigra* forests are grown only above a certain level of altitude.

7.2.2.2 Object-based classification of the Hyperion image

The step 3 consisted of Hyperion image segmentation and classification. All 147 bands of the Hyperion image were imported for use in object-oriented image analysis.

Image segmentation: the purpose behind image segmentation is to produce highly homogenous objects. Image layers were assessed differently depending on their importance and suitability for the segmentation result. The higher the weight is assigned to a layer the more of its information will be used during the segmentation process. Hyperion image layers that do not contain the information intended for representation by the image objects should be given little or no weight (Table 30). When segmenting the Hyperion reflectance image, all bands recommended in chapter 7 for vegetation discrimination were weighted with a highest value (three), while the ones that were not recommended were weighted with a lowest value (one). Finally, the bands above 1000 nm were all weighted with an average value of two due to the absence of field hyperspectral analysis in that range.

Table 30 Band weight assignments

Band numbers	Wavelength (nm)	Weight	Band numbers	Wavelength (nm)	Weight
8	428.441	3	40	753.863	3
11	458.961	3	42	774.236	3
13	479.311	3	43	784.430	3
14	489.488	3	44	794.641	3
16	509.820	3	48	835.421	3
24	591.037	3	51	865.941	3
25	601.194	3	83	957.738	3
27	621.506	3	84	967.828	3
30	651.995	3	85	977.918	3
32	672.346	3	86	988.048	3
35	702.917	3	Other bands	<1000 nm	1
37	723.305	3	All bands	>1000 nm	2
38	733.489	3	-	-	-

The scale 0.1 was chosen to keep as much as possible the spectral characteristics of every individual object in the image (Figure 67).

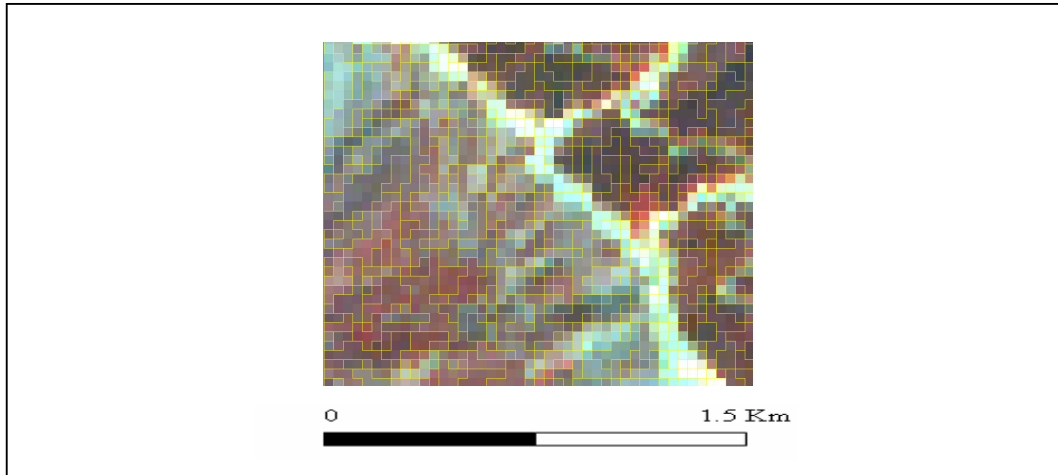


Figure 67 Image subset showing image objects created after segmentation

Image classification: after segmentation the image was made ready for classification. The previously described classification scheme (two classes and five subclasses of the class vegetation) are applied here. Each class of the classification scheme formulated in here contains a class description. Each class description consists of a set of fuzzy expressions allowing the evaluation of specific features and their logical operation. The output of the system is twofold: a fuzzy classification with detailed information of class mixture and reliability of class assignment, and a final crisp classification where each object is assigned to exactly one class (or none, if no assignment was possible). A fuzzy rule can have one single condition or can consist of a combination of several conditions which have to be fulfilled for an object to be assigned to a class. The conditions are defined by expressions, which are inserted into the class descriptions. Expressions of classification features were membership functions in the parent class ‘vegetation’ and nearest neighbour in the subclasses.

The feature used for the classification of the parent class ‘vegetation’ was NDVI. The NDVI was calculated from band 86 (998.048 nm) and band 32 (672.346 nm). These bands represented two of the previously recommended wavelengths for vegetation discrimination. It was essential to compare the lowest density of vegetation cover measured in the field to the correspondent image object in order to set up an NDVI threshold for the class ‘vegetation’. After the comparison, a threshold of 0.4 was set up (Figure 68).

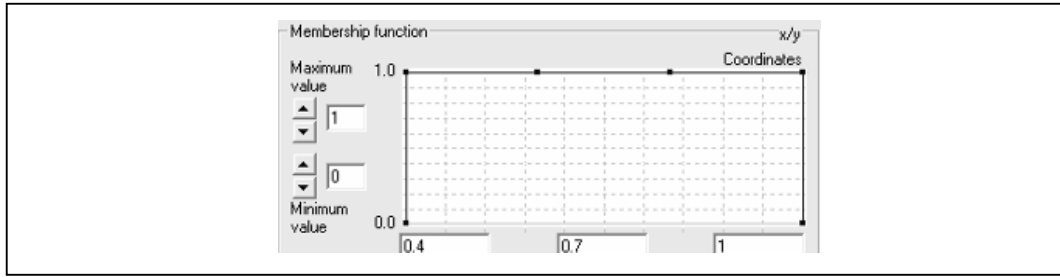


Figure 68 Membership function of NDVI for the class 'vegetation'

The nearest neighbour classifier was employed for the classification of the sub-classes. The nearest neighbour classifies image objects in a given feature space and with given samples for the classes of concern. The principle is simple: first, typical representative samples for each class are needed. As the analysis is based on an object oriented approach to image analysis, specific image objects are addressed to be the samples. After a representative set of sample objects has been declared for each class, the algorithm searches for the closest sample object in the feature space for each image object.

7.2.3 Results and discussion

Evaluation of the quality of a classification result is of high importance in remote sensing since it gives evidence of how well the generated or used classifier is capable of extracting the desired objects from the image. Commonly, for a first evaluation, simple visual inspection was used to evaluate the plausibility of the classification results. However, this is just a subjective method and thus difficult to quantify or be expressed in comparable values. The AOI1 image subset (Figure 69) showed large homogeneous areas of brutia mature forest. Patches of brutia regeneration and other regenerated vegetation are mainly observed within the burned areas. Most probably, the small spots of brutia regeneration surrounded by mature forest represent some misclassified objects or real young brutia trees. As for AOI2 a highly textured mosaic of vegetation regeneration makes difficult to visually interpret the results, therefore advanced analysis of the results will be required.

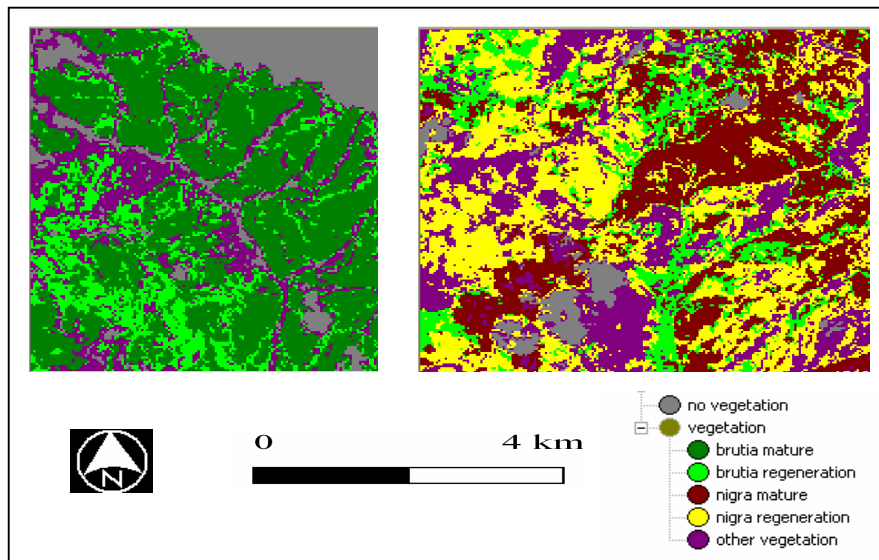


Figure 69 Final classification results on image subsets (left: AOI1, and right: AOI2)

When using fuzzy classification methods, objects can belong to several classes but with different degrees of membership, which is the case when class descriptions overlap. Thus, to evaluate the reliability or stability of classes it is necessary to survey the different degrees of membership of the classified objects. Objects whose feature values are within these overlapping ranges can be seen as ambiguous objects, since they fulfil the criteria of more than one class. Although fuzzy concepts make it possible to describe these ambiguities, the main aim of each classification should be to define classes as unambiguously as possible. It should be noted that obtaining ambiguous objects does not mean that the objects are misclassified; it rather means that there is no class to which these objects belong to explicitly. Hence, regarding the objects' statistics of the degrees of membership to the classes helps to evaluate the quality of the classes. In other words: the less ambiguous the objects, the more usable the classification results. Likewise, the more distinctly the classes differentiate the objects, the more clearly they express the image's content.

To quantify a class's quality regarding the statistics of its objects' degrees of membership is an appropriate method: the more objects having a membership degree of 1 to just this class, the better the class is, and vice versa. In addition, the statistics and some parameters such as minimum, maximum, standard deviation and mean of the several degrees of membership can give more evidence.

The best classification result (Table 31 and Table 32) is a statistical output for the best classification result evaluated per class. Due to the fuzzy classification concept, an image object has memberships to more than one class. The classification with the highest assignment value is taken as the best classification result. Basic statistical operations are performed on the best classification result of the image objects assigned to a class (number of image objects, mean, standard deviation, minimum value and maximum value).

Tables 31 can be interpreted as follows: at least one object fulfils the class description completely for the class ‘other vegetation’ and almost completely for the brutia classes, but there are some which do not. There is also at least one object per class which meets the class criteria poorly. But in general the objects in the brutia classes have a membership degree of $\mu = 0.81 \pm 0.14$ for ‘brutia mature’ and 0.71 ± 0.14 for ‘brutia regeneration’. This can be interpreted as “most objects of the class meet the class’s criteria sufficiently.”

While in Table 32 at least one object fulfils the class description completely for all the classes, but there are some as well which do not. There is also at least one object per class which meets the class criteria poorly. But in general the objects in all classes have acceptable StdDev in relation to the membership degrees. This can be interpreted as “most objects of the class meet the class’s criteria sufficiently.”

Table 31 Best classification results from AOI1

Class	Objects	Mean	StdDev	Minimum	Maximum
No vegetation	177	0.99	0.05	0.56	1
Brutia mature	198	0.81	0.14	0.5	0.99
Brutia regeneration	756	0.71	0.14	0.5	0.98
Other vegetation	559	0.7	0.16	0.5	1

Table 32 Best classification results from AOI2

Class	Objects	Mean	StdDev	Minimum	Maximum
No vegetation	1395	0.95	0.11	0.506972	1
Brutia regeneration	4137	0.76	0.11	0.500225	1
Nigra mature	5859	0.81	0.14	0.500457	1
Nigra regeneration	9846	0.76	0.13	0.500095	1
Other vegetation	6807	0.77	0.17	0.5	1

A comparison between the best and second best μ -values gives more evidence about the capability to separate the objects unambiguously. A simple operator which expresses the relativity between two values is their difference. The higher the μ 's difference, the more unambiguously an object belongs to its class.

Classification stability (Tables 33 and 34) is the difference between the best and the second best class assignment, calculated as a percentage. It was possible to explore the differences in degrees of membership between the best and the second best class assignments of each object, which can provide evidence about the ambiguity of an object's classification. The statistical output displays basic statistical operations such as, number of image objects, mean, standard deviation, minimum value and maximum value.

As it is already known, an image object has a membership degree to more than one class. With the classification stability statistics, it is possible to explore the differences in degrees of membership between the best and the second best class assignments of each object, which can give evidence about the ambiguity of an object's classification. Objects with 1.0 difference value are extremely non ambiguous and objects with a 0.0 difference value are absolutely ambiguous.

The statistical output displays, in terms of class, the basic statistical operations performed on the differences between the best and second best degrees of membership. In table 33 there isn't any object which belongs to another class with the same degree of membership as to any specific class (minimum is different from 0.00). There is no object of the brutia classes which does not belong to another class at the same time. If this was the case like for the class 'other vegetation', a maximum of 1.0 would occur. Based on the mean and StdDev values it can be concluded that all classes can be very acceptably separated among each others (mean = 0.07 ± 0.06 for 'brutia mature' and mean = 0.06 ± 0.05 for 'brutia regeneration'). In table 34, there is at least one object which belongs to another class with the same degree of membership as to any vegetation class (minimum = 0.00). There is no object of any of the pine classes which does not belong to another class at the same time. In general the objects of all classes can be acceptably separated among each others.

Table 33 Classification stability from AOI1

Class	Objects	Mean	StdDev	Minimum	Maximum
No vegetation	177	0.98	0.1	0.125995	1
Brutia mature	198	0.07	0.06	0.000204	0.44
Brutia regeneration	756	0.06	0.05	0.000125	0.31
Other vegetation	559	0.4	0.32	0.00003	1

Table 34 Classification stability AOI2

Class	Objects	Mean	StdDev	Minimum	Maximum
No vegetation	1395	0.91	0.22	0.01	1
Brutia regeneration	4137	0.26	0.19	0	0.71
Nigra mature	5859	0.4	0.24	0	0.91
Nigra regeneration	9846	0.4	0.23	0	0.81
Other vegetation	6807	0.55	0.34	0	1

Regarding the class descriptions, obviously and normally their membership functions, specifically those related to the spectral features do overlap in the value ranges. To solve the problem the membership functions must be adjusted to avoid overlapping value ranges (not possible to achieve with such a large number of bands).

The above examples showed one basic advantage of fuzzy classification methods: due to handling with degrees of membership instead of binary membership values, it is possible to evaluate the classifier's capability to extract the desired object classes from an image. Additionally, it is possible to detect unstable and unreliable classes. Nevertheless, it is necessary to compare the obtained classification results with references from the real world.

An accuracy measure, derived on the basis of a comparison of the classification in question with field reference data, was applied. These reference data were obtained by on-site ground measurements (Chapter 3), and are considered reliable and true, which is why sometimes the term "ground truth" is used. The term "reference classification" was used here to emphasize that it was essentially also a classification, the reliability of which must be assured and cannot be taken for granted. In order to assess the accuracy of the classification, field-collected data from 62 widely dispersed plots were employed. A so-called error matrix (Table 35) was derived by counting how many of the objects classified as class i in the classification are of class k in the reference classification.

The overall classification accuracy was found to be 75.81% (Table 36), while overall Kappa Index of Agreement (KIA) was 0.689 (Table 37). A closer examination of the tables revealed that the classes of mature pine forests were the most accurately identified. This is due to the fact that each of the mature pine species was classified in a different image subset. The classes of pine regeneration were mainly confused with the class ‘other vegetations’. This confusion can be explained by absence of large homogenously regenerated pine trees. A solution to resolve this problem could be provided by combining the Hyperion image to high spatial resolution imagery such as QuickBird. Still, the accuracy assessment of classification showed very promising results in mapping two different regenerated pine species and other vegetation regeneration after fire. An application that was not possible with other low spectral resolution images.

Table 35 Error Matrix

Reflectance	Reference data					
Classified Data	<i>P. brutia</i> mature	<i>P. brutia</i> regeneration	<i>P. nigra</i> mature	<i>P. nigra</i> regeneration	Other vegetations	Row total
<i>P. brutia</i> mature	4	1	0	0	0	5
<i>P. brutia</i> regeneration	0	9	0	1	2	12
<i>P. nigra</i> mature	0	1	15	0	0	16
<i>P. nigra</i> regeneration	0	0	1	8	5	14
Other vegetations	0	4	0	0	11	15
Column total	4	15	16	9	18	62

Table 36 Accuracy totals

Class name (Reflectance)	Reference totals	Classified totals	Number correct	Producers accuracy	Users accuracy
<i>P. brutia</i> mature	4	5	4	100 %	80 %
<i>P. brutia</i> regeneration	15	12	9	60 %	75 %
<i>P. nigra</i> mature	16	16	15	93.75 %	93.75 %
<i>P. nigra</i> regeneration	9	14	8	88.89 %	57.14 %
Other vegetations	18	15	11	61.11 %	73.33 %
Totals	62	62	47	-	-
Overall Classification Accuracy	75.81 %				

Table 37 Kappa Statistics

Class Name (Reflectance)	Kappa
<i>P. brutia</i> mature	0.7862
<i>P. brutia</i> regeneration	0.6702
<i>P. nigra</i> mature	0.9158
<i>P. nigra</i> regeneration	0.4987
Other vegetations	0.6242
Overall Kappa Statistics	0.6892

7.3 CHAPTER SUMMARY

In summary:

- The hyperspectral wavebands (0.4-1.1 μm) that best characterize pine vegetation were determined. Statistical analysis allowed a 97% reduction in data volume was feasible when 60 of hyperspectral wavebands were reduced to the first three principal components.
- The study resulted in recommending 14 best narrowbands (from 60 hyperspectral bands), in the range of 0.4 to 1.1 μm to discriminate among pine trees (age and species). The most frequently occurring waveband centres were: 428.441, 458.961, 479.311, 591.037, 621.506, 672.346, 702.917, 733.489, 794.641, 865.941, 907.288, 957.738, 967.828, and 988.048 nm. A *sig.* (2-tailed) analysis showed significant difference in reflectance due to change in pine age and species.
- Another study resulted in recommending 18 bands that best characterize the different shrub species. The most frequently occurring waveband centres were: 428.441, 458.961, 479.311, 489.488, 509.82, 601.194, 651.995, 672.346, 723.305, 753.863, 774.236, 784.43, 835.421, 865.941, 926.999, 937.568, 957.738, and 977.918 nm. The *sig.* (2-tailed) analysis showed a significant difference in reflectance due to change in species except between *C. incanus* and *L. nobilis* and between *Q. coccifera* and *A. unedo*.
- A couple of image transformation techniques, namely PCA and MNF were applied to the Hyperion image in order to reduce the large number of bands into more meaningful and noiseless bands.
- Only 10 PC bands were output of the analysis. The first PC band contained the largest percentage of data variance and the second PC band contains the second largest data variance, and so on. Principal Component bands produced more colourful composite images than spectral colour composite images because the data was made uncorrelated.
- The MNF transformation was used to determine the inherent dimensionality of image data, to segregate noise in the data, and to reduce the computational requirements for subsequent processing. Finally, only 17 eigenbands were selected.

- The classifications of the noise free images in addition to the use of field surveyed plots made possible locating the most representative training objects for the final classification of the Hyperion image.
- The interpretation of the classification results showed that the low spatial resolution of the image did not make it possible to identify accurately the pixels of mixed vegetation types. Also a spectral overlap was observed between different vegetation types because of topographic effects, canopy shadows, and illumination conditions.
- All 147 bands of the Hyperion image were imported for use in object-oriented image analysis. Previously selected training image objects were employed for standard nearest neighbour classification of the Hyperion reflectance image.
- Statistical evaluation of the classification results was twofold analysis. The first one was based on internal fuzzy analysis and the second one was based on external reference data. The fuzzy analysis showed that most objects of the different classes met the class's criteria sufficiently. Also it was concluded that almost all classes could be very acceptably separated among each others.
- Because of one basic advantage of the applied fuzzy classification method, it was possible to evaluate the classifier's capability to extract the desired object classes from an image. Additionally, it was possible to detect unstable, unreliable classes.
- By producing an error matrix, the overall classification accuracy was found to be 75.81%, while overall Kappa Index of Agreement (KIA) was 0.689. The accuracy showed very promising results in mapping two different regenerated pine species and other vegetation regeneration after fire.
- The classes of mature pine forests were the most accurately identified. Some confusion between the classes of pine regeneration and the class 'other vegetations' were recorded. This confusion can be explained by absence of large homogenously regenerated pine trees.
- A solution to resolve some problems observed in this classification could be provided in another kind of application combining the Hyperion image to high spatial resolution imagery such as QuickBird.

CHAPTER 8: MAPPING FOREST REGENERATION AND VEGETATION RECOVERY BY COMBINING VERY HIGH RESOLUTION AND HYPERSPECTRAL IMAGERY

Chapter 7 demonstrated how hyperspectral data with the typical high number of narrow bands could be used to spectrally characterize pine and shrub vegetation. Also, the use of hyperspectral imagery for vegetation regeneration mapping was demonstrated. Some classification confusions were recorded, and attributed to the low spatial resolution of the Hyperion image. In this chapter, a potential solution is presented by combining the Hyperion image to a high spatial resolution imagery of QuickBird. Hyperspectral data with the typical high number of bands could be used to provide the missing information in high spatial resolution imagery and vice versa.

Given that older generation sensors have many known limitations with respect to their suitability for studying complex biophysical characteristics (De Jong *et al.* 2000, Steininger 2000, Sampson *et al.* 2001, Salas *et al.* 2002), the need to benefit from new generation of high spatial and spectral resolution sensors is of critical importance. Accurate quantification of vegetation regeneration could be essential for biodiversity assessment, land cover characterization and biomass modelling (Blackburn and Milton 1995). High spectral resolution facilitates the identification of features while high spatial resolution permits accurate location of features (Gross and Scott 1998). Additionally, advanced multispectral sensors also allow significantly improved signal to noise ratios (Levesque and King 2003).

Many applications of remote sensing require high spatial resolution data for a correct determination of small objects. High spatial resolution imagery can be used before, during, and after a fire to measure fuel potential, access, progress, extent, as well as damage and financial loss. High spatial resolution multispectral data such as QuickBird (60 centimetres in panchromatic and 2.4 m in multispectral) can identify not only individual tree crowns, but often the type of tree, biomass, condition and age class (Wang *et al.* 2004). However, high spatial resolution image data contain often

limited spectral information. This poor spectral information leads often to classification errors between visible similar classes. Additional information is needed to separate these classes (Greiwe and Ehler 2005).

Hyperspectral data with the typical high number of bands could be used to provide this information (Okin *et al.* 2001) and allow a differentiation of material due to their typical spectra (Elvidge and Chen 1995). A number of recent studies have indicated the advantages of using discrete narrowband data from specific portions of the spectrum, rather than broadband data, to obtain the most sensitive quantitative or qualitative information on vegetation characteristics (i.e., Elvidge and Chen 1995, Carter 1998, Blackburn 1999, Thenkabail *et al.* 2000, Eckert and Kneubuhler 2004). Hyperspectral remote sensing has improved the feasibility of unambiguously identifying numerous vegetation absorption features, related to liquid water, chlorophyll, cellulose, and lignin contents (Smith *et al.* 1990, Gao and Goetz 1994). In the previous chapters it was shown how this is potentially useful in the analysis of vegetation characteristics and to what extent the Hyperion (Ungar *et al.* 2003) hyperspectral imagery (30-m resolution, 10-nm bands covering the spectrum from 400–2500 nm) could be useful in vegetation regeneration mapping.

None of these previously mentioned studies investigated the combination of both Hyperion and QuickBird for mapping post-fire forest regeneration, specifically in the Mediterranean. In the context of remotely sensed data, fusion is often performed by combining high spatial with high spectral resolution imagery on different levels (Pohl and Genderen 1998, Zhukov *et al.* 1999). Accurate mapping of post fire forest regeneration require high spatial and spectral resolution data for a correct determination of small re-vegetated areas and for a good discrimination among different vegetation type and species (Green *et al.* 1998, Shaw *et al.* 1998, Mumby *et al.* 1999).

Consequently, object-oriented image analysis (Batz and Shape 2000, Benz *et al.* 2004, Mitri and Gitas 2004a) is supposed to be most convenient not only for dealing with high spatial resolution imagery but also for combining and classifying multi-resolution imageries.

The aim of this study is to map post-fire forest vegetation on the island of Thasos by combining EO-1 Hyperion and QuickBird in an object-oriented analysis. The specific objectives are:

- to classify the Quickbird image using inputs from Hyperion and Landsat; and
- to assess the accuracy of the results using field data.

The same area that was studied in the previous chapter was considered in this study. The multispectral QuickBird image and the Hyperion image were employed. Two geometrically corrected Landsat-TM images acquired few days after the fire of 1985 and 1989 respectively were collected in order to be used in the object-oriented image analysis for specifically mapping burned and non burned areas.

8.1 METHODOLOGY

Different layers were selected to be imported to an object-oriented analysis. The same previously selected subsets were used. The imported layers were the following:

- Four multispectral QuickBird bands
- Hyperion reflectance bands (147 layers)
- PCA layers(only the first three PC bands)
- MNF layers (only the ten first MNF bands)
- Post fire Landsat TM images from 1985 and 1989

The flowchart of the methodology is represented in Figure 70 (the application of chapter 8 is highlighted in red).

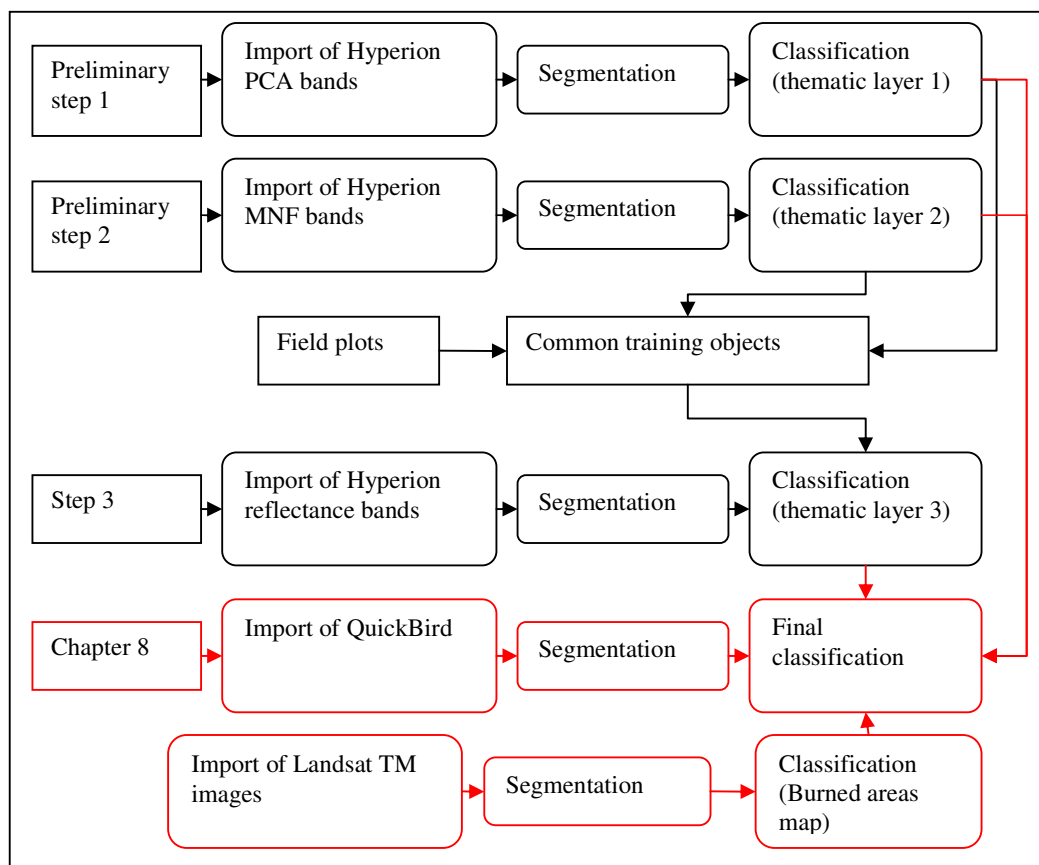


Figure 70 Flowchart of the methodology

8.1.1 Segmentation

The best segmentation result is the one that provides optimal information for further processing. In this study, the strategy before classifying the QuickBird image was to create a three-level graded scale of segmentation (Mao and Jain 1992, Hofmann *et al.* 1998). Thus, small objects at level 1 (regarded as sub-objects) and larger objects (regarded as super-objects) at level 3 would provide information for the final level of classification, which is the middle level (level 2).

After segmentation, all image objects were automatically linked to a network in which each image object knows its neighbours, thus affording important contextual information for later analysis. Subsequently, repetition of segmentation with different scale parameters creates a hierarchical network of image objects. Each middle-sized image object 'knows' its super-object and its sub-objects.

Level 2 was the first to be segmented with a scale of 10 taking into consideration the shape factor. This level was firstly segmented in order not to affect the segmentation results when employing the thematic layers. Then, level 1 was created with a scale 9 taking into consideration both the QuickBird image and the thematic layers. Finally, level 3 was created with a scale of 100 employing only the first four bands of Landsat-TM images. The output results showed large segments that fit well the burned areas.

8.1.2 Classification

After segmentation the different levels were classified. Level 1 was the first to be classified. A classification scheme was adopted (Figure 71). The following main classes were created: 'vegetation', 'shadows' (canopy and topographic shadows) and 'other' (bare ground urban expansion, etc.). Furthermore, the following sub-classes were added to the main class 'vegetation': 'brutia mature pure', 'brutia mature dense cover', 'brutia regeneration pure', 'brutia regeneration dense cover', 'nigra mature pure', 'nigra mature dense cover', 'nigra regeneration pure', 'nigra regeneration dense cover', and 'other vegetation'. In this sense 'pure' means that there is a minimal

mixing with other type of vegetation, while ‘dense cover’ means the vegetation might be mixed with other vegetation types or species.

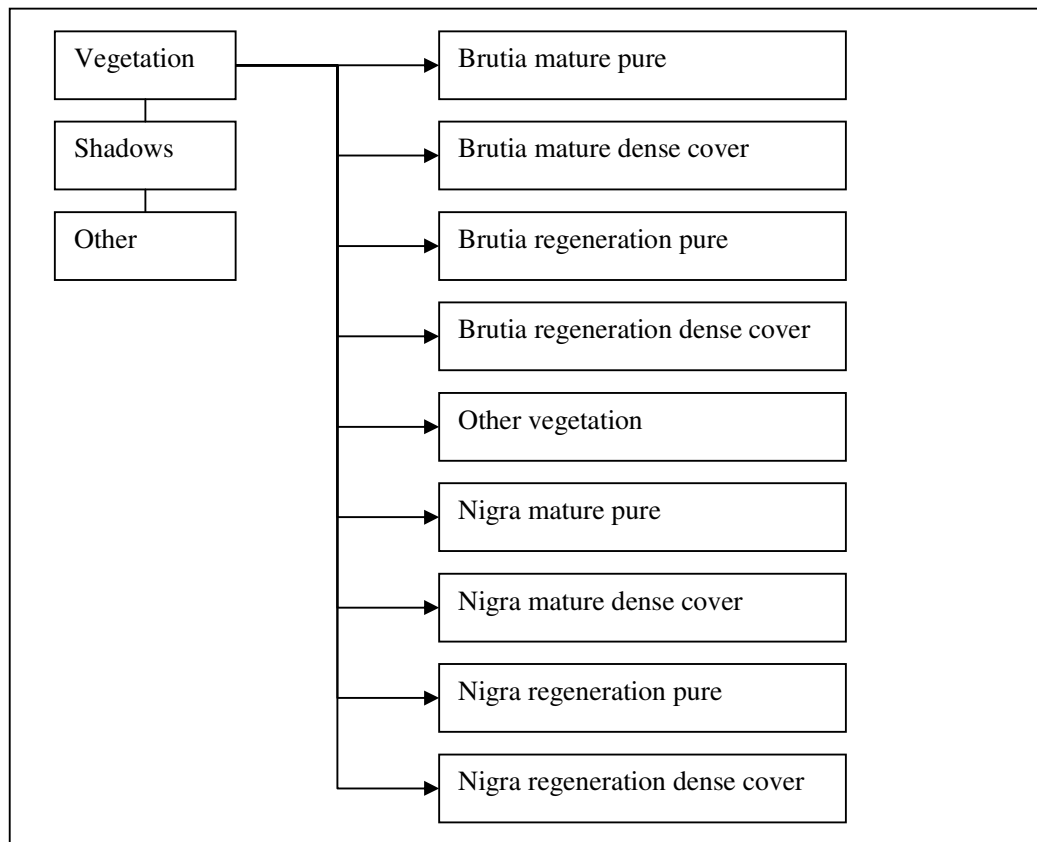


Figure 71 Classification scheme

Membership functions (Civanlar and Trussel 1986) were used to describe all the classes. Objects at level 1 were the first to be classified. The class ‘shadows’ describes the dark objects that represent mainly the canopy shadows and the shaded slopes. Membership function used in the description of this class was ratio of NIR from the QuickBird image (Figure 72).

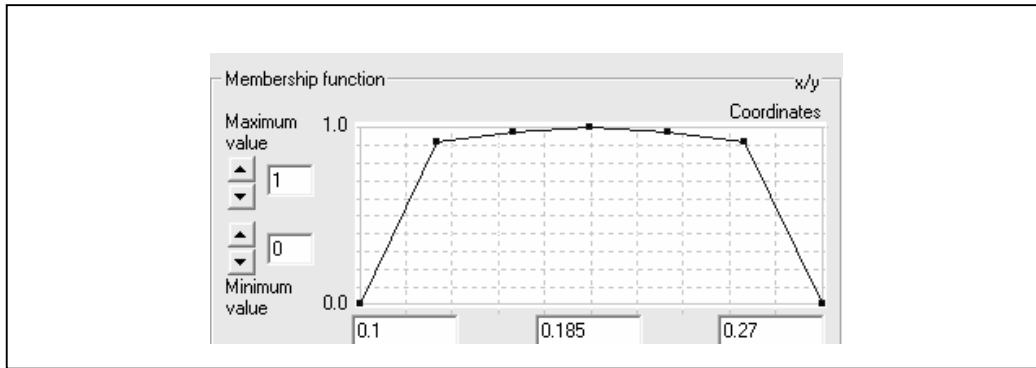


Figure 72 Ratio of NIR for the class ‘shadows’

The class vegetation was classified employing a membership function of NDVI (Figure 73).

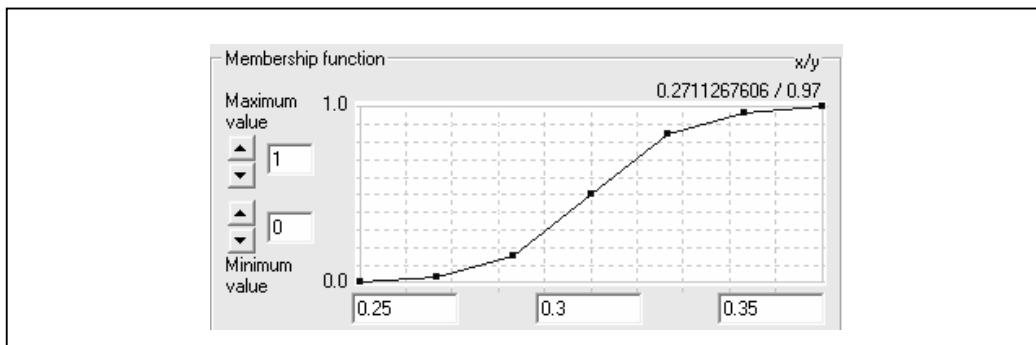


Figure 73 Membership function for the class ‘vegetation’

As for the subclasses a set of conditions was used in the description of each class. The sub-class ‘brutia mature pure’ had the following set of conditions:

If (thematic reflectance and thematic PCA and thematic MNF = brutia mature) then objects are classified as ‘brutia mature pure’.

The sub-class ‘brutia mature dense cover’ had the following set of conditions:

If (thematic reflectance and thematic PCA = brutia mature) or (thematic reflectance and thematic MNF = brutia mature) or (thematic PCA and thematic MNF = brutia mature) and (relative border to brutia mature is 0.01 or higher) then objects are classified as ‘brutia mature dense cover’.

The sub-class ‘brutia regeneration dense cover’ had the following set of conditions:

If (thematic reflectance and thematic PCA = 'brutia regeneration') or (thematic reflectance and thematic MNF = 'brutia regeneration') or (thematic PCA and thematic MNF = 'brutia regeneration') and (relative border to 'brutia mature' is 0.005 or higher) then objects are classified as 'brutia regeneration dense cover'.

The sub-class 'brutia regeneration pure' had the following set of conditions:

If (thematic reflectance and thematic PCA and thematic MNF = brutia regeneration pure) then objects are classified as 'brutia regeneration pure'.

Objects were classified as 'other vegetation' if none of the previous conditions was satisfied.

After classification, 'brutia regeneration pure' and 'brutia regeneration dense cover' were grouped under one class called 'brutia regeneration all'. Also, 'brutia mature pure' and 'brutia mature dense cover' were grouped under one class call 'brutia mature all'.

Level three was then classified. At this level two classes were created, 'burned' and 'not burned'. Not burned objected were classified using the band ratio of NIR from the Landsat-TM image (Figure 74).

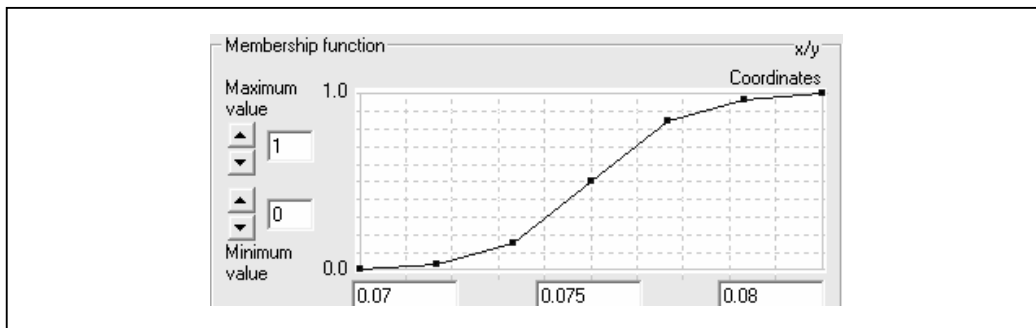


Figure 74 Membership function for the class 'not burned'

Finally, classification at level 2 was performed and a final output of classification was produced. At this level, four classes were created for the AOI1: 'brutia mature', 'brutia regeneration', 'other vegetations' and 'others'.

The class ‘brutia mature’ had the following set of conditions:

If (existence of ‘not burned’ super-objects and existence of ‘shadows’ sub-objects) or (existence of ‘brutia mature all’ sub-objects and existence of ‘not burned’ super-objects) or (existence of ‘not burned’ super-objects and existence of ‘other vegetation’ sub-objects and relative border to ‘brutia mature’ neighbour objects is 0.005 or higher) or (existence of ‘not burned’ super-objects and existence of ‘brutia regeneration all’ sub-objects) then objects are classified as ‘brutia mature’.

The class ‘brutia regeneration’ had the following set of conditions:

If (existence of ‘brutia regeneration all’ sub-objects and existence of ‘burned’ super-objects) or (existence of ‘burned’ super-objects and existence of ‘other vegetations’ sub-objects and relative border to ‘brutia regeneration’ neighbour objects is 0.45 or higher) then classify as ‘brutia regeneration’.

The class ‘other vegetations’ had the following set of conditions:

If (existence of ‘other vegetations’ sub-objects) or (existence of ‘brutia mature all’ sub-objects and existence of ‘burned’ super-objects) then classify as ‘other vegetation’.

Finally, objects were classified as ‘others’ when none of the previous conditions was satisfied. The final classification results are represented in Figure 75.

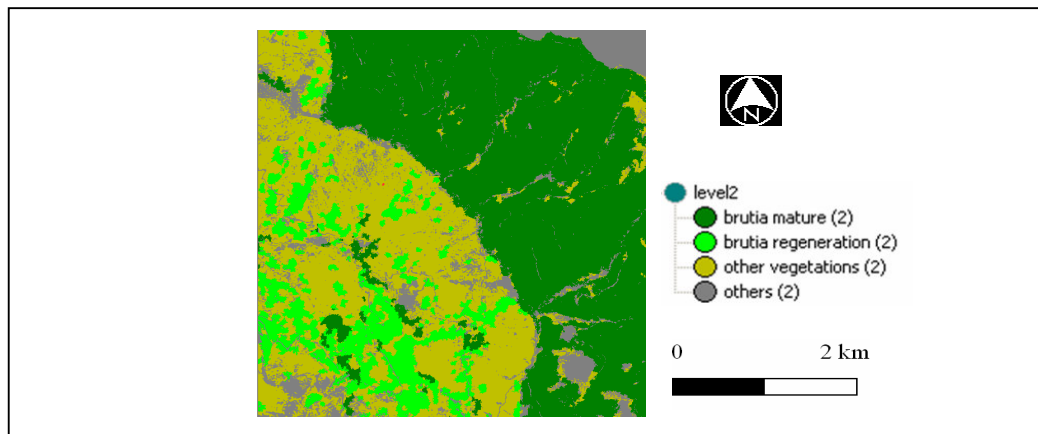


Figure 75 Final classification results at level 2 for AOI1

As for AOI2, the same previously applied procedure of object-oriented image analysis was performed by applying the classification scheme as shown in Figure 71.

As before, three main created and classified at level 1: 'vegetation', 'shadows' and 'no vegetation'. Seven sub-classes were defined in the main class vegetation: 'brutia regeneration pure', 'brutia regeneration dense cover', 'nigra mature pure', 'nigra mature dense cover', 'nigra regeneration pure', 'nigra regeneration dense cover', and 'other vegetations'. The same classification descriptions were used in the common classes. Also, membership functions were used to describe the new classes. Objects that were not attributed to any of these two classes were classified as 'others'.

The sub-class 'nigra mature pure' had the following set of conditions:

If (thematic reflectance and thematic PCA and thematic MNF = 'nigra pure') then objects are classified as 'nigra mature pure'.

The sub-class 'nigra mature dense cover' had the following set of conditions:

If (thematic reflectance and thematic PCA = 'nigra mature') or (thematic reflectance and thematic MNF = 'nigra mature') or (thematic PCA and thematic MNF = 'nigra mature') then objects are classified as 'nigra mature dense cover'.

The sub-class 'nigra regeneration pure' had the following set of conditions:

If (thematic reflectance and thematic PCA and thematic MNF = 'nigra regeneration') then objects are classified as 'nigra regeneration pure'.

The sub-class 'nigra regeneration dense cover' had the following set of conditions:

If (thematic reflectance and thematic PCA = 'nigra regeneration') or (thematic reflectance and thematic MNF = 'nigra regeneration') or (thematic PCA and thematic MNF = 'nigra regeneration') then objects are classified as 'nigra regeneration dense cover'.

The classes 'brutia regeneration pure' and 'brutia regeneration dense cover' were grouped into one class called 'brutia regeneration all'. The classes of 'nigra mature pure' and 'nigra mature dense cover' were grouped into another class called 'brutia

mature all'. Also, 'nigra regeneration pure' and 'nigra regeneration dense cover' were grouped into a class called 'nigra regeneration all'.

Like in the previous subset, the two classes at level 3, namely 'burned' and 'not burned' were created. The classification employed the two Landsat-TM images and objects were classified using the band ratio of NIR.

At the final level of classification (level 2), four new classes were created in addition to the 'brutia regeneration' class. These classes were: 'nigra mature', 'nigra regeneration', 'other vegetations' and 'others'.

'Nigra mature' had the following set of conditions:

If (existence of 'not burned' super-objects and existence of 'shadows' sub-objects and relative border to 'nigra mature' is 0.005 or higher) or (existence of 'nigra mature all' sub-objects and existence of 'not burned' super-objects) or (existence of 'not burned' super-objects and existence of 'other vegetations' sub-objects and relative border to 'nigra mature' neighbour objects is 0.35 or higher) then objects are classified as 'nigra mature'.

'Nigra regeneration' had the following set of conditions:

If (existence of 'burned' super-objects and existence of 'other vegetations' sub-objects and relative border to 'nigra regeneration' neighbour objects is 0.45 or higher) or (existence of 'burned' super-objects and existence of 'nigra regeneration all' sub-objects) then objects are classified as 'nigra regeneration'.

‘Other vegetations’ had the following conditions:

If (existence of ‘burned’ super-objects and existence of ‘nigra mature all’ sub-objects) or (existence of ‘nigra regeneration all’ sub-objects and existence of ‘not burned’ super-objects) or (existence of ‘brutia regeneration all’ sub-objects and existence of ‘not burned’ super-objects) or (existence of ‘other vegetations’ sub-objects) then objects are classified as ‘other vegetations’.

Finally, objects were classified as ‘others’ when none of the previous conditions was satisfied. The final output of the classification is presented in Figure 76.

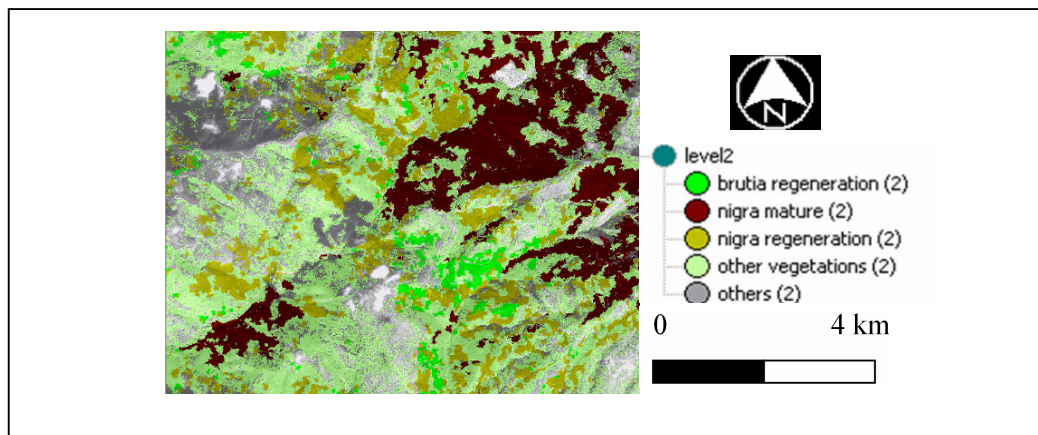


Figure 76 Final classification results at level 2 for AOI2

8.2 RESULTS AND DISCUSSION

By using an object-oriented approach for classifying very high spatial resolution imagery it was possible to create objects at a tree scale and attribute to these objects hyperspectral information from the thematic layers. To increase the accuracy of the results an object must satisfy a set of conditions based on both hyperspectral and high spatial resolution imagery. Moreover, in order to avoid confusions between certain type of vegetation and regenerated vegetation, two post-fire Landsat-TM images were employed. The use of these images helped in mapping burned areas, therefore restricting areas of possible pine regeneration.

In order to assess the accuracy of the results, the final maps were compared to 62 plots observed in field surveys. An error matrix was produced (Table 38) and accuracy totals were extracted (Table 39). Kappa statistics are shown in Table 40. The overall object-based classification accuracy of the total of classification was estimated to be 83.87% and the overall Kappa statistics was 0.79.

After a careful look at the results it was found that object-based classification performed with high accuracies on mature pine forests. Confusions between brutia and nigra regeneration were minimal. The main classification confusions were observed between 'brutia regeneration' and 'other vegetations' on one side and between 'nigra regeneration' and 'other vegetations' on the other side. This can be mainly attributed to areas with a very low density of pine regeneration.

Table 38 Error Matrix

Classified Data	Reference data					Row total
	P. brutia mature	P. brutia regeneration	P. nigra mature	P. nigra regeneration	Other vegetations	
P. brutia mature	4	0	0	0	0	4
P. brutia regeneration	0	13	0	1	3	17
P. nigra mature	0	0	16	1	1	18
P. nigra regeneration	0	0	0	7	2	9
Other vegetations	0	2	0	0	12	14
Column total	4	15	16	9	18	62

Table 39 Accuracy totals

Class name	Reference totals	Classified totals	Number correct	Producers accuracy	Users accuracy
P. brutia mature	4	4	4	100 %	100 %
P. brutia regeneration	15	17	13	86.67 %	76.47 %
P. nigra mature	16	18	16	100 %	88.89 %
P. nigra regeneration	9	9	7	77.78 %	77.78 %
Other vegetations	18	14	12	66.67 %	85.71 %
Totals	62	62	52	-	-
Overall Classification Accuracy	83.87 %				

Table 40 Kappa Statistics

Class Name	Kappa
P. brutia mature	1
P. brutia regeneration	0.6896
P. nigra mature	0.8502
P. nigra regeneration	0.7400
Other vegetations	0.7987
Overall Kappa Statistics	0.7900

The overall classification accuracy was found to be 75.81% when using only the Hyperion image. An improvement of 8.06% was recorded when combining both Hyperion and QuickBird (83.87 % of overall accuracy). A closer examination of the accuracy assessment tables showed that mapping brutia regeneration was notably improved while there was not a major improvement in mapping nigra regeneration. This can be explained by the very low cover density of nigra regeneration which is often mixed with other species of vegetation.

8.3 CHAPTER SUMMARY

In summary:

- The aim of this study was to map post-fire forest vegetation in the Mediterranean by combining EO-1 Hyperion and QuickBird in an object-oriented analysis. The presented approach used the benefits of combining high spatial with high spectral resolution remote sensing data.
- The object-based classification of QuickBird allowed extracting information not only from the image itself but also from other images such as Hyperion and Landsat-TM.
- Level 2 was the first to be segmented with a tree-scale of 10 taking into consideration the shape factor. Then, level 1 was created with a scale 9 taking into consideration both the QuickBird image and the thematic layers. Finally, level 3 was created with a scale of 100 employing Landsat-TM images.
- A classification scheme was developed and applied to the first image subset, namely AOI1 and then slightly modified and applied to the second image subset AOI2.
- Class description often consisted of combinations of conditions connected by operators like “and,” “or” and “not.” This gave flexibility to the classification process in terms of taking advantages from most useful information.
- When comparing the final forest regeneration map to plots surveyed in the field it was found that the overall classification accuracy was estimated to be 83.87% and the overall Kappa statistics was 0.79. Few classification confusions were observed in pine regeneration areas of very low density.
- An improvement of 8.06% was recorded when combining both Hyperion and QuickBird than by using only the Hyperion image. A closer examination of the accuracy assessment tables showed that mapping brutia regeneration was notably improved while there was not a major improvement in mapping nigra regeneration.
- Finally, this investigation of using multiresolution and multispectral imageries for mapping forest regeneration and vegetation recovery proved the importance of employing object-oriented analysis for better classification performance and results.

CHAPTER 9: GENERAL CONCLUSIONS AND RECOMMENDATIONS

9.1 GENERAL CONCLUSIONS

It has been emphasized throughout this work that detailed and current post-fire information concerning the extent of the burned areas, the type and severity of fire as well as forest regeneration and vegetation recovery, is important to understand the effects of forest fires in the short term and in the long term. Advanced tools in remote sensing provide the necessary means for gathering information about the burned areas, the regenerated forests and the recovered vegetations in a timely/cost effective manner.

The **aim** of this study was to assess the post-fire impact on vegetation in the Mediterranean ecosystem of Thasos using advanced tools in remote sensing. It was found that Ikonos imagery can be used to successfully map fire type and severity. Also, the combined use of QuickBird and Hyperion images can be used to map forest regeneration and vegetation recovery with a high degree of accuracy. Besides, the powerful method for object-oriented image analysis significantly extended the range of image analysis applications and turned the remotely sensing data into more accurately classified geographic post-fire information. The **specific objectives** of this work were:

1. to investigate the potential use of Very High Resolution (VHR) satellite imagery (Ikonos) in mapping the type and severity of fire;
2. to map vegetation recovery by using VHR satellite imagery (QuickBird) and to examine the relationship between fire severity and vegetation recovery;
3. to map forest regeneration and vegetation recovery by using hyperspectral remote sensing (field spectrometry and Hyperion); and
4. to examine the combination of VHR and hyperspectral imagery in forest regeneration and vegetation recovery mapping.

In relation to the above specific objectives of this work, the major findings and conclusions can be summarised as follows:

Objective 1: to investigate the potential use of Very High Resolution (VHR) satellite imagery (Ikonos) in mapping the type and severity of fire.

The main conclusion drawn from this task is that object-oriented classification employing Very High Spatial resolution imagery can be used to accurately distinguish and map areas of surface and crown fire spread (overall accuracy of 87% and Kappa Index of Agreement 0.74), especially that occurring in open Mediterranean forests. Classification accuracy was mainly affected by the density of the canopy. This could be attributed to the inability of the optical sensors to penetrate dense canopy to detect fire affected areas.

In a more advanced step, object-based classification resulted in mapping successfully the three classes of fire severity. When compared to field collected data the overall classification accuracy was estimated to be 83% while the KIA was 0.74. Classification accuracy percentages were consistently higher in the case of heavily burned areas. The shadowing from tree crowns, the poor spectral resolution of Ikonos together with the inability of the sensor to penetrate dense canopy were identified as being the main sources of confusion.

Objective 2: to map vegetation recovery by using VHR satellite imagery (QuickBird) and to examine the relationship between fire severity and vegetation recovery.

The classification of high spatial resolution image using object-oriented analysis successfully allowed vegetation survival mapping of canopy and shrub recovery within two different fire severity levels.

When comparing the produced map to plots surveyed in the field it was found that the overall classification accuracy was estimated to be 86% and the overall Kappa statistics was 0.83. Few classification confusions between forest and vegetation recovery (in areas of slight-moderate severity of fire) were observed.

A careful investigation of the results showed that mortality of *P. brutia* was very high within areas affected by high severity fire. Post-fire shrub vegetation dominated most

of the areas due to their sprouting and recovering ability. Seedling regeneration of *P. brutia* was almost absent.

Also, it was observed that fire was a driving force in landscape homogenization. The fires producing severely burned patches favoured the colonization of invasive, fire tolerant species at the expense of rare/endemic species less tolerant to post-fire conditions.

Objective 3: to map forest regeneration and vegetation recovery by using hyperspectral remote sensing (field spectrometry and Hyperion).

It was possible to extract the best wavebands for discriminating between pine age and species and among different post-fire shrub vegetation.

On one side, the study resulted in recommending 14 best narrowbands (from 60 hyperspectral bands), in the range of 0.4 to 1.1 μm . to discriminate among pine trees (age and species). The most frequently occurring waveband centres were: 428.441, 458.961, 479.311, 591.037, 621.506, 672.346, 702.917, 733.489, 794.641, 865.941, 907.288, 957.738, 967.828, and 988.048 nm.

On the other side, the study resulted in recommending 18 bands that best characterize the different shrub species. The most frequently occurring waveband centres were: 428.441, 458.961, 479.311, 489.488, 509.82, 601.194, 651.995, 672.346, 723.305, 753.863, 774.236, 784.43, 835.421, 865.941, 926.999, 937.568, 957.738, and 977.918 nm.

The *sig.* (2-tailed) analysis showed a significant difference in reflectance due to change in most pine and shrub species and in ages for pine trees.

Furthermore, the classification process of the Hyperion image successfully mapped two different forest species (*P. brutia* and *P. nigra*) and their regeneration. Also the different shrub species recovered after fire, were successfully mapped. The fuzzy analysis of the results showed that most objects of the different classes met the class's criteria sufficiently. The overall classification accuracy was found to be 75.81%,

while overall Kappa Index of Agreement (KIA) was 0.689. The accuracy showed very promising results in mapping two different regenerated pine species and other vegetation recovery after fire.

The classes of mature pine forests were the most accurately identified. Classification confusion between pine regeneration and the class 'other vegetations', was recorded in some places. This confusion was explained by absence of large homogenously regenerated pine trees.

Objective 4: to examine the combination of VHR and hyperspectral satellite imagery in forest regeneration and vegetation recovery mapping.

The combination of QuickBird and Hyperion resulted in the successful mapping of forest regeneration and vegetation recovery.

It was found that the overall classification accuracy was estimated to be 83.87% and the overall Kappa statistics was 0.79. Few classification confusions were observed in pine regeneration areas of very low density.

An improvement of 8.06% was recorded when combining both Hyperion and QuickBird than by using only the Hyperion image. A closer examination of the accuracy assessment tables showed that mapping brutia regeneration was notably improved while there was not a major improvement in mapping nigra regeneration.

Finally, this investigation of using data coming from different sources to map forest regeneration after fire proved the importance of using object-oriented analysis for better classification performance and results.

9.2 RECOMMENDATIONS AND FUTURE INVESTIGATIONS

Further research with respect to this work might follow two main directions. The first would be within the context of testing the transferability of the developed approach for post-fire impact assessment and the second in investigating the potential use of new sensing systems mainly active systems to avoid the encountered problems that were faced in this work.

In relation to the first direction, the existing constraints on automated data interpretation are so profound that an efficient integration of remote sensing and GIS is still a matter for research and development. The automated allocation and extraction of real world geographic objects from high resolution remotely sensed data is the central challenge for both the remote sensing and the GIS communities within the next few years. In this situation, object-oriented approach as applied in this work by integrating remote sensing and GIS into one analysis prospect is opening new paths and perspectives not only in post-fire impact assessment but also in much other kind of applications.

The methodology developed in this research study led to the implementation of an integrated approach for post-fire impact assessment. Thasos Island is a representative Mediterranean ecosystem; this developed methodology is worth being investigated in other countries of the Mediterranean basin to support forest management, subject to the availability of reliable databases and the necessary expertise. In this work, an integrated approach was developed using up-to-date sensors to assess the impact of fire on the Mediterranean vegetation of Thasos. Efforts might be made to develop ecosystem-specific algorithms for post-fire impact assessment on vegetation. Such algorithms could be developed and validated by the organizing of a network of study cases.

In relation to the second direction, it should be known that remote sensing technology is advancing at a rapid rate. There are currently active sensors and satellites in operation that have the potential to provide more detailed and accurate information about vegetation than that provided by passive Ikonos, QuickBird and Hyperion instruments, in particular, the LIDAR instruments. As mentioned before, one of the

main limitations of passive optical remote sensing system is the impossibility of discriminating forest understory. The discrimination of various shrub fuel types might probably be done with airborne LIDAR, since it has provided a height accuracy of up to 5-15 cm. The LIDAR is worthy of closer observation in combination with the previously mentioned sensors due to its ability to penetrate the forest canopy and senses the ground complexity.

REFERENCES

- Adams, J. (1974). "Visible and near-infrared diffuse reflectance: Spectra of pyroxenes as applied to remote sensing of solid objects in the solar system." *J. Geophys. Res.* 96: 475-484.
- Adler-Golden, S., Matthew, M., Bernstein, L., Levine, R., Berk, A., Richtsmeier, S., Acharya, P., Anderson, G., Felde, G., Gardner, J., Hoke, M., Jeong, L., Pukall, B., Ratkowski, A. and Burke, H. (1999). Atmospheric Correction for Shortwave Spectral Imagery Based on MODTRAN4. In: *SPIE proceedings Imaging Spectrometry*. pp. 61-69.
- Albini, F. and Stocks, B. (1986). "Predicted and observed rates of spread of crown fires in immature jack pine." *Combustion Science and Technology* 48: 65-76.
- Alexandrian, D. (1995). Coastal Forest Reconstruction and Protection Project - Republic of Croatia. Washington, DC, World Bank: 93.
- Amanatidis, G., Paliatsos, A., Repapis, C. and Bartzis, J. (1993). "Decreasing precipitation trend in the Marathon area, Greece." *International Journal of Climatology* 13: 191-201.
- Amiro, B., MacPherson, J., Desjardins, R., Chen, J. and Liu, J. (2003). "Post-fire carbon dioxide fluxes in the western Canadian boreal forest: evidence from towers, aircraft and remote sensing." *Agricultural and Forest Meteorology* 115: 91-107.
- Anon (1995). Analyse des causes des feux de forêt en Grèce. Les incendies de forêt en région méditerranéenne: 25: 33-39.
- Aoki, M., Yabuki, K. and Totsuka, T. (1981). An evaluation of chlorophyll content of leaves based on the spectral reflectivity in several plants, *The National Institute for Environmental Studies of Japan*: 125-130.
- Avrelo, J., Fernandez-Palacios, J., Jiménez, M. and Gil, P. (2001). "The effect of FIRE intensity on the understory species composition of two *Pinus canariensis* reforested stands in Tenerife (Canary Islands)." *Forest Ecology and Management* 148: 21-29.
- Baatz, M. and Schape, A. (1999). Object-Oriented and Multi-Scale Image Analysis in Semantic Networks. In: *2nd International Symposium on Operationalization of Remote Sensing*. pp. 15-20.
- Baatz, M. and Schape, A. (2000). Multiresolution segmentation - an optimization approach for high quality multi-scale image segmentation. In: J. e. a. h. STROBL, *Angewandte Geographische Informationsverarbeitung XII Beiträge zum AGIT-Symposium Salzburg 1999*, Karlsruhe, Herbert Wichmann Verlag. pp. 12-23.
- Bailey, J. and Covington, W. (2002). "Evaluating ponderosa pine regeneration rates following ecological restoration treatments in northern Arizona, USA." *Forest ecology and management* 155 (271-278).
- Baker, J., Briggs, S., Gordon, V., Jones, R., Settle, J., Townshend, J. and Wayatt, B. (1991). "Advances in classification for land cover mapping using SPOT HRV imagery." *International Journal of Remote Sensing* 12 (5).
- Baltsavias, E. (1999). "Airborne laser scanning: basic relations and formulas." *ISPRS Journal of Photogrammetry and Remote Sensing* 54: 199-214.

- Barbosa, P., Gregoire, J. and Pereira, J. (1999). "An algorithm for extracting burned areas from time series of AVHRR GAC data applied at a continental scale." *Remote Sensing of Environment* 69: 253-263.
- Bauer, M., Daughtry, C. and Vanderbilt, V. (1981). Spectral-agronomic relationships of corn, soybean, and wheat canopies Laboratory for Applications of Remote Sensing, Purdue University: 17.
- Beaty, R. and Taylor, A. (2001). "Spatial and temporal variation of fire regimes in a mixed conifer forest landscape, Southern Cascades, California, USA." *Journal of Biogeography* 28: 955-966.
- Belda, F. and Meliá, J. (2000). "Relationships between climatic parameters and forest vegetation: application to burned area in Alicante (Spain)." *Forest ecology and management* 135: 195-204.
- Belward, A. (1991). Spectral characteristics of vegetation, soil and water in the visible, near-infrared and middle-infrared wavelengths. In: A. Belward and C. Valenzuela, *Remote sensing and Geographical Information Systems for Resource Management in developing countries*, Kluwer, Netherlands. pp. 30-45.
- Benson, M. and Briggs, I. (1978). Mapping the extent and intensity of major forest fires in Australia using digital analysis of Landsat imagery. In: *International Symposium on Remote Sensing for Observation and Inventory of Earth Resources*, Freiburg. pp. 1965-1980.
- Benz, U. (1999). "Supervised Fuzzy Analysis of Single- and Multichannel SAR Data." *IEEE Transactions on Geoscience and Remote Sensing* 37 (2): 1023-1037.
- Benz, U., Hofmann, P., Willhauck, G., Lingenfelder, I. and Heynen, M. (2004). "Multi-resolution, object-oriented fuzzy analysis of remote sensing data for GIS ready information." *Journal of Photogrammetry and Remote Sensing* (58): 239-258.
- Berk, A., Bernstein, L., Anderson, G., Acharya, P., Robertson, D., Chetwynd, J. and Adler-Golden, S. (1998). "MODTRAN Cloud and Multiple Scattering Upgrades with Application to AVIRIS." *Remote Sensing of Environment* 65: 367-375.
- Berk, A., Bernstein, L. and Robertson, D. (1989). MODTRAN: a moderate resolution model for LOWTRAN7. GL-TR-89-0122, Air Force Geophys. Lab., Hanscom AFB, MA: 38.
- Bertolette, D. and Spotskey, D. (2001). Remotely sensed burn severity mapping. In: H. David Harmon, Michigan, *Crossing Boundaries in Park Management: Proceedings of the 11th Conference on research and Resource Management in Parks and on Public Lands*, The George Wright Society. pp. 44-51.
- Billings, W. and Morris, R. (1951). "Reflection of visible and infrared radiation from leaves of different ecological groups." *American Journal of Botany* 38: 327-331.
- Blackburn, G. (1999). "Relationships between spectral reflectance and pigment concentrations in stacks of deciduous broadleaves." *Remote Sensing of Environment* 70 (2): 224-237.
- Blackburn, G. and Milton, E. (1995). "Seasonal variations in the spectral reflectance of deciduous tree canopies." *International Journal of Remote Sensing* 16 (4): 709-720.

- Blackburn, G. and Steele, C. (1999). "Towards the remote sensing of matorral vegetation physiology: Relationships between spectral reflectance, pigment, and biophysical characteristics of semiarid bushland canopies." *Remote Sensing of Environment* 70: 278–292.
- Boardman, J. and Kruse, F. (1994). Automated spectral analysis: a geological example using AVIRIS data, north Grapevine Mountains, Nevada. In: *ERIM Tenth Thematic Conference on Geologic Remote Sensing*, Environmental Research Institute of Michigan, MI. pp. 407–418.
- Boardman, J., Kruse, F. and Green, R. (1995). Mapping target signatures via partial unmixing of AVIRIS data. In: *Fifth JPL Airborne Earth Science Workshop*, Pasadena. pp. 23–26.
- Broge, N. and Leblanc, E. (2000). "Comparing prediction power and stability of broadband and hyperspectral vegetation indices for estimation of green leaf area index and canopy chlorophyll density." *Remote Sensing of Environment* 76: 156–172.
- Brumby, D., Theiler, J., Bloch, J., Harvey, N., Perkins, S., Szymanski, J. and Young, A. (2002). Evolving land cover classification algorithms for multi-spectral and multi-temporal imagery. In: *SPIE 4480*. pp. 120–129.
- Brumby, S., Harvey, N., Bloch, J., Theiler, J., Perkins, S., Young, A. and Szymanski, J. (2001). Evolving Forest Fire Burn Severity Classification Algorithms for Multi-Spectra Imagery. In: *Proceedings SPIE 4381*, April 2001. pp. 20–30.
- Burns, R. (1970). *Mineralogical applications to crystal field theory*. Cambridge, Cambridge University Press.
- Caetano, M., Mertes, L., Cadete, L. and Pereira, J. (1995). Assessment of AVHRR data for characterizing burned areas and post-fire vegetation recovery. In: *International Workshop on Remote Sensing and GIS Applications to Forest Fire Management*, 7–9 September 1995, University of Alcalá de Henares, Spain. pp. 19–25.
- Caetano, M., Mertes, L. and Pereira, J. (1994). Using Spectral Mixture Analysis for Fire Severity Mapping. In: *2nd Int. Conf. Forest Fire Research*, Coimbra. pp. 667–677.
- Campbell, J. (1996). *Introduction to Remote Sensing*. London, Taylor & Francis.
- Canackcioglu, H. and Ozkazanc, O. (1997). What can we do to reduce forest fires in Mediterranean region? In: *XI. World Forestry Congress*, Antalya, Turkey. pp. 12–20.
- Canackcioglu, H. (1986). *Forest fires and fire problems in Turkey*. Valencia, Spain: 10.
- Carter, G. (1994). "Ratios of leaf reflectances in narrow wavebands as indicators of plant stress." *International Journal of Remote Sensing* 15: 697–703.
- Carter, G. (1998). "Reflectance bands and indices for remote estimation of photosynthesis and stomatal conductance in pine canopies." *Remote Sensing of Environment* (63): 61–72.
- Caturla, N., Raventós, J., Guàrdia, R. and Vallejo, R. (2000). "Early post-fire regeneration dynamics of *Brachypodium retusum* Pers. (Beauv.) in old fields of the Valencia region (eastern Spain)." *Acta Oecologica* 21 (1): 1–12.
- Chen, K., Jacobson, C. and Blong, R. (2001). Using NDVI image texture analysis for bushfire-prone landscape assessment. In: *22nd Asian Conference on Remote Sensing*, 5–9 November 2001, Singapore. pp. 45–51.

- Chuvieco, E. (1997). Foreword. A review of remote sensing methods for the study of large wildland fires. E. Chuvieco. Alcalá de Henares, Departamento de Geografía, Universidad de Alcalá: 3-5.
- Chuvieco, E. and Congalton, R. (1988a). "Using cluster analysis to improve the selection of training statistics in classifying remotely sensed data." *Photogrammetric Engineering & Remote Sensing* 54: 1275-1281.
- Chuvieco, E. and Congalton, R. (1988b). "Mapping and inventory of forest fires from digital processing of TM data." *Geocarto International* 4: 41-53.
- Chuvieco, E., Deshayes, M., Stach, N., Cocero, D. and Riaño, D. (1999). Short-term fire risk: foliage moisture content estimation from satellite data. *Remote Sensing of Large Wildfires in the European Mediterranean Basin*. E. Chuvieco. Berlin, Springer-Verlag: 17-38.
- Chuvieco, E. and Martin, P. (1994). "Global fire mapping and fire danger estimation using AVHRR images." *Photogrammetric Engineering and Remote Sensing* 60: 563-570.
- Chuvieco, E., Salas, F. and Vega, C. (1997). Remote sensing and GIS for long-term fire risk mapping. A review of remote sensing methods for the study of large wildland fires. E. Chuvieco. Alcalá de Henares, Departamento de Geografía, Universidad de Alcalá: 91-107.
- Civanlar, R. and Trussell, H. (1986). "Constructing Membership Functions Using Statistical Data." *Fuzzy Sets and Systems* 18 (1-13).
- Civco, D. (1989). "Topographic Normalization of Landsat Thematic Mapper Digital Imagery." *Photogrammetric Engineering and Remote Sensing* 55 (9): 1303-1309.
- Clark, R., Swayze, G., Kink, T., Eric Livo, K., Kokaly, R., Dalton, B., Vance, J., Rockwell, B. and McDougal, R. (1999). Surface Reflectance Calibration of Imaging terrestrial Spectroscopy Data: A tutorial using AVIRIS.
- Colby, J. (1991). "Topographic normalization in rugged terrain." *Photogrammetric Engineering and Remote Sensing* 57 (5): 531-537.
- Collins, W. (1978). "Remote sensing of crop type and maturity." *Photogrammetry Eng. and Remote Sensing* 44: 43-55.
- Collins, W., Chang, S., Raines, G., ACanney, F. and Ashley, R. (1983). "Airborne biogeochemical mapping of hidden mineral deposits." *Econ. Geology* 78: 737-743.
- Costa-Posada, C. (1997). The Topographic Effect in Visible and Near Infrared Satellite Imagery. PhD dissertation. Department of Geography. Cambridge, UK, University of Cambridge: 199.
- Costa-Posada, C. and Devereux, B. (1995). "Reduction of the topographic effect in SPOT imagery: An examination of the Minnaert model." In *Proceedings series, SPIE* 2579: 137-149.
- Critchfield, W. and Little, J. E. (1996). *Geographic Distribution of the Pines of the World*, USDA, Forest Service.
- Curran, P. (1994). "Imaging spectrometry." *Progress in Physical Geography* 18 (2): 247-266.

- Curran, P., Dungan, J., Macler, B. and Plummer, S. (1991). "The effect of a red leaf pigment on the relationship between red-edge and chlorophyll concentration." *Remote Sensing of Environment* 35: 69–75.
- Curran, P., Dungan, J., Macler, B., Plummer, S. and Peterson, D. (1992). "Reflectance specyrosopy of fresh whole leaves for the estimation of chemical concentration." *Remote Sensing of Environment* 39: 153-166.
- Dafis, S. (1990). Prevention of fire and postfire rehabilitation using silvicultural methods. In: Workshop on forest fires in Greece, Thessaloniki, Greece, Department of Forestry and Natural Environment, Aristotelian University of Thessaloniki. pp. 65-72.
- De Jong, B., Gaona, S., Santiago, M., Marcial, N. and Cairns, M. (2000). "Carbon flux and patterns of land-use/land-cover change in the Selva Lacandona, Mexico." *Ambio* 29 (8): 504-511.
- De Luis, M., Garcia-Cano, M., Cortina, J., Raventos, J., Gonzales-Hidalgo, J. and Sanchez, J. (2001). "Climatic trends, disturbances and short-term vegetation dynamics in a Mediterranean shrubland." *Forest ecology and management* (147): 25-37.
- De Wit, A. and Clevers, J. (2004). "Efficiency and accuracy of per-field classification for operational crop mapping." *International Journal of Remote Sensing* 20: 4091-4112.
- Delattre, E. (1993). Évaluation des actions communautaires: vers une coopération internationale: 271.
- Di Castri, F. and Mooney, A. (1973). *Mediterranean Type Ecosystems. Origin and Structure*, Ecological Studies, Springer-Verlag, Berlin.
- Diaz-Delgado, R., Lloret, F. and Pons, X. (2003). "Influence of fire severity on plant regeneration by means of remote sensing imagery." *International Journal of Remote Sensing* (24): 1751-1763.
- Díaz-Delgado, R. and Pons, X. (2001). "Spatial patterns of forest fires in Catalonia (NE of Spain) along the period 1975-1995. Analysis of vegetation recovery after fire." *Forest ecology and management* 147: 67-74.
- Diaz-Delgado, R., Salvador, R. and Pons, X. (1998). Monitoring of plant community regeneration after fire by remote sensing. In: L. Traboud, *Fire management and landscape ecology*, Fairfield, WA: International Association of Wildland Fire. pp. 315–324.
- Díaz-Delgado, R., Salvador, R., Valeriano, J. and Pons, X. (1999). Detection of burned forest areas in Catalonia using a temporal series of Landsat MSS imagery (period 1975-93). In: F. Neuenschwander, C. Ryan, E. Gollberg and D. Greer, *Joint Fire Science Conference and Workshop. Crossing the Millenium: Integrating Spatial Technologies and Ecological Principles for a New Age in Fire Management*, 15-17 June 1999, Boise, Idaho. pp. 15-24.
- Eckert, S. and Kneubuehler, M. (2004). Application of HYPERION data to agricultural land classification and vegetation properties estimation in Switzerland. In: ISPRS, Istanbul. pp. 24-32.
- Elvidge, C. and Chen, Z. (1995). "Comparison of broadband and narrowband red and near-infrared vegetation indices." *Remote Sensing of Environment* 54: 38–48.

- Elvidge, C., Chen, Z. and Groeneveld, D. (1993). "Detection of trace quantities of green vegetation in 1990 AVIRIS data." *Remote Sensing of Environment* 44: 271– 279.
- Elvidge, C. and Portigal, F. (1990). Change detection in vegetation using AVIRIS data. In: G. Vane, *PIE imaging spectroscopy of the terrestrial environment* Orlando, FL: International Society for Optical Engineering (SPIE). pp. 178– 189.
- Emberger, L. (1971). *Considerations complementaires au sujet des recherches bioclimatologiques et phytogeographiques*. Travaux de Botanique et d'Ecologie. E. L. Paris, Masson et Cie: 291-301.
- EPA (2001). *Inventory of U.S. Greenhouse Gas Emissions and Sinks: 1990 – 1999*. U.S., Environmental Protection Agency: 75-85.
- Escuin, S., Navarro, R. and Fernandez, P. (2002). "Using remote sensing and GIS to assess wildfire damage throughout the Mediterranean." *EOM* 11 (5): 19-22.
- Fiorella, M. and Ripple, W. (1993). "Analysis of conifer forest regeneration using Landsat Thematic Mapper data." *Photogrammetric Engineering and Remote Sensing* 59: 1383– 1388.
- Forman, R. and Godron, M. (1986). *Landscape Ecology*. New York, John Wiley and Sons.
- Fourty, T., Baret, F., Jacquemoud, S., Schmuck, G. and Verdebout, J. (1996). "Leaf optical properties with explicit description of its biochemical composition: direct and inverse problems." *Remote Sensing of Environment* 56: 104-117.
- Fox III, L. and Stuart, D. (1994). Detecting changes in forest condition following wildfire, using image processing and GIS. In: *ACSM/ASPRS Annual Convention & Exposition*, Baltimore, ACSM/ASPRS. pp. 197-206.
- Franklin, J., Syphard, D., Mladenoff, J., He, S., Simons, K., Martin, P., Deutschman, D. and A'Leary, F. (2001). "Simulating the effects of different fire regimes on plant functional groups in Southern California." *Ecological Modelling* 142: 261-283.
- Fraser, R. and Li, Z. (2002). "Estimating fire-related parameters in boreal forest using SPOT VEGETATION." *Remote Sensing of Environment* 82: 95-110.
- French, N., Kasischke, E., Johnson, R., Bourgeau-Chavez, L., Frick, A. and Ustin, S. (1996). Estimating fire-related carbon flux in Alaska boreal forests using multi-sensor remote sensing data. In: J. Levine, *Biomass burning and climate change*, Cambridge, MA: MIT Press. pp. 808–826.
- Gamon, J., Field, C., Goulden, M., Griffin, K., Hartley, A., Joel, G., Penuelas, J. and Valentini, R. (1995). "Relationships between NDVI, canopy structure, and photosynthesis in three Californian vegetation types." *Ecological and Applications* 5 (1): 28– 41.
- Gao, B. and Goetz, A. (1994). "Extraction of dry leaf spectral features from reflectance spectra of green vegetation,". *Remote Sensing of Environment* 47: 369-374.
- García-Haro, F., Gilabert, M. A. and Meliá, J. (2001). "Monitoring fire-affected areas using Thematic Mapper data." *International Journal of Remote Sensing* 22 (4): 533-549.
- García-Ruiz, J., Lasanta, T., Ruiz-Flano, P., Ortigosa, L., White, S., González, C. and Martí, C. (1996). "Land-use changes and sustainable development in mountain areas: A case study in the Spanish Pyrenees." *Landscape Ecology* 11: 267-277.

- Gates, D., Keegan, H., Schleter, V. and Weidner, V. (1965). "Spectral properties of plants." *Applied optics* 4: 11-20.
- Gausman, H., Allen, W., Cardenas, R. and Richardson, A. (1970). "Relationship of light reflectance to historical and physical evaluation of cotton leaf maturity." *Applied Optics* 4: 11-20.
- Gimeno, M., San-Miguel Ayanz, J., Barbosa, P. and Schmuck, G. (2002). Burnt area mapping from ERS-SAR time series using the principal component transformation. In: SPIE 9th International Symposium on Remote Sensing, 22-27 September 2002, Capsis Beach Hotel and Conference Center, Aghia Pelagia, Crete, Greece. pp. 60-72.
- Gitas, I. (1999). Geographical Information Systems and Remote Sensing in mapping and monitoring fire-altered forest landscapes. PhD dissertation. Department of Geography, University of Cambridge: 237.
- Gitas, I., Mitri, G. and Ventura, G. (2004). "Object-oriented image analysis for burned area mapping using NOAA-AVHRR imagery in Creus Cape, Spain." *Remote Sensing of Environment* 92 (3): 409-413.
- Gitas, I., Radoglou, K., Devereux, B. and Spanos, I. (2000). Comparative study of the post fire ecosystem recovery of *Pinus brutia* in Thasos by using experimental plots and Geographical Information Systems. In: Proceedings of the International Conference on Protection and Restoration of the Environment Thasos, Greece, July 2000.
- Gitas, I. and Rishmawi, K. (2003). "Burned area mapping with the use of low, medium-high and very high resolution satellite imagery." *Geotechnical Scientific Issues* 44: 4-15.
- Gluck, M. and Rempel, R. (1995). The effect of scale on structural measurements of post-disturbance vegetation in Northwestern Ontario. Remote Sensing and GIS applications to forest fire management, C. R. Chuvieco E. Alcalá de Henares, Universidad de Alcalá.
- Goetz, A. (1991). Imaging spectrometry for studying Earth, Air, Fire and Water. In: *EARSel Advances in Remote Sensing*, pp. 3-15.
- Goetz, A. and Rowan, L. (1981). "Geologic remote sensing." *Science* 218: 1020-1031.
- Gould, K., Fredericksen, T., Morales, F., Kennard, D., Putz, F., Mostacedo, B. and Toledo, M. (2002). "Post-fire tree regeneration in lowland Bolivia: implications for fire management." *Forest ecology and management* 165: 225-234.
- Green, A., Berman, M., Switzer, P. and Graig, M. (1988). "A transformation for ordering multispectral data in terms of image quality with implications for noise removal." *IEEE Trans. Geosci.Rem.Sens.* 26: 65-74.
- Green, E., Clarck, C., Mumby, P., Edwards, A. and Ellis, A. (1998). "Remote Sensing techniques for mangrove mapping." *International Journal of Remote Sensing* 19: 935-956.
- Greiwe, A. and Ehlers, M. (2005). Combined analysis of hyperspectral and high resolution image data in an object oriented classification approach. In: M. Moeller and E. Wentz, *ISPRS Tempe, AZ, USA*, pp. 19-23.
- Gross, H. and Scott, J. (1998). "Application of spectral mixture analysis and image fusion techniques or images sharpening." *Remote Sensing of Environment* 63: 85-94.

- Hall, D., Ormskby, J., Johnson, L. and Brown, J. (1980). "Landsat digital analysis of the initial recovery of burned tundra at Kokolik River, Alaska." *Remote Sensing of Environment* 10: 263-272.
- Harsanyi, J. and Chang, C. (1994). "Hyperspectral image classification and dimensionality reduction: An orthogonal subspace projection approach." *IEEE Trans. Geosci. and Remote Sensing* 32: 779-785.
- Hayes, D. and Sader, S. (2001). "Comparison of Change-Detection Techniques for Monitoring Tropical Forest Clearing and Vegetation Regrowth in a Time Series." *Photogrammetric Engineering & Remote Sensing* 67 (9): 1067-1075.
- Henry, M. and Hope, A. (1998). "Monitoring post-burn recovery of chaparral vegetation in southern California using multitemporal satellite data." *International Journal of Remote Sensing* 19 (16): 3097– 3107.
- Hitchcock, H. and Hoffer, R. (1974). Mapping a recent forest fire with ERTS-1 MSS data. West Lafayette, Indiana, The Laboratory for Applications of Remote Sensing information, note 032674, Purdue University.
- Hoffer, R. (1978). Biological and physical considerations in applying computer aided analysis techniques to remote sensor data. In: P. Swain and S. Davis, *Remote sensing: the quantitative approach*, McGraw Hill, New York. pp. 227-189.
- Hofmann, T., Puzicha, J. and Buhmann, J. (1998). "Unsupervised texture segmentation in a deterministic annealing framework." *IEEE Transactions on Pattern Analysis and Machine Intelligence* 13 (8): 478-482.
- Holben, B. and Justice, C. (1981). "An examination of spectral band ratioing to reduce the topographic effect on remotely sensed data." *International Journal of Remote Sensing* 2: 115-133.
- Hostert, P., Roder, A. and Hill, J. (2003). "Coupling spectral unmixing and trend analysis for monitoring of long-term vegetation dynamics in Mediterranean rangelands." *Remote Sensing of Environment* 87: 183 – 197.
- Hudak, A. and Brocket, B. (2002). Rangeland fire scar mapping using Landsat imagery. *Rapid Delivery of Remote Sensing Products*. In: Ninth Forest Service Remote Sensing Applications Conference, San Diego, California, The American Society for Photogrammetry and Remote Sensing. pp. 10-15.
- Huete, A., Jackson, R. and Post, D. (1985). "Spectral response of a plant canopy with different soil backgrounds." *Remote Sensing of Environment* 17: 37-53.
- Hunt, E. and Rock, B. (1989). "Detection of changes in leaf water content using near and middle-infrared reflectances." *Remote Sensing of Environment* 30: 43-54.
- Hunt, G. (1977). "Spectral signatures of particulate minerals in the visible and near-infrared." *Geophysics* 42: 501-513.
- Hunt, G. (1980). *Electromagnetic radiation: the communication link in remote sensing. Remote sensing in geology*. B. S. a. A. Gillespie. New York, Wiley: 702.

- Jakubauskas, M. (1988). Postfire vegetation change detection using LANDSAT MSS and TM data. School of Graduate Studies. Terre Haute, Indiana, Indiana State University: 99.
- Jakubauskas, M. (1989). Utilizing a geographic information system for vegetation change detection. In: GIS/LIS 1989 ASPIS. pp. 30-36.
- Jakubauskas, M., Lulla, K. and Mausel, P. (1990). "Assessment of vegetation change in a fire-altered forest landscape." *Photogrammetric Engineering and Remote Sensing* 56 (3): 371-377.
- Janetos, A. and Justice, C. (2000). "Land cover and global productivity: A measurement strategy for the NASA programme." *International Journal of Remote Sensing* 21: 1491-1512.
- Jensen, J. (1996). *Introductory Digital Image Processing. A Remote Sensing Perspective*. Upper Saddle River N.J., Prentice-Hall.
- Kafka, V., Gauthier, S. and Bergeron, Y. (2001). "Fire impacts and crowning in the boreal forest: study of a large wildfire in western Quebec." *International Journal of Remote Sensing* (10): 119-127.
- Karteris, M., Meliadis, I., Kritikos, G. and Nikolaidis, A. (1992). Forest classification and mapping of Mediterranean forests and maquis with satellite data. Chania, Greece, Mediterranean Agronomic Institute of Chania: 153.
- Kasischke, E., Bourgeau-Chavez, L. and French, N. (1994). "Observations of Variations in ERS-1 SAR Image Intensity Associated with Forest Fires in Alaska." *IEEE Transactions on Geoscience and Remote Sensing* 32 (1): 206-210.
- Kawata, Y., Ueno, S. and kusaka, T. (1988). "Radiometric correction for atmospheric and topographic effects on Landsat MSS images." *International Journal of Remote Sensing* 9 (4): 729-748.
- Keeley, J. (2000). Chaparral. In: M. Barbour and W. Billings, *North American terrestrial vegetation*, New York, Cambridge University Press. pp. 204-253.
- Kennard, D., Gould, K., Putz, F., Fredericksen, T. and Morales, F. (2002). "Effect of disturbance intensity on regeneration mechanisms in a tropical dry forest." *Forest ecology and management* 162: 197-208.
- Key, C. and Benson, N. (1999a). "The Composite Burn Index (CBI): Field rating of burn severity."
- Key, C. and Benson, N. (1999b). "The Normalized Burn Ratio (NBR): A Landsat TM radiometric measure of burn severity."
- Key, C. and Benson, N. (2000). Measuring and Remote Sensing of Burn Severity. In: 2000 Wildland Fire Workshop, Denver, CO, U.S. Geological Survey and Wildland Fire, U.S. Department of the Interior, U.S. Geological Survey. pp. 15-19.
- Key, C. and Benson, N. (2002). Measuring and Remote sensing of burn severity. In: J.L. Coffelt and R.K. Livingston, *U.S. Geological Survey Wildland Fire Workshop*, Los Alamos, USGS. pp. 55.

- Key, C., Benson, N., Sorbel, B., Zhu, Z., Ohlen, D., Howard, S. and Clement, B. (2002). "National Park Service-U.S. Geological Survey National Burn Severity Mapping Project, USGS EROS Data Center."
- Kornas, K. (1958). "Sucession regressive de la vegetation des guarrigues sur les clacaires compacts dans la montagne de la Gardiole, pres de Montpellier." *Acta Soc. Bot. Pol.* 27: 563-596.
- Koutsias, N. and Karteris, M. (1998). "Logistic regression modelling of multitemporal Thematic Mapper data for burned area mapping." *International Journal of Remote Sensing* (18): 3499-3514.
- Kraft, M., Weigel, H., Mejer, G. and Brandes, F. (1996). "Reflectance measurements of leaves for detecting visible and non-visible ozone damage to crops." *Journal of Plant Physiology* 148: 148-154.
- Kushla, J. and Ripple, W. (1998). "Assessing wildfire effects with Landsat Thematic Mapper data." *International Journal of Remote Sensing* 19: 2493– 2507.
- Lachowski, H. and Anderson, S. (1979). Assessment of fire damage within Seney wildlife refuge from aerial photography and Landsat imagery. In: 7th Biennial Workshop on Color Aerial Photography in the Plant Sciences and Related Fields, 15-17 May 1979. pp. 5-12.
- Landsberg, J. (1994). A review of prescribed fire and tree growth response in the genus *Pinus*. In: The Twelfth Conference on Fire and Forest Meteorology, Jekyll Island, Georgia, USA. pp. 326-346.
- Lauer, D. and Krumpe, P. (1973). Testing the usefulness of ERTS-1 Imagery for inventorying wildland resources in northern California. In: Symposium on significant results obtained from the Earth Resources Satellite -1, Goddard Space Flight Center, Maryland. pp. 97-104.
- Le Houerou, H. (1987). "Vegetation wildfires in the Mediterranean basin: evolution and trends." *Ecologia Mediterranea* 13: 13-24.
- Le Hou  rou, H. (1993). "Land degradation in Mediterranean Europe: can agroforestry be a part of the solution? A prospective review. ." *Agrofor. Sys.* 21: 43-61.
- Lee, Y., Towler, F., Bradatsch, H. and Finding, S. (1977). Computer assisted forest and land classification by means of several classification methods on the CCRS image 100. In: 4th Canadian Symposium on Remote Sensing, Quebec. pp. 37-46.
- Leisz, D. (1982). Concern and cost of managing Mediterranean-type ecosystems. In: Symposium on Dynamics and Management of Mediterranean-type ecosystems, San Diego, California, USDA Forest Service. pp. 3-5.
- Leopold, A., Cain, S., Cottam, C., Gabrielson, I. and Kimball, T. (1963). "Wildlife management in the national parks." 32-35.
- Levesque, J. and King, D. (2003). "Spatial analysis of radiometric fractions from high-resolution multispectral imagery for modelling individual tree crown and forest canopy structure and health." *Remote Sensing of Environment* 84 (4): 589– 602.
- Lichtenthaler, H., Gitelson, A. and Lang, M. (1996). "Non-destructive determination of chlorophyll content of leaves of a green and an aurea mutant of tobacco by reflectance measurements." *Journal of Plant Physiology* 148: 483– 493.

- Lillesand, T. and Kiefer, R. (1994). *Remote Sensing and Image Interpretation*. New York, John Wiley and Sons.
- Lloret, F. and Vilà, M. (1997). "Clearing of vegetation in Mediterranean garrigue: response after a wildfire." *Forest ecology and management* 93: 227-234.
- Lombrana, M. J. (1995). *Monitoring of Burnt Forest Areas with Remote Sensing Data: A Study in North-East Spain using LANDSAT and SPOT XS Data*. Ispra, Italy, Institute for Remote Sensing Applications, Joint Research Centre, European Commission.
- Lopez, G. and Casselles, V. (1991). "Mapping burns and natural reforestation using thematic Mapper data." *Geocarto International* 6: 31-37.
- Lucas, R., Honzak, M., Amaral, I., Curran, P. and Foody, G. (2002). "Forest regeneration on abandoned clearances in Central Amazonia." *International Journal of Remote Sensing* 23 (5): 965-988.
- Luckman, A., Baker, J., Kuplich, T., Da Costa Freitas Yanasse, C. and Frery, A. (1997). "A study of the Relationship between Radar Backscatter and Regenerating Tropical Forest Biomass for Spaceborne SAR Instruments." *Remote Sensing of Environment* 60: 1-13.
- Luque, S. (2000). "Evaluating temporal changes using Multi-Spectral Scanner and Thematic Mapper data on the landscape of a natural reserve. the New Jersey Pine Barrens, a case study." *International Journal of Remote Sensing* 21 (14): 2587-2611.
- Lyon, J., Yuan, D., Lunetta, R. and Elvidge, C. (1998). "A change detection experiment using vegetation indices." *Photogrammetric Engineering and Remote Sensing* 64: 143-150.
- Maheras, P. (1988). "Changes in precipitation conditions in the western Mediterranean over the last century." *J. Clim.* 8: 179-189.
- Makedos, I. (1987). The *Pinus Brutia* forest of Thasos. In: P. V., *Pinus halepensis and Pinus Brutia forests (Ecology, management and development)*, Chalkida, Greece, Hellenic Association of Foresters. pp. 153-160.
- Mao, J. and Jain, A. (1992). "Texture classification and segmentation using multiresolution simultaneous autoregressive models." *Pattern Recognition* 25: 173-188.
- Marchetti, M., Ricotta, C. and Volpe, F. (1995). "A qualitative approach to the mapping of post-fire regrowth in Mediterranean vegetation with Landsat-TM data." *International Journal of Remote Sensing* 16 (13): 2487-2494.
- Mariotti, M., Ercoli, L. and Masoni, A. (1996). "Spectral properties of irondeficient corn and sunflower leaves." *Remote Sensing of Environment* 58: 282-288.
- Martin, M., Newman, S., Aber, J. and Congalton, J. (1998). "Determining forest species composition using high spectral resolution remote sensing data." *Remote Sensing of Environment* (65): 249-254.
- Martín, M., Viedma, O. and Chuvieco, E. (1994). High versus low resolution satellite images to estimate burned areas in large forest fires. In: *Second International Conference on Forest Fire Research*, Coimbra, Portugal. pp. 653-663.

- Mass, S. (2000). "Linear mixture modeling approach for estimating cotton canopy ground cover using satellite multispectral imagery." *Remote Sensing of Environment* (3): 304-308.
- Mather, P. (1999). *Computer Processing of Remotely-sensed Images: An Introduction*. West Sussex, England, John Wiley & Sons.
- Matthew, M., Adler-Golden, S., Berk, A., Richtsmeier, S., Levine, R., Bernstein, L., Acharya, P., Anderson, G., Felde, G., Hoke, M., Ratkowski, A., Burke, H., Kaiser, R. and Miller, D. (2000). Status of Atmospheric Correction Using a MODTRAN4-based Algorithm. In: *SPIE Proceedings, Algorithms for Multispectral, Hyperspectral, and Ultraspectral Imagery* pp. 199-207.
- McGwire, K., Minor, T. and Fenstermaker, L. (1999). "Hyperspectral mixture modeling for quantifying sparse vegetation cover in arid environments." *Remote Sensing of Environment* 72: 360-374.
- Medler, M. and Yool, S. R. (1997). "Improving Thematic Mapper based classification of wildfire induced vegetation mortality." *Geocarto International* 12: 49-58.
- Metzler, J. and Sader, S. (2002). The use of IKONOS and LANDSAT ETM+ sensors in determining regeneration stand conditions. In: J. D. Greer, *Rapid Delivery of Remote Sensing Products*. Ninth Forest Service Remote Sensing Applications Conference. 8-12 April 2002, San Diego, California, The American Society for Photogrammetry and Remote Sensing. pp. 27-30.
- Meyer, P., Itten, K., Kellenbenberger, T., Sandmeier, S. and Sandmeier, R. (1993). "Radiometric corrections of topographically induced effects on Landsat TM data in an alpine environment." *ISPRS Journal of Photogrammetry and Remote Sensing* 48 (4): 17-28.
- Michalek, J., French, N., Kasischke, E., Johnson, R. and Colwell, J. (2000). "Using Landsat TM data to estimate carbon release from burned biomass in an Alaskan spruce forest complex." *International Journal of Remote Sensing* 21: 323-338.
- Miller, J. and Yool, S. (2002). "Mapping forest post-fire canopy consumption in several overstory types using multitemporal Landsat TM and ETM data." *Remote Sensing of Environment* 82 (2): 481-496.
- Milne, A. (1986). "The use of remote sensing in mapping and monitoring vegetational change associated with bushfire events in Eastern Australia." *Geocarto International* 1 (1): 25-34.
- Minnaert, M. (1941). "The reciprocity principle in Lunar photometry." *Astrophysical Journal* 93 (2): 403-410.
- Mitri, G. and Gitas, I. (2004a). "A semi-automated object-oriented model for burned area mapping in the Mediterranean region using Landsat-TM imagery." *International Journal of Wildland Fire* 13 (3): 367-376.
- Mitri, G. and Gitas, I. (2004b). "A performance evaluation of a burned area object-based classification model when applied to topographically and non-topographically corrected TM imagery." *International Journal of Remote Sensing*, 14: 2863-2870.
- Mitri, G. and Gitas, I. (2005). Fire type mapping using object-based classification of Ikonos imagery. In: E. Chuvieco, *5th International workshop on remote Sensing and GIS Applications to Forest Fire Management: Fire Effects Assessment*, Zaragoza, Spain. pp. 199-203.

- Molinier, R. (1968). "La dynamique de la vegetation provencale." *Collect. Bot. Et appliquees* 60: 119-208.
- Moreira, F., Ferreira, P., Rego, F. and Bunting, S. (2001). "Landscape changes and breeding bird assemblages in northwestern Portugal: the role of fire." *Landscape Ecology* 16: 175-187.
- Moreno, J. M. and Oechel, W. C. (1994). *The Role of Fire in Mediterranean-Type Ecosystems* (Preface). *The Role of Fire in Mediterranean-Type Ecosystems*. J. M. Moreno and W. C. Oechel. Berlin, Springer-Verlag: v-vii.
- Moreno, J. M., Pineda, F. and Rivas-Martinez, S. (1990). "Climate vegetation at the Eurosiberian- Mediterranean boundary in the Iberian Peninsula." *Journal of Vegetation Science* 1: 233-244.
- Mumby, P., Green, E., Edwards, A. and Clarck, C. (1999). "The cost effectiveness of remote sensing for tropical coastal resources assessment and management." *Journal of Environmental Management* 55: 157-166.
- Nahal, I. (1983). *Le pin brutia* (*Pinus brutia* Ten. subsp. *brutia*). Première partie, For. Médit.: 165-171.
- Nakos, G. (1995). *Desertification in the Mediterranean Area: A Decision Support System for the prevention of desertification resulting from forest fires*. Project Phoenix, European Commission. Athens, Institute of Mediterranean Forest Ecosystems.
- Naveh, Z. (1975). "The evolutionary significance of fire in the Mediterranean region." *Vegetatio* 29: 199-208.
- Naveh, Z. (1991). "The role of fire in Mediterranean vegetation." *Botanica Chronika* (Greece) 10: 385-405.
- Ne'eman, G., Fotheringham, C. J. and Keeley, J. (1999). "Patch to landscape patterns in post fire recruitment of a serotinous conifer." *Plant ecology* 12: 235-242.
- Nguyen, P. and Ho, D. (1988). Multiple source data processing in remote sensing. In *Digital Image Processing in Remote Sensing*, e. J.P. Muller. London, Taylor and Francis Ltd.
- Nilson, T. and Peterson, U. (1994). "Dependence of Forest Reflectance: Analysis of Main Driving Factors." *Remote Sensing of Environment* 48: 319-331.
- Okin, G., Roberts, D., Murray, B. and Okin, W. (2001). "Practical limits on hyperspectral vegetation discrimination in arid and semiarid environments." *Remote Sensing of Environment* (77): 212-225.
- Panetsos, K. (1981). "Monograph of *Pinus halepensis* Mill. and *Pinus brutia* Ten." *Ann. For. (Zagreb)* 9: 39-77.
- Parnot, J. (1988). Inventaire des feux de brousse au Burkina Faso saison seche 1986-1987. In: 22nd International Symposium on Remote Sensing of the Environment, Abidjan, Cote d'Ivoire, ERIM, Ann Arbor, Michigan. pp.
- Patterson, M. and Yool, S. (1998). "Mapping fire-induced vegetation mortality using Landsat thematic mapper data: A comparison of linear transformation techniques." *Remote Sensing of Environment* 65: 132-142.

- Pausas, J., Carbó, E., Caturla, R., Gil, J. and Vallejo, R. (1999). "Post-fire regeneration patterns in the eastern Iberian Peninsula." *Acta Oecologica* 20 (5): 499-508.
- Pausas, J. and Ramon, V. (1999). The role of fire in European Mediterranean ecosystems. *Remote Sensing of Large Wildfires in the European Mediterranean Basin*. E. Chuvieco. Berlin, Springer: 3-15.
- Pearlman, J., Carman, S., Segal, C., Jarecke, P., Barry, P. and Browne, W. (2001). Overview of the Hyperion imaging spectrometer for the NASA EO-1 mission. In: *IGARSS*, Sydney, Australia. pp. 3036–3038.
- Peneulas, J., Filella, I., Biel, C., Serrano, L. and Save, R. (1993). "The reflectance at the 950-970nm region as an indicator of plant water status." *International Journal of Remote Sensing* 14: 1887-1905.
- Penuelas, J., Filella, I., Lloret, P., Munoz, F. and Vilajeliu, M. (1995). "Reflectance assessment of mite effects on apple trees." *International Journal of Remote Sensing* 16: 2727– 2733.
- Pereira, J., Chuvieco, E., Beaudoin, A. and Desbois, N. (1997). Remote sensing of burned areas. A review of remote sensing methods for the study of large wildland fires, E. Chuvieco. Alcala de Henares, Universidad de Alcala.
- Pereira, J. and Setzer, A. (1993). "Spectral Characteristics of deforestation fires in NOAA/AVHRR images." *International Journal of Remote Sensing* (14): 583-597.
- Perez, B. and Moreno, J. (1998). "Methods for quantifying fire severity in shrubland-fires." *Plant Ecology* 139: 91–101.
- Perry, D. (1994). *Forest Ecosystems*. . Baltimore, The John Hopkins University Press.
- Piñol, J., Terradas, J. and Lloret, F. (1998). "Climatic warming hazard, and wildfire occurrence in coastal eastern Spain." *Climate Change* 38: 345-357.
- Pohl, C. and Genderen, J. (1998). "Multisensor image fusion in remote sensing: concepts, methods and applications." *International Journal of Remote Sensing* (19): 823-854.
- Pollet, J. and Omi, P. (2002). "Effect of thinning and prescribed burning on crown fire severity in ponderosa pine forests." *International Journal of Wildland Fire* 11: 1-10.
- Ponzoni, F. J., Lee, D. C. L. and Filho, P. H. (1986). Avaliacao da area queimada e da regeneracao da vegetacao afetada pelo fogo no Parque Nacional de Brasilia atraves de dados do TM/LANDSAT. In: R. Gramada, *Symposio Latino-Americano de Sensoriamento Remoto*, IV Simposio Brasileiro de Sensoriamento Remoto, INPE, Sao Jose dos Campos, Brazil. pp. 15-25.
- Pouliot, D., King, D., Bell, F. and Pitt, D. (2002). "Automated tree crown detection and delineation in high-resolution digital cam. imagery of coniferous forest regeneration." *Remote Sensing of Environment* 82: 322–334.
- Redmond, R., Winne, J., Opitz, D. and Mangrich, M. (2001). *Classifying and mapping wildfire severity. Imaging NOTES*.

- Rego, F. (1992). Land use changes and wildfires. In: A. Teller, P. Mathy and J. Jeffers, Response of forest fires to environmental change, London, Elsevier. pp. 367-373.
- Riaño, D., Chuvieco, E., Ustin, S., Zomer, R., Dennison, P., Roberts, D. and Salas, J. (2002). "Assessment of vegetation regeneration after fire through multitemporal analysis of AVIRIS images in the Santa Monica Mountains." *Remote Sensing of Environment* 79: 60-71.
- Richards, J. (1984). "Thematic mapping from multitemporal image data using the Principal Components Transformation." *Remote Sensing of Environment* 16: 35-46.
- Richards, J. (1999). *Remote Sensing Digital Image Analysis: An Introduction*. Berlin, Germany, Springer-Verlag: 240.
- Richter, R. (1990). "A Fast Atmospheric Correction Algorithm Applied To Landsat TM Images." *International Journal of Remote Sensing* 11 (1): 159-166.
- Ricotta, C., Avena, G., Olsen, E., Ramsey, R. and Winn, D. (1998). "Monitoring the landscape stability of the Mediterranean vegetation in relation to fire with a fractal algorithm." *International Journal of Remote Sensing* 19: 871– 881.
- Rignot, E., Despain, D. and Holecz, F. (1999). The 1988 Yellowstone fires observed by imaging radars. In: L. Neuenschwander, K. C. Ryan, G. Gollberg and J. Greer, Joint Fire Science Conference and Workshop, Crossing the Millenium: Integrating Spatial Technologies and Ecological Principles for a New Age in Fire Management, 15-17 June, Boise, Idaho. pp. 7-16.
- Rishmawi, K. and Gitas, I. (2001). Burned area mapping on the Mediterranean island of Thasos using low, medium-high and very high spatial resolution satellite data. In: RSPS2001, 12-14 September 2001, Westminster, London, Remote Sensing & Photogrammetry Society. pp. 26-32.
- Robinove, C. (1982). "Computation with physical values from Landsat digital data." *Photogrammetric Engineering and Remote Sensing* 48: 781-784.
- Rodriguez y Silva, F., Navarro, R., Navarro, C. and Gonzalez, M. P. (1997). Evaluation of forest fire damage with Landsat TM and ancillary information. A review of remote sensing methods for the study of large wildland fires. E. Chuvieco. Universidad de Alcala, Alcala de Henaras: 185-192.
- Rogan, J. and Franklin, J. (2001). "Mapping wildfire burn severity in southern California forests and shrublands using Enhanced thematic Mapper imagery." *Geocarto International* 4: 89-99.
- Rogan, J., Franklin, J. and Roberts, D. (2002). "A comparison of methods for monitoring multitemporal vegetation change using Thematic Mapper imagery." *Remote Sensing of Environment* 80: 143-156.
- Rogan, J. and Yool, S. (2001). "Mapping fire-induced vegetation depletion in the Peloncillo Mountains, Arizona and New Mexico." *International Journal of Remote Sensing* 22 (16): 3101-3121.
- Romero-Calcerrada, R. and Perry, G. (2004). "The role of land abandonment in landscape dynamics in the SPA 'Encinares del rio Alberche y Cofio, Central Spain, 1984-1999." *Landscape and Urban Planning*, 66: 217-232.

- Roy, D., Jin, Y., Lewis, P. and Justice, C. (2005). "Prototyping a global algorithm for systematic fire-affected area mapping using MODIS time series data." *Remote Sensing of Environment* 97: 137-162.
- Ruecker, G. and Siegert, F. (2000). Burn Scar Mapping and Fire Damage Assessment Using ERS-2 SAR Images in East Kalimantan, Indonesia. In: IAPRS, 17-21 August, Amsterdam. pp.
- Ryan, K. and Noste, N. (1985). Evaluating prescribed fires. In: J. Lotan, B. Kilgore, W. Fischer and R. Mutch, Symposium and workshop on wilderness fire, 15-18 November 1983, Missoula, MT. Gen. Tech. Rep. INT-182, Ogden, UT: US Department of Agriculture, Forest Service, Intermountain Forest and Range Experiment Station: 230-238. pp.
- Salas, W., Ducey, M., Rignot, E. and Skole, D. (2002). "Assessment of JERS-1 SAR for monitoring secondary vegetation in Amazonia: I. Spatial and temporal variability in backscatter across a chrono-sequence of secondary vegetation stands in Rondonia." *International Journal of Remote Sensing* 23 (7): 1357-1379.
- Salvador, R., Dnaz-Delgado, R., Valeriano, J. and Pons, X. (1998). Remote Sensing as a tool to map forest fires, to study the fire regime and their effects on plant communities and the integration into a GIS. In: GIS PlaNET'98 International Conference and Exhibition on Geographic Information 7-11 September 1998, Lisbon, Portugal. pp.
- Sampson, P., Treitz, P. and Mohammed, G. (2001). "Remote sensing of forest condition in tolerant hardwoods: An examination of spatial scale, structure and function." *Canadian Journal of Remote Sensing* 27 (3): 232-246.
- San Miguel-Ayanz, J., Annoni, A., Schmuck, G. and Meyer-Roux, J. (1998). Forest fire monitoring and damage assessment in Mediterranean landscapes through the integration of remote sensing and GIS techniques. In: The International Symposium on Resource and Environmental Monitoring: Local, Regional, Global, Budapest, Hungary. pp. 170-173.
- Schmidt, T., Koch, M., Gumuzzio, J. and Mathers, P. (2004). "A spectral library for a semi-arid wetland and its application to studies of wetland degradation using hyperspectral and multispectral data." *International Journal of Remote Sensing* 25: 2485-2496.
- Scott, J. and Reinhardt, E. (2001). Assessing crown fire potential by linking models of surface and crown fire behaviour, USDA, Forest service, Rocky Mountain Research station: 59.
- Shaw, D., Malthus, T. and Kupiec, J. (1998). "High-spectral resolution data for monitoring Scots pine (*Pinus sylvestris* L.) regeneration." *International Journal of Remote Sensing* 19 (13): 2601-2608.
- Siegert, F. and Nakayama, M. (2000). Comparison of ERS-2 and JERS for Fire Impact Assessment in Tropical Rainforests. In: International Geoscience and Remote Sensing Symposium, Honolulu Hawaii (IGARSS), 24/07-28/07, IEEE Geoscience and Remote Sensing Society, Spring, USA. pp. 35-50.
- Siegert, F. and Rueker, G. (2000). "Use of Multitemporal ERS-2 SAR Images for Identification of Burned Scars in South-East Asian Tropical Rainforest." *International Journal of Remote Sensing* 4: 831-837.
- Sifakis, N., Paronis, D. and Keramitsoglou, I. (2004). "An application of AVHRR imagery used in combination with CORINE Land Cover data for forestfire observations and

- consequences assessment." *International Journal of Applied Earth Observation and Geoinformation* 5: 263-274.
- Siljeström, P. and Moreno, A. (1995). "Monitoring burnt area by principal component analysis of multitemporal data." *International Journal of Remote Sensing* 16 (9): 1577-1587.
- Silva, J. M. N. (1996). Comparacao entre os indices de vegetao NDVI e IV7 para cartografia de areas ardidas com imagens LANDSAT-5 TM. Lisbon, Instituto Superior de Agronomia, Universidade Tecnica de Lisboa.
- Simpson, C. J. (1990). "Deep weathering, vegetation and fireburn. Significant obstacles for geoscience remote sensing in Australia." *International Journal of Remote Sensing* 11 (11): 2019-2034.
- Sinclair, T., Hoffer, R. and Schreiber, M. (1971). "Reflectance and internal structure of leaves from several crops during a growing season." *Agronomy Journal* 63: 864-868.
- Singer, R. and McCord, T. (1979). Mars: Large scale mixing of bright and dark surface materials and implications for analysis of spectral reflectance. In: *Proceedings of the 10th Lunar and Planetary Science Conference*, Houston. pp. 1835-1848.
- Smith, J., Lin, T. and Ranson, K. (1980). "The Lambertian assumption and Landsat data." *Photogrammetric Engineering and Remote Sensing* 46 (9): 1183-1189.
- Smith, M., Ustin, S., Adams, J. and Gillespie, A. (1990). "Vegetation in deserts: a regional measure of abundance from multispectral images." *Remote Sensing of Environment* 31: 1-26.
- Smith, R. and Woodgate, P. (1985). "Appraisal of fire damage and inventory for timber salvage by remote sensing in mountain ash forests in Victoria." *Australian Journal of Forestry* 48 (4): 252-263.
- Spanos, I. (1996). Natural regeneration of the Pinus Brutia forest in Thasos. In: *Second Balkan Scientific Conference on study, conservation and utilisation of forest resources*, Sofia, Bulgaria. pp. 40-56.
- Spanos, I., Daskalakou, E. and Thanos, C. (2000). "Postfire, natural regeneration of Pinus brutia forests in Thasos island, Greece." *Acta Oecologica* 21 (1): 13-20.
- Steininger, M. (2000). "Satellite estimation of tropical secondary forest above-ground biomass: Data from Brazil and Bolivia." *International Journal of Remote Sensing* 21 (6): 1139-1157.
- Stephens, S. (1998). "Evaluation of the effects of silvicultural and fuels treatments on potential fire behaviour in Sierra Nevada mixed conifer forests." *Ecology and Management* 105 (21-35).
- Tanaka, S., Kimura, H. and Suga, Y. (1983). "Preparation of a 1:25.000 LANDSAT map for assessment of burnt area on Etajima Island." *International Journal of Remote Sensing* 4 (1): 17-31.
- Tanaka, S. and Sugimura, T. (2001). "A new frontier of remote sensing from IKONOS images." *International Journal of Remote Sensing* 22: 1-5.

- Thenkabail, P. (2003). "Biophysical and yield information for precision farming from near-real-time and historical Landsat TM images." *International Journal of Remote Sensing* 24: 839-877.
- Thenkabail, P., Enclona, E., Ashton, M. and Der Meer, B. (2004a). "Accuracy assessments of hyperspectral waveband performance for vegetation analysis applications." *Remote Sensing of Environment* 91: 354-376.
- Thenkabail, P., Enclona, E., Ashton, M., Legg, C. and Jean De Dieu, M. (2004b). "Hyperion, IKONOS, ALI, and ETM+ sensors in the study of African rainforests." *Remote Sensing of Environment* (90): 23-43.
- Thenkabail, P., Smith, R. and De-Pauw, E. (2000). "Hyperspectral vegetation indices for determining agricultural crop characteristics." *Remote Sensing of Environment* 71: 158-182.
- Thenkabail, P., Smith, R. and De-Pauw, E. (2002). "Evaluation of narrowband and broadband vegetation indices for determining optimal hyperspectral wavebands for agricultural crop characterization." *Photogrammetric Engineering and Remote Sensing* 68: 607- 621.
- Torn, M. and Fried, J. (1992). "Predicting the impacts of global warming on wildland fire." *Climate Change* 21: 257-274.
- Trabaud, L. (1994). Plant and fire variability relationships more specifically in the Mediterranean basin. In: 2nd International Conference in Forest Fire Research, Coimbra, Portugal. pp. 53-58.
- Tsitsoni, T. (1997). "Conditions determining natural regeneration after wildfires in the *Pinus halepensis* (Miller, 1768) forests of Kassandra Peninsula (North Greece)." *Forest ecology and management* 92: 199-208.
- Turner, M., Romme, W. and Gardner, R. (1999). "Prefire Heterogeneity, Fire Severity, and Early Postfire Plant Reestablishment in Subalpine Forests of Yellowstone." *International Journal of Remote Sensing* 9 (1): 21-36.
- Twele, A. (2004). Post-fire vegetation regeneration: the case study of the Massif de l'etoile fire. Joint Research Centre, Directorate-General, European commission.
- Twele, A. and Barbosa, P. (2003). Monitoring vegetation regeneration after forest fires using satellite imagery, Joint Research Center, Institute for Environment and Sustainability, Land Management Unit.
- Ungar, S., Pearlman, J., Mendenhall, J. and Reuter, D. (2003). "Overview of the Earth Observing 1 (EO-1) mission." *IEEE Trans. Geosci. Remote Sensing* 41: 1149-1159.
- Ustin, S., Roberts, D., Jacquemoud, S., Pinzon, J., Gardner, M., Scheer, G., Castaneda, C. and Palacios, A. (1998). "Estimating canopy water content of chaparral shrubs using optical methods." *Remote Sensing of Environment* 65: 280- 291.
- Ustin, S. and Xiao, Q. (2001). "Mapping successional boreal forest in interior central Alaska." *International Journal of Remote Sensing* 22 (9): 1779- 1797.
- Van der Meer, F. and De Jong, S. (2000). "Improving the results of spectral unmixing of Landsat TM imagery by enhancing the orthogonality of end-members." *International Journal of Remote Sensing* 21: 2781-2797.

- Van der Meer, F. and De Jong, S. (2001). *Imaging spectrometry*. Kluwer Academic. 1-4020-0194-0.
- Van der Sande, C., De Jong, S. and De Roo, A. (2003). "A segmentation and classification approach of IKONOS-2 imagery for land cover mapping to assist flood risk and flood damage assessment." *International Journal of Applied Earth Observation and Geoinformation* 4: 217-229.
- Van Wagtendonk, J., Root, R., Key, C. and Running, S. (2004). "Comparison of AVIRIS and Landsat ETM+ detection capabilities for burn severity." *International Journal of Wildland Fire* 92: 397-408.
- Vane, G. and Goetz, A. (1988). "Terrestrial imaging spectrometry." *Remote Sensing of Environment* 24: 1-29.
- Vázquez, A. and Moreno, J. M. (2001). "Spatial distribution of forest fires in Sierra de Gredos (Central Spain)." *Forest ecology and management* 147: 55-65.
- Verdebout, J., Jacquemoud, S. and Schmuck, G. (1994). Optical properties of leaves: modelling and experimental studies. In: J. Hill and J. Megier, *Imaging spectrometry - a tool for environmental observations*, Brussels and Luxembourg. pp. 166-191.
- Viedma, O., Melia, J., Segarra, D. and García-Haro, J. (1997). "Modeling Rates of Ecosystem Recovery after Fires by Using Landsat TM data." *Remote Sensing of Environment* 61: 383-398.
- Wagner, W., Luckman, A., Vietmeier, J., Tansey, K., Balzter, H., Schmullius, C., Davidson, M., Gaveau, D., Gluck, M., Toan, T., Quegan, S., Shvidenko, A., Wiesmann, A. and Yu, J. (2002). "Large-scale mapping of boreal forest in SIBERIA using ERS tandem coherence and JERS backscatter data." *Remote Sensing of Environment* 5816: 1-20.
- Wahren, C., Papst, W. and Williams, R. (2001). "Early post-fire regeneration in subalpine heathland and grassland in the Victorian Alpine National Park, south-eastern Australia." *Austral Ecology* 26: 670-679.
- Wang, L., Sousa, W., Gong, P. and Biging, G. (2004). "Comparison of IKONOS and QuickBird images for mapping mangrove species on the Caribbean coast of Panama." *Remote Sensing of Environment* 91: 432-440.
- Wessmann, C. A., Aber, J., Peterson, D. and Melillo, J. (1988). "Remote Sensing of canopy chemistry and nitrogen cycling in temperate forest ecosystems." *Nature* 7: 449-461.
- White, J., Ryan, K., Key, C. and Running, S. (1996). "Remote Sensing of forest fire severity and vegetation recovery." *International Journal of Remote Sensing* 6 (3): 125-136.
- White, P. (1979). "Pattern, process, and natural disturbance in vegetation." *Bot. Rev.* 45: 229-299.
- Wicks, T., Smith, G. and Curran, P. (2002). "Polygon-based aggregation of remotely sensed data for regional ecological analysis." *International Journal of Applied Earth Observation and Geoinformation* (4): 161-173.
- Zhukov, B., Oertel, D., Lanzl, F. and Reinhäkel, G. (1999.). "Unmixing based multisensor multiresolution image fusion." *EEE Transactions on Geoscience and Remote Sensing* 37: 1212-1225.

APPENDICES

APPENDIX 1: Measuring fire severity in the field**A.1 DEVELOPED FIELD PROTOCOL FOR QUANTITATIVE VEGETATION DAMAGE ASSESSMENT (After Key and Benson 1999)**

Examiners: _____	Field date (mmdyyy): _____
Site name: _____	Registration code: _____
Plot ID: _____	Project code: _____

Coordinates (X,Y):	Coordinates (X,Y) Differential:
Elevation (m):	Elevation (m) Differential:
Slope (%):	Slope (DEM):
Aspect (field):	Aspect (DEM):
Sample size:	Name and date of fire:
Vegetation cover (%):	Percentage burned (%):
Vegetation type:	Vegetation type:
Presence of healthy trees (y/n):	Tree cover (%):
Plot photo IDs:	Dominant vegetation species after fire:

Strata Rating Factors	BURN SEVERITY SCALE							Factors Scores
	No Effect	Low		Moderate		High		
	0.0	0.5	1.0	1.5	2.0	2.5	3.0	
1. HERBS, LOW SHRUBS AND SMALL TREES								
%Foliage Altered (blk-brn)	Unchanged	--	30%	--	80%	95%	100%+branch loss	
%Living/Resprout (freq)	≥ 100%	--	90%	--	50%	≤20%	None	
Colonizers	Unchanged	--	Low	--	Moderate	High-Low	Low to None	
Spp. Comp. – Rel. Abund.	Unchanged	--	Little change	--	Moderate change	--	High change	
1. Sum of scores =		N Rated =			Mean =			
2. TALL SHRUBS, SAPLING TREES								
%Foliage Altered (blk-brn)	0%	--	20%	--	70%	80%	100%+branch loss	
%Green (volume unalter)	100%	--	80%	--	30%	5%	None	
%Living/Resprout (freq)	≥ 100%	--	90%	--	30%	15%	<1%	
Spp. Comp. – Rel. Abund.	Unchanged	--	Little change	--	Moderate change	--	High change	
2. Sum of scores =		N Rated =			Mean =			
3. INTERMEDIATE TREES (SUBCANOPY, POLE SIZED TREES)								
%Green Unaltered	100%	--	80%	--	40%	<10%	None	
%Black (Torch)	None	--	5-20%	--	60%	> 85%	100% + branch loss	
%Brown (Scorch/Girdle)	None	--	5-20%	--	40-80%	<40 or >80%	None due to torch	
%Canopy Mortality	None	--	15%	--	60%	80%	100%	
Char Height	None	--	1.5m	--	2.8m	--	>5m	
3. Sum of scores =		N Rated =			Mean =		%Girdled=	%Felled=
4. BIG TREES (UPPER CANOPY, DOMINANT TREES)								
%Green Unaltered	100%	--	95%	--	50%	<10%	None	
%Black (Torch)	None	--	5-10%	--	50%	> 80%	100% + branch loss	
%Brown (Scorch/Girdle)	None	--	5-10%	--	30-70%	<30 or >70%	None due to torch	
%Canopy Mortality	None	--	10%	--	50%	70%	100%	
Char Height	None	--	1.8m	--	4m	--	>7m	
4. Sum of scores =		N Rated =			Mean =		%Girdled=	%Felled=
Notes/Comments:		CBI = Sum of scores/N Rated:		Sum of scores		N Rated		CBI
		Understory (1+2)						
		Overstory (3+4)						
		Total Plot (1+2+3+4)						

A.2 PROTOCOL DESCRIPTION AND INSTRUCTIONS

The protocol is mainly addressed to assess fire damage on vegetation, specifically to assess fire severity qualitatively and quantitatively (Refer to chapter 3). Following, strata definitions are given:

Herbs, Low Shrubs and Small Trees - All grasses and forbs, plus shrubs and small trees less than 1 meter (3 ft) tall. Herbs are plants that die back to ground level each year. Shrubs retain persistent aboveground woody stems, from which subsequent years growth develops. Small trees, including tree seedlings, are like shrubs, but typically have only one central stalk, and eventually grow to heights far exceeding this one-meter size class.

Tall Shrub and Sapling Trees - Shrubs and small trees generally greater than 1 meter (3 ft) and less than 5 meters (15 ft) tall. If saplings or shrubs are between 5 meters (15 ft) and 8 meters (25 ft) tall, decide which stratum the life form fits best. They could be scored with intermediate trees, but only if they are distinctly tree-like and meet the characteristics of other intermediate trees.

Intermediate Trees (pole-sized trees, subcanopy) - Trees occupying space between the tall shrub/sapling layer and the uppermost canopy; generally 10 to 25 cm (4 to 10 in.) diameter, and 8 to 20 meters (25 to 65 ft) tall. If trees of this size are the uppermost canopy, then consider them as intermediate trees while not counting a big tree stratum. This stratum may itself be of stratified heights, with crown tops extending into the upper canopy. Still consider, however, that they are intermediate trees, if they receive little direct sunlight from above. Actual size of the intermediate trees is relative to height of upper canopy and may vary from community to community.

Big Trees (mature trees, dominant and co-dominant trees, upper canopy) – Dominant and co-dominant trees that are larger than intermediate trees. They occupy the uppermost canopy, and usually receive direct sunlight from above. These tree

crowns form the general or average level of the upper canopy, while some individuals may extend above that.

Understory - The region comprised of herbs/low shrubs/small trees, and tall shrubs/saplings.

Overstory - The region above the understory, consisting of intermediate and big trees.

Total Plot, or Overall - All strata of the plot combined.

A.2.1 Strata rating factors:

A.2.1.1 Herbs, low shrubs and trees less than 3 ft (1m) rating factors

As with substrates, field personnel must determine initially whether herb, low shrub, and/or small tree rating factors are sufficiently represented on a plot to justify scoring them. The stratum should have been sufficiently present to indicate severity after fire. In general, suspected pre-fire coverage of less than about 5 percent of the plot, or limited distribution throughout might not be enough and may lead you not to count at least some of the factors. Such cases may occur under dense conifer canopies where the pre-fire understory consisted solely of needle-cast litter and duff, or in other cases, where vegetation was sparse and exposed soil was relatively high.

Percent Foliage Altered - Percent of pre-fire woody-species cover that was impacted by fire as estimated by change in cover from green to brown or black. This only concerns the pre-fire low shrubs and small trees, not grasses and herbs. It includes girdle, scorch, and torch of needles, leaves, and stems. Resprouting from the base of shrubs or trees is not considered in this estimate of altered foliage, only the pre-fire foliage is. In other words, the entire blackened crown of a low shrub counts as pre-fire foliage altered, even though it may be resprouting. The amount of resprouting does not lessen the percent of pre-fire foliage altered. At high levels of severity, consumption of outer fine branching on low shrubs and small trees has occurred.

Frequency Percent Living - Percent of pre-fire vegetation that is still alive after fire. This is a measure of survivorship based on numbers of individuals and not necessarily on change in cover. Include unburned as well as burned, resprouting perennial herbs, low shrubs, and small trees plotwide. Resprouting plants are ones that burned but survive from living roots and stems. Include all green vegetation as well as burned plants that have not had enough time to resprout but remain viable. Burned plants may need to be examined for viable cambium or succulent buds near growth points. Dead stems will be brittle when bent; living ones will be supple. Do not include new colonizers or other plants newly germinating from seed. Make sure to take in the whole plot in the average score, including unburned areas.

New Colonizers - Potential dominance within 2 to 3 years post-fire of plants newly generating from seed (native or exotic) averaged over the plot. The basis for this rating is the proliferation of such species due to fire, that is, above and beyond what might be expected had fire not occurred. Relative frequency of colonizers compared to established plants may be more recognizable at first, with relative cover increasing over time. This includes herbs such as like fireweed, thistle and pokeweed, as well as new tree or shrub seedlings. It also includes increased dominance of nonvascular plants that proliferate after fire in some areas, such as fungi, bryophytes, lycopodium, and small fine-leaved moss. New colonizers also include aspen suckers that generate from former trees as well as similar tree to shrub responses from other species. Suckers are defined as stem growth originating from underground roots or rhizomes, as opposed to originating from branches or central trunks.

Species Composition and/or Relative Abundance - Change in species composition, and/or relative abundance of species anticipated within 2 to 3 years post-fire. This is a community-based assessment that gauges the ecological resemblance of the post-fire community compared to the community that existed before fire. It represents alterations in dominance among species (biomass or cover) as well as potential change in the species present, such as absence of pre-fire species and/or presence of new post-fire species. Consider the distribution of abundance or dominance among the species present after fire, compared to before fire. Such factors qualitatively determine the similarity or dissimilarity of the site from before to after fire. Increases

or decreases in certain species abundance and dominance, or changes in the species present after fire, raise the score for this rating factor.

A.2.1.2 Tall shrub and trees 3 to 16 ft (1 to 5 m) rating factors

Percent Foliage Altered - Percent of pre-fire foliage for tall shrubs and trees 3 to 16 ft (1 to 3 m) that was impacted by fire as estimated by change in crown volume from green to brown or black. This includes girdle, scorch, and torch of needles, leaves, and stems. The entire blackened top-killed crown of a tall shrub counts as pre-fire foliage altered, even though there may be a portion that is resprouting. The volume of the resprouting is ignored; it does not lessen the amount of pre-fire foliage altered. At high levels of severity, consumption of outer fine branching on shrubs and trees is evident. In fall burns and leaf-off conditions, base the score on effects to remaining boles and branches, the degree of outer branch consumption, and whether or not fire top-killed plants.

Frequency Percent Living - Percent of pre-fire tall shrubs and trees (3 to 16 ft) that are still alive after fire. This is a measure of survivorship based on numbers of individuals, not on change in cover or crown volume. Include unburned area as well as burned but resprouting tall shrubs and trees 3 to 16 ft (1 to 5 m) tall plotwide. Resprouting plants are ones that burned and survive from living roots and stems. Include all green plants, plus burned plants that have not had enough time to resprout but remain viable. Burned plants may need to be examined for viable cambium or succulent buds near growth points. Dead stems will be brittle when bent; living ones will be supple. Do not include new colonizers, such as aspen suckers or other plants newly germinating from seed. Account for potential mortality that could occur up to 2 years post-fire (for example, conifer saplings that are 70 percent brown will likely die in 2 years), and make sure to average plotwide, including unburned areas.

Percent Change in Cover - Overall *decrease* in cover of shrubs and trees between 3 and 16 ft (1 and 5 m) tall, relative to the area occupied by those plants before fire. Count resprouting from plants that burned, plus the unburned plants, as cover that mitigates against or lessens the amount of decrease in cover. Do not include new colonizers or other plants newly germinating from seeds, including suckers that

represent tree-to-shrub responses. Suckers from aspen and other species are counted as new colonizers that generate from underground roots or rhizomes, as opposed to coming from branches or central trunks. Make sure to average plotwide, including unburned areas. Account for potential mortality that could occur up to 2 years post fire. For example, conifer saplings that are 70 percent brown will likely die in 2 years.

Species Composition and/or Relative Abundance - Change in species composition, and/or relative abundance of species anticipated within 2 to 3 years post-fire. Include pre-fire tall shrubs and trees 3 to 16 ft (1 to 5 m) tall as well as big and intermediate trees resprouting from the base.

A.2.1.3 Intermediate and big tree rating factors (combined)

Generally for conifer forests, the sum of the first three factors - Percent Unaltered, Percent Black, and Percent Brown - will be 100 percent. That may not be the case, however, in some deciduous forests or southeastern pine forests, where crowns may have been blackened or torched but not killed and subsequently resprout. In such cases, continue to score the unaltered, black and brown factors as they appear on the site, even though they may add up to more than 100 percent. The balance of the three factors should still maintain appropriate overall ratings for severity in the overstory.

Percent Unaltered (Green) - Percent of pre-fire crown foliage volume (living or dead) unaltered by fire, relative to estimated pre-fire crown volume of the plot. Include resprouting from burned crowns, but not from tree bases, as unaltered/green.

Percent Black (torch) - Percent black is pre-fire crown foliage (living or dead) that actually caught fire, stems and leaves included, relative to estimated pre-fire crown volume plotwide; may or may not be viable crown foliage after fire. At high severity, consumption of fine branching is evident. Do not consider resprouting from black branches as lessening the percent black. In many cases, deciduous trees will not torch especially when leaves are off; yet high flame lengths from the ground may blacken virtually the entire tree. Due to the aerial intensity of such fire and its similarity to crown fire, this type of burn is also included in the percent black rating.

Percent Brown (scorch) - Percent of tree canopy affected by scorch or killed by girdling, in relation to the estimated pre-fire crown volume over the whole plot. This is foliage killed by proximal heating without direct flame contact (such as brown foliage that did not actually catch fire). It includes scorching effects at the time of fire as well as delayed mortality, often from heat impacts around tree boles and roots. Suspected insect and disease effects also may be included, if that is manifested in the crowns relatively soon after fire (within about 2 years). This avoids a need to separate burn impacts from similar-appearing and related foliage conditions caused by fire-induced pathogens. Include crowns obviously impacted by these effects, even though brown foliage may have fallen to the ground. Include deciduous trees burned in leaf-off condition that are not resprouting from crowns. In those cases, look for dead crowns or portions of crowns that do not contain any black but may show severe charring around lower trunks or at ground level.

Percent Canopy Mortality - Of trees killed by fire or expected to die within 2 years, this should represent the proportion of crown volume now contributed by fire-killed trees (the proportion of once living crown volume that is now dead). Consider in relation to crown volume still contributed by surviving trees. Only count trees that are completely dead, not the fire-killed portions of crowns that may still exist on living trees. One can count completely top-killed crowns on trees that show shrubby basal resprout. The factor is viewed as the proportion of a plot's total once-living canopy now lost because of recently dead trees. Suspected insect and disease effects also may be included, if that has contributed to killing whole trees relatively soon after fire (within about 2 years). This avoids a need to separate burn impacts from similar appearing and related foliage conditions caused by fire-induced insects or disease.

Char Height - The average height of char on tree trunks resulting from ground flames. This is the mean height on individual trees averaged over all trees in the plot. The mean height on a given tree is determined as halfway between upper char height and lower char height. Trees on slopes typically have char running up higher on the up-slope side, and wind-driven flames usually result in char running up higher on the leeward side of trees. Include unburned trees (char height = 0) and burned trees only where demarcation of ground char height is discernable. This rating does not include the black on upper boles resulting from crown fire. Trees that do not clearly show

where ground flames ended and crown fire began are not included in the score. Thus, char height may not be applicable where crown fire predominates.

Percent Girdled (at root or lower bole) - Percent of trees effectively killed by heat through the lower bark, affecting the cambium around the circumference of lower boles or buttress roots. Girdling may or may not actually char through the bark and into the wood. It is often indicated a year or more after fire by sheets of bark loosely attached or sloughing off the lower bole. Include trees either dead or likely to die within 1 to 2 years. Do not include trees killed by crown fire or other scorching to crown.

Percent Felled (downed) - Percent of trees, whether dead or alive, that were standing before fire but now are lying on the ground. Such trees usually result from wind throw after fire. They typically exhibit fresh upturned

A.3 REFERENCES

Key, C. and Benson, N. (1999), Measuring and remote sensing of burn severity. In Joint Fire Science Conference and Workshop, Ryan, C. (Ed.), Moscow, pp. 284.

Key, C. and Benson, N. (2002), Measuring and Remote sensing of burn severity. In J.L. Coffelt and R.K. Livingston, U.S. Geological Survey Wildland Fire Workshop, Los Alamos, NM October 31-November 3, 2000. USGS Open-File Report 02-11. pp. 55.

Key, C., Benson, N., Sorbel, B., Zhu, Z., Ohlen, D., Howard, S. and Clement, B. (2002), National Park Service-U.S. Geological Survey National Burn Severity Mapping Project, USGS EROS Data Center.

Key, C.H. and Benson, N.C. (2004), FIREMON Landscape Assessment (LA): Sampling and Analysis methods, NPS-USGS, USA.

A.4 DATA COLLECTED: GENERAL INFORMATION

Plot Nb.	GPS1 (East)	GPS1 (North)	Elevation (m)	Slope (%)	Aspect	Dominant vegetation	Canopy (%)	Substratum (%)
1	565145	4509496	70	40	S	coccifera	0	90
2	565406	4509314	77	40	S	brutia, coccifera	40	10
3	565614	4509569	82	30	NE	coccifera	0	90
4	565569	4509873	76	25	NE	coccifera	0	80
5	565516	4509951	85	25	NE	coccifera	0	80
6	565228	4510047	110	40	NW	brutia, cistus i.	15	80
7	565168	4510004	60	40	N-NE	l. nobilis	0	40
8	565062	4510107	70	50	N-NE	l. nobilis, cistus i.	0	80
9	564887	4510294	80	15	W	brutia, coccifera	90	60
10	564659	4510116	60	45	NE	brutia, fern	10	20
11	564485	4510321	30	30	E	brutia, fern	70	80
12	564324	4510519	25	40	E	brutia, cistus i.	0	60
13	564754	4510491	23	20	W	brutia, l. nobilis	20	80
14	564829	4509335	115	45	SW	brutia, coccifera	15	35
15	564912	4509452	100	30	E	coccifera	0	80
16	564910	4509454	130	45	E	brutia	40	30
17	564954	4509696	140	30	SE	coccifera	0	30
18	564147	4509759	218	20	S	cistus, rosmarie	0	90
19	565022	4509866	200	40	N	brutia, nobilis	20	60
20	564957	4509915	173	30	N-NW	brutia	40	20
21	564871	4509890	180	30	N	nobilis, brutia	5	80
22	564672	4509934	183	55	N	nobilis, brutia	0	50
23	564568	4509936	183	50	N	brutia	20	15
24	564489	4509974	192	60	N	coccifera	0	10
25	564236	4510085	209	35	N	brutia	35	10
26	564146	4510093	223	30	N-NE	brutia, fern	80	5
27	563916	4510107	232	55	N-NE	brutia	95	5
28	564019	4510074	237	55	N	brutia	95	5
29	564182	4510058	216	35	N-NE	brutia	95	2
30	564394	4509772	298	501	N	fern	0	20
31	564209	4509831	319	40	N-E	coccifera	0	15
32	564229	4509842	286	25	NE	brutia	50	20
33	564168	4509754	330	45	S	brutia	30	5
34	564093	4509768	330	30	S	brutia	0	5
35	564366	4509404	136	45	SE	brutia, coccifera	2	95
36	564559	4509415	118	40	SE	brutia	30	50

A.5 COLLECTED DATA: RATED SCORES

1. Herbs, low shrubs and small trees < 1m							
Plot Nb.	% Foliage altered	% Living/Resprout	Colonizers	Spp.Comp.-Rel. Abund.	B. sum of scores	N Rated	Mean
1	3	2	2	0	7	4	1.75
2	3	2	2	0	7	4	1.75
3	3	2	2	0	7	4	1.75
4	3	3	2	0	8	4	2
5	3	1.5	1	0	5.5	4	1.375
6	3	1	1.5	0	5.5	4	1.375
7	3	2	1	0	6	4	1.5
8	3	2	1.5	0	6.5	4	1.625
9	3	1	0.5	0	4.5	4	1.125
10	3	1	1	0	5	4	1.25
11	0.5	0	0	0	0.5	4	0.125
12	3	3	2	0	8	4	2
13	3	1	0.5	0	4.5	4	1.125
14	1	1	1	0	3	4	0.75
15	3	2	2	0	7	4	1.75
16	-	-	-	-	-	-	-
17	3	2.5	1.5	0	7	4	1.75
18	3	2	2	0	7	4	1.75
19	2.5	1.5	1	0	5	4	1.25
20	3	1.5	1	0	5.5	4	1.375
21	3	1	2.5	0	6.5	4	1.625
22	3	2	0.7	0	5.7	4	1.425
23	3	1.5	1	0	5.5	4	1.375
24	3	2.5	1	0	6.5	4	1.625
25	-	-	-	-	-	-	-
26	-	-	-	-	-	-	-
27	-	-	-	-	-	-	-
28	-	-	-	-	-	-	-
29	-	-	-	-	-	-	-
30	3	2.5	1.5	0	7	4	1.75
31	-	-	-	-	-	-	-
32	3	2.5	0.5	0	6	4	1.5
33	3	2.5	1	0	6.5	4	1.625
34	2.7	1.5	1	0	5.2	4	1.3
35	3	2	1	0	6	4	1.5
36	1.2	1	1	0	3.2	4	0.8

2. Tall shrubs, sapling trees (between 1 and 5 m)							
Plot Nb.	% Foliage altered	Green (volume unalt.)	Living/Respro ut	Spp. Comp.- Rel.Abund.	C. sum of scorres	N Rated	Mean
1	3	3	2	0	8	4	2
2	-	-	-	-	-	-	-
3	3	3	2	0	8	4	2
4	-	-	-	-	-	-	-
5	3	3	3	0	9	4	2.25
6	3	3	2.5	0	8.5	4	2.125
7	-	-	-	-	-	-	-
8	-	-	-	-	-	-	-
9	-	-	-	-	-	-	-
10	-	-	-	-	-	-	-
11	-	-	-	-	-	-	-
12	-	-	-	-	-	-	-
13	3	2.2	1	0	6.2	4	1.55
14	-	-	-	-	-	-	-
15	3	3	2.5	0	8.5	4	2.125
16	-	-	-	-	-	-	-
17	-	-	-	-	-	-	-
18	-	-	-	-	-	-	-
19	-	-	-	-	-	-	-
20	-	-	-	-	-	-	-
21	-	-	-	-	-	-	-
22	3	3	2.5	0	8.5	4	2.125
23	-	-	-	-	-	-	-
24	-	-	-	-	-	-	-
25	-	-	-	-	-	-	-
26	-	-	-	-	-	-	-
27	-	-	-	-	-	-	-
28	-	-	-	-	-	-	-
29	-	-	-	-	-	-	-
30	-	-	-	-	-	-	-
31	-	-	-	-	-	-	-
32	-	-	-	-	-	-	-
33	-	-	-	-	-	-	-
34	-	-	-	-	-	-	-
35	3	3	2.5	0	8.5	4	2.125
36	-	-	-	-	-	-	-

3. Intermediate Trees (subcanopy) (10-25 cm, 5-20 m)								
Plot Nb.	% Green (unaltered)	% Black (Torch)	% Brown (Scorch/Girdle)	% canopy Mortality	Char height	D. sum of scores	N Rated	Mean
1	-	-	-	-	-	-	-	-
2	1.5	2	1	1.7	1	7.2	5	1.44
3	-	-	-	-	-	-	-	-
4	-	-	-	-	-	-	-	-
5	3	2	1	3	2	11	5	2.2
6	2	2	1		1	6	4	1.5
7	3	-	-	-	2	5	2	2.5
8	3	-	-	-	3	6	2	3
9	-	-	-	-	-	-	-	-
10	0.2	0.1	0.1	0	0.1	0.5	5	0.1
11	-	-	-	-	-	-	-	-
12	-	-	-	-	-	-	-	-
13	2.5	2	1.5	1.5	2	9.5	5	1.9
14	-	-	-	-	-	-	-	-
15	-	-	-	-	-	-	-	-
16	1.5	1	1		1	4.5	4	1.12
17	3	-	-	-	1.9	4.9	2	2.45
18	-	-	-	-	-	-	-	-
19	-	-	-	-	-	-	-	-
20	2.5	2	1.5		0.5	6.5	4	1.62
21	-	-	-	-	-	-	-	-
22	-	-	-	-	-	-	-	-
23	-	-	-	-	-	-	-	-
24	3	-	-	-	2	5	2	2.5
25	-	-	-	-	-	-	-	-
26	0.2	0.3	0.2		0.1	0.8	4	0.2
27	0.5	1	1		0.5	3	4	0.75
28	1	1	1		0.5	3.5	4	0.87
29	-	-	-	-	-	-	-	-
30	-	-	-	-	-	-	-	-
31	1	1	1		1	4	4	1
32	1.2	1	1		0.5	3.7	4	0.92
33	-	-	-	-	-	-	-	-
34	-	-	-	-	-	-	-	-
35	2.2	2	1.5	-	0.5	6.2	4	1.55
36	-	-	-	-	-	-	-	-

4. Big Trees (.25cm)								
Plot Nb.	% Green (unaltered)	% Black (Torch)	% Brown (Scorch/Girdle)	% canopy Mortality	Char height	E. sum of scores	N Rated	Mean
1	-	-	-	-	-	-	-	-
2	2.3	2.2	1.5	1.3	1.4	8.7	5	1.74
3	-	-	-	-	-	-	-	-
4	-	-	-	-	-	-	-	-
5	-	-	-	-	-	-	-	-
6	-	-	-	-	-	-	-	-
7	-	-	-	-	-	-	-	-
8	-	-	-	-	-	-	-	-
9	1.5	1	0.5	0	0.5	3.5	5	0.7
10	-	-	-	-	-	-	-	-
11	-	-	-	-	-	-	-	-
12	-	-	-	-	-	-	-	-
13	-	-	-	-	-	-	-	-
14	1	1	1	-	1.2	4.2	4	1.05
15	-	-	-	-	-	-	-	-
16	2.5	2	1.5	-	1	7	4	1.75
17	-	-	-	-	-	-	-	-
18	3	-	-	-	1.5	4.5	2	2.25
19	2.5	1.5	1	-	1.2	6.2	4	1.55
20	2	1.7	2	-	0.8	6.5	4	1.625
21	2.5	2	2	-	1.8	8.3	4	2.075
22	3	-	-	-	2	5	2	2.5
23	2	2	1	-	0.7	5.7	4	1.425
24	-	-	-	-	-	-	-	-
25	1	1.5	1.2	-	0.5	4.2	4	1.05
26	1.5	1	1	-	0.5	4	4	1
27	2	2.2	2	-	1	7.2	4	1.8
28	1.5	1	1	-	0.5	4	4	1
29	1.9	1.5	1.2	-	1.2	5.8	4	1.45
30	3	2.5		-	2.5	8	3	2.66
31	1.5	1.5	1	-	3	7	4	1.75
32	1.5	1.5	2	-	1.5	6.5	4	1.625
33	2.5	2.5	1.5	-	2	8.5	4	2.125
34	3	2	1	-	2.5	8.5	4	2.125
35	-	-	-	-	-	-	-	-
36	1.7	1.3	1	-	0.7	4.7	4	1.175

FINAL SCORES

Plot Nb.	Understory (1+2)			Canopy/Overstory (3+4)			Total plot (1+2+3+4)			
	Sum of Scores	N Rated	CBI (Sum of Scores/N Rated)	Sum of Scores	N Rated	CBI (Sum of Scores/N Rated)	Sum of Scores	N Rated	CBI (Sum of Scores/N Rated)	Severity class
1	15	8	1.875	-	-	-	15	8	1.875	3
2	7	4	1.75	15.9	10	1.59	22.9	14	1.635714	2
3	15	8	1.875	-	-	-	15	8	1.875	3
4	8	4	2	-	-	-	8	4	2	3
5	14.5	8	1.8125	11	5	2.2	25.5	13	1.961538	3
6	14	8	1.75	6	4	1.5	20	12	1.666667	2
7	6	4	1.5	5	2	2.5	11	6	1.833333	3
8	6.5	4	1.625	6	2	3	12.5	6	2.083333	3
9	4.5	4	1.125	3.5	5	0.7	8	9	0.888889	1
10	5	4	1.25	0.5	5	0.1	5.5	9	0.611111	1
11	0.5	4	0.125	-	-	-	0.5	4	0.125	1
12	8	4	2	-	-	-	8	4	2	3
13	10.7	8	1.3375	9.5	5	1.9	20.2	13	1.553846	2
14	3	4	0.75	4.2	4	1.05	7.2	8	0.9	1
15	15.5	8	1.9375	-	-	-	15.5	8	1.9375	3
16	-	-	-	11.5	8	1.4375	11.5	8	1.4375	2
17	7	4	1.75	4.9	2	2.45	11.9	6	1.983333	3
18	7	4	1.75	4.5	2	2.25	11.5	6	1.916667	3
19	5	4	1.25	6.2	4	1.55	11.2	8	1.4	2
20	5.5	4	1.375	13	8	1.625	18.5	12	1.541667	2
21	6.5	4	1.625	8.3	4	2.075	14.8	8	1.85	3
22	14.2	8	1.775	5	2	2.5	19.2	10	1.92	3
23	5.5	4	1.375	5.7	4	1.425	11.2	8	1.4	2
24	6.5	4	1.625	5	2	2.5	11.5	6	1.916667	3
25	-	-	-	4.2	4	1.05	4.2	4	1.05	2
26	-	-	-	4.8	8	0.6	4.8	8	0.6	1
27	-	-	-	10.2	8	1.275	10.2	8	1.275	2
28	-	-	-	7.5	8	0.9375	7.5	8	0.9375	1
29	-	-	-	5.8	4	1.45	5.8	4	1.45	2
30	7	4	1.75	8	3	2.666667	15	7	2.142857	3
31	-	-	-	11	8	1.375	11	8	1.375	2
32	6	4	1.5	10.2	8	1.275	16.2	12	1.35	2
33	6.5	4	1.625	8.5	4	2.125	15	8	1.875	3
34	5.2	4	1.3	8.5	4	2.125	13.7	8	1.7125	2
35	14.5	8	1.8125	6.2	4	1.55	20.7	12	1.725	2
36	3.2	4	0.8	4.7	4	1.175	7.9	8	0.9875	1

APPENDIX 2: Collection of hyperspectral data in the field

Averaged and filtered field spectrometry of pine trees:

<i>Wavelengths (nm)</i>	<i>brutia-young</i>	<i>brutia-mature</i>	<i>nigra-young</i>	<i>nigra-mature</i>
428.441	0.016174	0.042095	0.016538	0.02912
438.611	0.019023	0.029266	0.020618	0.022907
448.791	0.020741	0.034577	0.020366	0.027256
458.961	0.022023	0.034823	0.025831	0.027416
469.141	0.023045	0.039137	0.026595	0.026216
479.311	0.023438	0.039809	0.025766	0.029977
489.488	0.025149	0.040725	0.027092	0.03332
499.651	0.028931	0.040256	0.027696	0.034747
509.82	0.038772	0.048765	0.034314	0.037961
519.974	0.062636	0.063555	0.052099	0.054599
530.135	0.079609	0.074187	0.065221	0.064079
540.283	0.090652	0.080652	0.075444	0.069819
550.439	0.09532	0.084965	0.078196	0.074634
560.584	0.094191	0.08587	0.077525	0.072889
570.738	0.093293	0.078974	0.068454	0.065647
580.892	0.0938	0.075423	0.062287	0.060179
591.037	0.086857	0.073467	0.059613	0.0575
601.194	0.090769	0.074451	0.057899	0.055362
611.343	0.080653	0.071279	0.054325	0.053336
621.506	0.059996	0.069342	0.050325	0.051279
631.662	0.05795	0.074944	0.051826	0.051102
641.831	0.059996	0.068854	0.048746	0.047933
651.995	0.047726	0.066096	0.042151	0.043412
662.172	0.040838	0.064171	0.038998	0.039903
672.346	0.033676	0.062163	0.035084	0.035335
682.535	0.03647	0.064568	0.036069	0.037401
692.72	0.064029	0.081143	0.054968	0.053978
702.917	0.140824	0.13207	0.118864	0.106823
713.107	0.198518	0.175004	0.177806	0.155867
723.305	0.271555	0.234556	0.263375	0.228208
733.489	0.3111	0.2676	0.316694	0.273509
743.679	0.338431	0.290311	0.350571	0.300478
753.863	0.351354	0.307286	0.372304	0.319048
764.039	0.354108	0.316036	0.38123	0.325742

774.236	0.359461	0.317986	0.386602	0.33099
784.43	0.361249	0.322167	0.390209	0.332441
794.641	0.362848	0.325583	0.390634	0.336054
804.841	0.365182	0.329919	0.396131	0.340728
815.047	0.365231	0.330536	0.395927	0.340234
825.235	0.367453	0.33679	0.399595	0.340905
835.421	0.368535	0.33591	0.39956	0.344171
845.591	0.370276	0.341793	0.401903	0.345307
855.771	0.371688	0.342221	0.403492	0.347878
865.941	0.372931	0.345643	0.40488	0.348922
876.12	0.374117	0.35212	0.407354	0.353352
886.29	0.374739	0.350652	0.403137	0.356585
896.47	0.373344	0.356946	0.406068	0.349101
906.64	0.373122	0.344228	0.403959	0.354839
916.819	0.373654	0.351866	0.406215	0.355367
926.999	0.36928	0.352462	0.391431	0.35613
897.198	0.372803	0.355859	0.398833	0.351
907.288	0.373412	0.343685	0.40371	0.355518
917.388	0.37354	0.352283	0.404339	0.355188
927.478	0.369733	0.345944	0.395875	0.340681
937.568	0.367258	0.349682	0.359823	0.339559
947.658	0.36486	0.34441	0.346143	0.354952
957.738	0.356778	0.30468	0.346761	0.326634
967.828	0.349454	0.352995	0.352498	0.302467
977.918	0.346392	0.320688	0.352991	0.321426
988.048	0.348882	0.335748	0.340473	0.312276

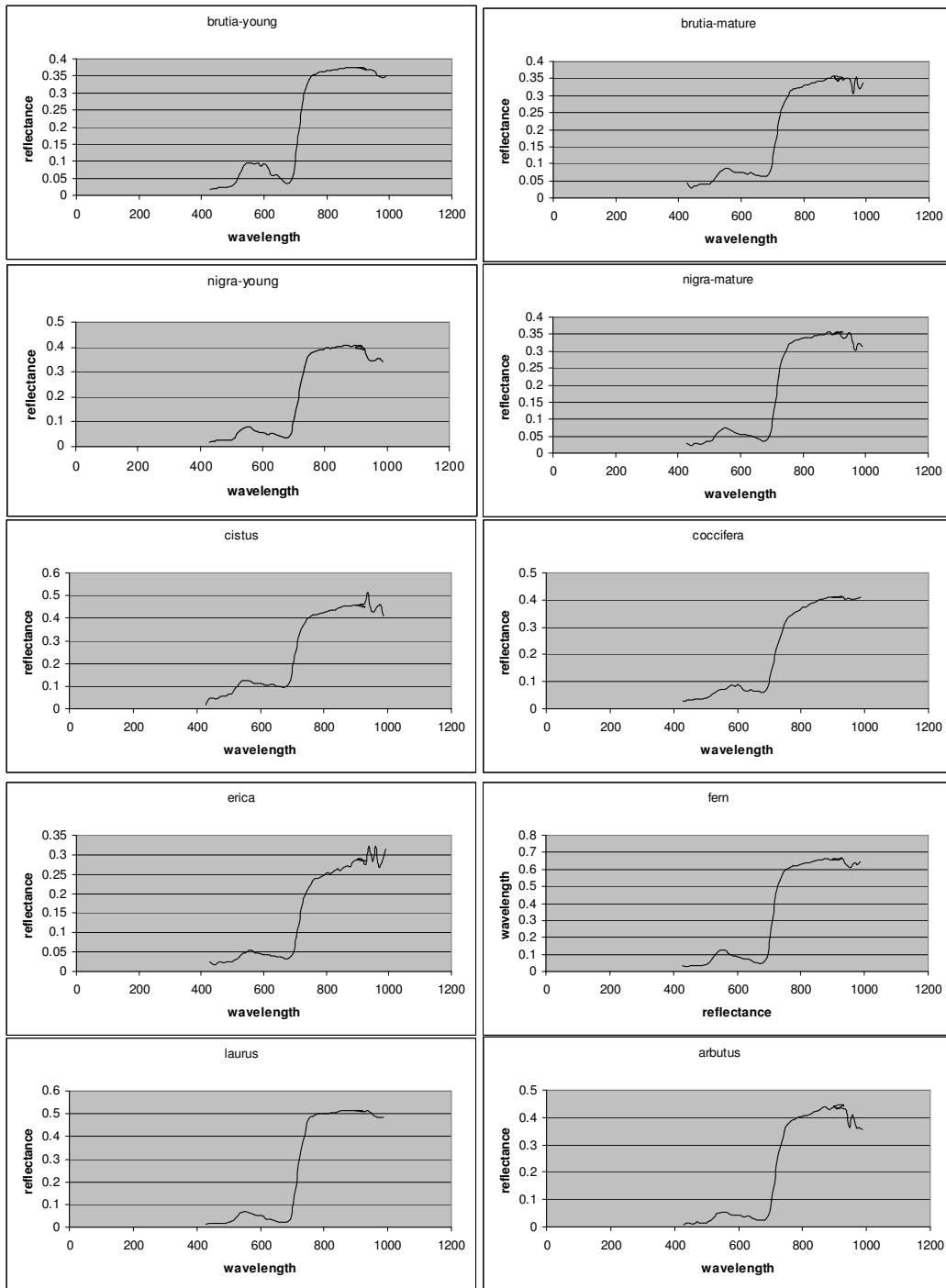
Averaged and filtered field spectrometry of shrub species:

<i>wavelengths</i>	<i>C. incanus</i>	<i>Q. coccifera</i>	<i>E. manipuliflora</i>	<i>fern</i>	<i>L. nobilis</i>	<i>A. unedo</i>
428.441	0.016995	0.027629	0.025258	0.032373	0.014981	0.008406
438.611	0.042669	0.030464	0.017897	0.031425	0.016523	0.012951
448.791	0.046846	0.031953	0.020692	0.031025	0.017411	0.012795
458.961	0.042907	0.033484	0.025787	0.032012	0.018089	0.011619
469.141	0.049343	0.034449	0.022019	0.031887	0.017966	0.016461
479.311	0.054571	0.035324	0.024762	0.034948	0.018219	0.015429
489.488	0.054405	0.036551	0.025235	0.033387	0.018813	0.013523
499.651	0.062863	0.038715	0.024995	0.038838	0.020941	0.015817
509.82	0.064392	0.042437	0.030529	0.047068	0.024709	0.023039

519.974	0.090372	0.052265	0.037269	0.072622	0.038897	0.03223
530.135	0.105492	0.060241	0.046118	0.098963	0.052203	0.045118
540.283	0.119601	0.067083	0.048652	0.117634	0.063363	0.050623
550.439	0.126731	0.07069	0.052199	0.126465	0.067947	0.053129
560.584	0.125556	0.072869	0.055926	0.125592	0.066537	0.054259
570.738	0.119033	0.079601	0.047981	0.109278	0.059905	0.046262
580.892	0.114203	0.08586	0.048	0.09687	0.0572	0.044154
591.037	0.112363	0.082855	0.045244	0.093911	0.052007	0.042667
601.194	0.111431	0.090045	0.043902	0.087626	0.052195	0.042528
611.343	0.109	0.084529	0.043225	0.081338	0.045607	0.039221
621.506	0.105315	0.066605	0.04037	0.075027	0.034573	0.036018
631.662	0.106436	0.063335	0.04071	0.074675	0.033836	0.038769
641.831	0.106158	0.072007	0.038783	0.068296	0.032084	0.033275
651.995	0.099298	0.065289	0.037	0.056983	0.025829	0.029474
662.172	0.097737	0.064173	0.03586	0.052298	0.022736	0.026613
672.346	0.093	0.061175	0.033667	0.045167	0.019802	0.024336
682.535	0.100067	0.062618	0.036266	0.050969	0.021325	0.025669
692.72	0.125149	0.076288	0.046605	0.079353	0.035155	0.04314
702.917	0.202875	0.121917	0.087831	0.201671	0.106356	0.096891
713.107	0.259128	0.16173	0.123022	0.316882	0.181418	0.157449
723.305	0.329879	0.219925	0.170266	0.462583	0.298144	0.251198
733.489	0.365382	0.262619	0.197542	0.5332	0.378074	0.307107
743.679	0.38643	0.29554	0.216342	0.573785	0.436323	0.347982
753.863	0.40181	0.323718	0.229333	0.600262	0.477079	0.375524
764.039	0.413941	0.340236	0.239797	0.609856	0.486791	0.390118
774.236	0.413643	0.349881	0.240333	0.619807	0.496242	0.393657
784.43	0.419753	0.357596	0.244646	0.623387	0.498751	0.397828
794.641	0.422499	0.364311	0.250055	0.627359	0.500067	0.402496
804.841	0.428594	0.372743	0.253594	0.632634	0.502258	0.407602
815.047	0.430469	0.374972	0.252979	0.639333	0.502072	0.406375
825.235	0.435533	0.383164	0.26041	0.64159	0.505011	0.415352
835.421	0.437267	0.388444	0.263514	0.645348	0.506995	0.41981
845.591	0.445255	0.393559	0.258844	0.648833	0.509472	0.423387
855.771	0.44837	0.399194	0.267956	0.654541	0.51207	0.428405
865.941	0.453157	0.40251	0.27298	0.655027	0.513906	0.437912
876.12	0.45138	0.406475	0.269038	0.661218	0.515086	0.434714
886.29	0.454866	0.409207	0.281533	0.659831	0.515669	0.429224
896.47	0.458	0.409266	0.286667	0.658256	0.513811	0.44055
906.64	0.455549	0.410299	0.290272	0.663278	0.513302	0.432018

916.819	0.459461	0.411287	0.28406	0.658103	0.513199	0.435064
926.999	0.448092	0.411603	0.283287	0.660352	0.511442	0.444959
897.198	0.456057	0.408825	0.286667	0.655486	0.514093	0.443204
907.288	0.457314	0.41024	0.290815	0.660834	0.513321	0.434055
917.388	0.46232	0.411482	0.287277	0.656673	0.512656	0.436493
927.478	0.464545	0.412067	0.274543	0.666962	0.511444	0.431446
937.568	0.51516	0.403241	0.321977	0.636977	0.513042	0.426008
947.658	0.437229	0.408082	0.283018	0.618922	0.506402	0.36257
957.738	0.426693	0.402598	0.323436	0.609944	0.493537	0.411374
967.828	0.452693	0.403248	0.269152	0.637864	0.482575	0.364662
977.918	0.459588	0.405885	0.278934	0.626415	0.483412	0.364666
988.048	0.41086	0.411814	0.313556	0.64181	0.484722	0.354864

Spectral signatures of the spectrally targeted vegetation (400-1000 nm):



APPENDIX 3: Selected publications

- Mitri, G. and Gitas, I. Mapping the severity of fire using object-based classification of Ikonos imagery. *International Journal of Wildland Fire* (In press).
- Moufllis G., Gitas, I., Iliadou, S., Mitri, G.. Assessment of the visual impact of marble quarry expansion (1984-2000) on the landscape of Thasos island, NE Greece. *International Journal of Landscape and Urban Planning* (In press).
- Mitri, G. and Gitas, I. 2007. Mapping post-fire vegetation regeneration using EO-1 Hyperion. The 6th International Workshop of the EARSeL Special Interest Group (SIG) on Forest Fires, Thessaloniki, Greece. 26 - 29 Sept. 2007.
- Gitas, I., Moufllis, G., Mitri, G., Tsakalidis, S., Iliadou, S., Minakou, H. 2007. Assessment of the impact of forest fires and marble quarries on the environment of Thasos island. *Landscape Architecture and New Technologies*. 25-26 May, Kavala, Greece.
- Mitri, G. and Gitas I. 2006. Fire type mapping using object-based classification of Ikonos imagery. *International journal of wildland Fire*, Volume 15, Number 4, 457-462.
- Gitas, I., Mitri, G., Kazakis, G., Ghosn, D. and Xanthopoulos, G. 2006. Fuel type mapping in Anopolis, Crete by employing QuickBird imagery and object-based classification. *Forest Ecology and Management*. Vol. 234, P. 228.
- Gitas, I., Mitri, G., Kazakis, G., Ghosn, D., Xanthopoulos, G. 2006. Fuel type mapping in Anopolis, Crete by employing QuickBird imagery and object-based classification. 5th International Conference on Forest Fire Research. 27 to 30 November 2006, Portugal.
- Polychronaki, A., Gitas, I. and Mitri, G. 2006. The development of an object-oriented model for burned area mapping using an atmospherically and non-atmospherically corrected ASTER image. RSPSoc Annual Conference 5-8th September 2006 Fitzwilliam College, Cambridge, U.K.
- Mitri G., Gitas I., 2004. A semi-automated object-oriented model for burned area mapping in the Mediterranean region using Landsat-TM imagery. *International Journal of Wildland Fire*, Volume 13, Number 3, 367–376.
- Gitas I., Mitri G., and Ventura G., 2004. Object-oriented image analysis for burned area mapping using NOAA-AVHRR imagery in Creus Cape, Spain. *Remote Sensing of Environment*. Volume 92, Number 3, 409-413.
- Mitri G. and Gitas I., 2004. A performance evaluation of a burned area object-based classification model when applied to topographically and non-topographically corrected TM imagery. *International Journal of Remote Sensing*. Volume 25, Number 14, 2863–2870.
- Gitas I., Mitri G., Avyikou I and Diamanti E. 2004. Vegetation greenness mapping of Greece using MODIS imagery. MODIS workshop, June 24-25, University of Valladolid, Spain.
- Mitri G. and Gitas I., 2003. A performance evaluation of a burned area object-oriented classification model when applied to topographically and non-topographically corrected TM imagery. 4th EARSeL Workshop on Forest Fire Monitoring and Mapping (Emilio Chuvieco). EARSeL, 5-7 June, Ghent, Belgium, 187-191.
- Gitas I., Chuvieco E., Mitri G., and Ventura G., 2003. Object-oriented image analysis for burned area mapping using NOAA-AVHRR imagery in Creus Cape, Spain. 4th EARSeL Workshop on Forest Fire Monitoring and Mapping (Emilio Chuvieco). EARSeL, 5-7 June, Ghent, Belgium, 177-181.
- I.Z. Gitas, G.H. Mitri, P. Barbosa, N. Assad, I. Jomaa, C. Papageorgiou, and T.Turk, 2003. Land Cover Change Detection Using NOAA-AVHRR Images taken from 1989 to 2002 for the Eastern Part of the Mediterranean Region as a Tool to Support Decision-Making. Options Méditerranéennes (CIHEAM), Série B – n° 46.
- Karydas, C. G., Silleos, N. G., Gitas, I. Z., and Mitri, G. H., 2002. Development of an object oriented classification model for managing and monitoring citrus plantations. In: Proceedings of the 9th International Symposium on Remote Sensing, SPIE, Agia Pelagia, Crete, Greece, 23-27 September.